MCEER
EARTHQUAKE ENGINEERING TO EXTREME EVENTS

ISSN 1520-295X

Statistical and Mechanistic Fragility Analysis of Concrete Bridges

by
M. Shinozuka, Swagata Banerjee and Sang-Hoon Kim

Technical Report MCEER-07-0015

September 10, 2007

This research was conducted at the University of California, Irvine and was supported by the Federal Highway Administration under contract number DTFH61-98-C-00094.

NOTICE

Statistical and Mechanistic Fragility Analysis of Concrete Bridges

by

M. Shinozuka,[1] Swagata Banerjee[2] and Sang-Hoon Kim[3]

Publication Date: September 10, 2007
Submittal Date: February 28, 2006

Technical Report MCEER-07-0015

Task Number 094-B-1.3

FHWA Contract Number DTFH61-98-C-00094

1 Distinguished Professor, Department of Civil and Environmental Engineering, University of California, Irvine
2 Ph.D. Candidate, Department of Civil and Environmental Engineering, University of California, Irvine
3 Former Ph.D. Student, Department of Civil and Environmental Engineering, University of California, Irvine

MCEER
University at Buffalo, The State University of New York
Red Jacket Quadrangle, Buffalo, NY 14261
Phone: (716) 645-3391; Fax (716) 645-3399
E-mail: *mceer@buffalo.edu*; WWW Site: *http://mceer.buffalo.edu*

Preface

The Multidisciplinary Center for Earthquake Engineering Research (MCEER) is a national center of excellence in advanced technology applications that is dedicated to the reduction of earthquake losses nationwide. Headquartered at the University at Buffalo, State University of New York, the Center was originally established by the National Science Foundation in 1986, as the National Center for Earthquake Engineering Research (NCEER).

Comprising a consortium of researchers from numerous disciplines and institutions throughout the United States, the Center's mission is to reduce earthquake losses through research and the application of advanced technologies that improve engineering, pre-earthquake planning and post-earthquake recovery strategies. Toward this end, the Center coordinates a nationwide program of multidisciplinary team research, education and outreach activities.

MCEER's research is conducted under the sponsorship of two major federal agencies, the National Science Foundation (NSF) and the Federal Highway Administration (FHWA), and the State of New York. Significant support is also derived from the Federal Emergency Management Agency (FEMA), other state governments, academic institutions, foreign governments and private industry.

The Center's Highway Project develops improved seismic design, evaluation, and retrofit methodologies and strategies for new and existing bridges and other highway structures, and for assessing the seismic performance of highway systems. The FHWA has sponsored three major contracts with MCEER under the Highway Project, two of which were initiated in 1992 and the third in 1998.

Of the two 1992 studies, one performed a series of tasks intended to improve seismic design practices for new highway bridges, tunnels, and retaining structures (MCEER Project 112). The other study focused on methodologies and approaches for assessing and improving the seismic performance of existing "typical" highway bridges and other highway system components including tunnels, retaining structures, slopes, culverts, and pavements (MCEER Project 106). These studies were conducted to:

- assess the seismic vulnerability of highway systems, structures, and components;
- develop concepts for retrofitting vulnerable highway structures and components;
- develop improved design and analysis methodologies for bridges, tunnels, and retaining structures, which include consideration of soil-structure interaction mechanisms and their influence on structural response; and
- develop, update, and recommend improved seismic design and performance criteria for new highway systems and structures.

The 1998 study, "Seismic Vulnerability of the Highway System" (FHWA Contract DTFH61-98-C-00094; known as MCEER Project 094), was initiated with the objective of performing studies to improve the seismic performance of bridge types not covered under Projects 106 or 112, and to provide extensions to system performance assessments for highway systems. Specific subjects covered under Project 094 include:

- development of formal loss estimation technologies and methodologies for highway systems;
- analysis, design, detailing, and retrofitting technologies for special bridges, including those with flexible superstructures (e.g., trusses), those supported by steel tower substructures, and cable-supported bridges (e.g., suspension and cable-stayed bridges);
- seismic response modification device technologies (e.g., hysteretic dampers, isolation bearings); and
- soil behavior, foundation behavior, and ground motion studies for large bridges.

In addition, Project 094 includes a series of special studies, addressing topics that range from non-destructive assessment of retrofitted bridge components to supporting studies intended to assist in educating the bridge engineering profession on the implementation of new seismic design and retrofitting strategies.

This report elaborates on the seismic performance of reinforced concrete bridges subjected to earthquake ground motion by integrating probabilistic, statistical and mechanistic aspects of bridge damageability in the form of two-parameter lognormal fragility curves. To simulate general patterns of the progressive nature of bridge damage and failure mechanisms, the study performs nonlinear time history analyses of typical California RC bridges by finite element method (FEM). The analyses demonstrate that under normal conditions, the most prominent bridge damage that is first observed after a significant earthquake is the formation of plastic hinges at the ends of bridge columns. Therefore, damage due to pounding of girders at expansion joints, unseating of bridge decks and shear failure of bridge columns are considered but not as governing failure modes in this study. Another purpose of these FEM analyses is to simulate the enhancement of bridge fragility characteristics due to seismic retrofit, primarily because neither empirical nor experimental results are available to evaluate such enhancements. In addition, these FEM analyses develop fragility curves with and without retrofit. In fact, the main purpose of these FEM analyses is to develop analytical fragility curves without retrofit that can be calibrated with empirical fragility curves. In the process of calibration, intervals of rotational ductility values that represent states of bridge damage are adjusted to form contiguous intervals over the one-dimensional space of rotational ductility. If the rotational ductility is between upper and lower bounds in one of the intervals, the bridge is assumed to have suffered from the state of damage corresponding to the rotational ductility specified by that interval. This calibration is made for each bridge separately, although it is envisioned to perform combined calibration to derive common damage states for all types of bridges. In addition to time history analysis, nonlinear static procedure is performed to assess seismic vulnerability of the bridge and results from these two methods are in good agreement. Furthermore, the effect of ground motion directionality on bridge fragility characteristics is demonstrated, which indicates that directionality may significantly influence bridge seismic damageability.

ABSTRACT

In highway transportation system, bridges are one of the most seismically vulnerable structures. Development of fragility curves that incorporates various sources of uncertainty related to seismic hazard, bridge characteristics, site conditions etc., is an appropriate way to express the seismic vulnerability associated with various damage states of bridges. It gives a physical understanding of the structural reliability under an earthquake ground motion having certain intensity level. Thus construction of fragility curve is a widely accepted and well populated approach to express seismic vulnerability information.

This report represents dynamic progressive failure modes that are defined and used for interpreting fragility characteristics of typical Caltrans' bridges of various dimensions and configurations. To investigate the effect of ground motion intensity on the variation of bridge response behavior, a model bridge is analyzed under ground acceleration time histories at different levels of annual exceedance probability. The bridge is analyzed as a system with the aid of finite element method integrating appropriate nonlinear elements to represent plastic hinge formation at the column ends, pounding at the expansion joints and restrainer failures. The analysis shows that the dynamic progressive failure represents important progression of bridge failures.

The effect of seismic retrofitting is analytically investigated by means of steel jacketing of bridge columns and restrainers at expansion joints in order to strengthen the existing bridges. Two parameter lognormal distribution functions are used to develop fragility curves as a function of PGA. The improvement in the fragility characteristics of bridges after retrofit is examined by comparing two fragility curves before and after retrofit. The fragility enhancement is quantified by computing the change in the median values of the fragility curves before and after retrofit.

This study also mechanistically defines and quantifies the damage states of bridges in calibration with damage data of bridges under past earthquakes to the extent that these damage states can be used for fragility curve construction by nonlinear dynamic analysis. This makes the fragility

curves, developed analytically, more consistent with the empirical curves developed from past earthquake damage data.

This study also deals with the directionality effect of earthquake ground motion. As we know, earthquake ground motion has two horizontal and one vertical components. In the practice of seismic response analysis, it is almost impossible to identify the principal direction of these orthogonal horizontal components, and let alone that of all the three components. The assessment of this directionality effect on structure will not be mathematically feasible to model for the purpose of fragility curve development. In this report, a more practice-oriented concept and design criteria are developed on the basis that the structure must resist an earthquake ground motion from all possible directions. Furthermore, exploratory research is performed to construct fragility curves of bridges utilizing pushover method, in conjunction with performance-based structural design currently used in profession. To check the reliability of this procedure, developed fragility curves are compared with those obtained from time history analysis.

ACKNOWLEDGMENT

This study was supported by the Federal Highway Administration under contract DTFH61-98-C-00094 (Task Entitled 'Fragility Curves for Seismically Retrofitted Bridges and Effect of Retrofit on Transportation Performance') through the Multidisciplinary Center for Earthquake Engineering Research (MCEER) in Buffalo, NY.

Authors would like to thank Dr. Shigeru Kushiyama for providing moment-rotation program and Mr. Ung Jin Na for performing analysis to compute the effect of stiffness and strength degradation of moment-curvature relation on fragility characteristics of bridges.

TABLE OF CONTENTS

TABLE OF CONTENTS (cont'd)

LIST OF ILLUSTRATIONS

LIST OF ILLUSTRATIONS (cont'd)

LIST OF ILLUSTRATIONS (cont'd)

LIST OF ILLUSTRATIONS (cont'd)

LIST OF ILLUSTRATIONS (cont'd)

LIST OF ILLUSTRATIONS (cont'd)

LIST OF TABLES

LIST OF TABLES (cont'd)

SECTION 1
INTRODUCTION

Representation of seismic vulnerability of highway bridges in terms of fragility curves is a modern, well accepted and appropriate way for a meaningful risk assessment, not only the bridges but also for ensuing assessment of performance of transportation networks in which bridges are important components. A fragility curve represents structural reliability in the form of a probability distribution function, which is again a function of the ground motion intensity. The measures such as PGA, SA and SI are often deployed to represent such intensity.

Several recent destructive earthquakes, particularly the 1989 Loma Prieta and 1994 Northridge earthquakes in California, and the 1995 Hanshin-Awaji (Kobe) earthquake in Japan, caused significant damage to a large number of highway structures that were seismically deficient (Basoz and Kiremidjian 1998, Buckle 1994). In addition to this, Roberts (2005) documented different types of failure modes of reinforced concrete bridges in most recent earthquake events around the world. The investigation of these negative consequences brought forward the discussions about seismic design deficiency, probable failure modes, possible ways to upgrade the performance by retrofitting of the existing bridges and the seismic design of new bridges. In this respect, a comparative study on response analysis of a bridge as a system tracing the dynamic progressive failure will provide a better understanding and insight for the global performance of the bridge to seismic ground motion. In addition, the analysis identifies and prioritizes locations of retrofit for the enhancement of its capability to future strong earthquakes. Indeed, the present research focuses on comparative study of different types of bridge failures and collapse and their individual time of occurrences to demonstrate a progressive failure mechanism of bridge as a system in response to a specific earthquake ground motion. Obviously, specific bridge models reflect their unique structural characteristics. It is envisioned, however, that a class of bridges of similar configuration, materials, and size will have correspondingly similar failure mechanism that applies to that class. However, difference in the number of spans, skewness and site soil conditions are the parameters that substantially influence the seismic fragility of bridges (Shinozuka et al. 2003a). Accordingly, the calibrations of analytical fragility curves and damage state quantification are carried out simultaneously with empirical ones for a specific combination of these parameters in Section 5.

Two-parameter lognormal distribution is traditional way to construct fragility curves. This study develops the fragility curves of five (5) reinforced concrete bridges for different damage states. For that, nonlinear time history analyses of these bridges are carried out for sixty (60) ground motion time histories. Both longitudinal and transverse analysis is performed to construct fragility curves in both directions of bridges. This study also provides an approach for the seismic performance assessment of older bridges retrofitted by steel jacketing of bridge columns. Result shows a considerable improvement in the seismic performance of existing bridges. Therefore, using this approach to estimate the enhancement in fragility characteristics, it is now possible to evaluate the improvement of seismic performance of a highway network after retrofitting the bridges associated with that system.

The damage report of Caltrans' bridges under the Northridge earthquake documented five damage states of bridges as 'almost no', 'minor', 'moderate', 'major' (extensive) damage and 'collapse' as often used for fragility analysis. Effort has been given, however, for developing mechanistic model of bridge damage in calibration with Caltrans' damage data to the extent that the models can be used for fragility curve construction by nonlinear dynamic analysis. The damage models are developed to specify mechanistically the range of physical damage (upper and/or lower bounds) for each damage state. In this respect, the damage observation as reported by Caltrans serves as invaluable field experiments the nature provided according to which mechanistic calibration of damage model is achieved. Analytical fragility curves of Caltrans bridges at different damage states are calibrated with the empirical result reported by Shinozuka et al. (2003b) for bridges with similar geometric configuration and site condition.

This study also develops nonlinear static procedure involving Capacity Spectrum Method for construction of fragility curves consistent with current professional design and vulnerability assessment procedure incorporating performance-based engineering concept. This method provides a graphical representation of the force-displacement capacity curve of the bridge and develops inelastic demand spectrum of earthquake ground motion from its elastic demand spectrum through an interaction with capacity curve of the bridge. Thereafter, performance displacements are obtained from the intersection of the inelastic demand spectra and capacity spectrum and used to generate fragility curves at different damage levels. Comparison of thus developed fragility curves with that developed in time history analysis indicates well consistency that proves the reliability of this analytical procedure.

Most analytical investigations of nonlinear response of structural systems to seismic excitation in the past have considered one component of ground motion. Although in reality, the reliability of any important structure depends on its capability of resisting the ground motion coming from any possible horizontal direction. Also, a recorded ground motion may have two horizontal orthogonal components, N-S and E-W. In the practice of seismic response analysis, it is almost impossible to identify the principal directions of these orthogonal components and position of the structure relative to them. Although it is possible to model the ground motion acceleration time history as a 2D or 3D vector random process (Shinozuka, et al., 1996), the model results in time varying principal axis of the process and becomes too complex for our purposes. This report provides a practice-oriented concept and analytical procedure to address the issue of directional effect of earthquake ground motion on bridges. Fragility curves are developed considering that the ground motions are approaching to the bridge such a way that they will have maximum effect on structural response. It is believed that this theoretical concept will provide a basis to estimate the effect of directionality of earthquake ground motion on seismic performance of structures.

SECTION 2
NONLINEAR BRIDGE MODELS AND RETROFIT OF REINFORCED CONCRETE COLUMNS

To examine the performance of bridges under seismic ground motions, finite element modeling of five (5) typical reinforced concrete bridges with various dimensions, configurations and site conditions in California is done and analyzed using commercially available structural analysis computer code. Bridge dynamic characteristics are simulated numerically so that obtained response can be utilized to develop analytical fragility curves. The following sections described the procedure in detail.

2.1 Bridge Description

A short description of the five (5) sample bridges used for analysis is given in table 2-1. Bridge 1 is a three span bridge having overall length of 34 m. The superstructure consists of a longitudinally reinforced concrete deck slab of 10 m width. The bridge is supported on two pairs of three circular columns of 0.8 m diameter and an abutment at each end. Bridge 2 has an overall length of 242 m and an expansion joint. This bridge is supported on four 21 m high identical circular columns of diameter 2.4 m. The deck has a 3-cell concrete box girder (13 m x 2 m). Bridge 3 has an overall length of 226 m consisting of three frames separated by two expansion joints. The superstructure consists of a RC box girder in the outer spans and a prestressed box girder in the interior (central) span. The deck has a 6-cell box girder (20 m x 2.6 m). The columns are octagonal in shape and with varying lengths. Bridge 4 is of 483 m long and it has four expansion joints. This bridge is supported on nine columns of all different heights. Each column has a rectangular cross section (1.2 m x 3.7 m). The deck has a 5-cell concrete box type girder section (17 m x 2 m). Bridge 5 has an overall length of 500 m with twelve spans and an expansion joint. It is supported on eleven oblong columns of equal height (12.8 m) and cross-sections. The deck is consisting of 4-cell concrete box type girder section (15 m x 2 m). The geometric configurations of example bridges are shown in figure 2-1.

TABLE 2-1 Description of Five (5) Sample Bridges

Bridges	Overall Length	Number of Spans	Number of Hinges	Column Height
1	34 m	3	0	4.7 m
2	242 m	5	1	21.0 m
3	226 m	5	2	9.5 ~ 24.7 m
4	483 m	10	4	9.5 ~ 34.4 m
5	500 m	12	1	12.8 m

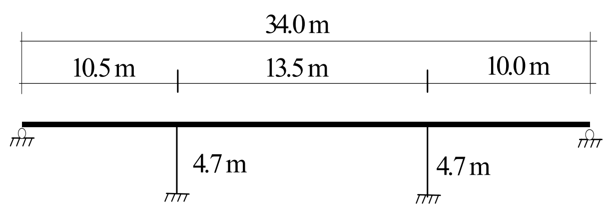

(a) Bridge 1

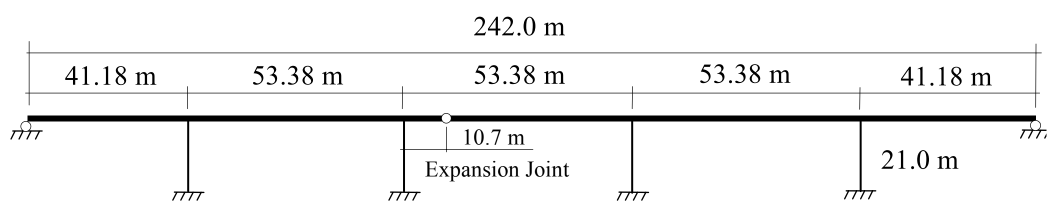

(b) Bridge 2

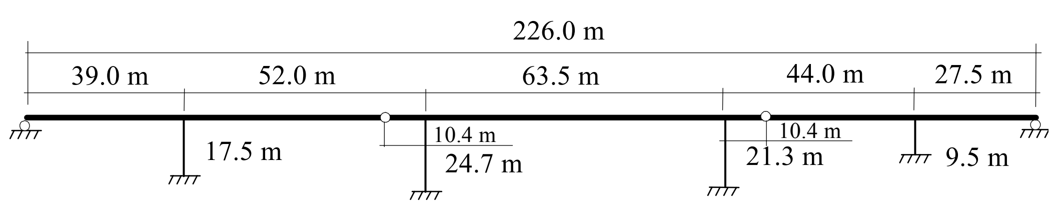

(c) Bridge 3

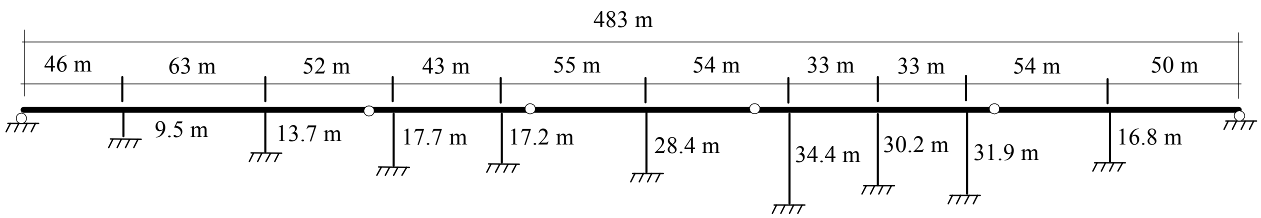

(d) Bridge 4

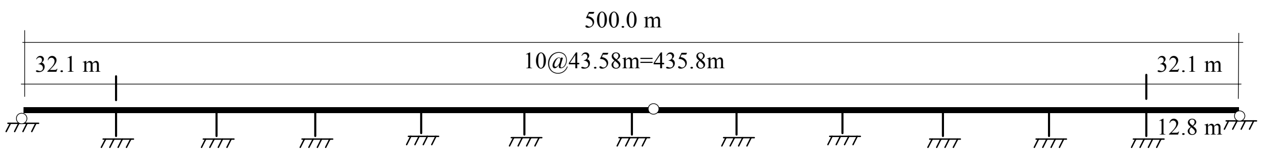

(e) Bridge 5

FIGURE 2-1 Elevation of Sample Bridges

2.2 Nonlinear Modeling of Bridges

Finite element computer code SAP2000 Nonlinear (Computer and Structures, 2002) is used in the ensuing time history analysis. The bridge deck is integrated with the column bents, so full continuity is considered at its girder-column joints. The bridge superstructure is free to rotate at the abutment locations for longitudinal in-plane excitation, although the translational motion is limited to the initially provided gap between the bridge girder and abutment. If the relative displacement of the bridge girder at abutment locations exceeds this gap, axial force develops at the interface due to the passive earth pressure of embankment soil. According to Caltrans recommendation (Bridge Design Criteria, 2004), the longitudinal abutment stiffness is

$$K_{abut} = K_i \times w \times \left(\frac{h}{5.5} \right) \quad \text{in S.I. units} \tag{2-1}$$

where K_i is the initial embankment stiffness (=11.5 kN/mm/m), w is the width of the backfill in m and h is the height of the backfill in m. During transverse out-of-plane motion, it can rotate freely while movement is restrained by wingwalls and concrete shear keys which are, in general, assumed to be rigidly connected with abutments and not to dissipate any energy through yielding

(Federal Highway Administration, 1996). Therefore, during transverse motion, the bridge end and the abutment move together as rigidly joined. To incorporate the soil effects behind wingwalls at abutments, translational (linear) springs are attached at the end of bridge girder. Spring stiffness is determined according to Caltrans recommendation for abutment stiffness in transverse direction.

Bridges with expansion joint(s) are modeled such that the two ends of an expansion joint can move independently in longitudinal direction and rotate in longitudinal plane while they have no relative vertical movement. During out-of-plane motion, they are assumed as pin connections as the lateral translations of the two ends of bridge deck at expansion joint are same.

Due to the seismic excitation, bending moment is generated in columns which may lead to the formation of plastic hinges at both ends of the columns. The approximate nonlinearities in a bridge are shown in figure 2-2 and as described immediately below. Moment-curvature relationship at the plastic hinges can generate a complex hysteretic behavior. For the sake of simplicity and design compatibility, however, rotational springs with bilinear moment-curvature relationship are introduced to represent the nonlinearity at both ends of bridge columns. Also linear translational and rotational springs are introduced at the bases of the columns to account for soil effect in longitudinal and transverse directions. An effective moment of inertia is considered to take care of the cracked state of concrete bridge columns.

The computer code (SAP 2000) permits the use of a gap element to take care of the effect of pounding between two adjacent bridge decks at expansion joints and abutment locations during longitudinal movement of the bridge. At abutment locations, an initial gap of 0.0508 m (2 in) is provided between the bridge deck and abutment (figure 2-3a). The gap element at expansion joint is modeled as a linear spring having stiffness not more than 1000 times of that of the adjacent element (Kim and Shinozuka, 2003). Here the initially provided gap is 0.0254 m (1 in) (figure 2-3b) and during oscillation, pounding develops (compressive force) at the interface of the two adjacent bridge decks when relative displacement exhausts this initial gap width. The hook element represents the restraining bar or cable that can be severed under excessive tensile stress, or producing failure of anchorages though which restrainers are tied to decks. Figure 2-3c shows that the initial slack in the restrainer is 0.013 m (0.5 in) and axial force generates when the restrainer gets engaged by loosing this initial slack.

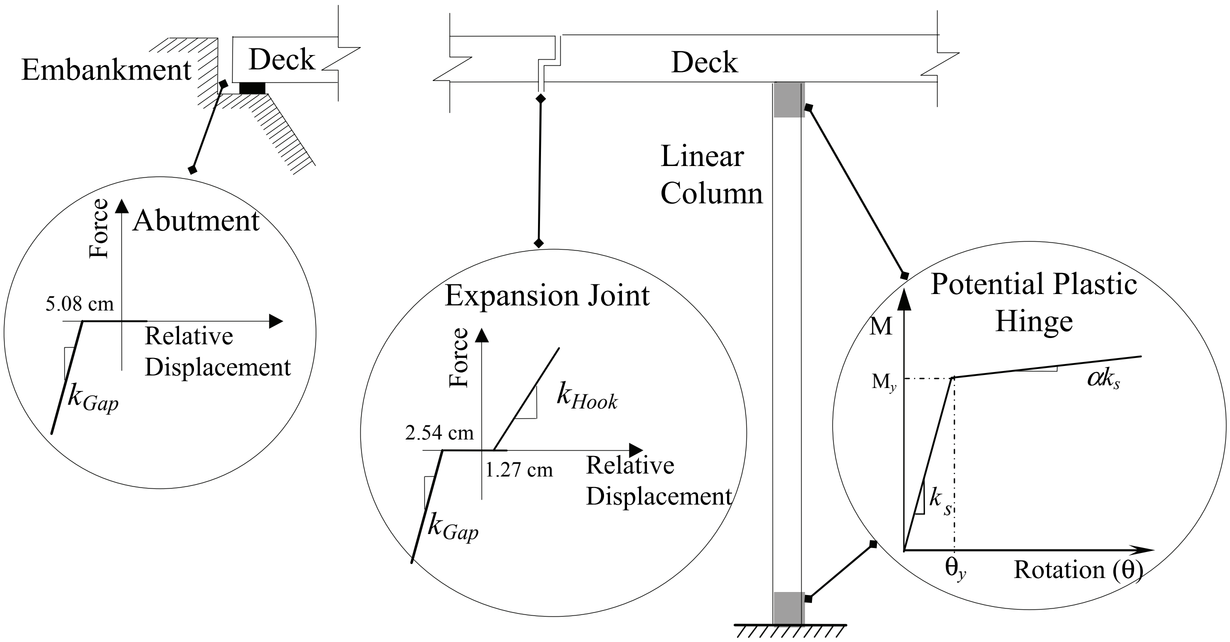

FIGURE 2-2 Nonlinearities in Bridge Model

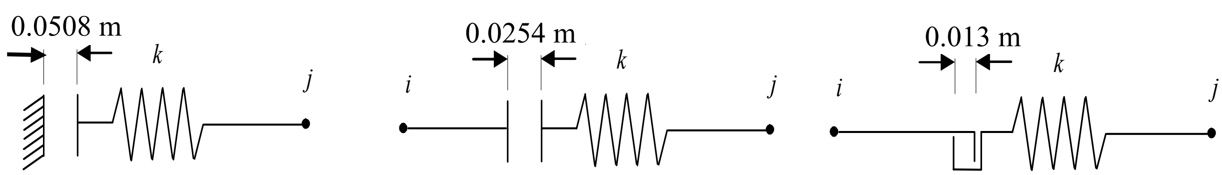

(a) Gap Element for Pounding at Abutment (b) Gap Element for Pounding at Expansion Joint (c) Hook Element for Restrainer at Expansion Joint

FIGURE 2-3 Nonlinear Modeling of Gap and Hook Elements

2.3 Retrofit of Reinforced Concrete Columns

During seismic excitation, concrete columns often lack flexural strength, flexural ductility and shear strength. One of the main causes for these structural inadequacies is lap splices in critical regions and/or premature breakdown of longitudinal reinforcement. A number of column-retrofit techniques, such as steel jacketing, wire pre-stressing and composite material jacketing, have been developed and tested. Among all these, the steel jacketing has been widely applied to bridge retrofit as the most common retrofit technique.

Chai *et al*. (1991) observed that confinement of the concrete columns could be improved by placing transverse reinforcement layers closely along the longitudinal axis that will restrain the lateral expansion of the concrete during seismic excitation. By doing this, the compression zone will be able to sustain higher compressive stresses and much higher compressive strains before failure. However, this method is applicable for new design and construction, but not for existing bridge columns.

This study focuses on the steel jacketing technique for retrofitting existing bridge columns to improve their seismic performance.

2.4 Steel Jacketing

Chai *et al*. (1991) performed an experiment to investigate the retrofit of circular columns with steel jacketing. In this experiment with circular columns, two half shells of steel plate rolled to a radius slightly larger than that of the column. These plates are site-welded along the vertical plane, and placed over the area to be retrofitted to provide a continuous tube with a small annular gap around the column. This gap is grouted with pure cement. Typically the jacket is cut to provide a space of about 0.05 m between the jacket and any supporting member. It is noted that the jacket is effective only in passive confinement and the level of confinement depends on the hoop strength and stiffness of the steel jacket.

The thickness of steel jacket is calculated from the following equation (Priestley *et al*., 1996).

$$t_j = \frac{0.18(\varepsilon_{cm} - 0.004)Df'_{cc}}{f_{yj}\varepsilon_{sm}} \tag{2-2}$$

where ε_{cm} is the strain at maximum stress in concrete, ε_{sm} the strain at maximum stress in steel jacket, D the diameter of circular column, $f_{cc}^{'}$ the compressive strength of confined concrete and f_{yj} the yield stress of steel jacket.

2.5 Compression Stress-Strain Relationships for Confined Concrete

The effect of confinement is to increase the compression strength and ultimate strain of concrete as illustrated in figure 2-4 (after Priestley *et al*., 1996). Many different stress-strain relationships have been developed for confined concrete. Most of these are applicable under certain conditions. A recent (Priestley et al., 1996) model, applicable to all cross-sectional shapes and at all levels of confinement, is used for the analysis.

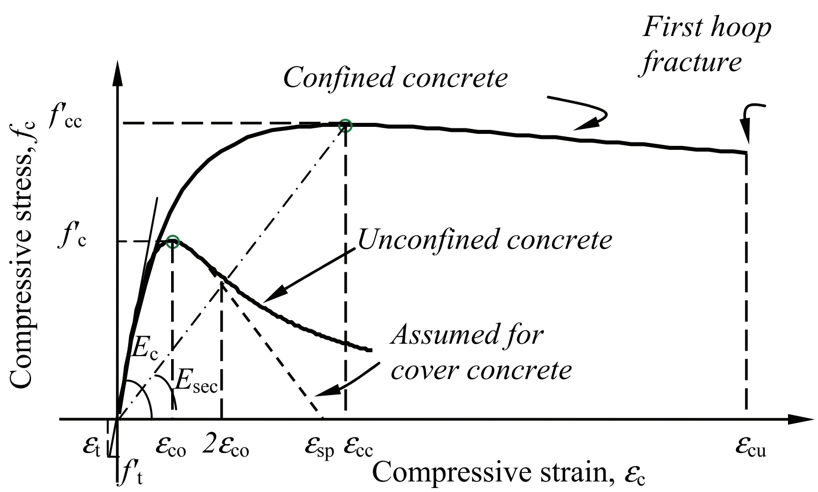

FIGURE 2-4 Stress-Strain Model for Concrete in Compression

2.6 Moment-Curvature Relationship

The moment-curvature relationship of each bridge column is obtained using the column ductility program developed by Kushiyama (2002) that follows the concept and equations given in Priestley et al. (1996). The rotational ductility demand at each column end is defined as θ / θ_y, where θ is the rotation of a bridge column in its plastic hinge region and θ_y is the corresponding yield rotation. Figure 2-5 shows the cross-section of column 1 of Bridge 1 and their bilinear hysteretic behavior before and after retrofit as obtained from the column ductility program and figure 2-6 shows the same for column 2 of Bridge 1. The moment rotation curves before and after retrofit of bridge columns of Bridge 2 to 5 in both longitudinal and transverse directions are shown in Appendix A.

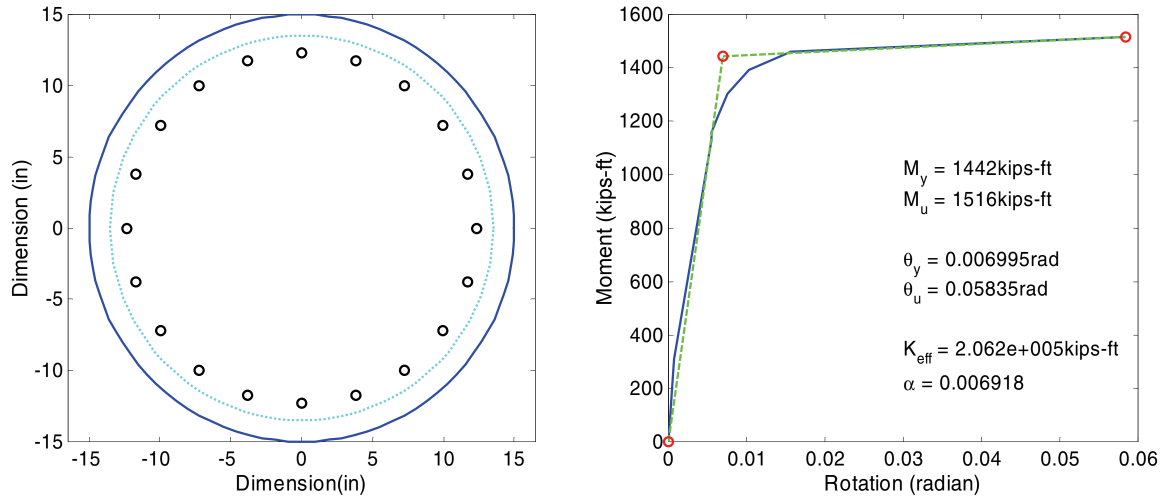

Section of Column Moment-Rotation Curve

(a) Before Retrofit

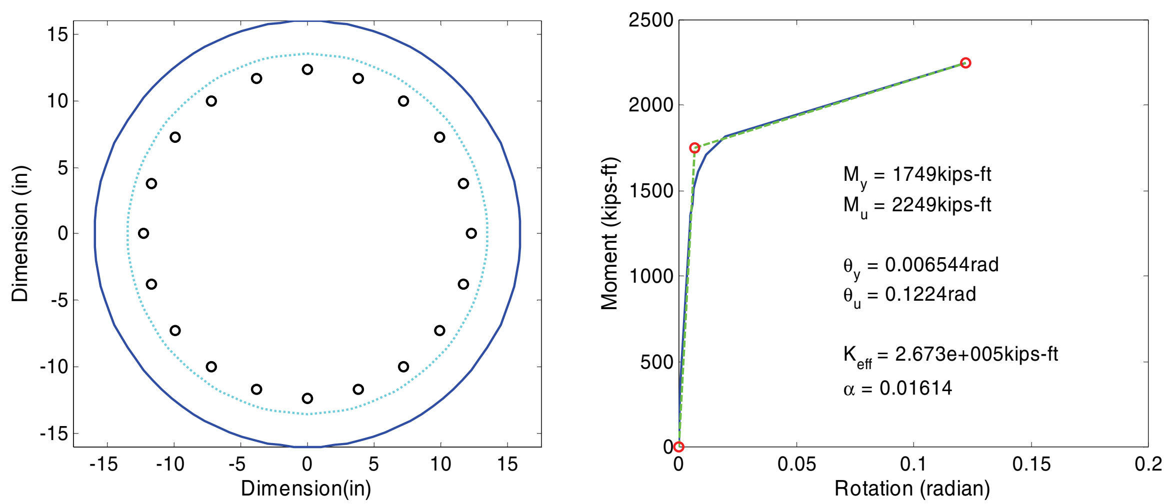

Section of Column Moment-Rotation Curve

(b) After Retrofit

FIGURE 2-5 Moment-Curvature Analysis of Column 1 of Bridge 1

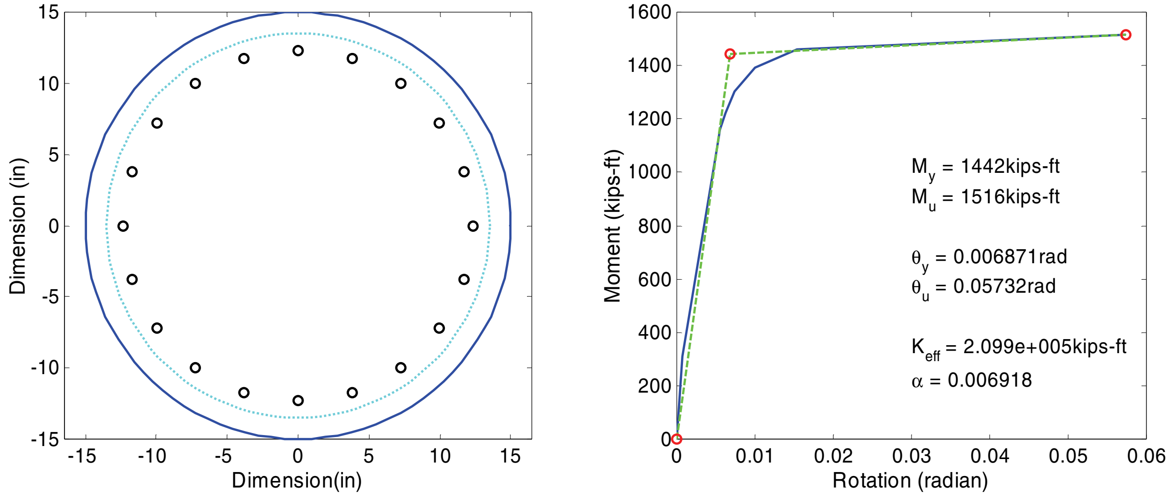

Section of Column Moment-Rotation Curve

(a) Before Retrofit

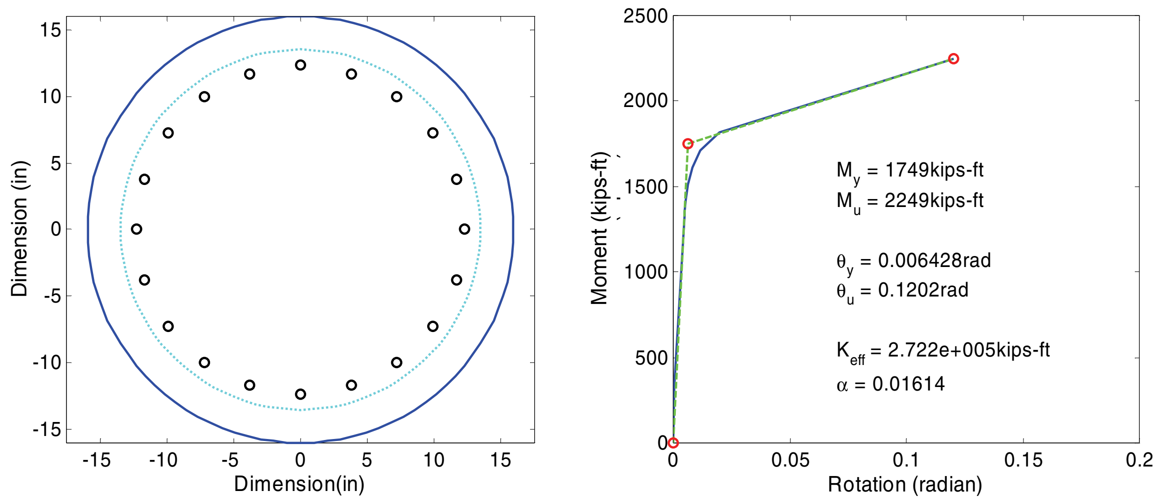

Section of Column Moment-Rotation Curve

(b) After Retrofit

FIGURE 2-6 Moment-Curvature Analysis of Column 2 of Bridge 1

SECTION 3
PROGRESSIVE FAILURE ANALYSIS OF BRIDGES

The seismic performance of bridges depends on their geometric configuration, material properties, nonlinear behavior under earthquake loading, soil condition at site as well as the characteristics of specific earthquake ground motion to which they are subjected. Earthquake ground motion, depending on its intensity and major direction of propagation at bridge site, may lead to complete collapse of bridges resulting from various failure mechanisms. Unseating of superstructure at abutments and at expansion joints due to restrainer failure and insufficient seat width, pounding between two adjacent decks at expansion joints as well as at abutments, formation of plastic hinges at all column ends are some examples of such failure mechanisms. Also, premature shear failure in bridge column may lead to collapse by preventing full utilization of rotational ductility capacities at the probable plastic hinge regions of columns. This type of shear failure is prominent in shorter and stiffer columns of a long bridge having several columns with different heights. Using *SAP2000 Nonlinear* computer code, nonlinear finite element analysis is carried out assuming bilinear hysteretic behaviors of the bridge columns and nonlinear characteristics of the expansion joints arising from pounding and restrainer failures. This analysis focuses on comparative study of different types of bridge collapse and their individual time of occurrences.

3.1 Input Ground Motions

Sixty (60) earthquake time histories in Los Angeles area (originally developed for FEMA/SAC project; http://nisee.berkeley.edu/data/strong_motion/sacsteel/ground_motions.html), listed in table 3-1, are utilized in this study. They consists of 3 sets of 20 actual earthquake records, each set are scaled linearly so as to have return periods of 2500 yrs, 475 yrs and 67 yrs that are representative of earthquakes with exceedance probabilities, respectively of 2, 10 and 50% in 50 years. Among these 60 records, three representative earthquakes one from each set, observed during 1994 Northridge earthquake (LA27; PGA: 908.70cm/sec^2), 1940 El Centro Earthquake (LA02; PGA: 662.88cm/sec^2), and 1979 Imperial Valley Earthquake (LA44; PGA:

109.45cm/sec^2), are considered to demonstrate the progressive failure modes of bridges. Horizontal acceleration time histories of these three ground motions are shown in figure 3-1.

Kim (2003) showed that assumption of identical support ground motions underestimates the peak ductility demands of the bridge columns. In this study, example bridges are analyzed under a number of scenario earthquakes. For each scenario earthquake, the bridge under consideration is analyzed using identical and differential support ground motion. The following ratio is then computed for each section of the bridge in order to quantify the effect of the spatial variation of ground motion on the response of the structure:

$$\rho = \frac{\text{max of response quantity computed using } \textit{differential} \text{ support ground motion}}{\text{max of same quantity computed using } \textit{identical} \text{ support ground motion}}$$

According to this observation, a conservative factor of 1.5 is used in the earlier research during the analysis of Bridge 2 and 5 in order to highlight the effect of spatial variation of PGA. For other bridges, it is kept as 1.0.

TABLE 3-1 Description of Los Angeles Ground Motions

10% Exceedence in 50 yr				2% Exceedence in 50 yr				50% Exceedence in 50 yr			
SAC Name	DT (sec)	Duration (sec)	PGA (cm/sec^2)	SAC Name	DT (sec)	Duration (sec)	PGA (cm/sec^2)	SAC Name	DT (sec)	Duration (sec)	PGA (cm/sec^2)
LA01	0.02	39.38	452.03	LA21	0.02	59.98	1258.00	LA41	0.01	39.38	578.34
LA02	0.02	39.38	662.88	LA22	0.02	59.98	902.75	LA42	0.01	39.38	326.81
LA03	0.01	39.38	386.04	LA23	0.01	24.99	409.95	LA43	0.01	39.08	140.67
LA04	0.01	39.38	478.65	LA24	0.01	24.99	463.76	LA44	0.01	39.08	109.45
LA05	0.01	39.38	295.69	LA25	0.005	14.945	851.62	LA45	0.02	78.60	141.49
LA06	0.01	39.38	230.08	LA26	0.005	14.945	925.29	LA46	0.02	78.60	156.02
LA07	0.02	79.98	412.98	LA27	0.02	59.98	908.70	LA47	0.02	79.98	331.22
LA08	0.02	79.98	417.49	LA28	0.02	59.98	1304.10	LA48	0.02	79.98	301.74
LA09	0.02	79.98	509.70	LA29	0.02	49.98	793.45	LA49	0.02	59.98	312.41
LA10	0.02	79.98	353.35	LA30	0.02	49.98	972.58	LA50	0.02	59.98	535.88
LA11	0.02	39.38	652.49	LA31	0.01	29.99	1271.20	LA51	0.02	43.92	765.65
LA12	0.02	39.38	950.93	LA32	0.01	29.99	1163.50	LA52	0.02	43.92	619.36
LA13	0.02	59.98	664.93	LA33	0.01	29.99	767.26	LA53	0.02	26.14	680.01
LA14	0.02	59.98	644.49	LA34	0.01	29.99	667.59	LA54	0.02	26.14	775.05
LA15	0.005	14.945	523.30	LA35	0.01	29.99	973.16	LA55	0.02	59.98	507.58
LA16	0.005	14.945	568.58	LA36	0.01	29.99	1079.30	LA56	0.02	59.98	371.66
LA17	0.02	59.98	558.43	LA37	0.02	59.98	697.84	LA57	0.02	79.46	248.14
LA18	0.02	59.98	801.44	LA38	0.02	59.98	761.31	LA58	0.02	79.46	226.54
LA19	0.02	59.98	999.43	LA39	0.02	59.98	490.58	LA59	0.02	39.98	753.70
LA20	0.02	59.98	967.61	LA40	0.02	59.98	613.28	LA60	0.02	39.98	469.07

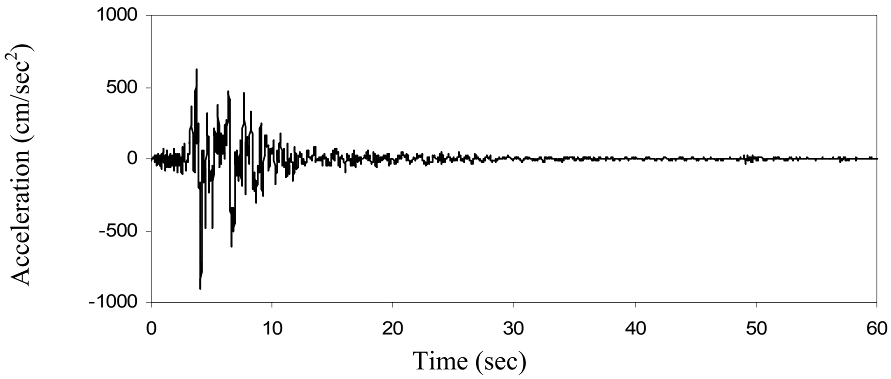

(a) Ground Motion 1
(1994 Northridge earthquake (LA27) with exceedance Probability 2% in 50 yrs)

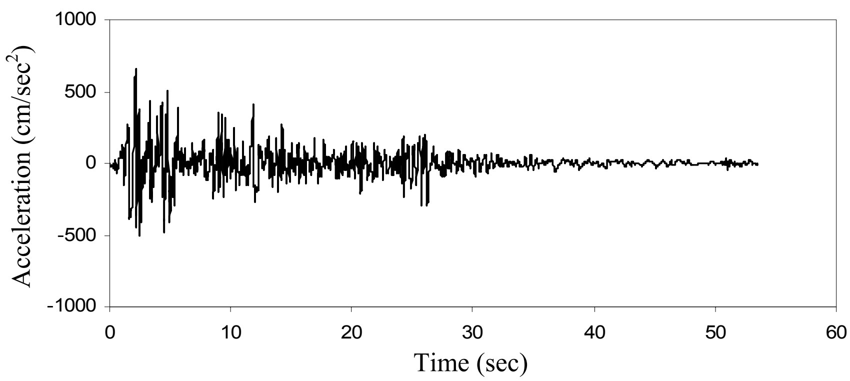

(b) Ground Motion 2
(1940 El Centro Earthquake (LA02) with exceedance Probability 10% in 50 yrs)

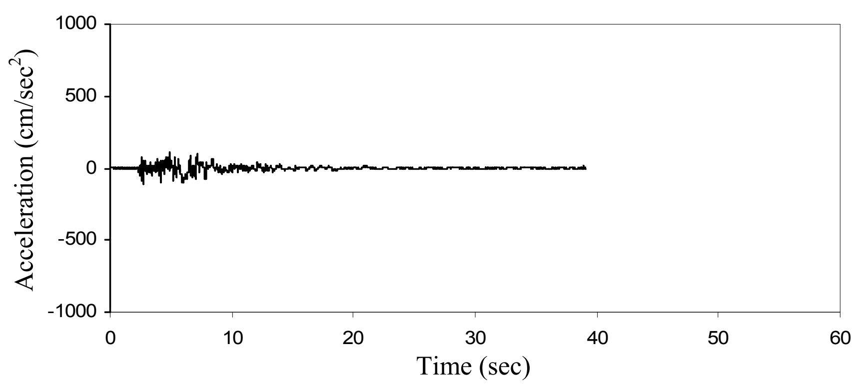

(c) Ground Motion 3
(1979 Imperial Valley Earthquake (LA44) with exceedance Probability 50% in 50 yrs)

FIGURE 3-1 Acceleration Time Histories Generated for Los Angeles

3.2 Damage States

The rotational ductility demand can be described as the ratio of rotation (θ) of the column end, modeled as nonlinear spring, to its yield rotation (θ_y). According to Dutta and Mander (1998), five different damage states namely 'Almost no', 'Minor', 'Moderate', 'Major' and 'Collapse' can be defined based on column drift which is the ratio of maximum displacement response (Δ) to the height of the column pier/bent (H) and given in table 3-2. Priestley *et al*. (1996) recommended that drift limit corresponding to yield state is 0.005. In this study, rotational ductility demands at plastic hinge regions of bridge columns are used as the signature representing the bridge damage levels. Therefore, rotational ductility demands corresponding to 'Almost no damage' (i.e., yield state with drift limit 0.005) and 'Column collapse' (i.e., ultimate state with drift limit 0.075) are, respectively of, θ_y/θ_y (=1.0) and θ_u/θ_y, which can be computed from moment-curvature relationship of bridge columns. Rotational ductility demands corresponding to other states of damage are obtained in proportional to the drift limits presented in table 3-2. Tables 3-3 and 3-4 list the ductility demands at the two ends of column of five (5) example bridges where plastic hinges are likely to form during the longitudinal and transverse movement. It should be noted that tables 3-3 and 3-4 give idea about the ductility demands only at left most columns of example bridges. Although in analysis, damage state of a particular column is determined on the basis of the seismic performance and rotational ductility of that column.

Table 3-2 Damage States and Ductility Capacities for the Bridge Columns

Damage state	Description	Drift Limits (Δ/H)
Almost no	First yield	Yield
Minor	Cracking, spalling	0.01
Moderate	Loss of anchorage	0.025
Major	Incipient column collapse	0.050
Complete	Column collapse	0.075

TABLE 3-3 Peak Ductility Demand of First Left Column of Example Bridges During the Longitudinal Motion

Damage States	Bridge 1	Bridge 2	Bridge 3	Bridge 4	Bridge 5
Almost no	1.00	1.00	1.00	1.00	1.00
Minor	1.52	1.58	1.40	1.82	2.05
Moderate	3.10	3.33	2.58	4.27	5.20
Major	5.72	6.24	4.56	8.36	10.45
Complete	8.34	9.16	6.54	12.44	15.70

TABLE 3-4 Peak Ductility Demand of First Left Column of Sample Bridges During the Transverse Motion

Damage States	Bridge 1	Bridge 2	Bridge 3	Bridge 4	Bridge 5
Almost no	1.00	1.00	1.00	1.00	1.00
Minor	1.52	1.58	1.30	1.56	1.82
Moderate	3.10	3.33	2.19	3.25	4.27
Major	5.72	6.24	3.69	6.07	8.36
Complete	8.34	9.16	5.18	8.89	12.44

3.3 Responses of Bridge 2

To demonstrate different progressive failure modes, Bridge 2 is analyzed for three ground motions indicated in figure 3-1. Responses are measured at column ends in terms of ductility demand and in the interface of adjacent bridge decks in terms of axial force in restrainer and the pounding force due to impact. Also, generated shear force in plastic hinge regions is estimated to check for premature shear failure of bridge columns. It should be noted that bridge failure due to liquefaction is not considered here. The following section elaborates different failure modes of Bridge 2.

3.3.1 Rotation at Column Ends

Figures 3-2(a) and 3-2(b) show the different damage states and variation of ductility demand with time for four column tops and bottoms respectively under ground motion 1. These figures indicate that the variation of ductility factors at all column ends is same as all columns are identical. Though this bridge has one expansion joint, but the stiffness of the hook element (restrainer) is considerably high and no out-of-phase motion is observed between right and left subsystems of the bridge separated by the joint during longitudinal excitation of the bridge. The two column ends have same nature of variation of ductility demand with time. Bridge response at plastic hinge regions under ground motion 2 and 3 are shown in figures 3-3 and 3-4.

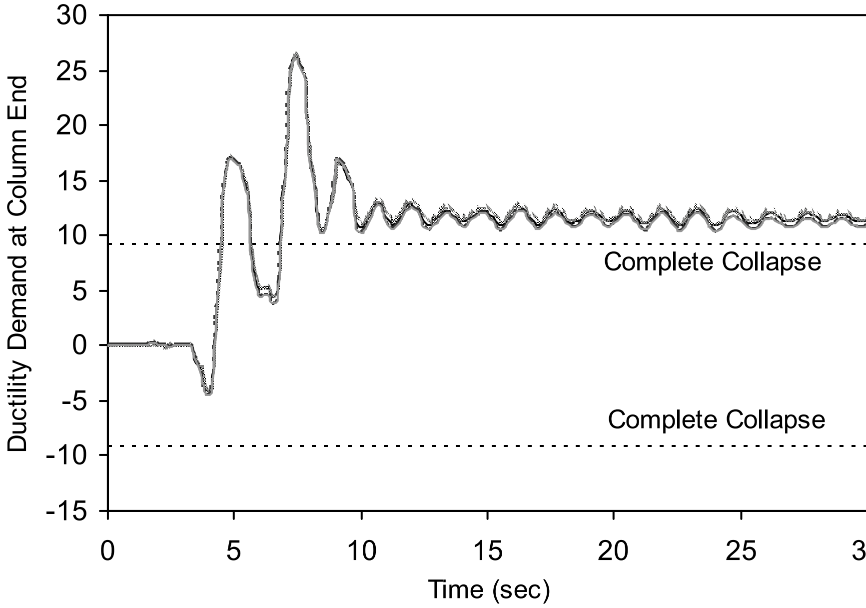

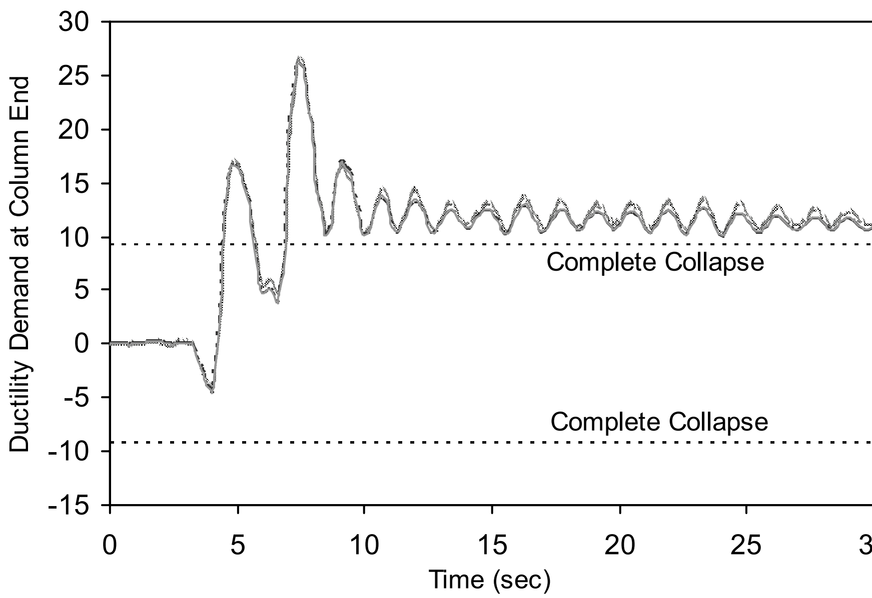

(b) All Column Bottoms

FIGURE 3-2 Ductility Demand for Ground Motion 1

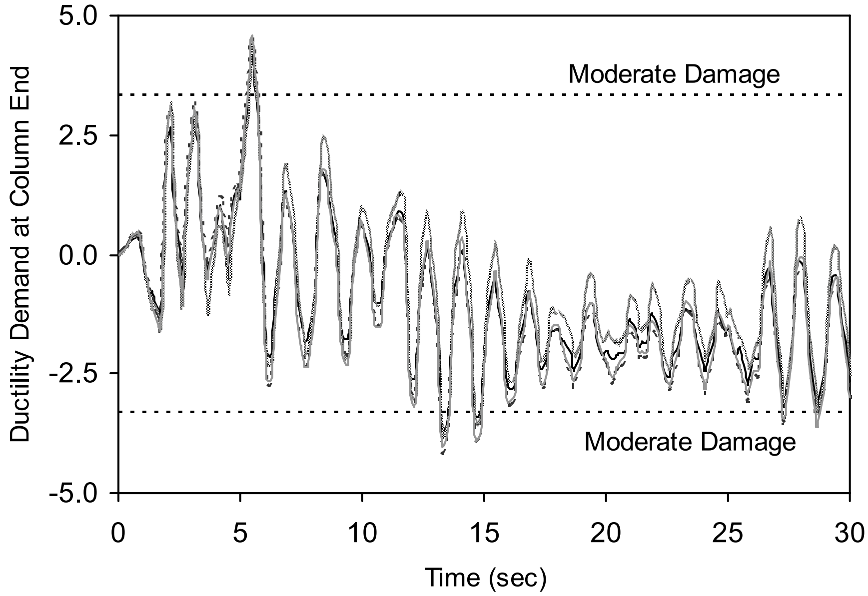

(a) All Column Tops

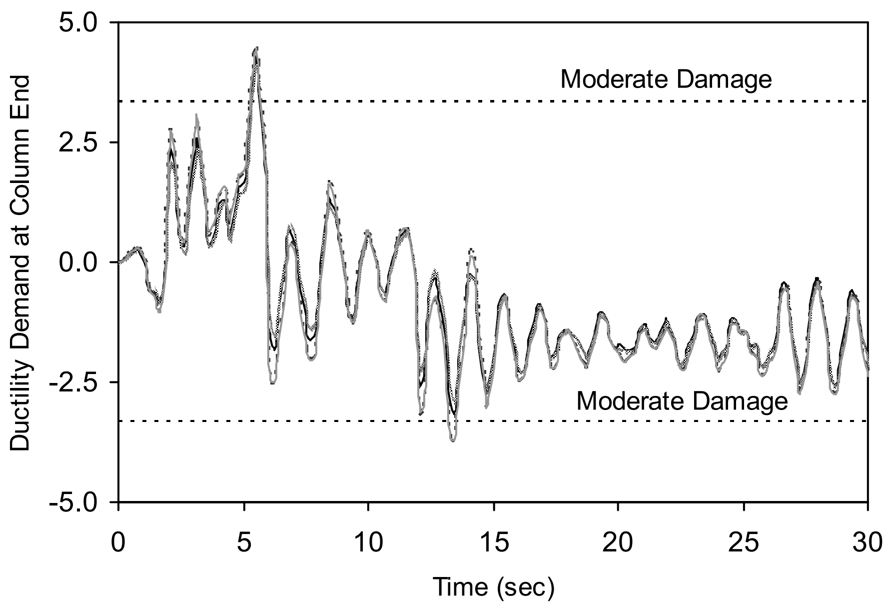

(b) All Column Bottoms

FIGURE 3-3 Ductility Demand for Ground Motion 2

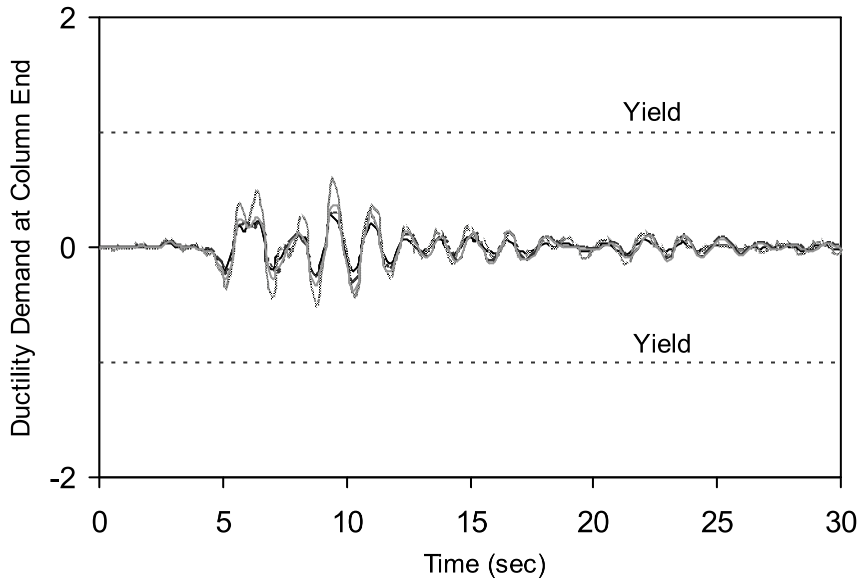

(a) All Column Tops

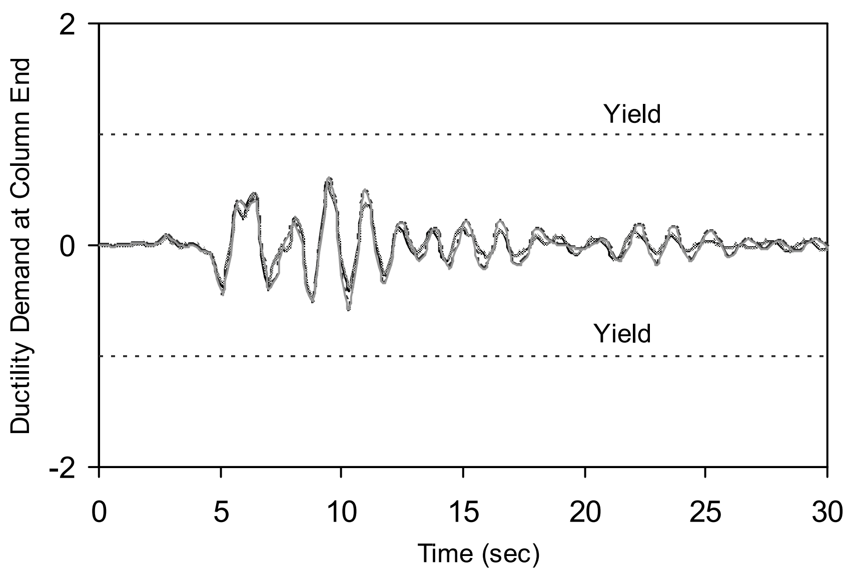

FIGURE 3-4 Ductility Demand for Ground Motion 3

3.3.2 Pounding and Restrainer Failure

For ground motion 1, the relative displacement time history at the two ends of expansion joint is plotted in figure 3-5. Impact force develops at the interface of the adjacent bridge decks when the relative displacement becomes zero exhausting the initially provided gap equal to 0.0254 m and hence causing the pounding. Figure 3-6 depicts that pounding force generates only at that time instance when relative inward movement of decks is more than the specified value. The bridge experiences a maximum of 10870 kN impact force at 15.4 sec due to ground motion 1. The outward movement between the adjacent bridge decks at the expansion joint results in the development of the axial force in restrainer as the hook element gets engaged by losing initially provided slack equal to 0.013 m. This axial force in the restrainer is transmitted to the nearby concrete block through anchors that hold the restrainer in position. Figure 3-7 shows the development of axial force in the restrainer. The anchors fail when the axial force exceeds the anchor design capacity and this failure is assumed conservatively to lead to the collapse of bridge. Depending on the design, however, the restrainer itself fails before anchorage fails. This also is assumed to result in the bridge collapse.

For other two ground motions, the relative displacement at the expansion joint and axial force in the restrainer are shown in figures 3-8 ~ 3-11.

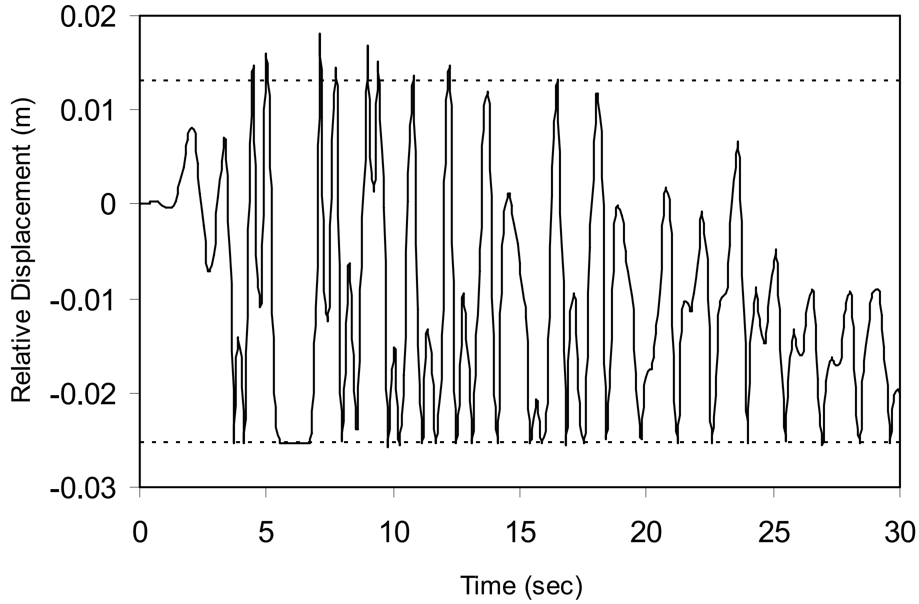

FIGURE 3-5 Relative Displacement at Expansion Joint for Ground Motion 1

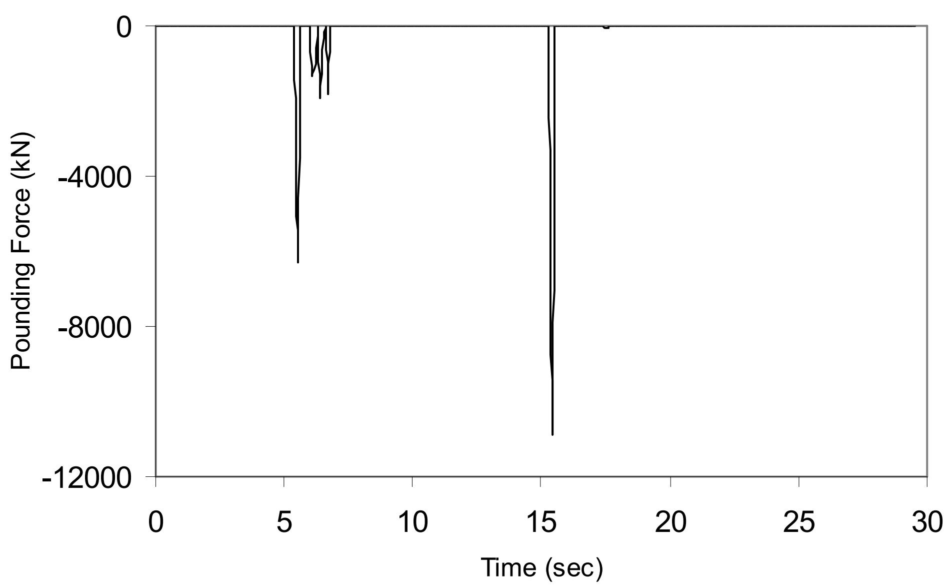

FIGURE 3-6 Pounding Force Developed at Expansion Joint for Ground Motion 1

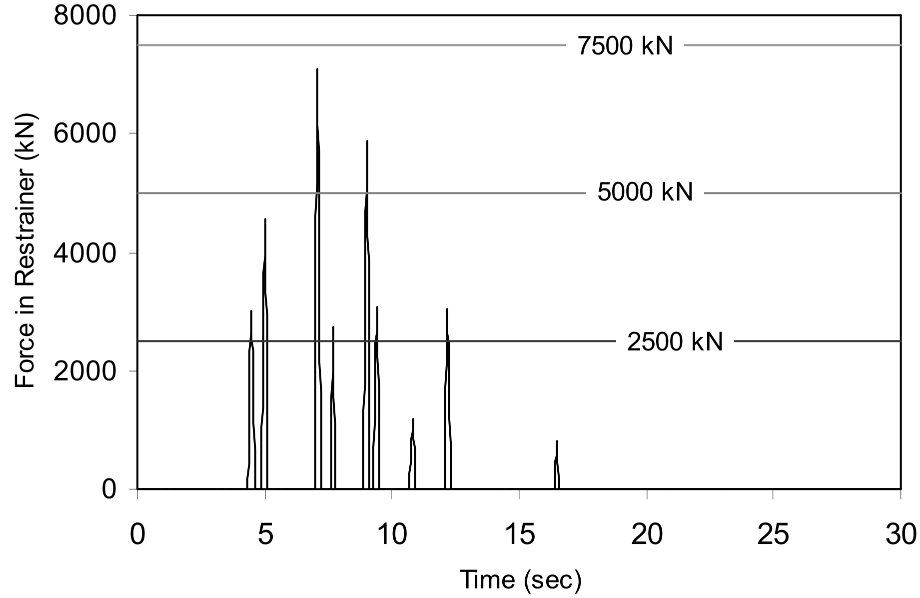

FIGURE 3-7 Axial Force in Restrainer for Ground Motion 1

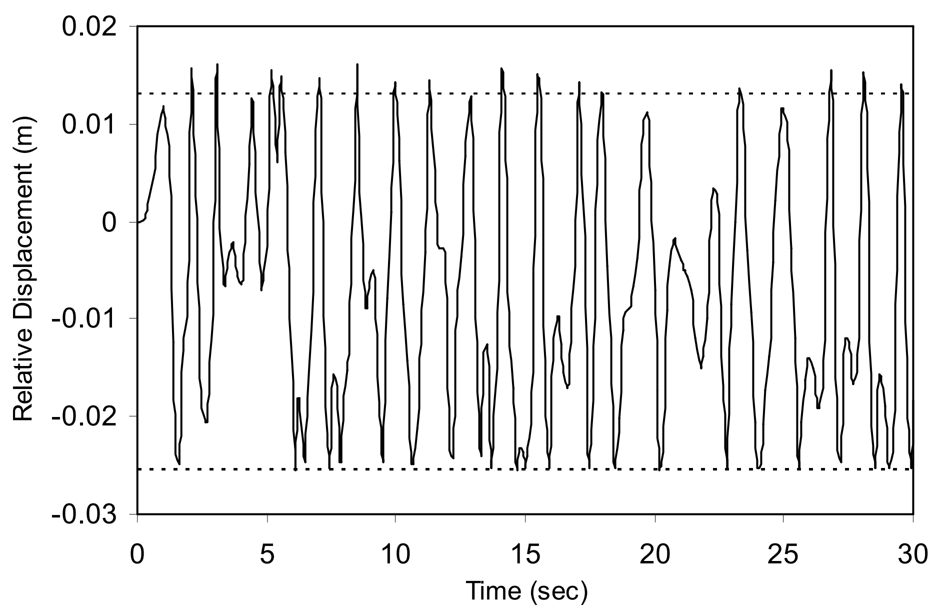

FIGURE 3-8 Relative Displacement at Expansion Joint for Ground Motion 2

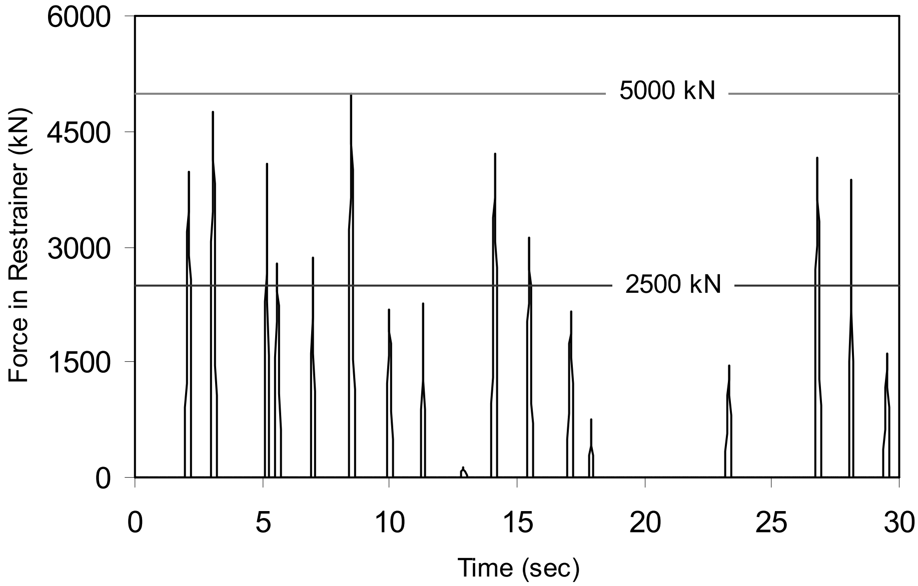

FIGURE 3-9 Axial Force in Restrainer for Ground Motion 2

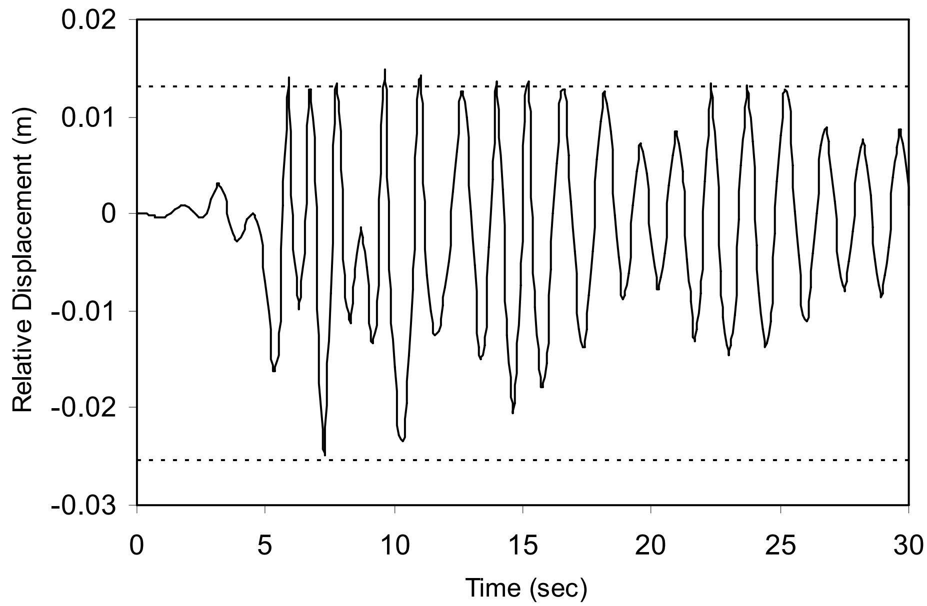

FIGURE 3-10 Relative Displacement at Expansion Joint for Ground Motion 3

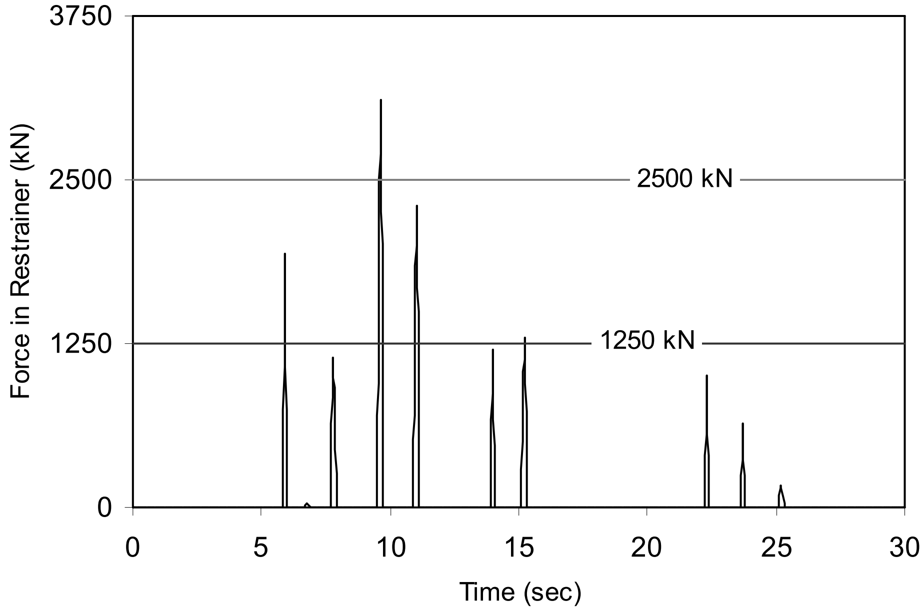

FIGURE 3-11 Axial Force in Restrainer for Ground Motion 3

3.3.3 Premature Shear Failure

Development of shear force in the region of plastic hinges of column may lead to premature shear failure preventing flexural ductility capacity at those regions from full utilization. Priestley et al. (1996) focused on this issue and prescribed the analytical estimation of shear capacity in the plastic hinge regions in relation to the curvature ductility factor at those regions. They expressed the nominal shear capacity of concrete, $V_c = k\left(\sqrt{f_c^{'}}\right)A_e$ where A_e is 0.8 times the gross area of column, f_c' is the compressive strength of unconfined concrete, and k is presented graphically as a function of curvature ductility factor μ_ϕ. Outside the plastic hinge regions, value of k for $\mu_\phi = 1$ is suggested. To check the possibility of having a premature shear failure, shear strength (capacity) of column is compared with the generated shear force due to seismic excitation. This generated shear force at plastic hinge regions can be obtained directly from the flexural strength developed in these locations. Therefore, for the purpose of comparison the flexural moment-curvature relationship is expressed in terms of equivalent shear force-curvature relationships (shear demand). Following this procedure, the shear capacity and equivalent shear force (i.e. demand) at the plastic hinge regions of Bridge 2 are estimated and presented in figures 3-12 and 3-13 respectively.

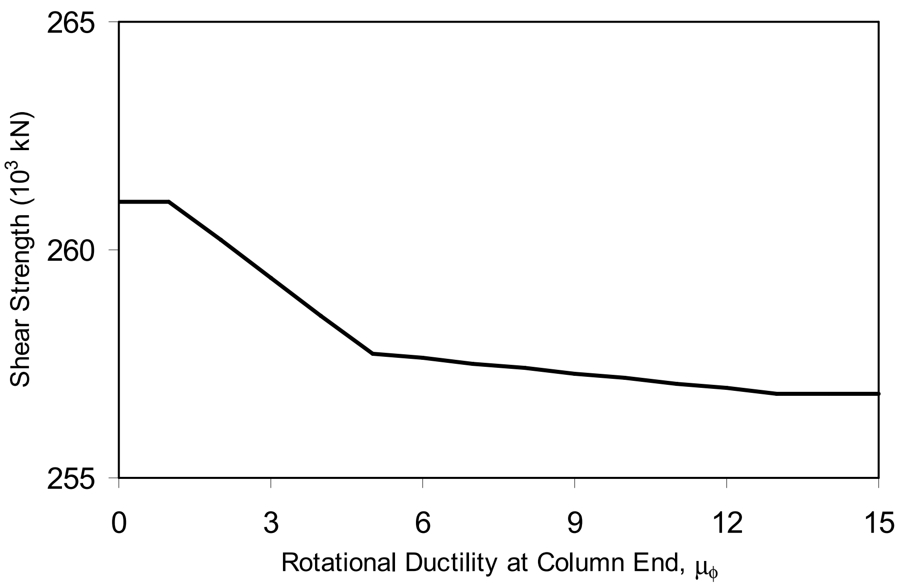

FIGURE 3-12 Shear Strength Envelope: Shear Strength in Column at Plastic Hinge Locations

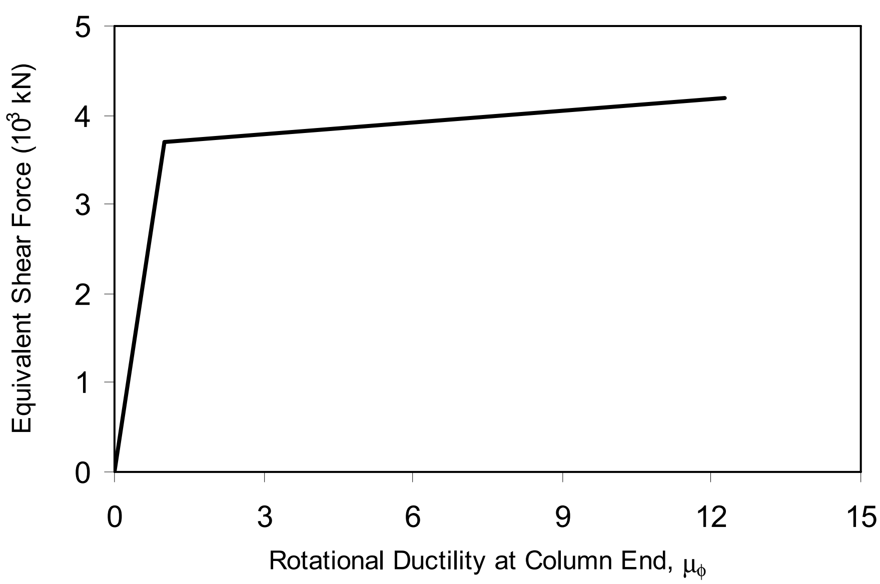

FIGURE 3-13 Equivalent Shear Force-Curvature Relation from Moment-Curvature Relation

3.4 Modes of Progressive Failure

The progressive failure modes of the bridge under these three ground motions are summarized in the following sub-sections.

3.4.1 Ground Motion 1

All of these failure mechanisms can lead to the collapse of the bridge in such a way that mechanism which has the shortest time to occurrence controls failure. Figures 3-2(b), 3-6 and 3-7 highlight three failure mechanisms described above under ground motion 1. Governing failure mechanism changes with different capacities of the restrainer. For example, if the restrainer is assigned to a design capacity of 2500 kN or less, bridge collapses due to the restrainer or anchorage failure while for restrainer capacity of 5000 kN or more, plastic hinges are formed at the four column ends simultaneously at 4.5 sec, which results in the complete 'collapse' of the bridge. Whereas the compressive stress (F/A where F is the impact force and A is the contact area of bridge deck) develops due to the face-to-face impact of the adjacent bridge decks during pounding. This stress, however, is much less than the compressive strength of concrete, and therefore, does not contribute to failure. However, localized damage can be attributed to the generation of a significantly high stress field resulted from local contact (not uniform face-to-face contact) of the adjacent decks.

3.4.2 Ground Motion 2

Bridge response at plastic hinge regions under ground motion 2 (as shown in figure 3-3) clearly indicates that the rotation of bridge columns produces 'moderate damage' to the bridge but does not lead to 'collapse'. Pounding at the interface of the adjacent decks does not develop at all, as nowhere the inward relative movement exceeds 0.0254 m (figure 3-8). For this ground motion, bridge fails in 'collapse' only when either restrainer or anchor fails i.e. restrainer failure occurs. Figure 3-9 depicts the tensile force developed in the restrainer. Failure occurs at 2.1 sec if restrainer capacity is less than 2500 kN or at 8.5 sec if capacity is less than 5000 kN.

3.4.3 Ground Motion 3

As this is the least intensive among three considered ground motions, the sample bridge has a lesser level of response than other two cases. The rotations of the columns are within elastic range (as shown in figure 3-4) and therefore no damage occurs at these locations. As it is depicted in figure 3-11, bridge collapses only when the developed tension in the restrainer exceeds its limit. As an example, 'collapse' due to the restrainer failure occurs at 5.9 sec if the restrainer capacity is less than 1250 kN.

3.4.4 Failure in Premature Shear

Comparison of figures 3-12 and 3-13 indicate the developed shear force (figure 3-13) is well below than the resistant capacity (figure 3-12) of the bridge columns at plastic hinge regions. Hence, no premature shear failure of the bridge column occurs in the current analysis.

SECTION 4
DEVELOPMENT OF FRAGILITY CURVES

4.1 Fragility Analysis of Bridges

It is well accepted that the fragility curves can be expressed in the form of two-parameter lognormal distribution functions, and the estimation of the two parameters (median and log-standard deviation) is performed with the aid of the maximum likelihood method. A common log-standard deviation, which forces the fragility curves not to intersect, can also be estimated. The following likelihood formulation described by Shinozuka et al. (2000) and (2003a) is introduced for the purpose of this method.

Although this method can be used for any number of damage states, for the ease of demonstration of analytical procedure it is assumed in this study that there are five states of damage including the state of (almost) no damage. A family of four (4) fragility curves exists in this case where events E_1, E_2, E_3, E_4 and E_5, respectively, indicate the state of (almost) no, (at least) slight, (at least) moderate, (at least) extensive damage and complete collapse. $P_{ik} = P(a_i, E_k)$ in turn indicates the probability that a bridge selected randomly from the sample will be in the damage state E_k when subjected to ground motion intensity expressed by PGA = a_i. All fragility curves are then represented

$$F_j\left(a_j; c_j, \zeta_j\right) = \Phi\left[\frac{\ln\left(a_i / c_j\right)}{\zeta_j}\right] \tag{4-1}$$

where $\Phi(*)$ is the standard-normal distribution function, c_j and ζ_j are the median and log-standard deviation of the fragility curves for the damage state of "(at least) minor", "(at least) moderate", "(at least) major" and "complete" identified by j = 1, 2, 3 and 4. From this definition of fragility curves, and under the assumption that the log-standard deviation is equal to ζ common to all the fragility curves, one obtains;

$$P_{i1} = P\left(a_i, E_1\right) = 1 - F_1\left(a_i; c_1, \zeta\right) \tag{4-2}$$

$$P_{i2} = P(a_i, E_2) = F_1(a_i; c_1, \zeta) - F_2(a_i; c_2, \zeta) \tag{4-3}$$

$$P_{i3} = P(a_i, E_3) = F_2(a_i; c_2, \zeta) - F_3(a_i; c_3, \zeta) \tag{4-4}$$

$$P_{i4} = P(a_i, E_4) = F_3(a_i; c_3, \zeta) - F_4(a_i; c_4, \zeta) \tag{4-5}$$

$$P_{i5} = P(a_i, E_5) = F_4(a_i; c_4, \zeta) \tag{4-6}$$

The likelihood function can then be introduced as

$$L(c_1, c_2, c_3, c_4, \zeta) = \prod_{i=1}^{n} \prod_{k=1}^{5} P_k(a_i; E_k)^{x_{ik}} \tag{4-7}$$

where x_i represents realizations of the Bernoulli random variable X_i and x_i =1 or 0 depending on whether or not the bridge sustains the state of damage under PGA = a_i. The maximum likelihood estimates c_{0j} for c_j and ζ_0 for ζ are obtained by solving the following equations,

$$\frac{\partial \ln L(c_1, c_2, c_3, c_4, \zeta)}{\partial c_j} = \frac{\partial \ln L(c_1, c_2, c_3, c_4, \zeta)}{\partial \zeta} = 0 \qquad (j = 1,2,3,4) \tag{4-8}$$

by implementing a straightforward optimization algorithm.

There is a question whether PGA or PGV (peak ground velocity) or, other indices are better measure of ground motion intensity for fragility curve development. Actually Shinozuka et al. (2003a) compared various indices (PGA, PGV, SA, SV and SI) and concluded that none is exclusively superior over others in their definition of utility of fragility curve. Their definition for the utility is such that the fragility curve is more useful when the curve more sharply divides the sample population into two groups, ideally in the form of a unit step function. Note that a lognormal distribution function can approach to a unit step function in the limit as $\zeta \to 0$ with the jump occurring at the value of median c.

4.2 Analytical Fragility Curves in Longitudinal Direction

To construct analytical fragility curves of the example bridges, bridge models (described in Section 2) are analyzed under sixty (60) ground motion time histories (given in Section 3). According to the damage states definition given by Dutta and Mander (1998), ductility demands at each damage states are calculated. Progressive failure analysis of Bridge 2 in time domain showed that formation of the plastic hinge at column ends is the most probable failure mode, and is followed by failure at the expansion joint. Restrainer failure depends on the capacity of restraining cables, therefore not likely to occur in reality. On this basis, only bridge response at column ends is considered for fragility analysis of bridges. Readers are referred to Shinozuka et al. (2003a) for detail procedure about the fragility curve development.

In order to assess the individual and combined effects of various factors (such as, pounding and restrainer at expansion joint, soil effect at the column bases) and retrofitting of columns on seismic performance of bridge, fragility analysis is performed and discussed in the later part of this section.

It should be noted that in this report, bilinear model of moment-rotation curve is considered. However, to compute the effect of stiffness and strength degradation of moment-rotation relation on fragility characteristics of bridges, one example bridge is analyzed for different models of moment-curvature relation and documented in Appendix B. From this exercise, little difference in girder displacement and column rotation is observed when bridge deformation is in moderate range (i.e., at low to moderate performance level of the bridge). Only when column rotation is very close to its ultimate point, the degradation model develops somewhat larger deformation (typically 8% more) than the bilinear model.

All analytical fragility curves reported here are developed for 60 ground motions. In this regard, another research (Zhou 2006) showed that variations in median values are within 15% for minor, moderate and major damage states when a sample of size 64 is used. Additionally, hypothesis testing is performed to check the goodness of fit. This indicates that analytical fragility curves developed using 60 samples are accepted with a 10% significance level.

4.2.1 Fragility Analysis Considering No Abutment Stiffness in Longitudinal Direction

Bridges are analyzed considering no resistance from embankment soil at abutment locations such that superstructure can move freely in longitudinal direction. Numbers of damaged bridges in each damage state and fragility parameters are tabulated in tables 4-1 ~ 4-5 while figures 4-1 to 4-5 show the analytical fragility curves of Bridge 1 to 5 respectively.

TABLE 4-1 Number of Damaged Bridges and Fragility Parameters of Bridge 1

Damage States	Damaged Bridges (Sample Size 60)	Fragility Parameters	
		$c(g)$	ζ
Almost No Damage	56	0.1806	0.781
Minor Damage	50	0.2306	
Moderate Damage	38	0.4490	
Major Damage	27	0.6398	
Collapse	17	0.8306	

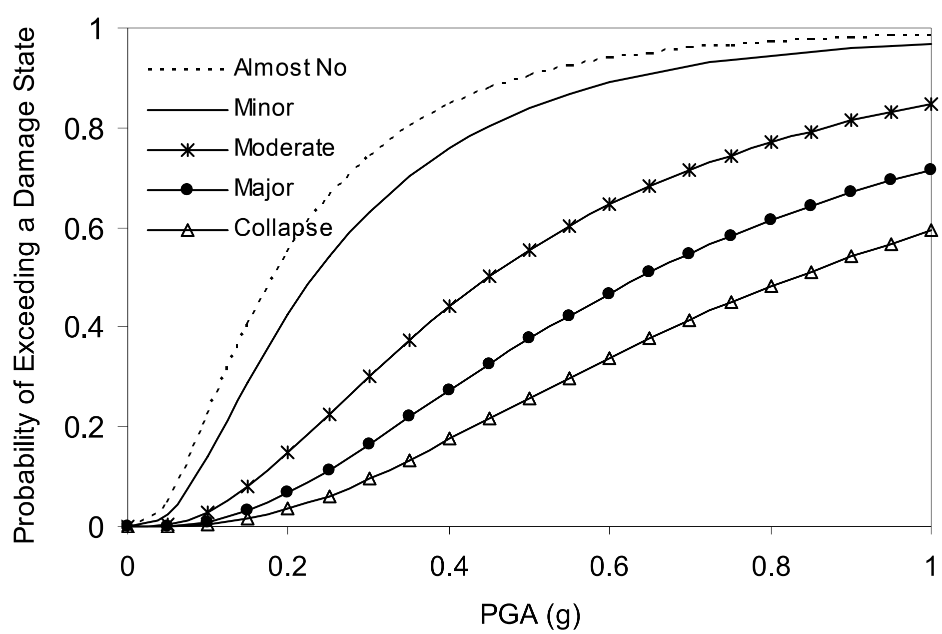

FIGURE 4-1 Fragility Curves of Bridge 1 for Five Damage States

TABLE 4-2 Number of Damaged Bridges and Fragility Parameters of Bridge 2

Damage States	Damaged Bridges (Sample Size 60)	Fragility Parameters	
		$c(g)$	ζ
Almost No Damage	50	0.1959	0.931
Minor Damage	41	0.4020	
Moderate Damage	31	0.5550	
Major Damage	17	0.8410	
Collapse	9	1.8353	

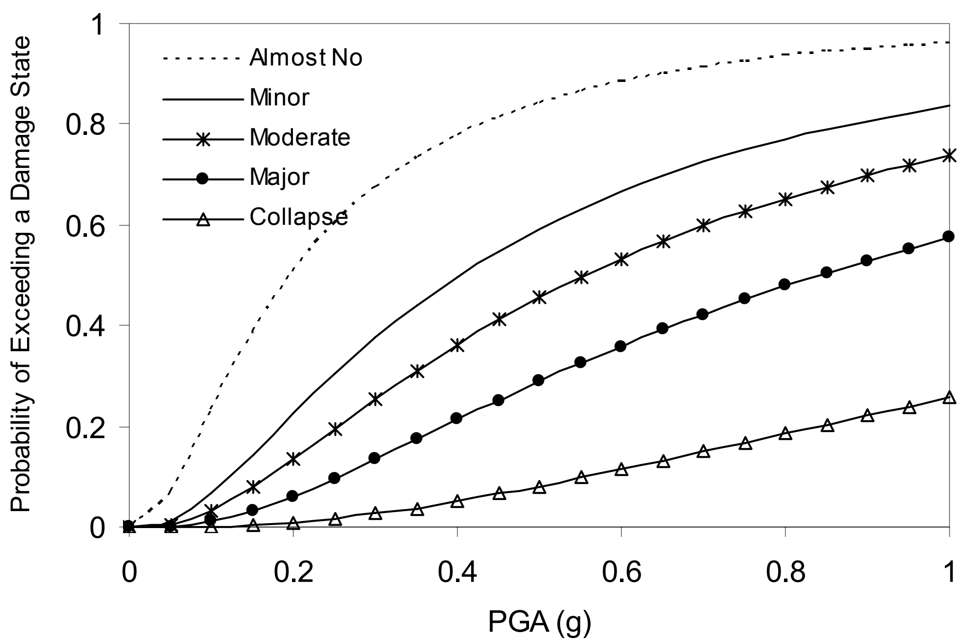

FIGURE 4-2 Fragility Curves of Bridge 2 for Five Damage States

TABLE 4-3 Number of Damaged Bridges and Fragility Parameters of Bridge 3

Damage States	Damaged Bridges (Sample Size 60)	Fragility Parameters	
		$c(g)$	ζ
Almost No Damage	58	0.1041	0.825
Minor Damage	55	0.1490	
Moderate Damage	47	0.2847	
Major Damage	39	0.4306	
Collapse	36	0.4745	

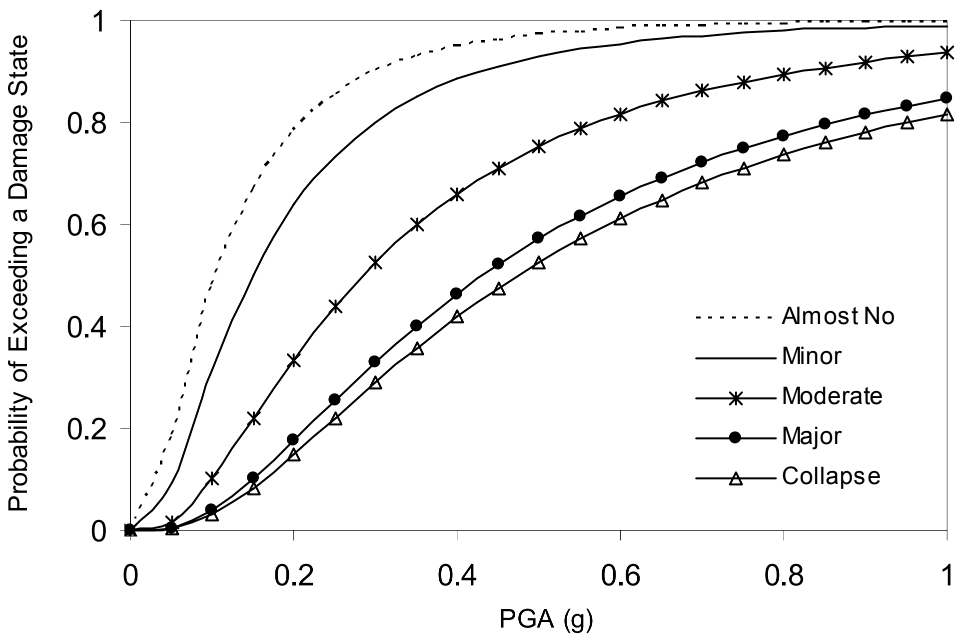

FIGURE 4-3 Fragility Curves of Bridge 3 for Five Damage States

TABLE 4-4 Number of Damaged Bridges and Fragility Parameters of Bridge 4

Damage States	Damaged Bridges (Sample Size 60)	Fragility Parameters	
		$c(g)$	ζ
Almost No Damage	57	0.1316	0.867
Minor Damage	50	0.2163	
Moderate Damage	37	0.4492	
Major Damage	27	0.6357	
Collapse	22	0.7265	

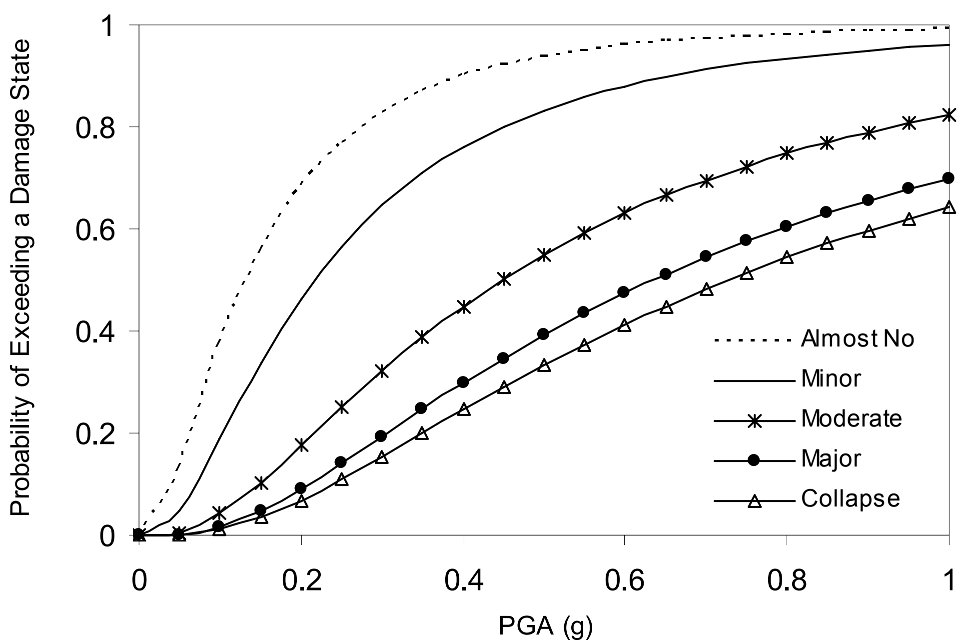

FIGURE 4-4 Fragility Curves of Bridge 4 for Five Damage States

TABLE 4-5 Number of Damaged Bridges and Fragility Parameters of Bridge 5

Damage States	Damaged Bridges (Sample Size 60)	Fragility Parameters	
		$c(g)$	ζ
Almost No Damage	57	0.1255	0.814
Minor Damage	51	0.2908	
Moderate Damage	37	0.4714	
Major Damage	21	0.7439	
Collapse	13	0.9092	

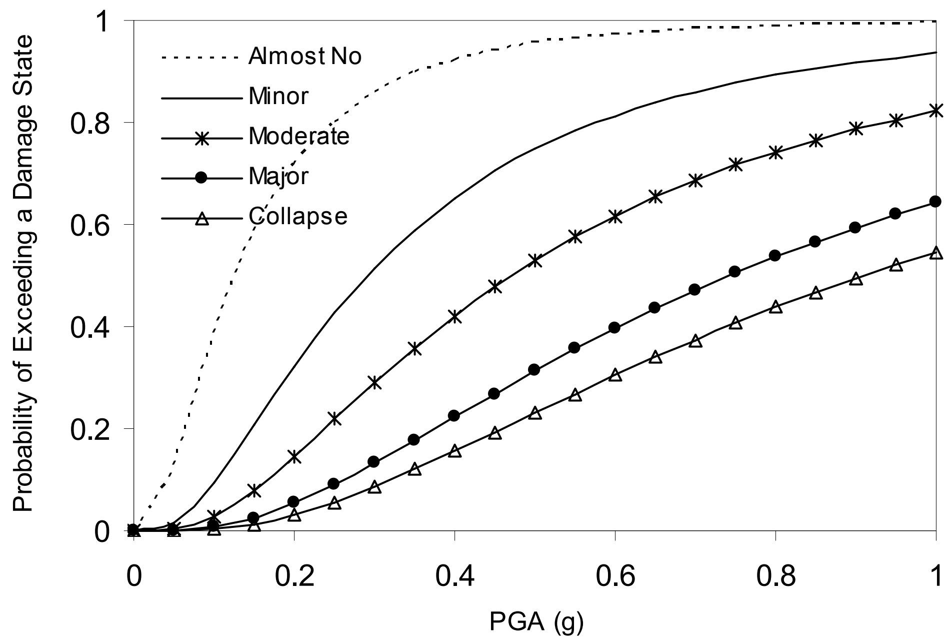

FIGURE 4-5 Fragility Curves of Bridge 5 for Five Damage States

4.2.2 Fragility Analysis Considering Abutment Stiffness in Longitudinal Direction

Bridge 2 is analyzed considering the resistance from embankment soil due to passive earth pressure at abutment locations. The abutment stiffness is computed as described in (2-1). The connection between bridge deck and abutment is modeled as a gap element which is active only in compression. An initial gap of 0.0508 m (2 in) is provided in the gap element (figure 2-3(a)). Axial force develops due to pounding when the bridge deck strikes the abutment by loosing initially provided gap. Numbers of damaged bridges in each damage state and fragility parameters are tabulated in table 4-6 and the analytical fragility curves are shown in figure 4-6.

TABLE 4-6 Number of Damaged Bridges and Fragility Parameters of Bridge 2 Considering Abutment Stiffness

Damage States	Damaged Bridges (Sample Size 60)	Fragility Parameters	
		$c(g)$	ζ
Almost No Damage	51	0.245	0.932
Minor Damage	45	0.365	
Moderate Damage	27	0.638	
Major Damage	9	1.060	
Collapse	2	1.610	

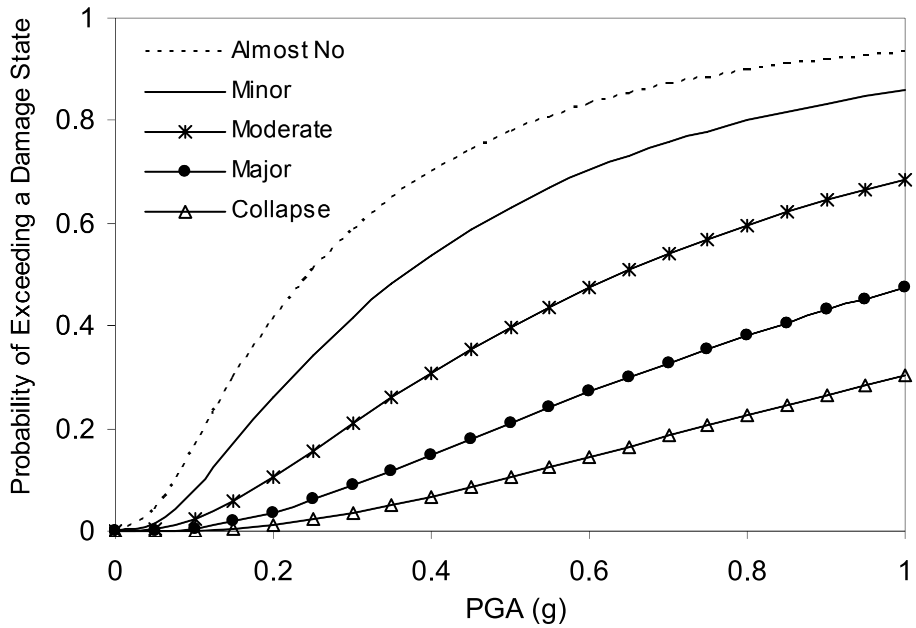

FIGURE 4-6 Fragility Curves of Bridge 2 for Five Damage States Considering Abutment Stiffness

4.2.3 Effect of Abutment Stiffness on Fragility Curves in Longitudinal Direction

Comparison of figures 4-6 and 4-2 shows that there is no significant improvement of the fragility characteristics of Bridge 2 if the abutment stiffness in longitudinal direction is considered. Though it is very difficult to draw any conclusion depending on one sample test result, but the comparison procedure is general and applicable for all other bridges.

4.3 Pounding and Soil Effect on Fragility Curves

Kim and Shinozuka (2003) carried out a finite element analysis on impact phenomena as well as effects of seismically induced pounding at expansion joints of typical California bridges. They found that impact due to pounding affects the acceleration and velocity response, but does not contribute much to displacement response depending on the size of the impulse, and the rotations of the column ends are sensitive to the time duration of impact. Although pounding effect is found to have negligible effect on the ductility demand, a need is felt to quantify the effect of pounding at the expansion joints by developing fragility curves of highway bridges, particularly for multi-span long bridges with expansion joints.

In order to investigate the effect of pounding, bridges are analyzed with and without pounding under sixty time histories indicated earlier. Also to see the effect of soil-structure interaction, analysis is done considering the soil effect (introducing linear springs at column bottoms) and without considering soil effect (fixed condition at column bottoms). The fragility curves for the four (4) sample bridges (Bridge 2 to 4) associated with the states of damage mentioned in the previous section are plotted as a function of peak ground acceleration in figures 4-7, 4-8, 4-9 and 4-10, while the percent changes in median values of fragility curves are listed in tables 4-7, 4-8, 4-9 and 4-10, respectively considering CASE 1 as a standard case. Each figure has four (4) curves for the following four (4) cases: CASE 1: without pounding effects and without soil effects; CASE 2: with pounding effects and without soil effects; CASE 3: without pounding effects and with soil effects; CASE 4: with pounding effects and with soil effects. For the purpose of comparing the fragility curves from above four cases, these are plotted in one figure for each damage state. It is noted that the log-standard deviation in each of figures 4-7, 4-8, 4-9 and 4-10 is obtained such that no two fragility curves will intersect each other.

This shows a mixed result in such a way that the pounding and/or soil effects are beneficial for some damage states, while it appears detrimental for other cases. Even at a certain state of damage of all bridges, it is very difficult to mention any common trend for the effect of pounding and/soil.

TABLE 4-7 Percent Change in Median Values of Fragility Curves

Damage States	Case1	Case2	Case3	Case4
Almost No	0.0	3.6	3.6	10.7
Slight	0.0	-17.3	17.3	3.8
Moderate	0.0	5.7	10.0	0.0
Extensive	0.0	0.0	-3.9	5.9
Complete	0.0	0.0	11.5	11.5

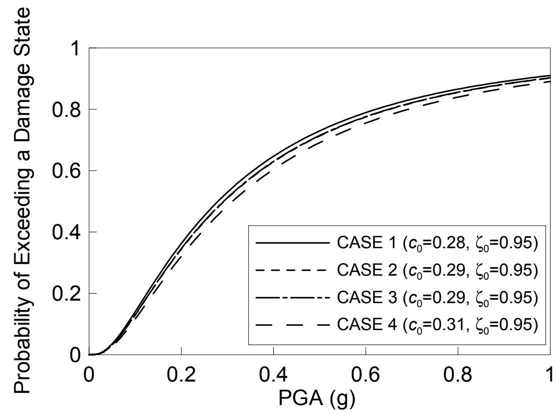

(a) Almost No Damage

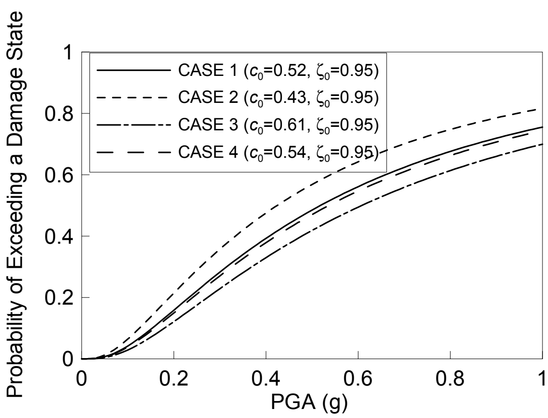

(b) Slight Damage

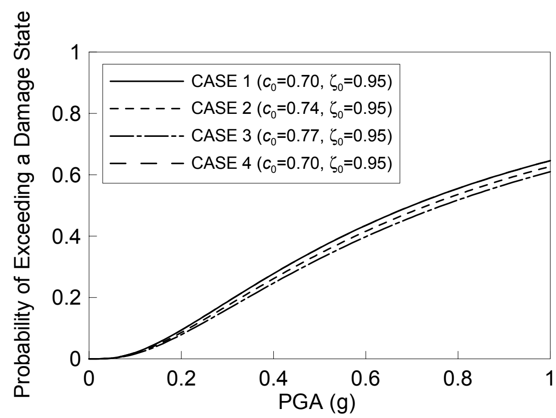

(c) Moderate Damage

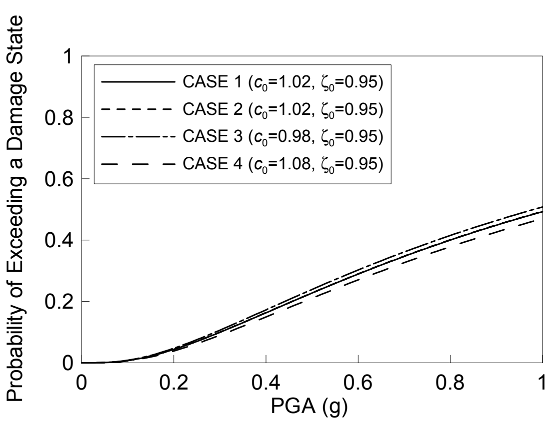

(d) Extensive Damage

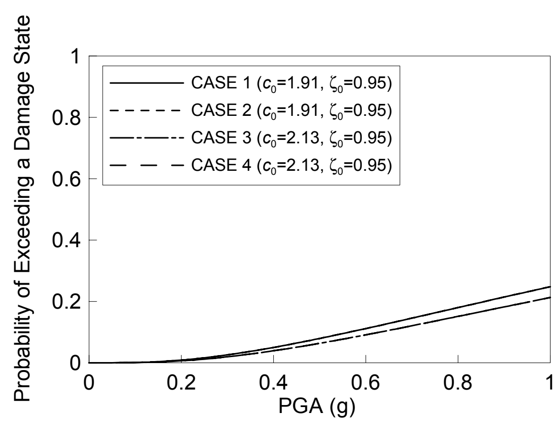

(e) Complete Collapse

FIGURE 4-7 Fragility Curves of Bridge 2

TABLE 4-8 Percent Change in Median Values of Fragility Curves

Damage States	Case1	Case2	Case3	Case4
Almost No	0.0	0.0	0.0	83.3
Slight	0.0	11.8	41.2	82.3
Moderate	0.0	-2.9	17.6	17.6
Extensive	0.0	-13.0	4.3	-2.2
Complete	0.0	-6.1	4.5	0.0

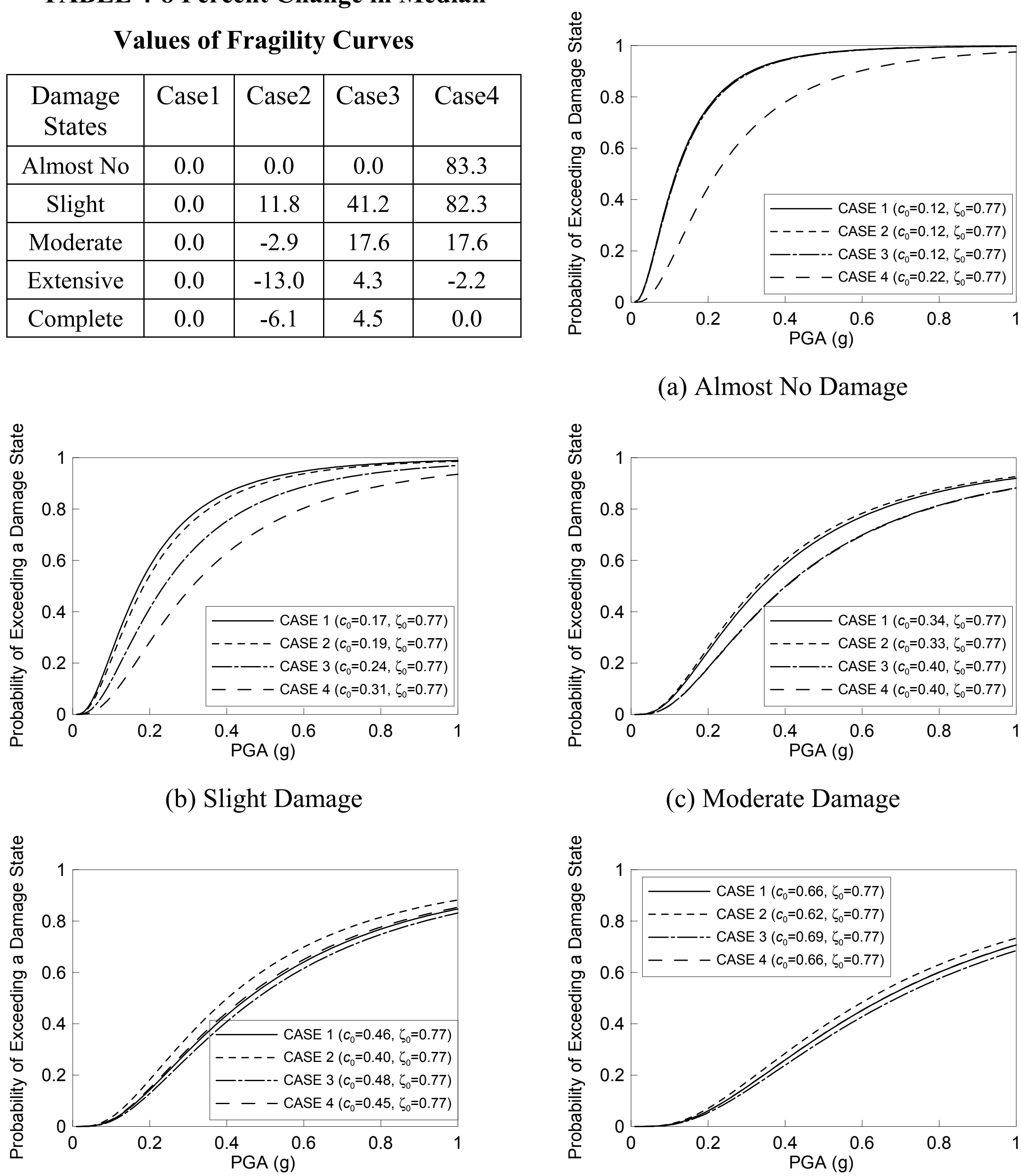

(a) Almost No Damage

(b) Slight Damage

(c) Moderate Damage

(d) Extensive Damage

(e) Complete Collapse

FIGURE 4-8 Fragility Curves of Bridge 3

TABLE 4-9 Percent Change in Median Values of Fragility Curves

Damage States	Case1	Case2	Case3	Case4
Almost No	0.0	-55.6	16.7	-72.2
Slight	0.0	-24.0	20.0	-4.0
Moderate	0.0	-32.7	10.2	-14.3
Extensive	0.0	-27.5	2.9	-17.4
Complete	0.0	-19.3	6.4	-10.8

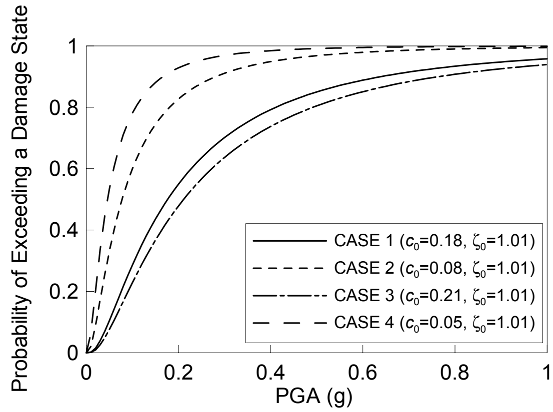

(a) Almost No Damage

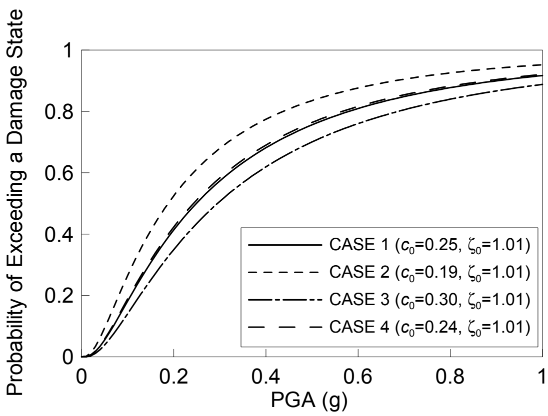

(b) Slight Damage

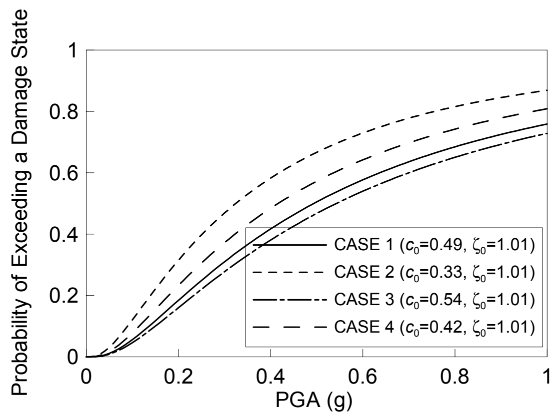

(c) Moderate Damage

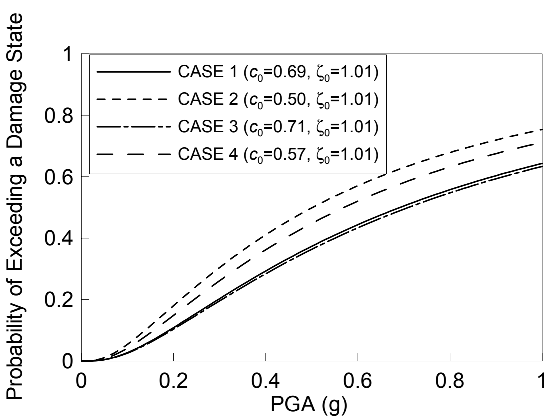

(d) Extensive Damage

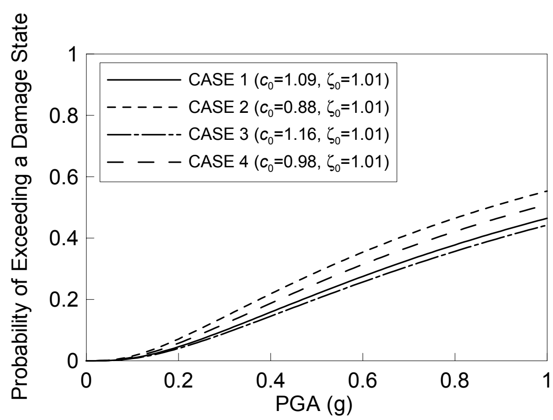

(e) Complete Collapse

FIGURE 4-9 Fragility Curves of Bridge 4

TABLE 4-10 Percent Change in Median Values of Fragility Curves

Damage States	Case1	Case2	Case3	Case4
Almost No	0.0	0.0	-20.5	-27.3
Slight	0.0	-1.8	-9.1	-14.5
Moderate	0.0	0.0	-9.1	-9.1
Extensive	0.0	0.0	0.0	0.0
Complete	0.0	0.0	0.5	0.5

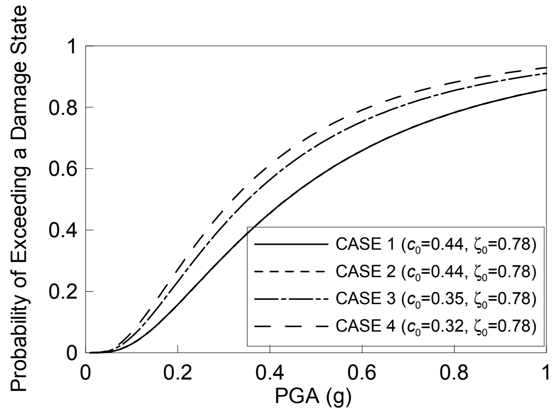

(a) Almost No Damage

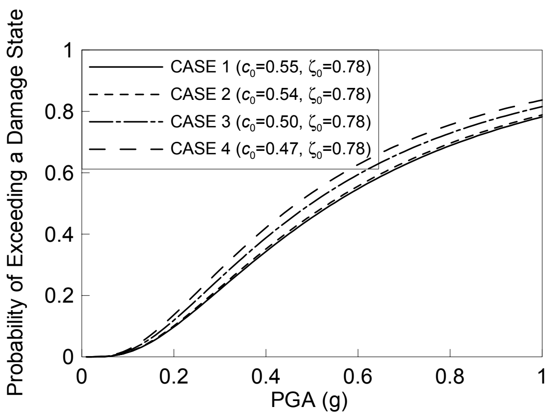

(b) Slight Damage

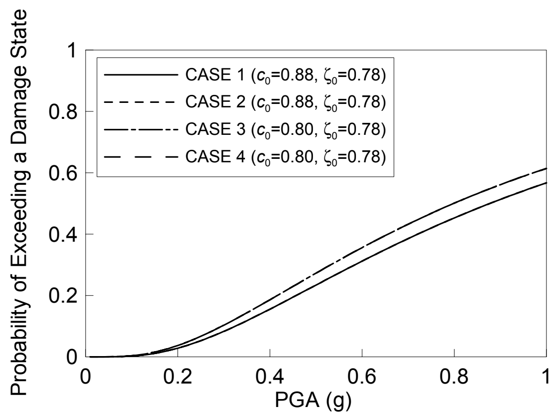

(c) Moderate Damage

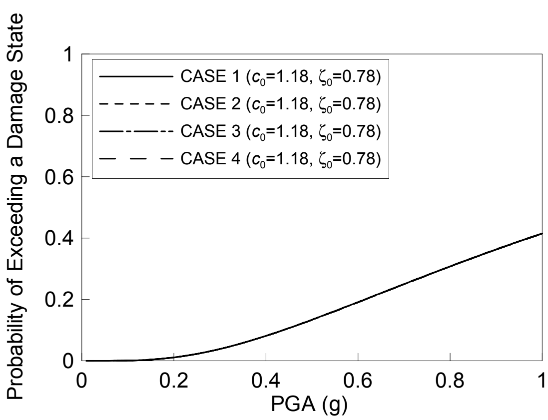

(d) Extensive Damage

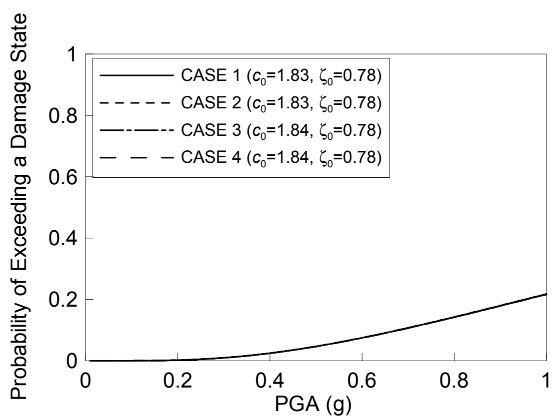

(e) Complete Collapse

FIGURE 4-10 Fragility Curves of Bridge 5

4.4 Jacketing and Restrainer Effect on Fragility Curve

In order to investigate the effect of bridge retrofit by confining columns with steel jackets, fragility curves of each bridge after retrofit are developed and compared with that of before retrofit. Also, a parametric study is performed to observe the effect of restrainer in the fragility characteristics of bridges by analyzing the bridge with and without applying restrainer.

The fragility curves for the four (4) sample bridges associated with the states of damage mentioned in the previous section are plotted as a function of peak ground acceleration in figures 4-11, 4-12, 4-13 and 4-14, while the percent changes in median values of fragility curves are listed in tables 4-11, 4-12, 4-13 and 4-14, respectively considering CASE 1 as a standard case. Each figure has four (4) curves for the following four (4) cases: CASE 1: without jacketing and without restrainer; CASE 2: with jacketing and without restrainer; CASE 3: without jacketing and with restrainer; CASE 4: with jacketing and with restrainer. For the purpose of comparing the fragility curves from above four cases, these are plotted in one figure for each damage state. It is noted that the log-standard deviation in each of figures 4-11, 4-12, 4-13 and 4-14 is obtained such that the fragility curves in each figure will not intersect each other.

The damage state of a bridge is defined in terms of the maximum value of the peak ductility demands sustained by all the column ends. In this context, comparison between fragility curves in figures 4-11 ~14 (CASE: 1 vs. 2 and 3 vs. 4) indicates considerable improvement in the fragility characteristics of bridge after column retrofit. This parametric study does not provide clear idea about the effect of restrainers at expansion joints.

TABLE 4-11 Percent Change in Median Values of Fragility Curves

Damage States	Case1	Case2	Case3	Case4
Almost No	0.0	34.5	0.0	58.6
Slight	0.0	64.1	25.6	64.1
Moderate	0.0	70.0	5.7	70.0
Extensive	0.0	87.6	0.0	138.1
Complete	0.0	220.4	45.5	220.4

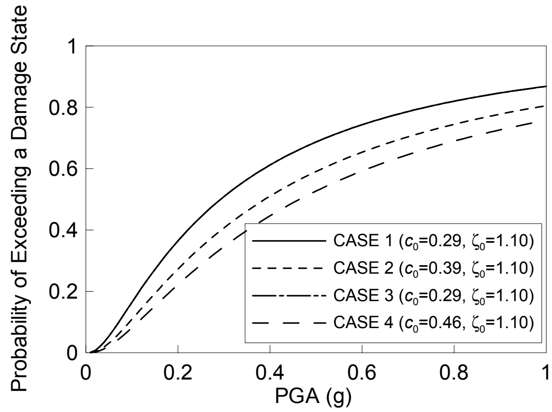

(a) Almost No Damage

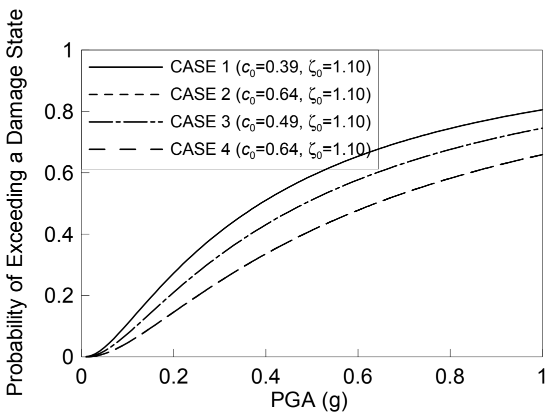

(b) Slight Damage

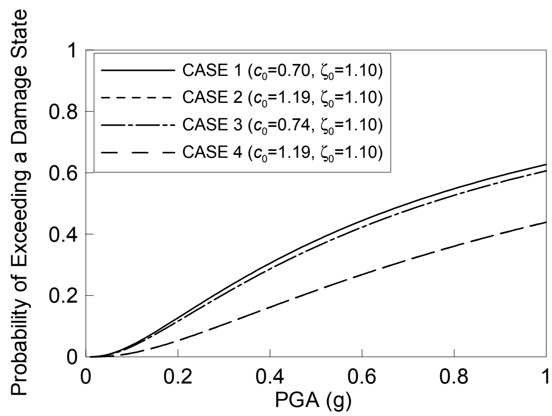

(c) Moderate Damage

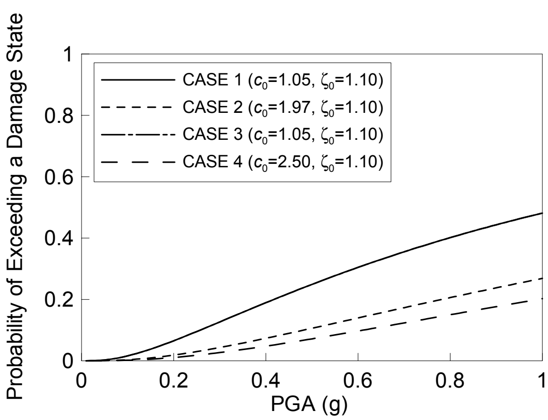

(d) Extensive Damage

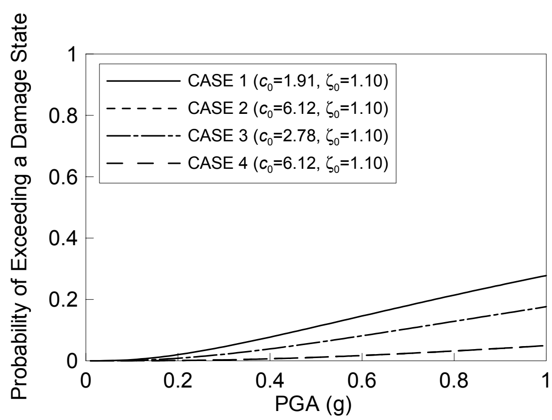

(e) Complete Collapse

FIGURE 4-11 Fragility Curves of Bridge 2

TABLE 4-12 Percent Change in Median Values of Fragility Curves

Damage States	Case1	Case2	Case3	Case4
Almost No	0.0	45.5	-9.1	36.4
Slight	0.0	89.5	-21.1	42.1
Moderate	0.0	87.9	-18.2	45.5
Extensive	0.0	115.0	-2.5	82.5
Complete	0.0	272.6	-22.6	85.5

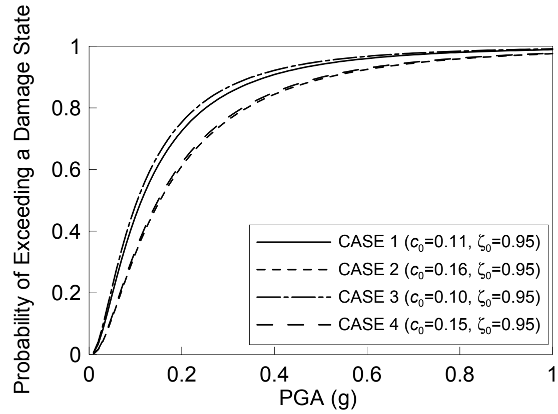

(a) Almost No Damage

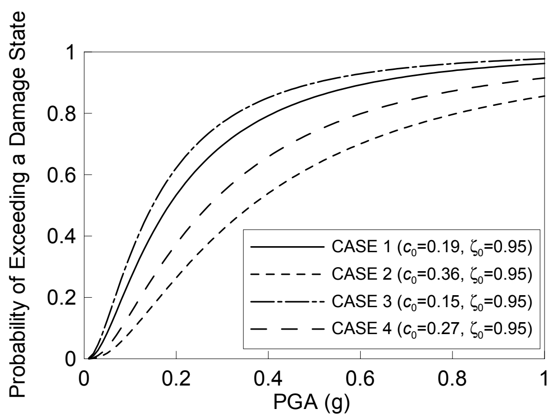

(b) Slight Damage

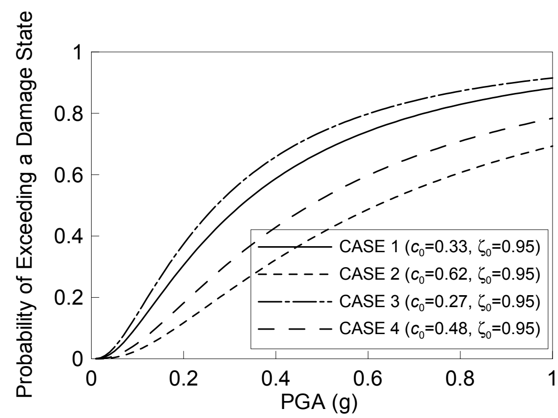

(c) Moderate Damage

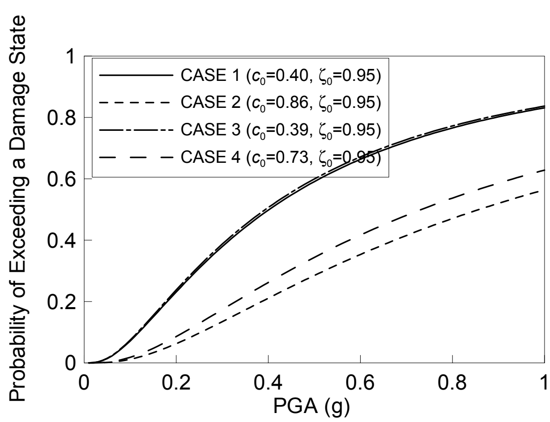

(d) Extensive Damage

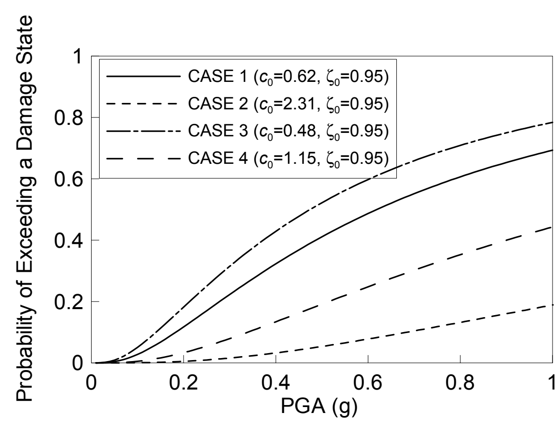

(e) Complete Collapse

FIGURE 4-12 Fragility Curves of Bridge 3

TABLE 4-13 Percent Change in Median Values of Fragility Curves

Damage States	Case1	Case2	Case3	Case4
Almost No	0.0	125.0	62.5	150.0
Slight	0.0	105.3	10.5	100.0
Moderate	0.0	109.1	18.2	87.9
Extensive	0.0	104.0	0.0	62.0
Complete	0.0	114.9	-17.2	165.5

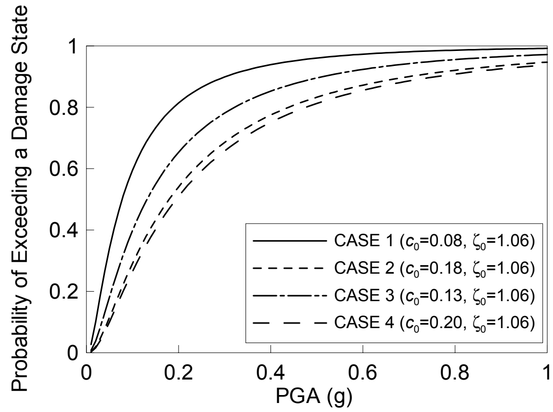

(a) Almost No Damage

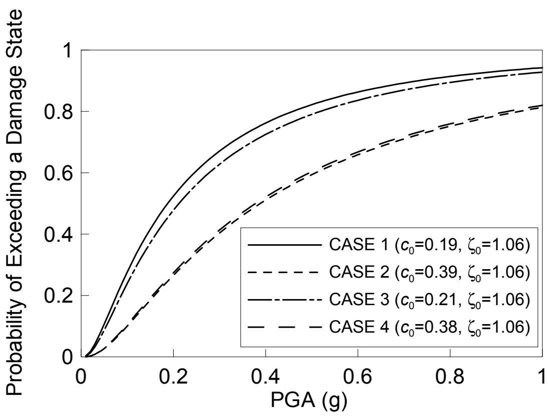

(b) Slight Damage

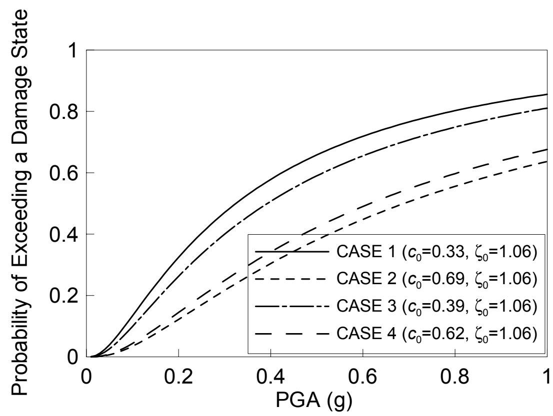

(c) Moderate Damage

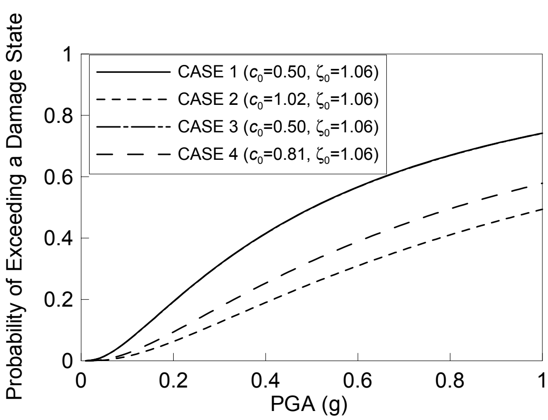

(d) Extensive Damage

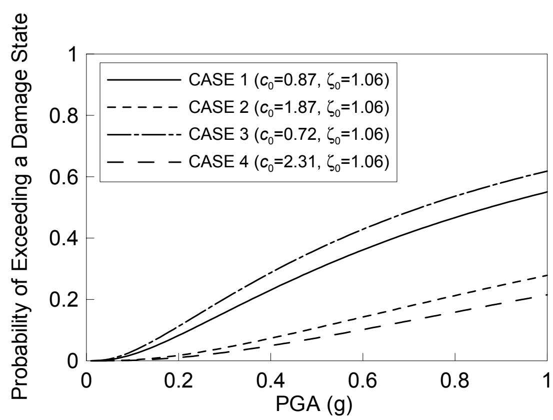

(e) Complete Collapse

FIGURE 4-13 Fragility Curves of Bridge 4

TABLE 4-14 Percent Change in Median Values of Fragility Curves

Damage States	Case1	Case2	Case3	Case4
Almost No	0.0	33.3	-24.2	12.1
Slight	0.0	24.1	0.0	27.6
Moderate	0.0	50.0	0.0	50.0
Extensive	0.0	47.5	4.2	53.3
Complete	0.0	54.0	4.6	54.0

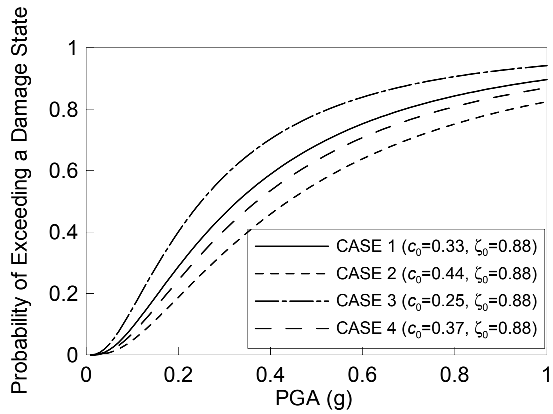

(a) Almost No Damage

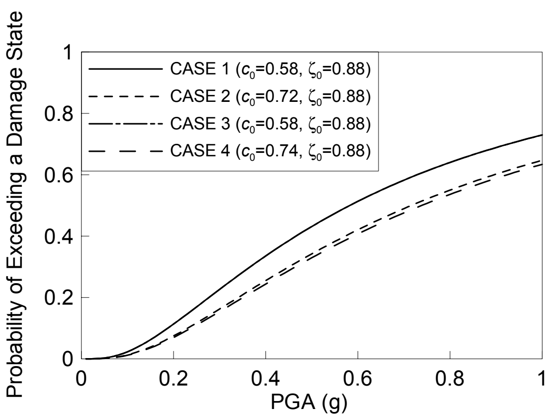

(b) Slight Damage

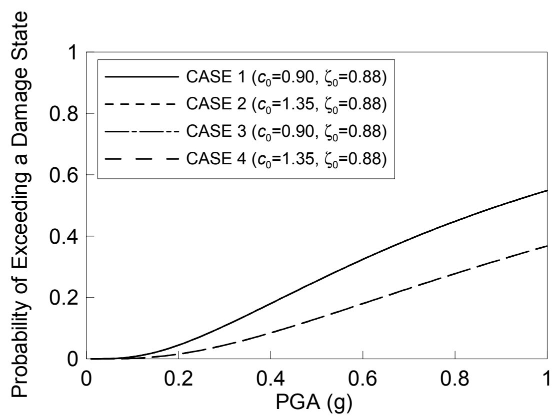

(c) Moderate Damage

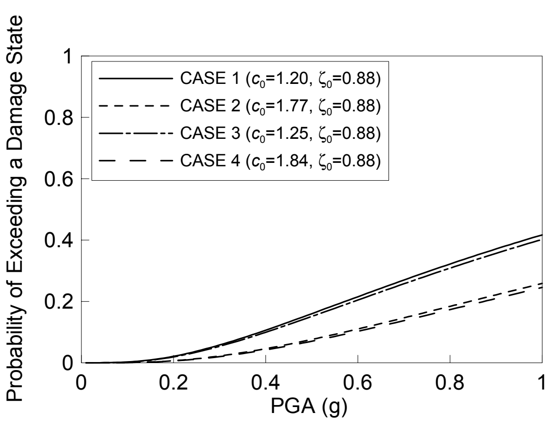

(d) Extensive Damage

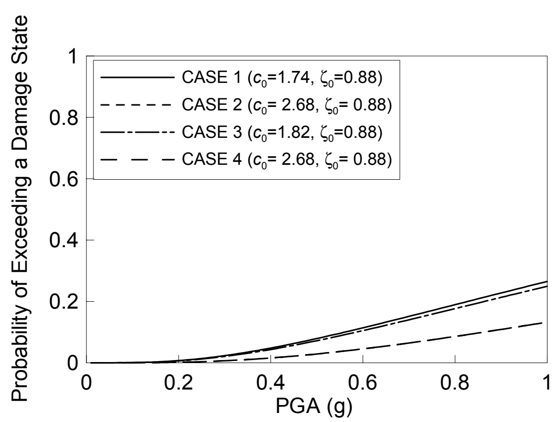

(e) Complete Collapse

FIGURE 4-14 Fragility Curves of Bridge 5

4.5 Fragility Enhancement after Column Retrofit

As observed from the previous figures (figures 4-11 ~ 14), bridge performance in seismic ground motion is improving after retrofitting the bridge columns with steel jackets. In the following sections, the enhancements are computed separately for different shapes of bridge columns. The percent increase in fragility parameter (*c*) after retrofit with respect to the same before retrofit represent the "Enhancement" by definition.

4.5.1 Bridges with Circular Columns

Average fragility enhancements of Bridge 1 and 2 at each state of damage are computed from the corresponding sets of fragility curves for before and after retrofit and plotted as a function of the state of damage. An analytical function is interpolated and the "enhancement curve" is plotted on the basis of the least square fit as shown in figure 4-15. Five damage states are mentioned as indices, x = 1, to 5 and described on the figure. This curve shows 20%, 34%, 58%, 98% and 167% improvement for 'Almost No' damage, 'Minor' damage, 'Moderate' damage, 'Major' damage and 'Collapse' respectively.

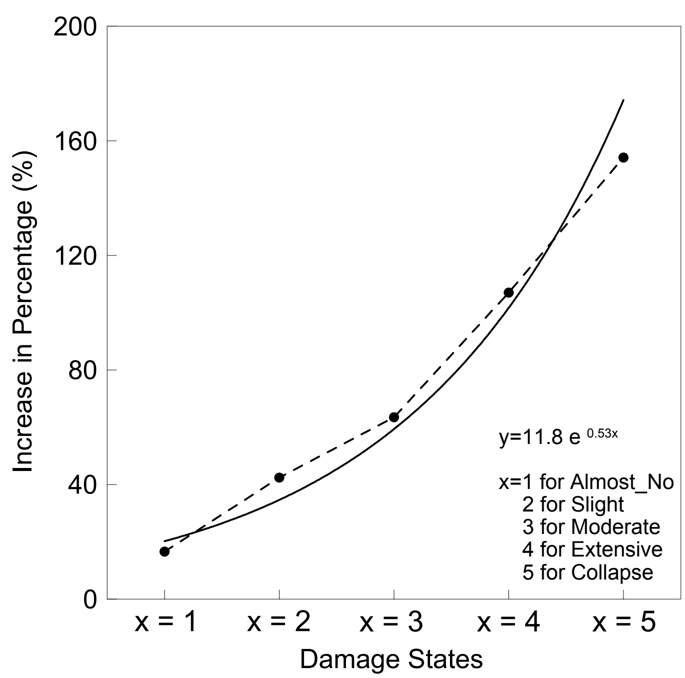

FIGURE 4-15 Enhancement Curve for Circular Columns with Steel Jacketing

4.5.2 Bridges with Oblong Shape Columns

For Bridge 3 and 5 with oblong columns, the fragility enhancement is developed in figure 4-16.

Average fragility enhancements of these two bridges at each state of damage are computed from the corresponding sets of fragility curves for before and after retrofit and plotted as a function of the state of damage. An analytical function is interpolated and the "enhancement curve" is plotted on the basis of the least square fit as shown in figure 4-16. Five damage states are mentioned as indices, x = 1, to 5 and described on the figure. This curve shows 20%, 34%, 58%, 99% and 170% improvement for 'Almost No' damage, 'Minor' damage, 'Moderate' damage, 'Major' damage and 'Collapse' respectively.

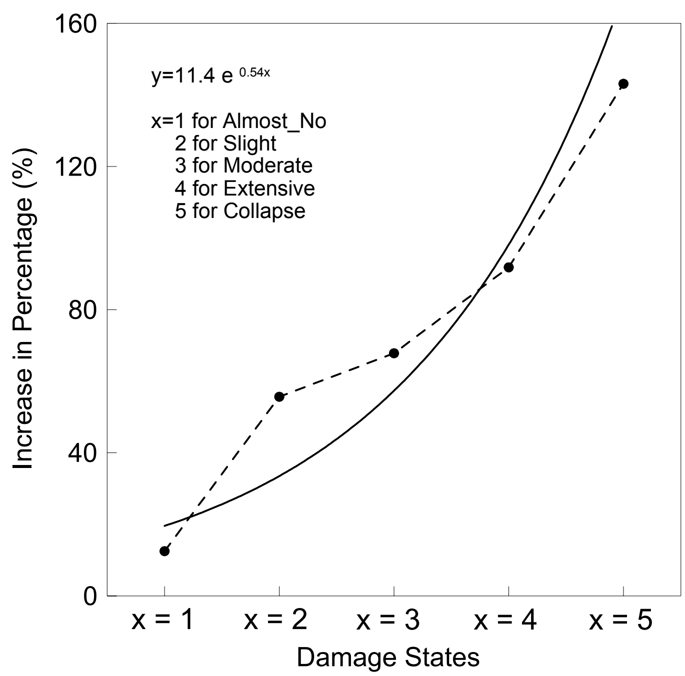

FIGURE 4-16 Enhancement Curve for Oblong Columns with Steel Jacketing

4.5.3 Bridge with Rectangular Columns

For Bridge 4 with rectangular columns, the fragility enhancement is developed in figure 4-17.

Fragility enhancements of this bridge at each state of damage are computed from the corresponding sets of fragility curves for before and after retrofit and plotted as a function of the state of damage. An analytical function is interpolated and the "enhancement curve" is plotted on the basis of the least square fit as shown in figure 4-17. Five damage states are mentioned as indices, x = 1, to 5 and described on the figure. This figure does not indicate any good correlation among the enhancement records from at five (5) damage states. This is because the rectangular columns of Bridge 4 are not efficiently confined with elliptical steel jackets after retrofit (figures A-6(b) ~ A-14(b)).

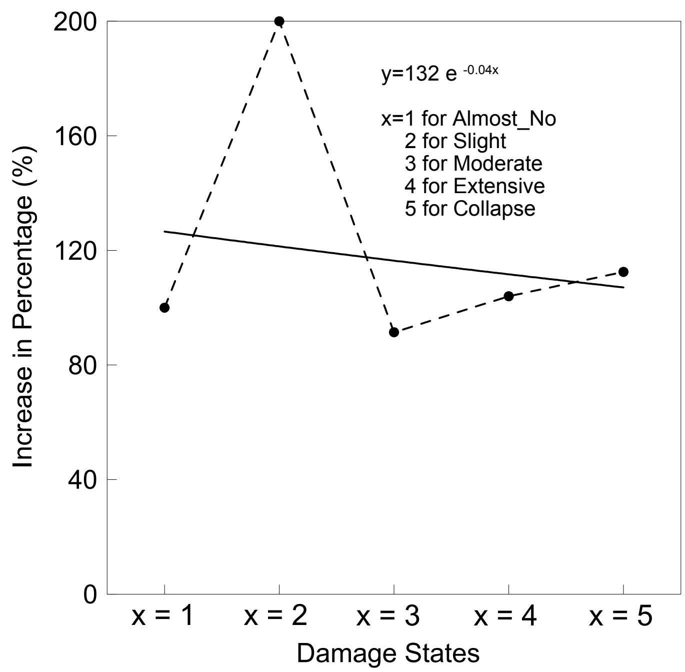

FIGURE 4-17 Enhancement Curve for Rectangular Columns with Steel Jacketing

4.5.4 Enhancement in All Bridges

For Bridges 1~5, the fragility enhancement is developed in figure 4-18.

Considering all the sample bridges and corresponding sets of fragility curves before and after retrofit at each state of damage is computed and plotted as a function of the state of damage. An analytical function is interpolated and the "enhancement curve" is plotted on the basis of the least square fit as shown in figure 4-18. Five damage states are mentioned as indices, x = 1, to 5 and described on the figure. This curve shows 40%, 55%, 75%, 104% and 143% improvement for 'Almost No' damage, 'Minor' damage, 'Moderate' damage, 'Major' damage and 'Collapse' respectively. This curve shows improvement for each damage state described on the *x* axis in figure 4-18.

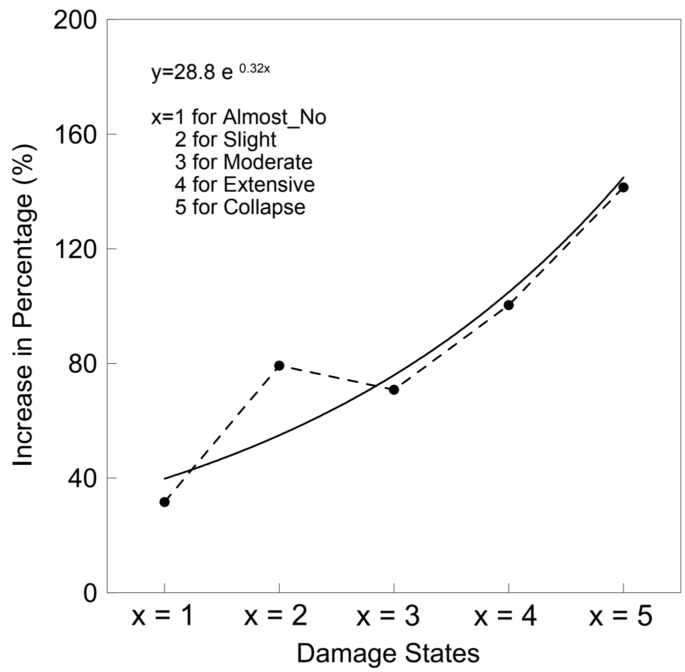

FIGURE 4-18 Enhancement Curve for Five Sample Bridges with Steel Jacketing

4.6 Analytical Fragility Curves in Transverse Direction

To construct analytical fragility curves of the example bridges, bridge models (described in Section 2) are analyzed under sixty (60) ground motion time histories. According to the damage states definition given by Dutta and Mander (1998), ductility demands at each damage states are calculated.

4.6.1 Fragility Analysis Considering No Abutment Stiffness in Transverse Direction

For no abutment stiffness (zero resistance from backfill soil), bridge acts as a single degree of freedom system in transverse direction. Very low abutment stiffness (14.57 kN/m, nearly zero resistance from backfill soil) is considered to analyze Bridge 1 and 2 under earthquake ground motions. Numbers of damaged bridges in each damage state and fragility parameters are tabulated in tables 4-15 and 4-16 while figures 4-19 and 4-20 show the analytical fragility curves of Bridge 1 and 2.

TABLE 4-15 Number of Damaged Bridges and Fragility Parameters of Bridge 1 for Abutment Stiffness 14.57 kN/m

Damage States	Damaged Bridges (Sample Size 60)	Fragility Parameters	
		$c(g)$	ζ
Almost No Damage	55	0.1765	0.730
Minor Damage	49	0.2969	
Moderate Damage	39	0.4459	
Major Damage	27	0.6418	
Collapse	15	0.8969	

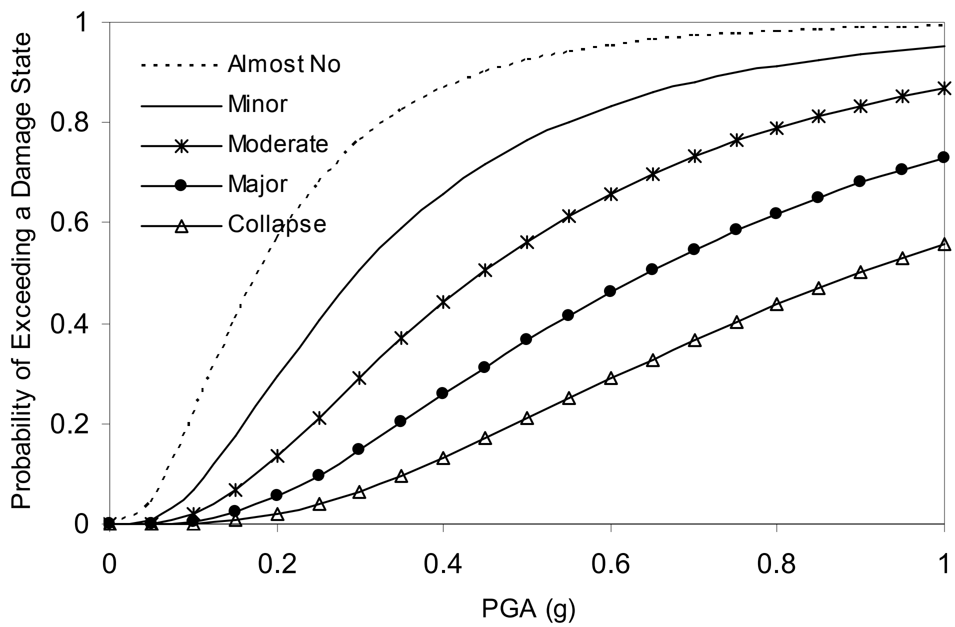

FIGURE 4-19 Fragility Curves of Bridge 1 for Five Damage States for Abutment Stiffness 14.57 kN/m

TABLE 4-16 Number of Damaged Bridges and Fragility Parameters of Bridge 2 for Abutment Stiffness 14.57 kN/m

Damage States	Damaged Bridges (Sample Size 60)	Fragility Parameters	
		$c(g)$	ζ
Almost No Damage	56	0.0255	1.527
Minor Damage	45	0.1745	
Moderate Damage	34	0.4857	
Major Damage	19	0.8908	
Collapse	12	1.0929	

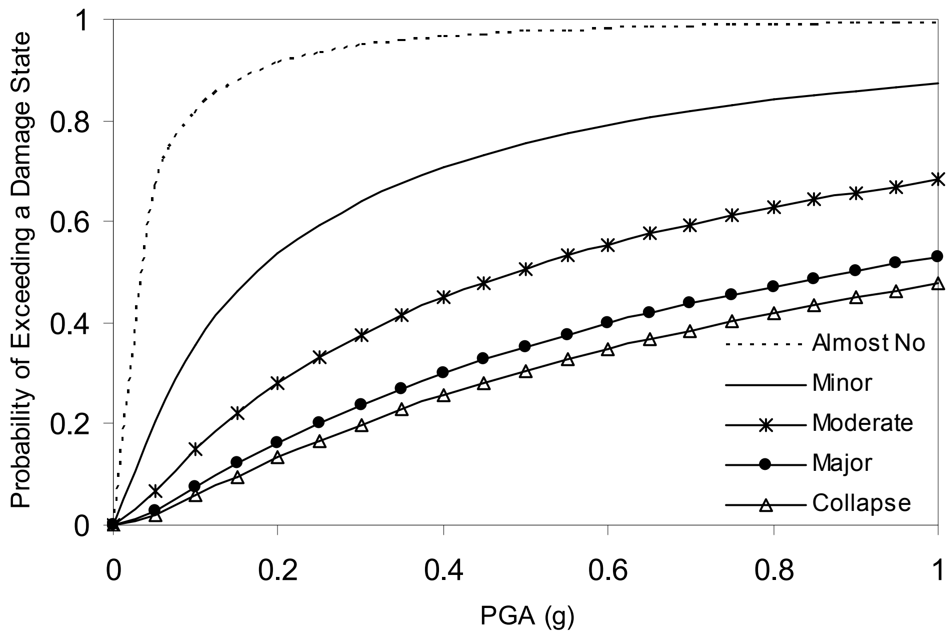

FIGURE 4-20 Fragility Curves of Bridge 2 for Five Damage States for Abutment Stiffness 14.57 kN/m

4.6.2 Fragility Analysis Considering Abutment Stiffness in Transverse Direction

Bridge 1 and 2 are analyzed considering the lateral abutment stiffness of 7287.68 kN/m (500 kips/ft) and 29150.73 kN/m (2000 kips/ft) respectively. Numbers of damaged bridges in each damage state and fragility parameters are tabulated in tables 4-17 and 4-18 and the analytical fragility curves are shown in figures 4-21 and 4-22.

TABLE 4-17 Number of Damaged Bridges and Fragility Parameters of Bridge 1 for Abutment Stiffness 7287.68 kN/m

Damage States	Damaged Bridges (Sample Size 60)	Fragility Parameters	
		$c(g)$	ζ
Almost No Damage	50	0.3061	0.707
Minor Damage	41	0.3990	
Moderate Damage	28	0.6194	
Major Damage	16	0.8633	
Collapse	6	1.1990	

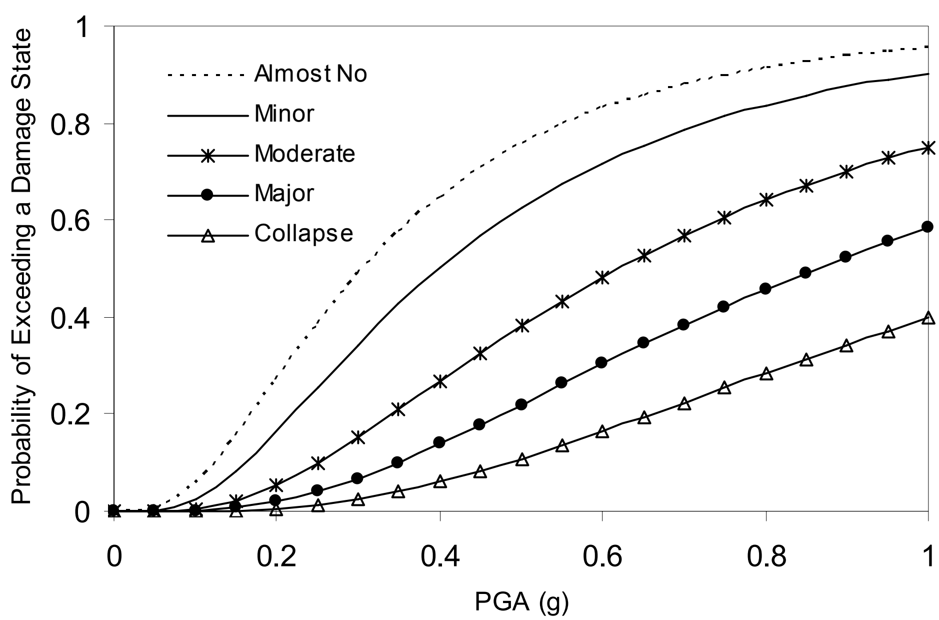

FIGURE 4-21 Fragility Curves of Bridge 1 for Five Damage States for Abutment Stiffness 7287.68 kN/m

TABLE 4-18 Number of Damaged Bridges and Fragility Parameters of Bridge 2 for Abutment Stiffness 29150.73 kN/m

Damage States	Damaged Bridges (Sample Size 60)	Fragility Parameters	
		$c(g)$	ζ
Almost No Damage	53	0.212	0.968
Minor Damage	45	0.295	
Moderate Damage	28	0.617	
Major Damage	16	0.856	
Collapse	8	1.738	

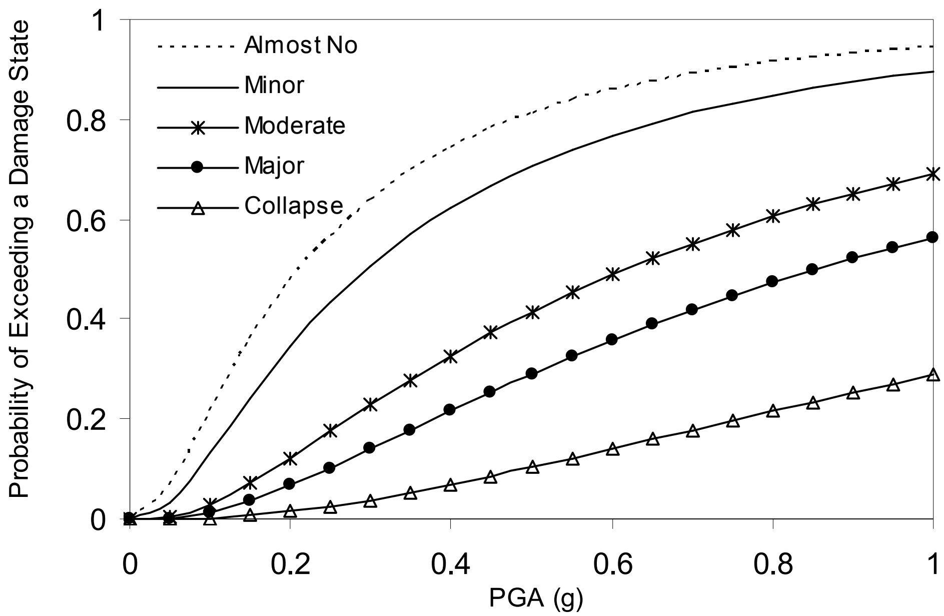

FIGURE 4-22 Fragility Curves of Bridge 2 for Five Damage States for Abutment Stiffness 29150.73 kN/m

4.6.3 Effect of Abutment Stiffness on Fragility Curves in Transverse Direction

Considerable improvement in fragility characteristics of Bridge 1 and 2 are noticed due to the lateral resistance of backfill soil at abutment locations. In reality, it is rational to consider that the lateral movement of bridge is resisted by the wingwalls. Therefore, it is important to consider the lateral stiffness of abutments during transverse movement of the bridge.

SECTION 5
CALIBRATION OF ANALYTICAL FRAGILITY CURVES WITH DAMAGE DATA

The damage report of Caltrans' bridges under the Northridge earthquake serves as invaluable field experiments that the nature provided. For the analytical purpose, mechanistic model of bridge damage should be in accordance with that past earthquake damage data. Shinozuka et al. (2003b) developed the empirical fragility curves for Caltrans' bridges utilizing ShakeMap (*http://www.trinet.org/shake/index.html*) for 1994 Northridge Earthquake and the bridge damage data associated with it. They statistically analyzed 1998 damaged bridges and categorized them according to bridge configurations (such as 'single or multiple span' and 'skew angle') and 'soil type'. Each of these classes is again subdivided into more detailed sets; (a) two span types (single or multiple); (b) three sets of skew angles (0° ~ 20°, 20° ~ 60° and > 60°); and (c) three soil types (A: hard, B: medium, C: soft as per Uniform Building Code 1993). They generated empirical fragility curves for four different subset levels; (i) Level 1 subset considering all 1998 bridges in a same class, (ii) Level 2 subset for different bridge classes according to their span, soil type and skewness, (iii) Level 3 subset for bridges with any two combinations of their span, soil type and skewness, and (iv) Level 4 subset for bridges with all possible combinations of span, soil type and skewness. Among these, Level 4 is the most statistically sophisticated and consisting of 18 combinations of bridge span, skew angle, and soil type. Figure 5-1 shows a set of empirical fragility curves developed in Level 4 subset with a combination of 'multiple span', skew angle '0° ~ 20°' and soil type 'C'. In this section, these empirical fragility curves are used to mechanically calibrate of analytical damage model of Caltrans' bridges. Definitions of bridge damage states are also quantified through this process for which analytical fragility curves become consistent with empirical damage data.

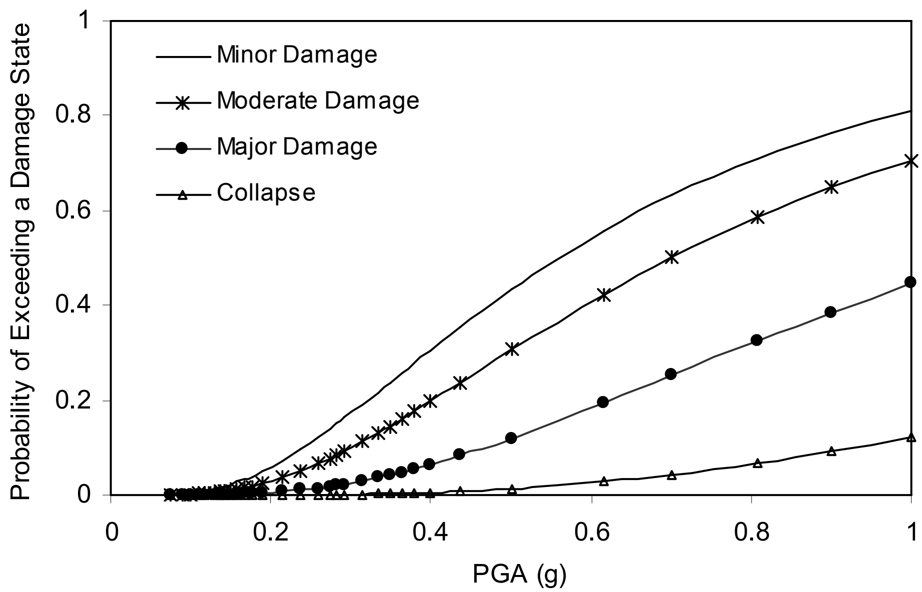

FIGURE 5-1 Empirical Fragility Curves for Level 4 Subset (Multiple Span, Skew angle 0° ~ 20° and Soil Type C)

5.1 Comparison of Fragility Curves

In the present study, empirical fragility curves for a third level subset (considering 'multiple span' and 'soil type C') are used to compare these curves with the analytically obtained fragility curves (figures 5-2 ~ 5-4). Comparison indicates that the analytical curves tend to be substantially conservative in the sense that bridges are more probable to suffer from more severe damage state than they are when empirical fragility curves suggest. In order to minimize the discrepancies observed between the analytical and empirical fragility curves, definition of the damage states of bridges is revised for the development of analytical fragility curves and it is found that the damage state definition given by Dutta and Mander (1998) can be adjusted to produce analytical fragility curves much more consistent with empirical one.

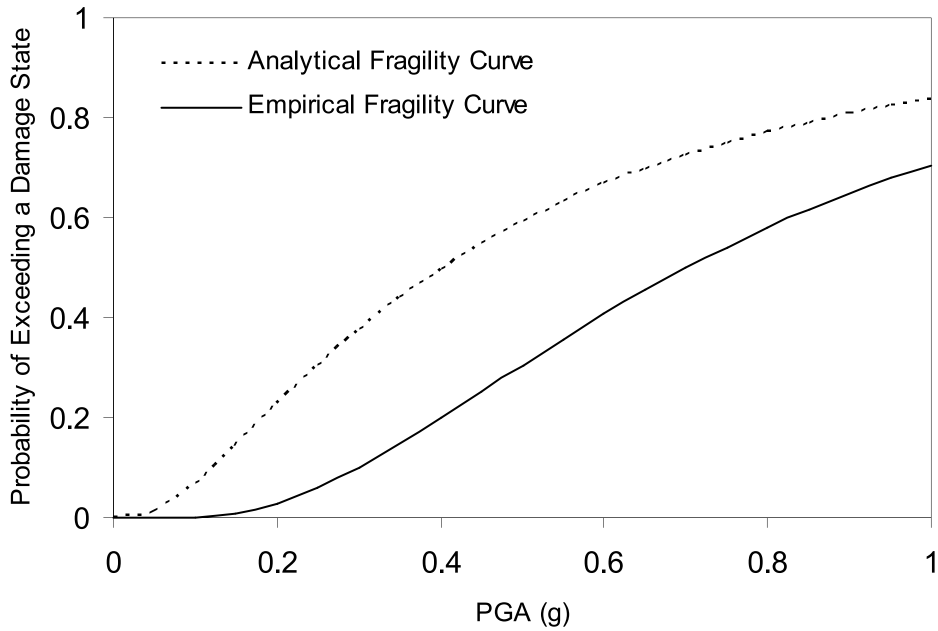

FIGURE 5-2 Comparison of Empirical and Analytical Fragility Curves of Bridge 2 at Minor Damage State

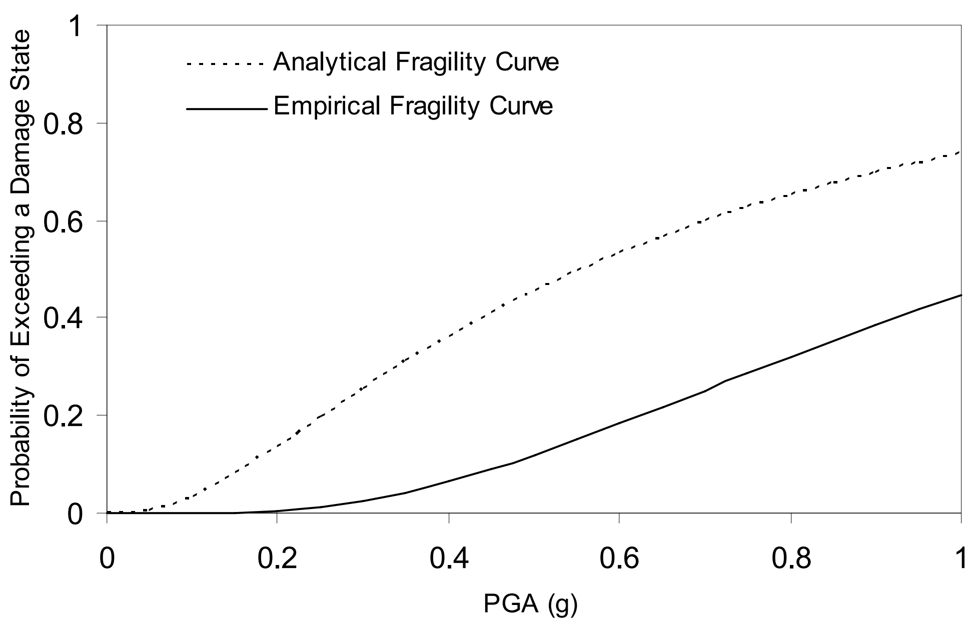

FIGURE 5-3 Comparison of Empirical and Analytical Fragility Curves of Bridge 2 at Moderate Damage State

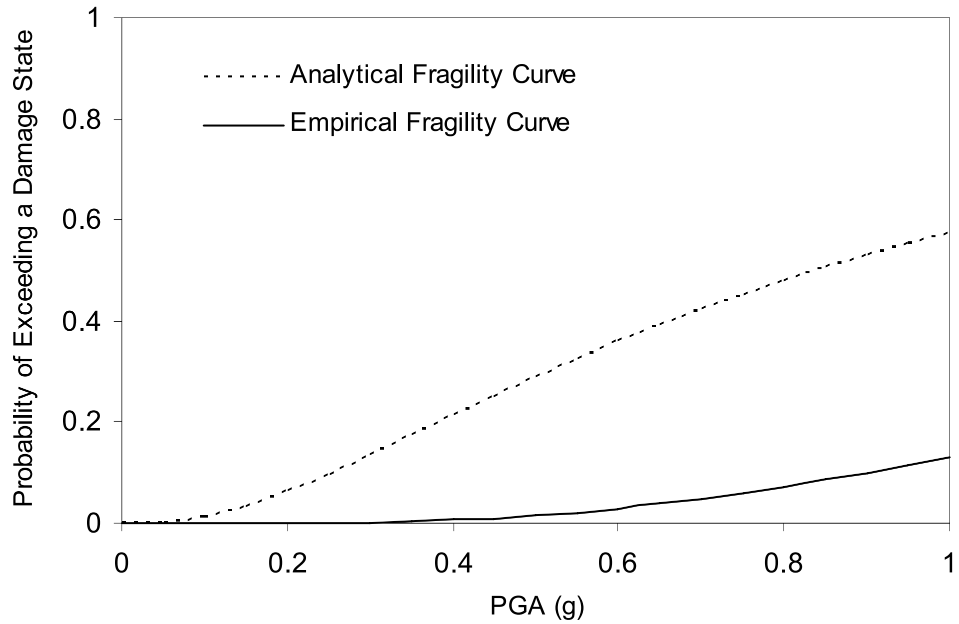

FIGURE 5-4 Comparison of Empirical and Analytical Fragility Curves of Bridge 2 at Major Damage State

5.2 Estimation of Ductility Capacities at Various Damage States

Seismic response of bridges from nonlinear time history analysis (*SAP2000 Nonlinear* analysis) for sixty ground motions is used as input in this part of analysis. While comparing with empirical fragility curves, numerical analysis is done to get best-fit distribution, for minor, moderate and extensive damage states and their corresponding ductility capacities. The parameters (median and log-standard deviation) of each fragility curve are independently estimated by means of the maximum likelihood procedure as described in section 4. The two fragility parameters are computed as c_0 and ζ_0 satisfying (4-8).

Second optimization is done to minimize the difference between parameters of empirical fragility curves (median, c_{emp} and log-standard deviation, ζ_{emp}) and those obtained in the analytical procedure (i.e. c_0 and ζ_0). In order to capture the proper value of threshold ductility capacity at each damage state, which will produce the analytical fragility curves consistent with empirical curves, the above two optimization procedures are performed simultaneously. Figures 5-5 represents a flowchart that represents the procedure. The entire procedure is carried out independently for Bridge 2, 4 and 5. Table 5-1 presents the median values (c) for empirical fragility curves and calibrated analytical fragility curves. Result indicates that at minor and moderate damage states, calibrated median values are well in accordance with that from empirical fragility curves, although dispersion is observed in the major damage state for Bridges 4 and 5. This is because of the limited failure cases observed in major damage state while analyzing these example bridges under 60 ground motion time histories. Analysis with many severe ground motions that may cause major damage to Bridge 4 and 5 will produce better correspondence with empirical data. Figures 5-6 and 5-7 show the empirical fragility curves and calibrated fragility curves of three example bridges respectively for minor and moderate damage states.

Calibrated rotational ductility capacities for minor, moderate and major damage states of these three example bridges are presented in table 5-2. Figure 5-8 plots these calibrated rotational ductility capacities for different damage states in which indices 1, 2, and 3 stand for 'Minor Damage', 'Moderate Damage' and 'Major Damage' respectively. This figure indicates that in all damage states threshold rotational ductility for Bridge 4 and 5 almost overlap with each other while that for Bridge 2 lay far apart. A clear increasing trend is common for all bridges which can be represented on the basis of least square fit. It can be stated from this result that empirical fragility curve for more detailed bridge classification is needed in order to calibrate analytical result. For example, additional consideration of bridge length and number of span in current classification will enhance calibrated result significantly.

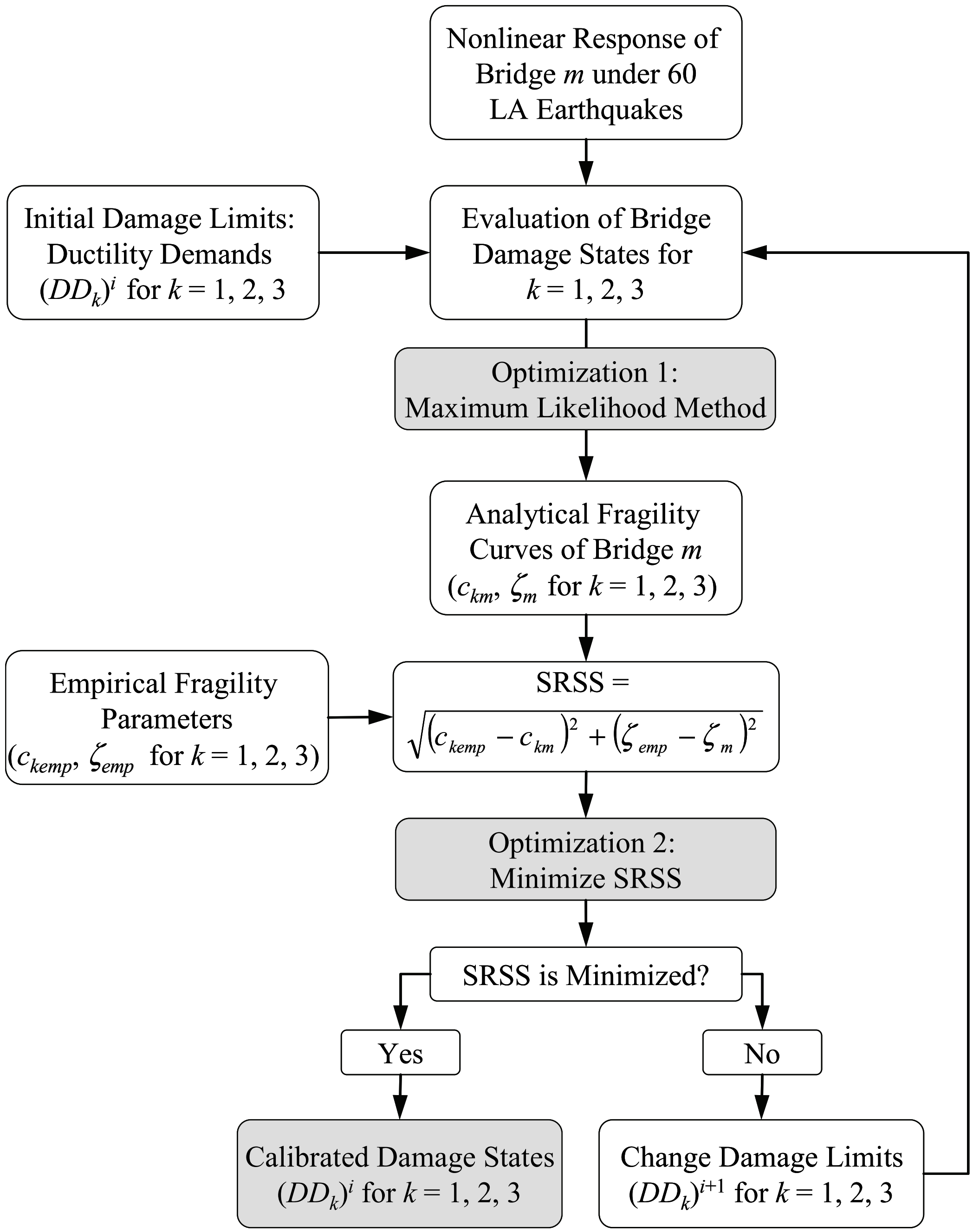

FIGURE 5-5 Flow Chart: Estimation of Bridge Damage States through the Calibration of Analytical and Empirical Bridge Fragility Curves

Table 5-1 Fragility Parameters (Median Values in g) for Empirical and Calibrated Analytical Fragility Curves

Damage States	Median Values (g)			
	Empirical Fragility Curves	Calibrated Analytical Fragility Curves		
		Bridge 2	Bridge 4	Bridge 5
Minor	0.56	0.56	0.53	0.54
Moderate	0.70	0.70	0.67	0.67
Major	1.09	1.06	0.73	0.83

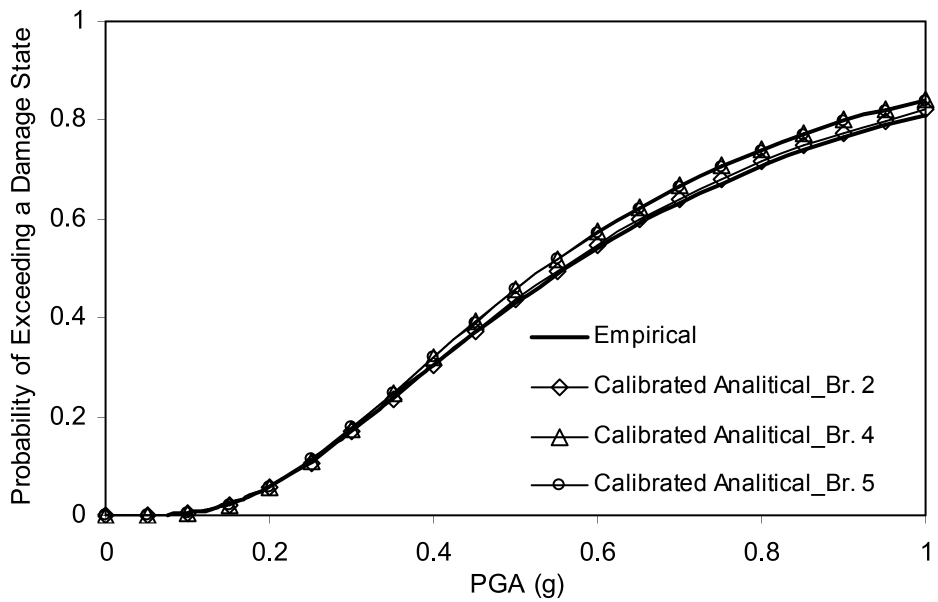

FIGURE 5-6 Empirical and Calibrated Analytical Fragility Curves at Minor Damage

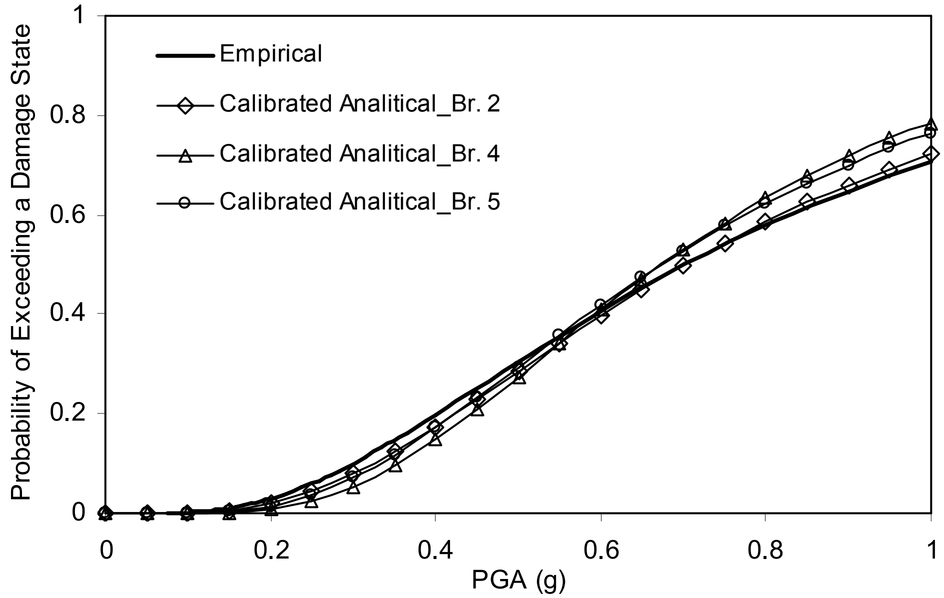

FIGURE 5-7 Empirical and Calibrated Analytical Fragility Curves at Moderate Damage

Table 5-2 Lower Bound of Calibrated Rotational Ductility of Bridges

Bridge No	Threshold Rotational Ductility at Different Damage States		
	Minor	Moderate	Major
2	3.39	4.75	8.43
4	6.43	9.02	12.35
5	5.93	9.06	12.18

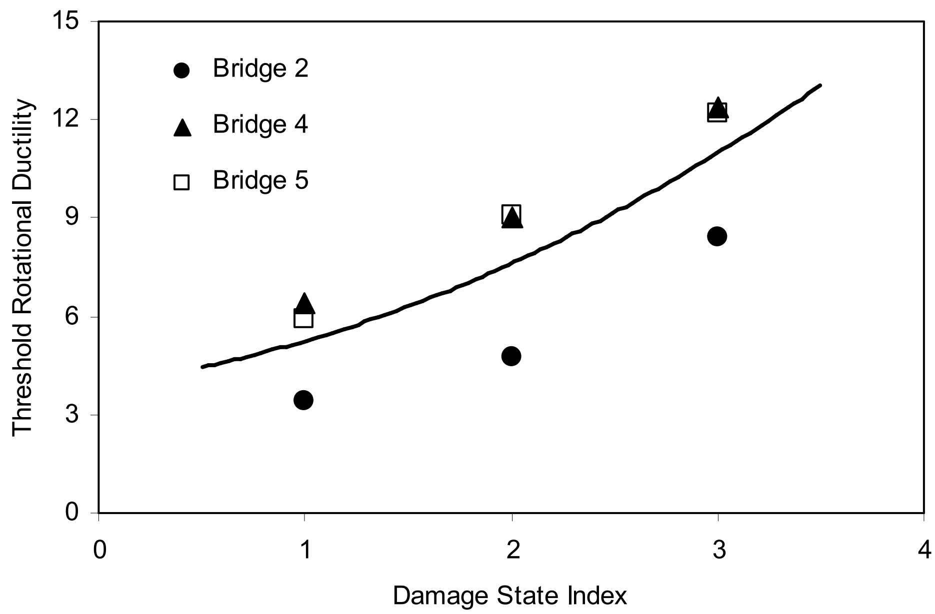

FIGURE 5-8 Rotational Ductility Capacities at Various Damage States

SECTION 6
EFFECT OF GROUND MOTION DIRECTIONALITY ON FRAGILITY CHARACTERISTICS OF BRIDGES

Most of the studies on the seismic performance of structures are conducted using earthquake ground motions acting along one of the principle axes of those structures. According to ATC-6 (1981), "It would be better to use a set of three or more acceleration time histories with an average elastic response spectrum similar to the design spectrum. This discussion is intended to emphasize that the design ground shaking is not a single motion, but rather a concept that encompasses a family of motions having the same overall intensity and frequency content but differing in some potentially important details of the time sequences of the motions". In general recorded ground motions have two components, N-S and E-W. A typical bridge under two components of ground motion is shown in figure 6-1. Figure 6-2 shows the trajectory of an earthquake ground motion with two orthogonal components. It is almost impossible to identify the principal directions of these orthogonal components and position of the structure relative to them. Although it is possible to model the ground motion acceleration time history as a 2D or 3D vector random process (Shinozuka, et al., 1996), the model results in time varying principal axis of the process and becomes too complex for our purposes. Recently some researchers [Stefano et al. (1998), Riddell and Santa-Maria (1999), Ghersi and Rossi (2001)] evaluated structural response considering bi-directional earthquake ground motions acting along principal axes of the structure. However, well-designed structure should be capable of resisting earthquake motion from all possible directions. Therefore directionality of the earthquake ground motion components and its effect on structure is an important issue in seismic performance analysis. The word 'directionality' is used here as opposed to 'directivity' used in engineering seismology with a specific definition related to fault motion unique to that field.

Wilson et al. (1982), Wilson et al. (1995) and Hernandez et al. (2002) showed how to estimate the maximum structural response to more than one translational seismic component of ground motion by a response spectrum analysis. They considered one component of ground motion as some proportion of other and showed the variation in response at a certain location of the structure due to varying inclination of ground motion components. Following their approach, this study presents a practice-oriented technique to compute the effect of directionality of earthquake ground motion on seismic performance of bridges in terms of fragility curves.

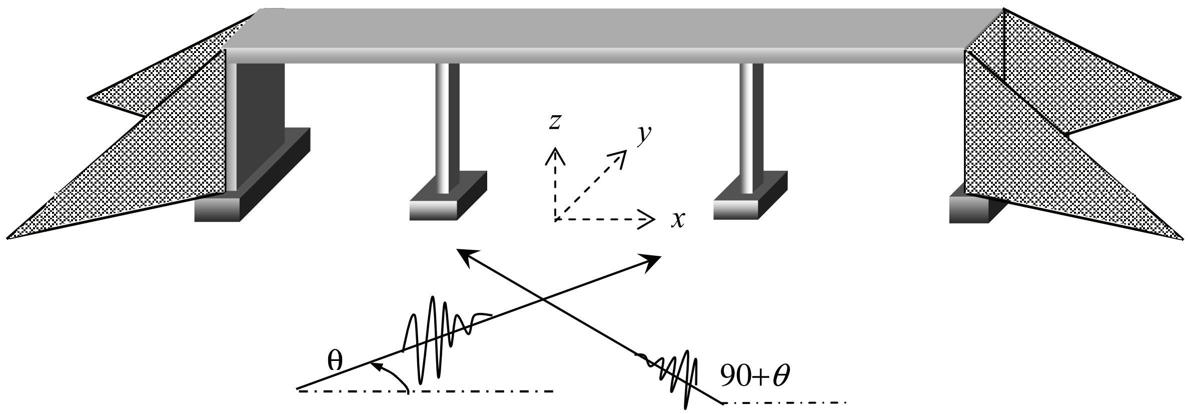

FIGURE 6-1 Bridge under Two Orthogonal Components of Ground Motion Acting at Any Angle θ

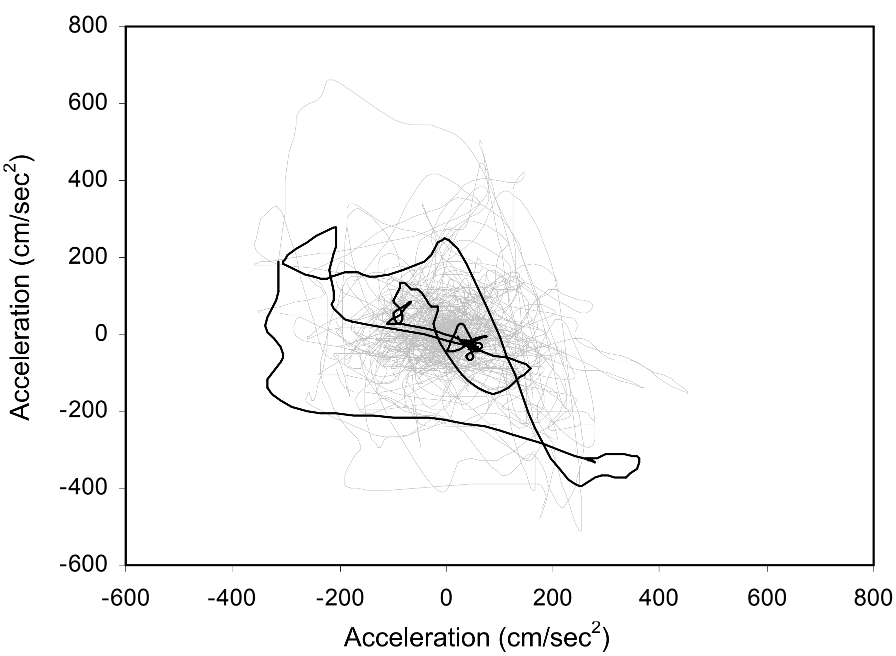

FIGURE 6-2 Trajectory of Ground Acceleration Time Histories of El Centro Earthquake, 1940

6.1 Bridge Under One Inclined Component of Ground Motion

To investigate the directionality effect of earthquake ground motion, it is considered that the ground motion (GM) acts at all possible angles θ with respect to longitudinal (x) axis of the example bridge (figure 6-1), as shown in figure 6-3.

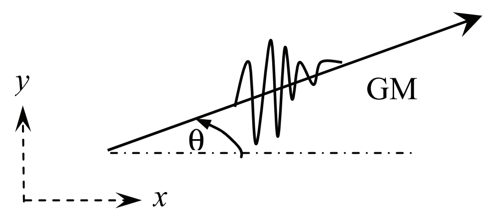

FIGURE 6-3 Earthquake Ground Motions Input (Plan View)

For the purpose of demonstration, it is considered that two separate analyses of the example bridge, under ground motion 'GM' acting along longitudinal and transverse directions, yield the responses R_x and R_y respectively in longitudinal and transverse directions at any location 'A' of the bridge. This response could be in terms of generated force, moment or deformation in any bridge component. At any inclined direction (θ), the response components are computed from R_x and R_y as shown in figure 6-4.

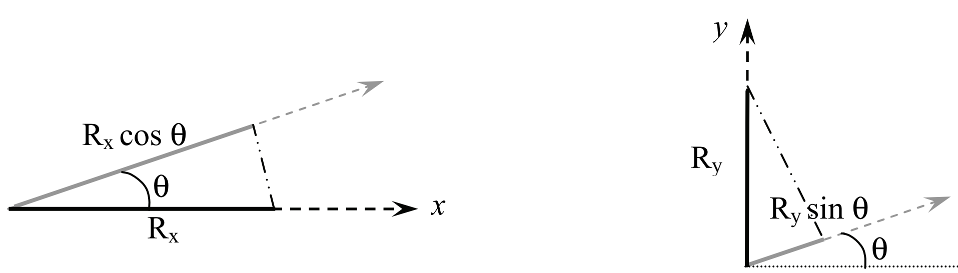

(a) Longitudinal Analysis (b) Transverse Analysis

FIGURE 6-4 Response Components in any Inclined Direction (Plan View)

Hence, the response of the bridge at location 'A' due to GM when acting with an angle θ with longitudinal axis of bridge is a combination of R_x and R_y and can be expressed as

$$R_\theta = R_x \cos\theta + R_y \sin\theta \tag{6-1}$$

To get the maximum response, $\frac{\partial R_{\theta}}{\partial \theta} = 0$

Therefore, the critical angle θ_{cr}, at which the demand of the ground motion is maximum, will be

$$tan\, 2\theta_{cr} = \frac{2R_x R_y}{R_x^2 - R_y^2} \tag{6-2}$$

and the maximum response of the bridge at location A becomes,

$$R_{max} = R_x \cos\theta_{cr} + R_y \sin\theta_{cr} = \sqrt{R_x^2 + R_y^2} \tag{6-3}$$

6.2 Bridge Under Two Orthogonal Components of Ground Motion

To investigate the directionality effect of two orthogonal components of earthquake ground motion, it is considered that one component, GM_1 acts at all possible angles θ with respect to *x* (longitudinal) axis and at the same time the orthogonal component, GM_2 acts an angle $90+\theta$. The following figure (figure 6-5) shows the plan view these motions schematically.

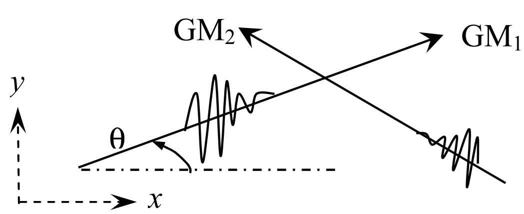

FIGURE 6-5 Earthquake Ground Motions Input (Plan View)

Figure 6-6 shows the responses of the bridge R_{1x} and R_{2x} in *x* direction (at any location 'A') as observed under GM_1 and GM_2, respectively, when they are acting along the longitudinal direction. Similar analyses are done considering motions are acting along the transverse direction of the bridge and corresponding response quantities (at location 'A') are measured as R_{1y} and R_{2y}. In order to compute the response of the bridge under two orthogonal components, it is considered that ground motions are statically independent.

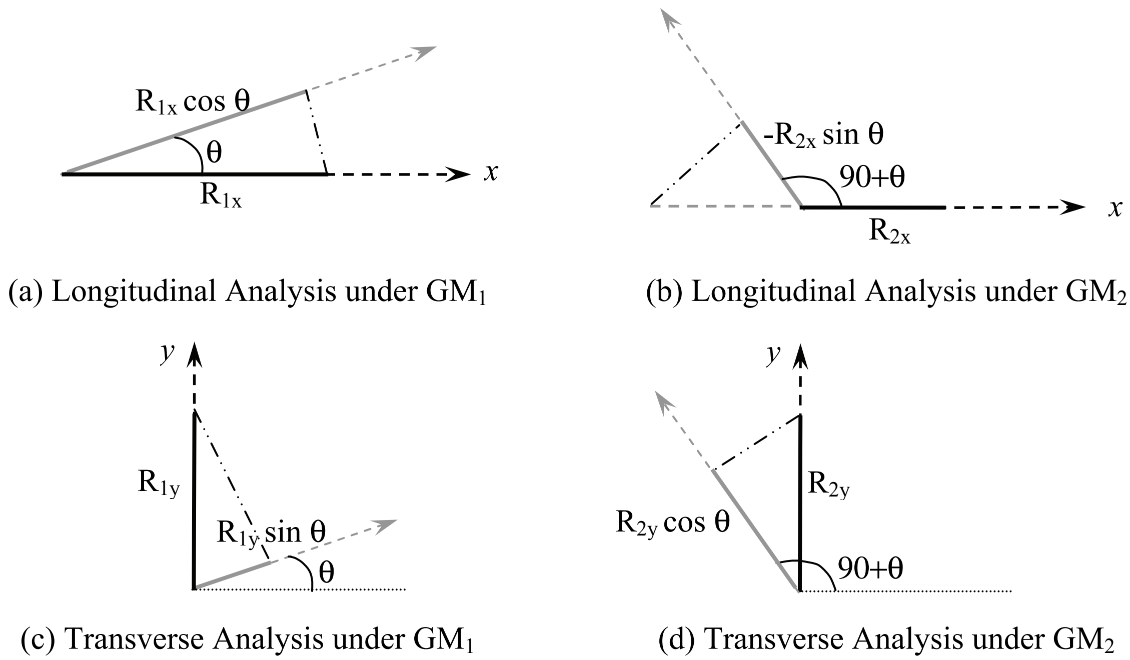

FIGURE 6-6 Response Components under two Orthogonal Components of Ground Motion (Plan View)

The response of the bridge at location 'A' due to GM_1 when acting with an angle θ with longitudinal axis of bridge is

$$R_{1\theta} = R_{1x}\cos\theta + R_{1y}\sin\theta \tag{6-4}$$

and the same due to GM_2, acting at an angle $90+\theta$ with longitudinal axis of bridge is

$$R_{2\theta} = -R_{2x}\sin\theta + R_{2y}\cos\theta \tag{6-5}$$

As ground motions are statistically independent, the response of the bridge at location 'A' under GM_1 and GM_2 is

$$R = \sqrt{R_{1\theta}^2 + R_{2\theta}^2} = \sqrt{\left(R_{1x}\cos\theta + R_{1y}\sin\theta\right)^2 + \left(-R_{2x}\sin\theta + R_{2y}\cos\theta\right)^2} \tag{6-6}$$

To get the maximum response, $\dfrac{\partial R}{\partial \theta} = 0$

Therefore, the critical angle, θ_{cr} at which the bridge will have maximum response at 'A' under GM_1 and GM_2, can be expressed as

$$tan\,2\theta_{cr} = \frac{2\left(R_{1x}R_{1y} - R_{2x}R_{2y}\right)}{\left(R_{1x}^2 + R_{2y}^2 - R_{1y}^2 - R_{2x}^2\right)} \tag{6-7}$$

So the maximum response of the bridge at location 'A' under GM_1 and GM_2 will be,

$$R_{max} = \sqrt{\left(R_{1x}\,cos\,\theta_{cr} + R_{1y}\,sin\,\theta_{cr}\right)^2 + \left(-R_{2x}\,sin\,\theta_{cr} + R_{2y}\,cos\,\theta_{cr}\right)^2} \tag{6-8}$$

6.3 Development of Fragility Curve for One Inclined Component of Ground Motion

Nonlinear time history analysis of Bridge 2 under 60 pre-stated ground motions is conducted separately to compute the response (in this case, rotation at column ends) for each earthquake in both longitudinal and transverse directions. According to (6-1), rotations of bridge column ends for each ground motion are obtained considering motions are acting at certain angle to the longitudinal axis of the bridge. Therefore, to check the failure possibility of bridge in any damage level, maximum rotations at all column ends of bridge are computed under each time history of ground motion. Fragility curves are developed considering θ as 15^0, 30^0, 45^0, 60^0 and 75^0 and plotted in figures 6-7 ~ 6-11. Tables 6-1 to 6-5 show the number of cases of bridge failure at each damage states and the corresponding fragility parameters for different inclinations of ground motion.

TABLE 6-1 Number of Damaged Bridges and Fragility Parameters of Bridge 2 for $\theta = 15^0$

Damage States	Damaged Bridges (Sample Size 60)	Fragility Parameters	
		c (g)	ζ
Almost No Damage	57	0.0694	1.096
Minor Damage	49	0.2847	
Moderate Damage	35	0.4990	
Major Damage	17	0.8500	
Collapse	5	1.2398	

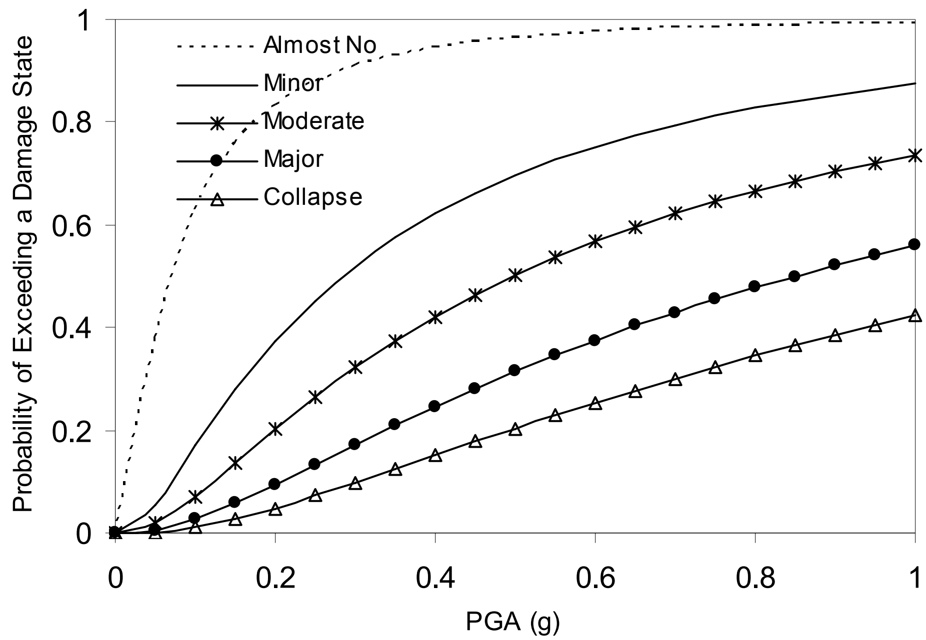

FIGURE 6-7 Fragility Curves of Bridge 2 for Five Damage States for $\theta = 15^0$

TABLE 6-2 Number of Damaged Bridges and Fragility Parameters of Bridge 2 for $\theta = 30^0$

Damage States	Damaged Bridges (Sample Size 60)	Fragility Parameters	
		c (g)	ζ
Almost No Damage	57	0.1041	1.001
Minor Damage	49	0.2541	
Moderate Damage	35	0.4755	
Major Damage	17	0.7755	
Collapse	5	1.0816	

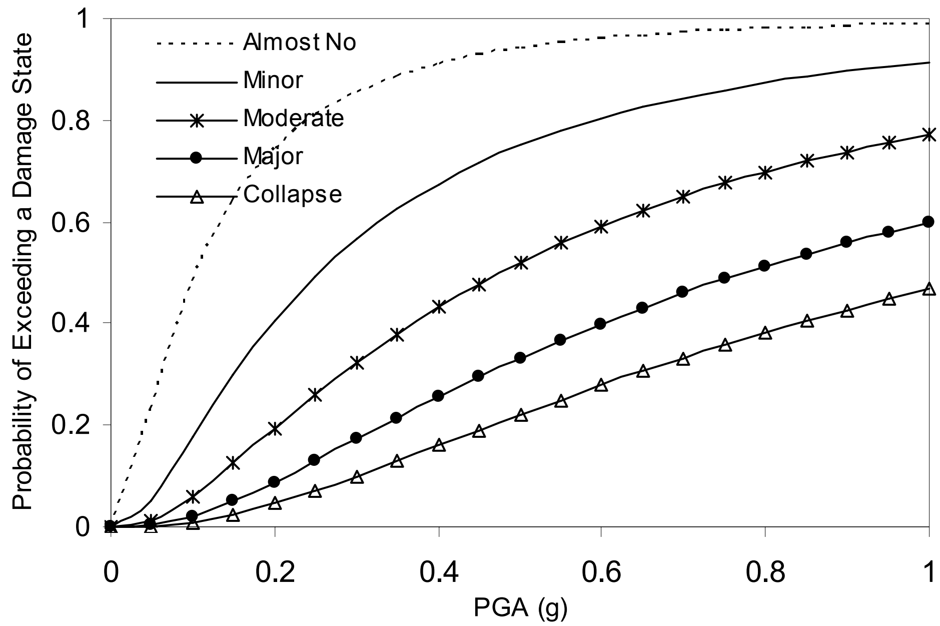

FIGURE 6-8 Fragility Curves of Bridge 2 for Five Damage States for $\theta = 30^0$

TABLE 6-3 Number of Damaged Bridges and Fragility Parameters of Bridge 2 for $\theta = 45^0$

Damage States	Damaged Bridges (Sample Size 60)	Fragility Parameters	
		c (g)	ζ
Almost No Damage	58	0.1041	0.962
Minor Damage	52	0.2541	
Moderate Damage	37	0.4531	
Major Damage	22	0.7255	
Collapse	13	1.0296	

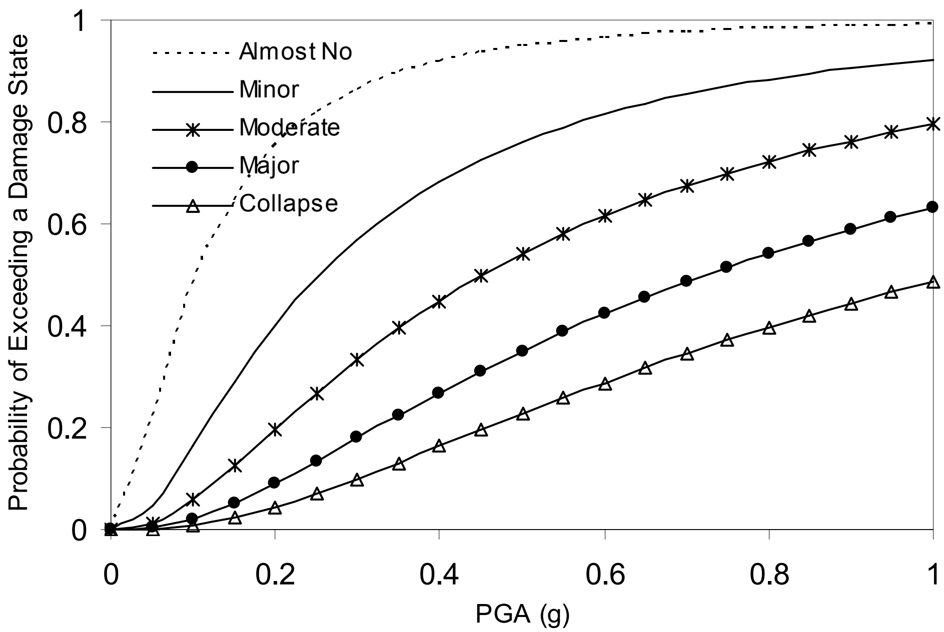

FIGURE 6-9 Fragility Curves of Bridge 2 for Five Damage States for $\theta = 45^0$

TABLE 6-4 Number of Damaged Bridges and Fragility Parameters of Bridge 2 for $\theta = 60^0$

Damage States	Damaged Bridges (Sample Size 60)	Fragility Parameters	
		c (g)	ζ
Almost No Damage	59	0.0286	1.011
Minor Damage	52	0.2541	
Moderate Damage	35	0.4898	
Major Damage	20	0.7602	
Collapse	14	0.9694	

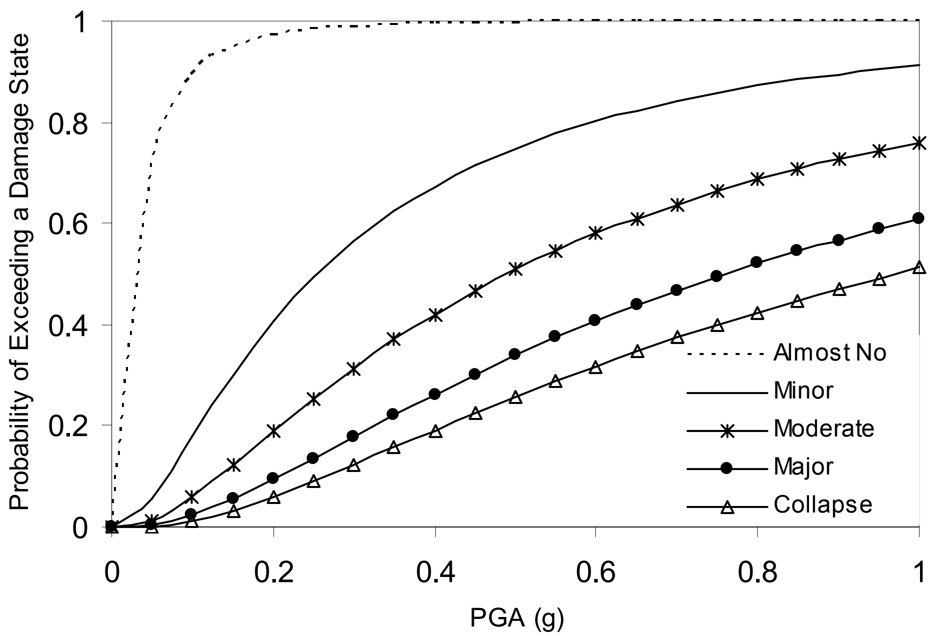

FIGURE 6-10 Fragility Curves of Bridge 2 for Five Damage States for $\theta = 60^0$

TABLE 6-5 Number of Damaged Bridges and Fragility Parameters of Bridge 2 for $\theta = 75^0$

Damage States	Damaged Bridges (Sample Size 60)	Fragility Parameters	
		c (g)	ζ
Almost No Damage	57	0.0694	1.015
Minor Damage	51	0.2510	
Moderate Damage	34	0.5174	
Major Damage	19	0.7776	
Collapse	11	1.2592	

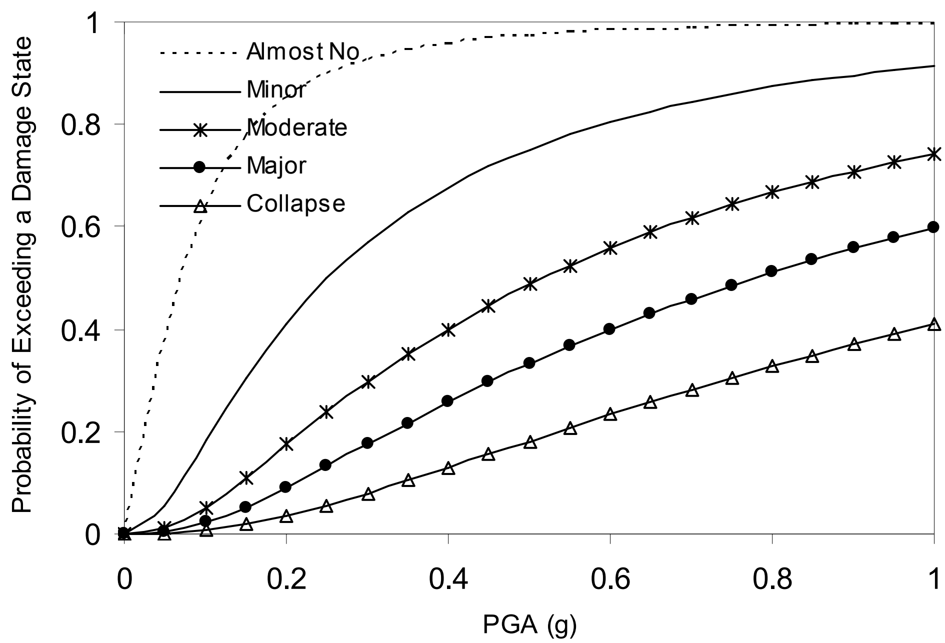

FIGURE 6-11 Fragility Curves of Bridge 2 for Five Damage States for $\theta = 75^0$

6.4 Effect of Ground Motion Directionality on Fragility Curves

From figures 6-7 ~ 6-11 it is clear that the bridge has nearly same failure probabilities in a particular damage state starting from 'Minor' to 'Major', when θ is varying from 30^0 to 60^0. The following figures (figures 6-12, 6-13 and 6-14) compare the fragility curves of Bridge 2 for 'Minor', 'Moderate' and 'Major' damage states respectively, for different inclinations (θ) of ground motions to the longitudinal axis of the bridge. Result shows that when ground motions come along the longitudinal axis of the bridge (i.e. $\theta = 0^0$), it has least probability of failure while that is maximum for $\theta = 45^0$. Fragility curves for $\theta = 90^0$ (along transverse direction) are stronger than that for $\theta = 45^0$ but weaker than those for $\theta = 0^0$. The trend is similar for all three damage states. Therefore, it can be concluded that for Bridge 2, the ground motions have maximum demand when they come with an inclination of 30^0 to 60^0 with the longitudinal direction of the bridge. Seismic performance analysis only considering ground motions along longitudinal or transverse directions of the bridge, underestimates the structural impact under the earthquake ground motions.

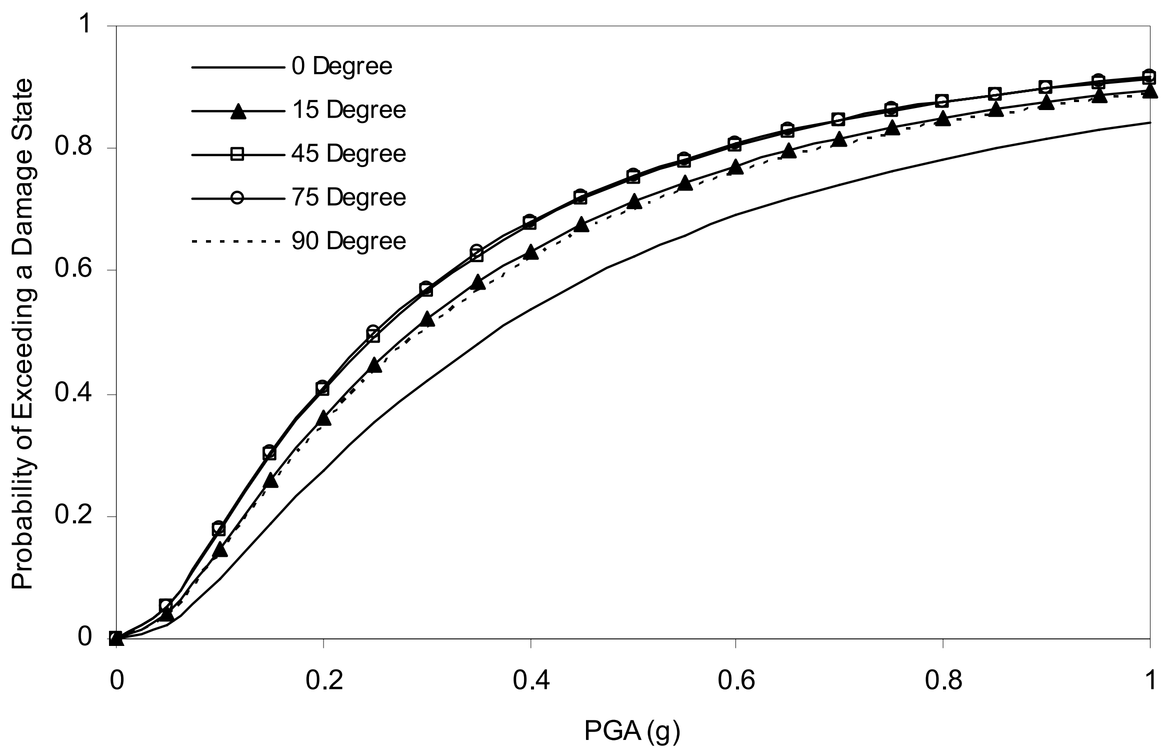

FIGURE 6-12 Fragility Curves of Bridge 2 for State of Minor Damage

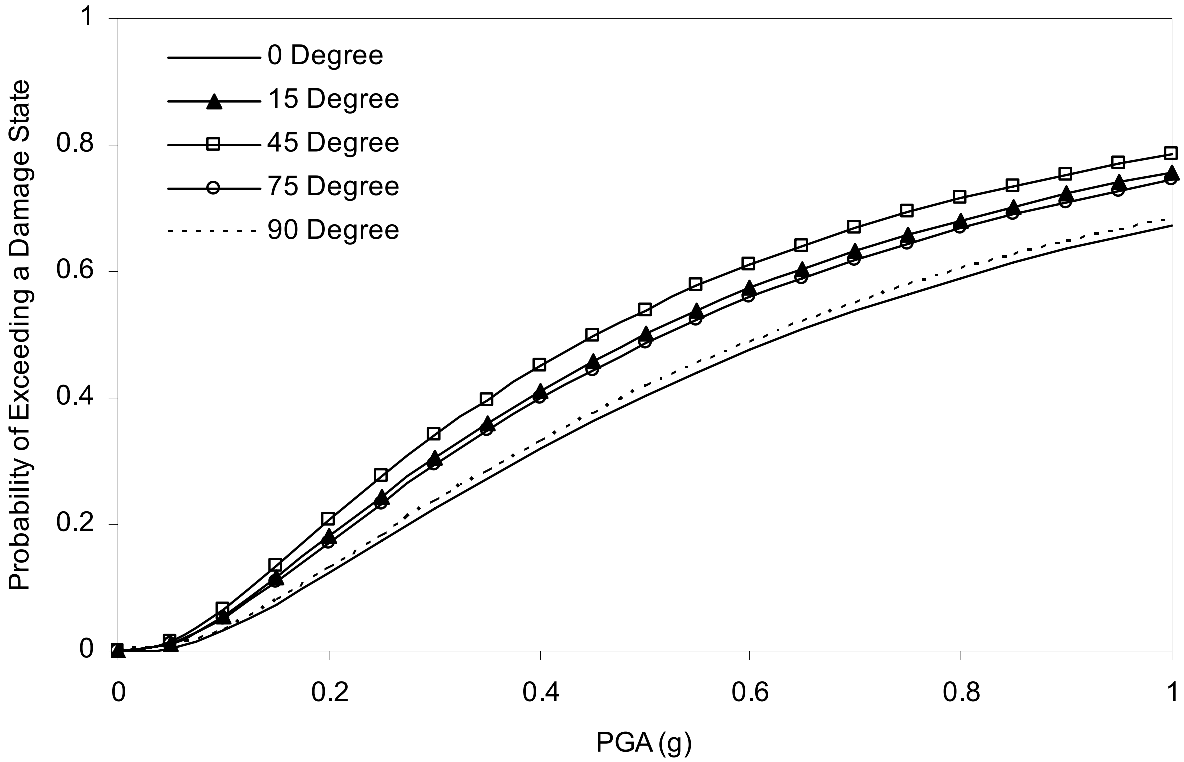

FIGURE 6-13 Fragility Curves of Bridge 2 for State of Moderate Damage

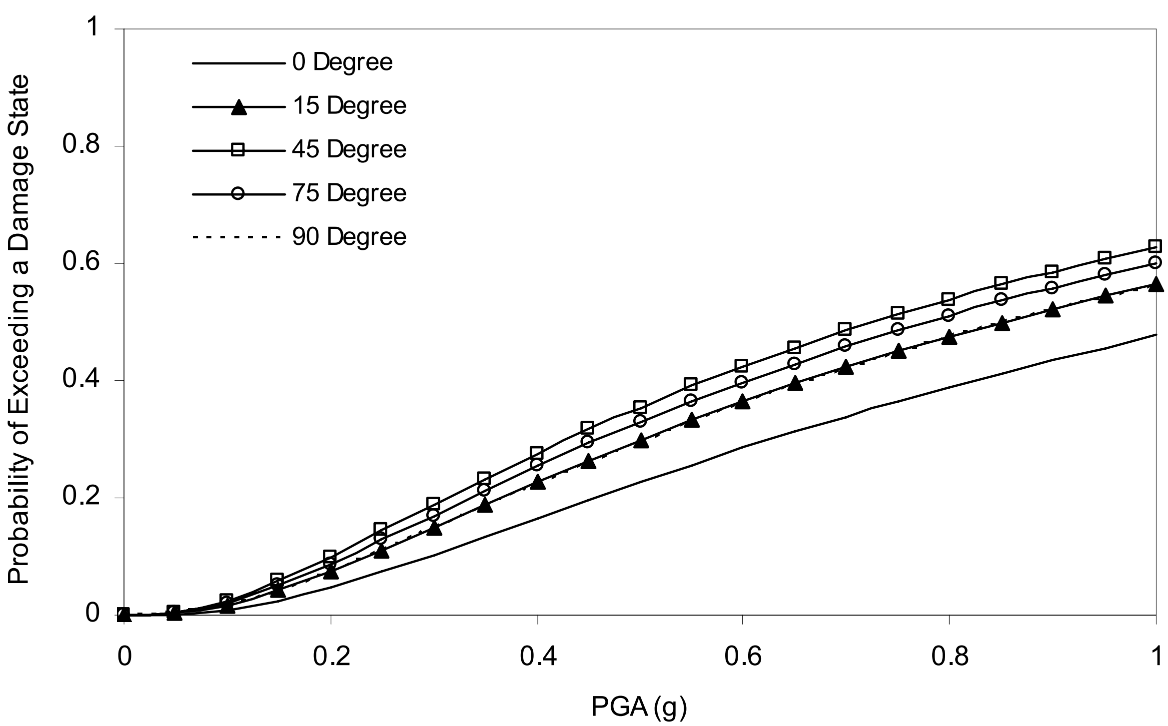

FIGURE 6-14 Fragility Curves of Bridge 2 for State of Major Damage

SECTION 7
FRAGILITY CURVE DEVELOPMENT USING CAPACITY SPECTRUM METHOD

Currently Capacity Spectrum Method (CSM), popularly known as pushover analysis, is in use for a rapid evaluation of structural performance under earthquake ground motion. It correlates structural capacity with the demand related to earthquake ground motion by means of graphical representation. Applied Technology Council (ATC-40, 1996) documented nonlinear static analysis procedures including CSM for seismic evaluation of concrete buildings. For the purpose of vulnerability assessment of bridges, this section develops the nonlinear static procedure involving CSM for construction of fragility curves incorporating performance-based engineering concept. Although analytical methods are available to perform nonlinear time history analysis, this method, as more practice-oriented, is expected to attract more interest and support from the profession.

Over past few years, CSM has been studied and applied for the seismic evaluation of structures, mainly RC buildings. This concept is currently under investigation for the use in bridge analysis, design and seismic evaluation (Fajfar et al., 1997, Abeysinghe et al., 2002 and Zheng at al., 2003). Fragility curves of Memphis bridges were developed using CSM following the procedure prescribed in ATC-40 (ATC, 1996) (Shinozuka et al., 2000). The fragility curves thus developed were in a good agreement with those developed by the nonlinear time-history analysis for one damage state but did not match very well for other damage state. Recently following the same methodology, pushover analysis was carried out for the evaluation of Grevniotikos Bridge in Greece (Abeysinghe et al., 2002), indicating that the use of CSM for the performance-based seismic evaluation of bridges is now acceptable.

In this study, CSM is used to evaluate the seismic performance of Bridge 2 for sixty (60) ground acceleration time histories in Los Angeles (table 3-1). Two spectra, “Demand Spectrum” that represents intensity of the seismic ground motion to which bridges are subjected, and “Capacity Spectrum” that represents the bridges’ ability to resist the seismic demand and the “Performance

Point" (i.e. the intersecting point of demand and capacity spectra) are the key elements in CSM. Because of the hysteretic damping of the structure during excitation, elastic response spectrum (5% damped) should be reduced to the inelastic response spectrum by an appropriate spectral reduction factor. Here one simplified approach (Reinhorn, 1997), alternative to the current professional design procedure given in ATC-40 (1996), is followed to reduce the seismic demand curve to take care of structural nonlinearity. Fragility curves at different damage levels are developed by numerically simulating the performance displacements. To check the reliability of this current analytical procedure, developed fragility curves are compared with those obtained from time history analysis of the bridge.

7.1 Fragility Analysis in Longitudinal Direction

7.1.1 Capacity Spectrum

Capacity curve is force-displacement curve that represents the capacity of the structure within and beyond elastic limit. To develop this plot, static nonlinear analysis (pushover analysis) is performed using *SAP2000 Nonlinear* computer code. Computation of total shear force generated at bridge supports as a function of displacement of the bridge girder constitutes the capacity curve by definition.

As stated in ATC-40 (1996) the 'lateral' forces (i.e., force in a horizontal plane acting along longitudinal/transverse direction) are applied in proportion to the fundamental mode shape, and is described as

$$F_i = \left(w_i \phi_i \Big/ \sum_{i=1}^{N} w_i \phi_i \right) V \tag{7-1}$$

where F_i is the 'lateral' force on node i $(i = 1, 2, \cdots, N)$, w_i is the dead weight assigned to node i, ϕ_i is the amplitude of the fundamental mode at node i, V the total base shear and N the number of nodes. To generate the capacity curve for building structures, the horizontal displacement at roof level is considered as a most critical displacement component. However, for bridge structures the displacements of the bridge girder in longitudinal direction is used to develop the capacity curve. In order to develop the capacity spectrum in any mode other than the fundamental mode, the effect of each of the higher modes should be incorporated in the lateral load pattern and all the modal parameters should be taken corresponding to the mode under consideration.

Bridge 2 has 1st mode (T_1 = 1.94 sec) of vibration in transverse direction and the next two modes (T_2 = 1.56 sec and T_3 = 1.39 sec) are in longitudinal direction as shown in figure 7-1. As second (2nd) and third (3rd) modes are very close to each other, modal combination rule is applied for these two modes to determine the 'lateral' forces at each node (7-1) of the bridge for longitudinal pushover analysis. Figures 7-2(a) and (b) are the capacity curves of the bridge obtained from pushover analysis which represent, respectively, the variation of the bridge girder displacement and rotation of plastic hinge regions at bridge column ends with the overall base shear force.

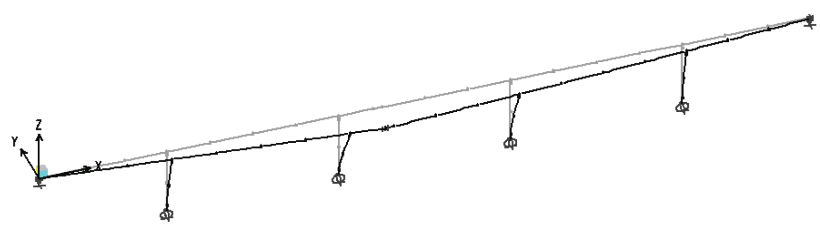

(a) Mode 1 in Transverse Direction

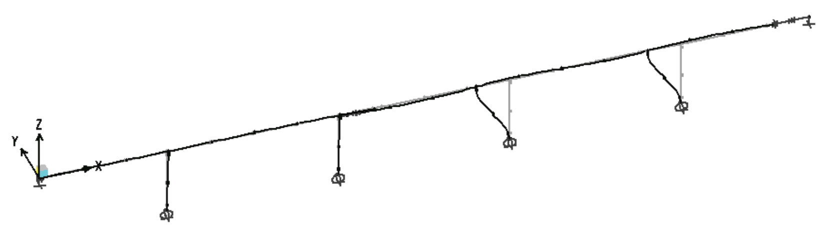

(b) Mode 2 in Longitudinal Direction

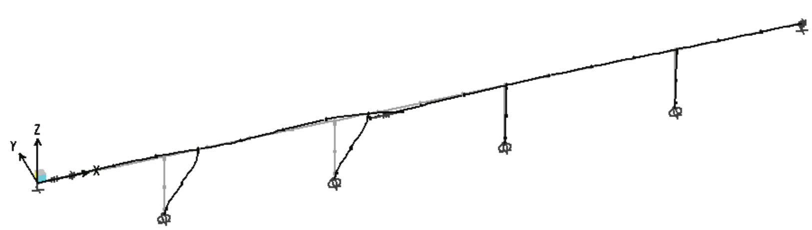

(b) Mode 3 in Longitudinal Direction

FIGURE 7-1 Mode Shapes of Bridge 2 in First 3 Modes

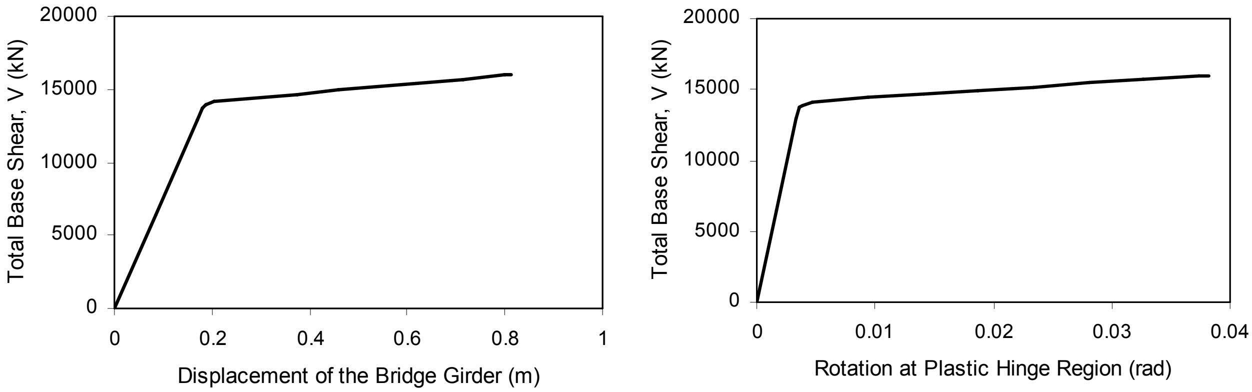

(a) (b)

FIGURE 7-2 Capacity Curves of Bridge 2 Derived from Pushover Analysis

According the general trend of CSM, it is required to convert the capacity curve to the capacity spectrum in ADRS (Acceleration-Displacement Response Spectra) format. Two measures of capacity spectrum, spectral acceleration S_a and spectral displacement S_d, can be estimated using the following equations;

$$S_a = \frac{V/W}{\alpha} \tag{7-2}$$

$$S_d = \frac{\Delta_{girder}}{PF\phi_{girder}} \tag{7-3}$$

where W overall dead weight of bridge, Δ_{girder} horizontal displacement of girder, ϕ_{girder} amplitude of the fundamental mode at girder, α and PF are modal mass coefficient and modal participation factor of the fundamental mode defined as follows

$$\alpha = \frac{\left[\sum_{i=1}^{N} (w_i \phi_i)/g\right]^2}{\left[\sum_{i=1}^{N} w_i/g\right]\left[\sum_{i=1}^{N} \left(w_i \phi_i^2\right)/g\right]} \tag{7-4}$$

$$PF = \left[\frac{\sum_{i=1}^{N} (w_i \phi_i)/g}{\sum_{i=1}^{N} \left(w_i \phi_i^2\right)/g}\right] \tag{7-5}$$

For longitudinal pushover analysis, modal combination rule is also applied to obtain α and PF and therefore, S_a and S_d. Figure 7-3 shows capacity spectrum of Bridge 2.

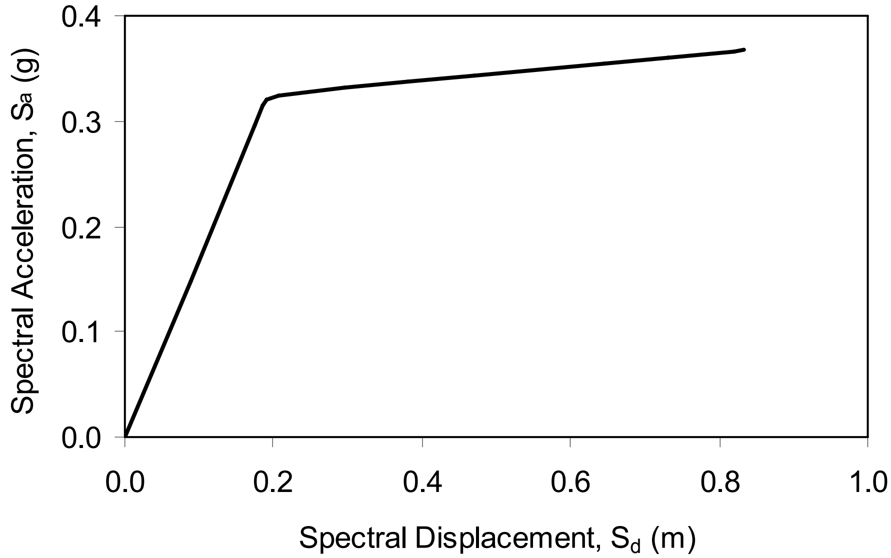

FIGURE 7-3 Capacity Spectrum of Bridge 2 in Longitudinal Direction

7.1.2 Demand Spectrum

Sixty elastic acceleration response spectra (5% damped) are generated from ground motion time histories (table 3-1). To use the CSM, these are converted to ADRS format as follows

$$S_d = \frac{T^2}{4\pi^2} S_a g \tag{7-6}$$

Figures 7-4 and 7-5 show the elastic acceleration response spectrum and corresponding demand spectrum for ground motion LA01.

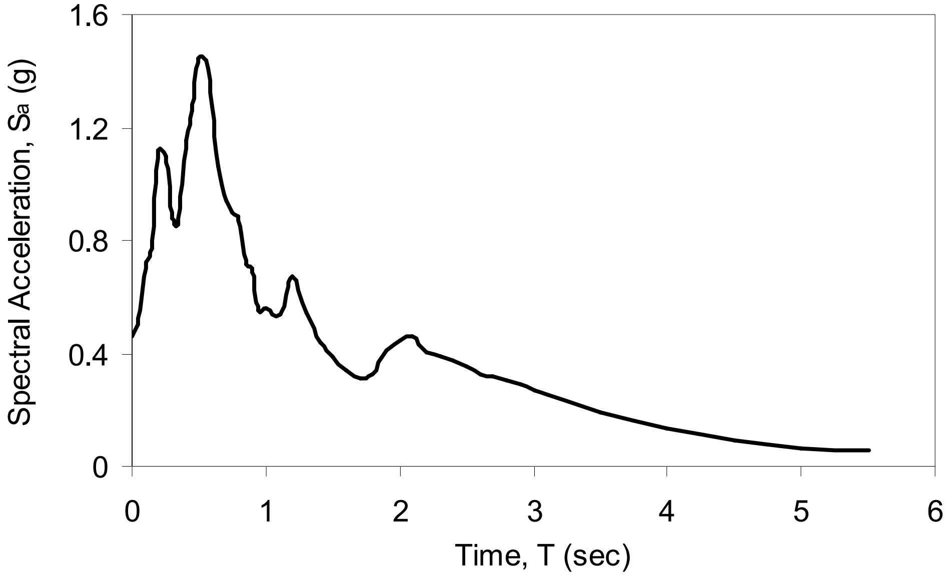

FIGURE 7-4 Elastic Acceleration Response Spectrum (5% Damped)

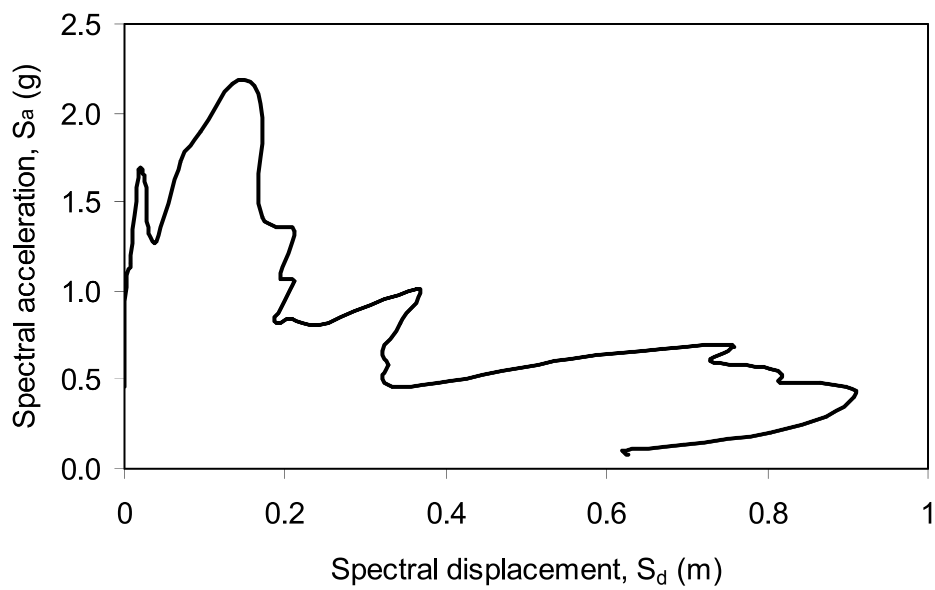

FIGURE 7-5 Acceleration-Displacement Response Spectrum

7.1.3 Performance Point

Performance point is the intersecting point of capacity spectrum with demand spectrum. To incorporate the energy dissipation of the structure through hysteretic behavior beyond yield, the elastic demand curve of the earthquake ground motion should be reduced. In a variation of ATC-40 (1996), recent studies developed few methods to determine inelastic demand spectra from elastic spectra (Fajfar, 1999, Miranda, 1994, Reinforn, 1997). In this study, the procedure given by Reinforn (1997) is used to produce the inelastic demand spectrum and, hence the inelastic response. According to this procedure, the inelastic spectral displacement (S_d^{in}) and inelastic spectral acceleration (S_a^{in}) can be expressed as

$$S_d^{in} = \frac{S_d^e}{R}\left\{1+\frac{1}{c}\left(R^c-1\right)\right\} \geq \frac{S_d^e}{R} \tag{7-7}$$

$$S_a^{in} = \frac{S_a^e}{R}\left[1+\alpha_{PY}\left\{\frac{1}{c}\left(R^c-1\right)\right\}\right] \tag{7-8}$$

where S_d^e and S_a^e, respectively are the elastic spectral displacement and acceleration, R is the reduction factor, c is a constant and α_{PY} is the post-yield hardening coefficient of the structure. The reduction factor R is defined as the ratio of maximum elastic force (Q^e/W) to the yield force (Q^y/W) as shown in figure 7-6. The constant c can be computed according to the following equation

$$c = \frac{T_o^a}{1+T_o^a}+\frac{b}{T_o} \tag{7-9}$$

where T_o is the initial time period of the capacity spectrum, a and b are factors as given in table 7-1 (Krawinkler and Nasser, 1992).

TABLE 7-1 Coefficients as Given in Krawinkler and Nasser (1992)

α_{PY}	a	b
0%	1.0	0.42
2%	1.0	0.37
10%	0.80	0.29

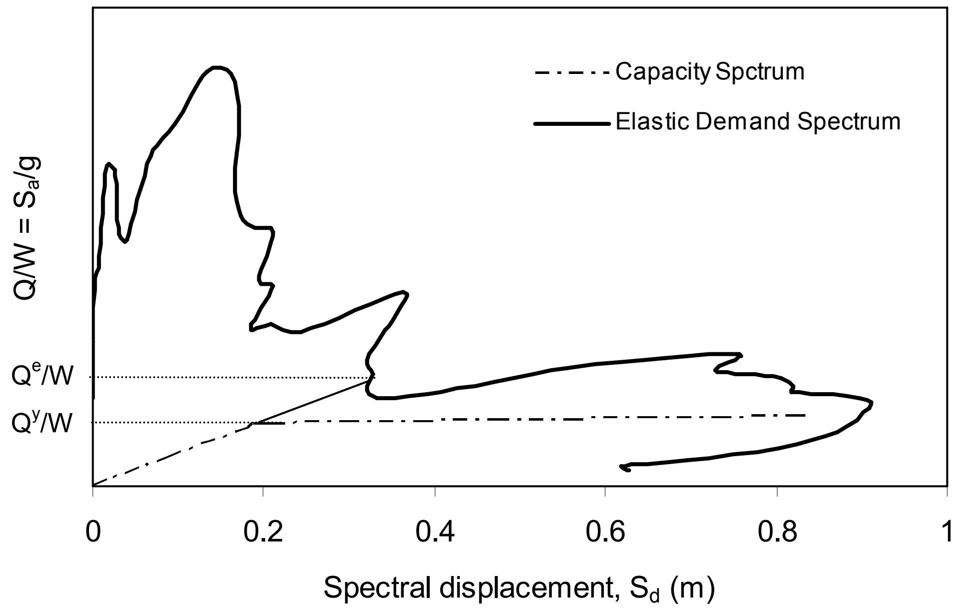

FIGURE 7-6 Estimation of Spectral Reduction Factor, *R*

Following this procedure, 60 inelastic demand spectra are generated from corresponding elastic demand spectra. Figure 7-7 shows the inelastic demand spectrum generated from the elastic spectrum of LA01.

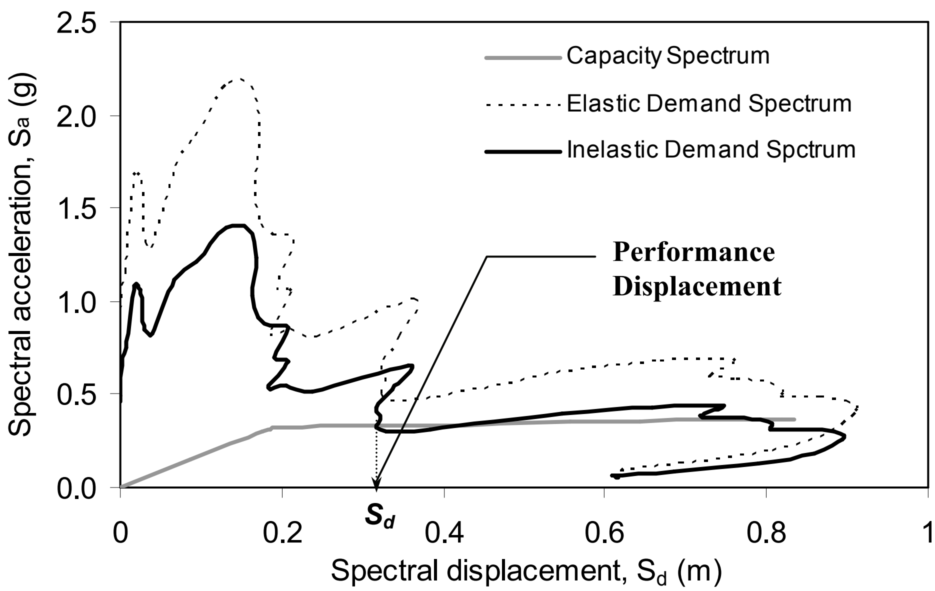

FIGURE 7-7 Calculation of Performance Displacement for LA01

The intersecting point of capacity and inelastic demand spectra represents structural performance under that particular ground motion (figure 7-7). It should be noted that the reduction factor R depends on the capacity curve of the structure as well as on the elastic demand curve of the ground motion under consideration. Hence, it is obvious that R will vary with different structures and earthquake ground motions.

7.1.4 Development of Fragility Curves in Longitudinal Direction

For sixty earthquake ground motions, sixty performance (spectral) displacements (S_d) are obtained separately and converted to the displacement of the bridge girder with the aid of following equation.

$$\Delta_{girder} = S_d \times PF \times \phi_{girder} \tag{7-10}$$

In correspond to the estimated displacements of the bridge girder for all sixty ground motions, rotations at plastic hinge regions of bridge columns are computed and used to develop the fragility curves as the damage states are defined on the basis of rotational ductility demand. To be consistent with the analytical fragility curves developed in the earlier section, the definition of damage states is kept unaltered. Number of damaged bridges for each damage states and fragility parameters are listed in table 7-2. In addition, figure 7-8 shows the fragility curves of Bridge 2 for all damage states.

TABLE 7-2 Number of Damaged Bridges and Fragility Parameters in Longitudinal Direction

Damage States	Damaged Bridges (Sample Size 60)	Fragility Parameters	
		$c(g)$	ζ
Almost No Damage	47	0.2184	1.249
Minor Damage	37	0.4020	
Moderate Damage	24	0.7122	
Major Damage	8	1.1520	
Collapse	3	1.4340	

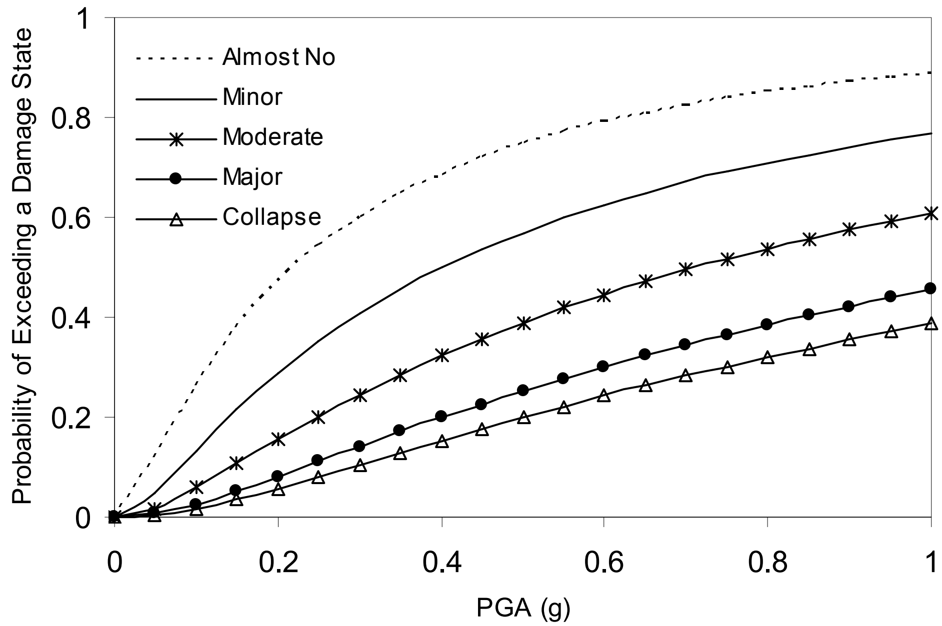

FIGURE 7-8 Fragility Curves of Bridge 2 for Five Damage States

7.2 Fragility Analysis in Transverse Direction

As stated earlier, Bridge 2 has its fundamental mode of vibration (T_1 = 1.95 sec) in transverse direction. Following the procedure described in the earlier part, the capacity of the bridge in transverse direction is computed and shown in is shown in figure 7-9.

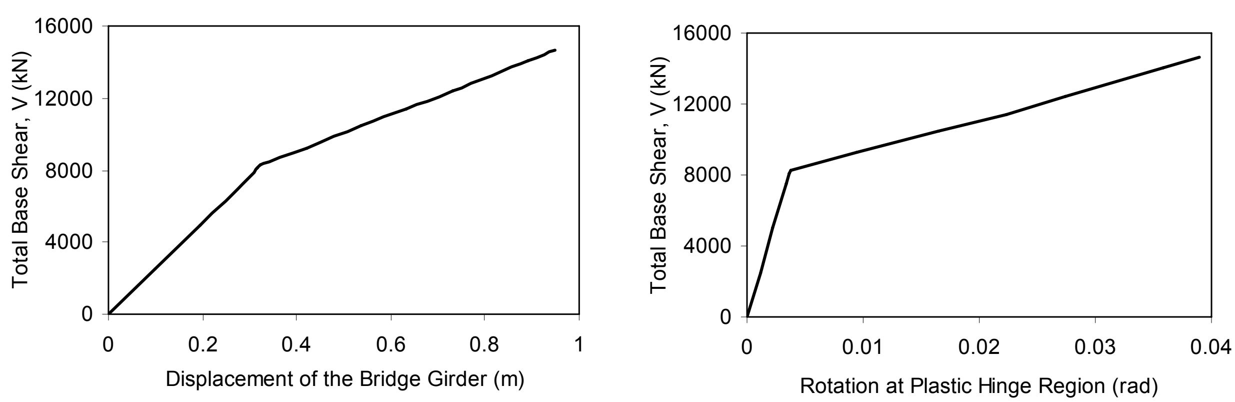

(a) (b)

FIGURE 7-9 Capacity Curves of Bridge 2 Derived from Pushover Analysis

Figure 7-9(a) is converted to the capacity spectrum and is shown in the following figure (figure 7-10).

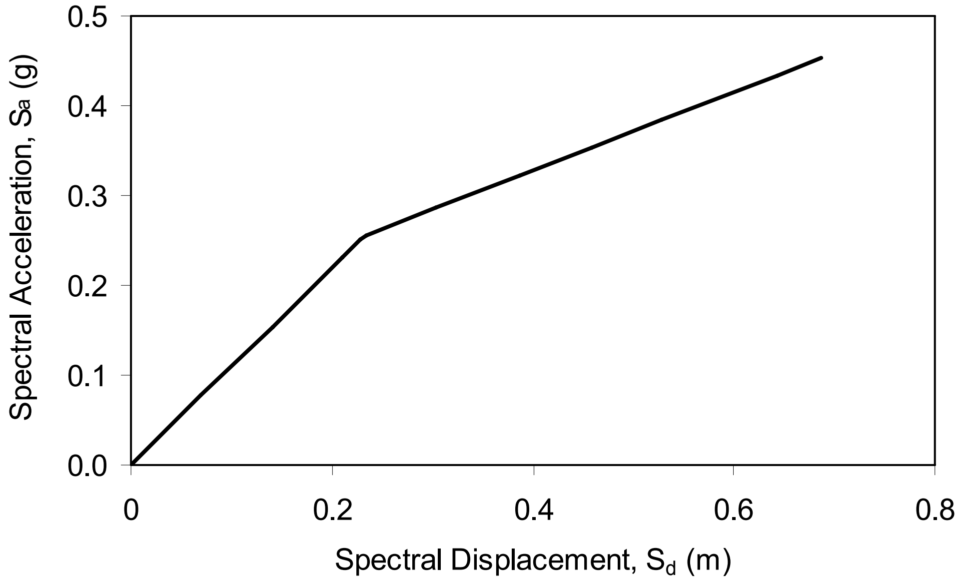

FIGURE 7-10 Capacity Spectrum of Bridge 2 in Transverse Direction

Fragility analysis in transverse direction of the bridge is done as described in Section 7.1.4. Number of damaged bridges for each damage states and fragility parameters are listed in table 7-3. In addition, figure 7-11 shows the fragility curves of Bridge 2 for all damage states.

TABLE 7-3 Number of Damaged Bridges and Fragility Parameters in Transverse Direction

<table>
<tr><th rowspan="2">Damage States</th><th rowspan="2">Damaged Bridges (Sample Size 60)</th><th colspan="2">Fragility Parameters</th></tr>
<tr><th>$c(g)$</th><th>ζ</th></tr>
<tr><td>Almost No Damage</td><td>43</td><td>0.2680</td><td rowspan="5">0.96</td></tr>
<tr><td>Minor Damage</td><td>38</td><td>0.3880</td></tr>
<tr><td>Moderate Damage</td><td>27</td><td>0.6408</td></tr>
<tr><td>Major Damage</td><td>17</td><td>0.8929</td></tr>
<tr><td>Collapse</td><td>10</td><td>1.0745</td></tr>
</table>

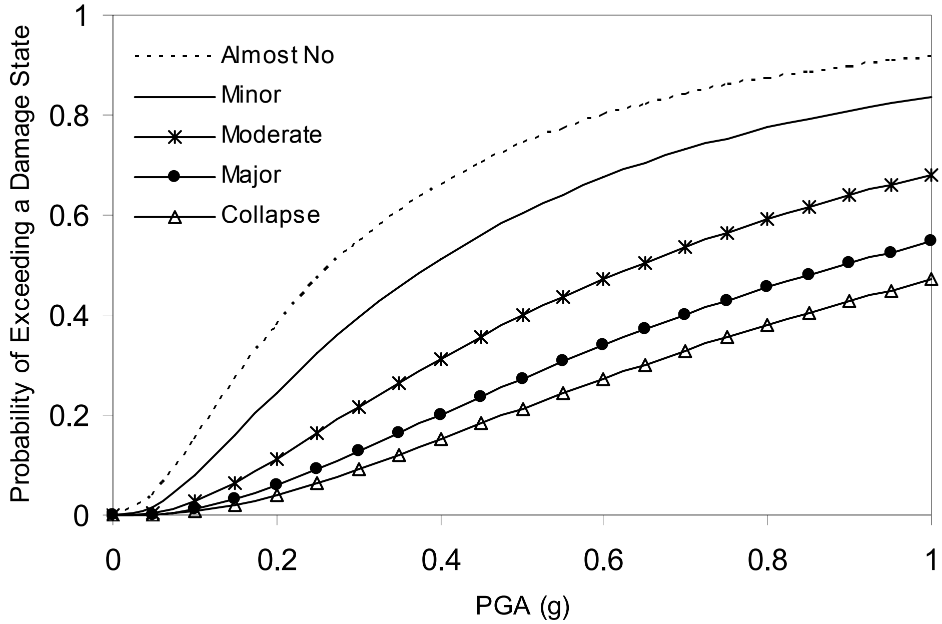

FIGURE 7-11 Fragility Curves of Bridge 2 for Five Damage States in Transverse Direction

7.3 Comparison of Analytical Fragility Curves

Since nonlinear time history analysis is commonly considered as accurate procedure to judge the performance of any structure, the analytical fragility curves developed using static nonlinear analysis are verified by considering the bridge response in time history analysis as an ideal guideline (figures 4-6 and 4-22). Figures 7-12 and 7-13 show the comparison in ‘Almost No’, ‘Minor’, ‘Moderate’ and ‘Major’ damage states of Bridge 2 in longitudinal and transverse direction, respectively.

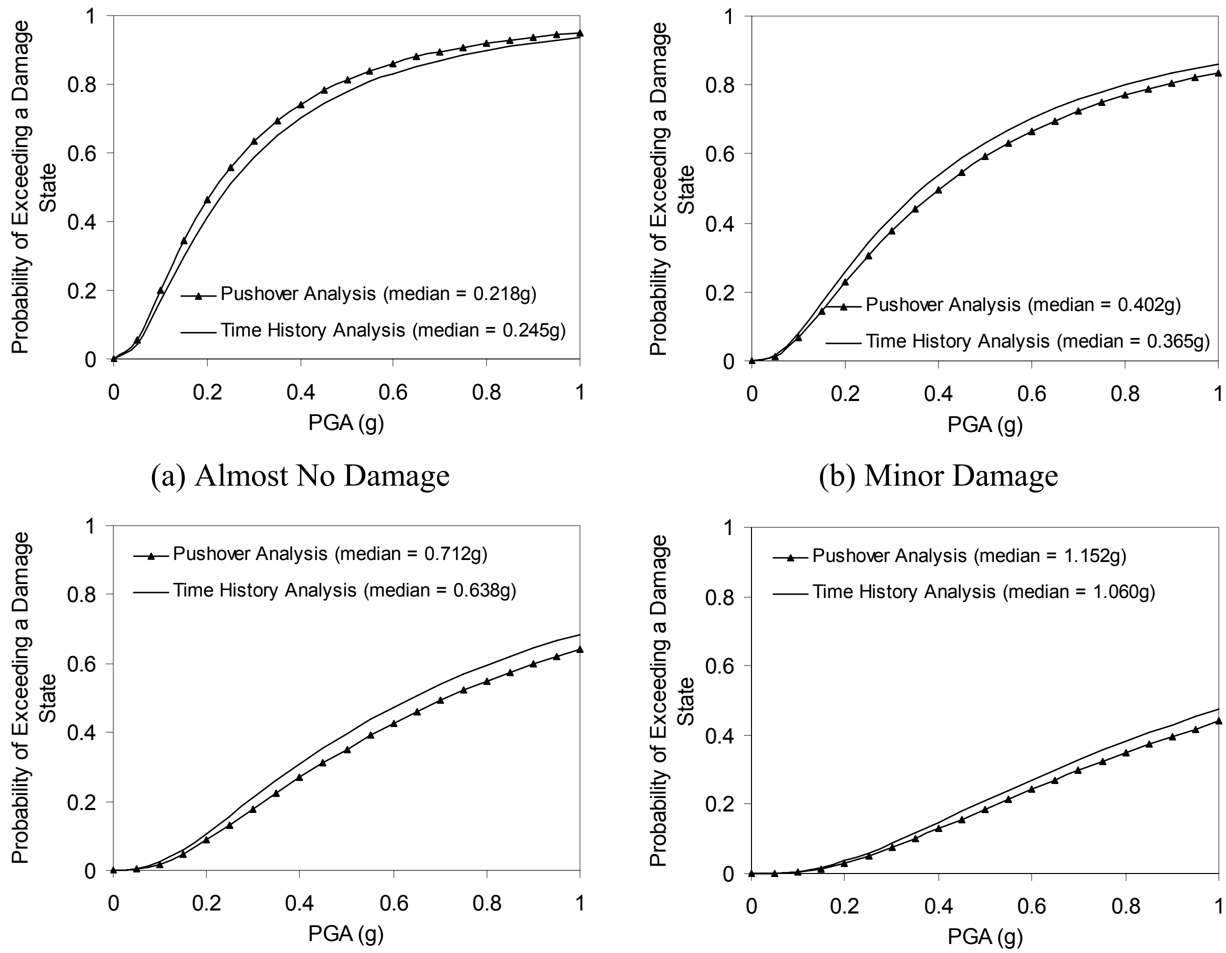

(a) Almost No Damage (b) Minor Damage

(c) Moderate Damage (d) Major Damage

FIGURE 7-12 Comparison of Fragility Curves of Bridge 2 in Longitudinal Direction

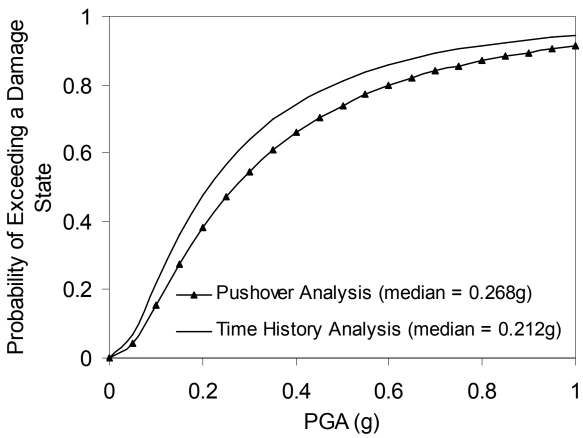

(a) Almost No Damage

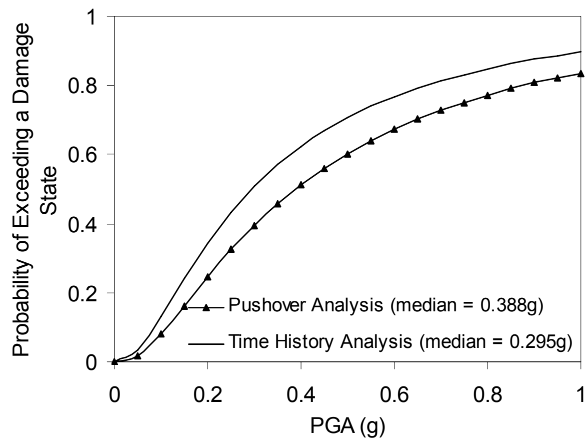

(b) Minor Damage

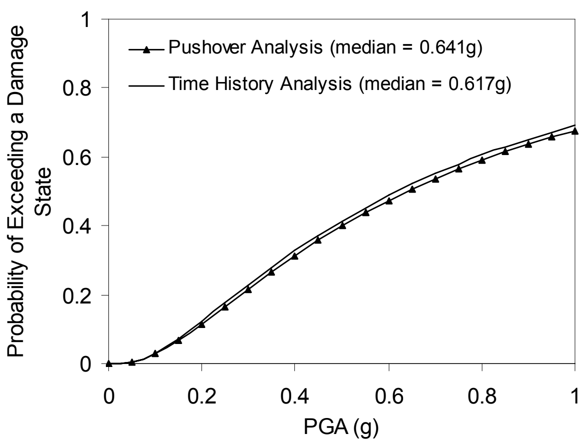

(c) Moderate Damage

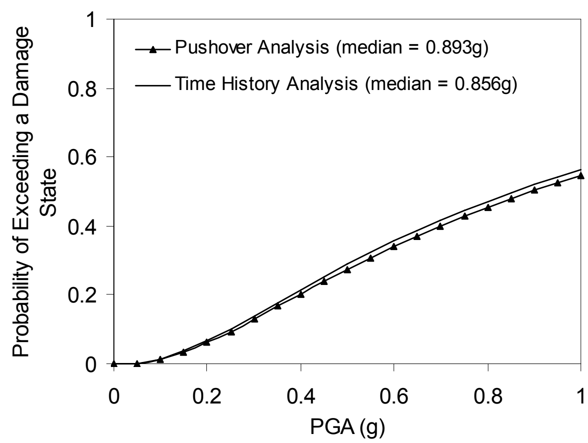

(d) Major Damage

FIGURE 7-13 Comparison of Fragility Curves of Bridge 2 in Transverse Direction

Result indicates, in all cases (four damage states in both longitudinal and transverse directions) analytical fragility curves derived from pushover analysis are in well accordance with those from time history analysis. Therefore this nonlinear static analysis method can be use successfully in seismic vulnerability analysis of bridges. Also this provides confidence to use this method to conduct seismic performance analysis of bridges when ground motion comes from any arbitrary direction.

SECTION 8
CONCLUSIONS

This report represents the seismic performance analysis of reinforced concrete bridges in the form of fragility curves which is a function of ground motion intensity. Nonlinear time history analyses of five (5) Caltrans' bridges are performed before and after column retrofit with steel jacketing. In addition to the dynamic analysis, pushover (nonlinear static) analysis is also conducted as it is more practice-oriented and appealing to the profession. To be consistent, developed fragility curves are calibrated with damage data of bridges from past earthquakes. Furthermore, this report addresses the issue of directionality effect of earthquake ground motion on structures in order to reflect on the fact that earthquake can come from any arbitrary direction to the structure.

Following are the conclusions that can be drawn from this study:

1. The result of progressive failure mechanism indicates that damage may result due to the formation of plastic hinges at column ends or due to the failure at expansion joint. Restrainer performs an important role in bridge failure to the bridge having expansion joints. There is also a probability, though small, of having shear failure at the plastic region of a shorter and stiffer bridge column. Bridge failure can also result from anchorage failure if restrainer and anchor are not designed properly.
2. Pounding does not result in any significant damage to the structure. Also impact force generated by pounding is not enough to make any significant change in the columns rotation. In reality, however, there is a high possibility of having non-uniform contact of adjacent decks at expansion joints due for example to the yaw motion of joining decks at different frequency. This may lead to localized damage by generating highly concentrated local stress field, even if the bridge has no geometrical skewness.
3. Seismic retrofit of bridge columns with steel jackets helps to improve the fragility characteristics of the bridges enormously. The enhancement curves of bridge retrofit are represented on the basis of least square fit of enhancement records from different damage states.

4. Fragility performance of a bridge in transverse direction is highly influenced by the abutment lateral stiffness coming from the backfill soil resistance. This stiffness should be considered carefully, as abutment lateral stiffness influences the bridge movement in transverse direction significantly.
5. The present analysis integrated statistical and mechanistic aspects of fragility curve development and revealed that ductility capacity converted from drift limits and used as definition of damage states results in excessively conservative estimate of fragility curves of bridges. To remedy this problem, this study established a method of adjusting mechanistic definition of damage state and produced analytical fragility curves from nonlinear time history analysis consistent with empirical damage data.
6. This study developed a practice-oriented method for seismic performance analysis of a structure, in the form of fragility curves, considering earthquake ground motions are coming from any arbitrary horizontal direction to the bridge structure. Result indicates that in seismic performance analysis, consideration of ground motion acting only along longitudinal and/or transverse directions of the bridge may underestimate the maximum seismic demand.
7. Fragility curves developed utilizing pushover (static nonlinear) procedure show excellent consistency with that obtained from nonlinear time history analysis. This method was further extended to evaluate the effect of ground motion directionality on bridge response.

There are some aspects that require further future study including:

1. Non-uniform (not face-to-face) impact at expansion joint and its effect of structural behavior.
2. At a more sophisticated level of analysis considering the random nature of 2D ground motion time histories, sensitivity of the bridge response to the correlation between the orthogonal components will be studied.

SECTION 9
REFERENCES

1. Abeysinghe, R. S., Gavaise, E., Rosignoli, M. and Tzavas, T., (2002), "Pushover Analysis of Inelastic Seismic Behavior of Grevniotikos Bridge", Journal of Bridge Engineering, ASCE, 7(2), 115-126.

2. Applied Technology Council (ATC), (1981), "ATC-6, Seismic Design Guidelines for Highway Bridges", Berkeley, California.

3. Applied Technology Council (ATC), (1996), "ATC-40, Seismic Evaluation and Retrofit of Concrete Buildings", Redwood City, California.

4. Basoz, N., and Kiremidjian, A. S., (1998), "Evaluation of bridge damage data from the Loma Prieta and Northridge, California earthquake", Technical Report MCEER-98-0004.

5. Buckle, I. G., (Editor) (1994), "The Northridge, California Earthquake of January 17, 1994: Performance of Highway Bridge", Technical Report, NCEER-94-0008, National Center for Earthquake Engineering Research, State University of New York, Buffalo.

6. California Department of Transportation, (2004), Bridge Design Criteria.

7. Chai, Y.H., Priestley, M.J.N. & Seible F., (1991), "Seismic Retrofit of Circular Bridge Columns for Enhanced Flexural Performance", ACI Structural Journal, V. 88 (No. 5), 572-584.

8. Computer and Structures, Inc., (1998), SAP2000/Nonlinear Users Manual, Berkeley, CA.

9. Dutta, A. & Mander, J.B., (1998), "Seismic Fragility Analysis of Highway Bridges", Proc., INCEDE-MCEER Center-to-Center Workshop on Earthquake Engineering Frontiers in Transportation Systems, Tokyo, Japan, 311-325.

10. Fajfar, P., Gaspersic, P. and Drobnic, D., (1997), "A Simplified Nonlinear Method for Seismic Damage Analysis of Structures", Seismic Design Methodologies for the Next Generation of Codes, Edited by P. Fajfar and H. Krawinkler, A.A. Balkema Publishers, Rotterdam, 183-194.

11. Fajfar, P., (1999), "Capacity Spectrum Method Based on Inelastic Demand Spectra", Earthquake Engineering and Structural Dynamics, 28, 979-993.

12. Federal Highway Administration (1996), Seismic Design of Bridges, Design Example No. 9 FHWA-SA-97-006.

13. Ghersi, A. and Rossi, P. P., (2001), "Influence of Bi-directional Ground Motions on the Inelastic Response of One-story In-pane Irregular Systems", J. Engineering Structures, 23(6), 579-591.

14. Hernandez, J. J. and Lopez, O. A., (2002), "Response to Three-Component Seismic Motion of Arbitrary Direction", J. Earthquake Engrg, and Struct. Dyn, 31, 55-77.

15. Kim, S-H., (2003), "Fragility Analysis of Bridges under Ground Motion with Spatial Variation", Ph.D. Dissertation, Department of Civil and Environmental Engineering, University of California, Irvine, CA.

16. Kim, S-H., and Shinozuka, M., (2003), "Effects of Seismically Induced Pounding at Expansion Joints of Concrete Bridges", J. Engrg. Mech., ASCE, 129(11), 1225-1234.

17. Krawinkler, H. and Nasser, A.A., (1992) "Seismic Design Based on Ductility and Cumulative Damage Demands and Capacities", Nonlinear Seismic Analysis and Design of Reinforced Concrete Buildings, Edited by Peter Fajfar and Helmut Krawinkler, Elsevier Science Publisher Ltd., New York, N.Y., 23-40.

18. Kushiyama, S., (2002), "Calculation Moment-Rotation Relationship of Reinforced Concrete Member with/without Steel Jacket", Unpublished Report at University of Southern California, CA, USA.

19. Miranda, E., and Bertero, V. V., (1994), "Evaluation of Strength Reduction Factors for Earthquake-resistance Design", Earthquake Spectra, 10(1), 357-379.

20. Priestley, M. J. N., Seible, F., and Calvi, G. M., (1996), Seismic Design and Retrofit of Bridges, John Wiley and Sons, Inc., NY.

21. Reinhorn, A.M., (1997), "Inelastic Analysis Techniques in Seismic Evaluation", Seismic Design Methodologies for the Next Generation of Codes, Edited by Peter Fajfar and Helmut Krawinkler, A.A. Balkema Publishers, Rotterdam, 277-287.

22. Riddell, R. and Santa-Maria, H., (1999), "Inelastic Response of One-story Asymmetric plan Systems Subjected to Bi-directional Earthquake Motions", J. Earthquake Engrg, and Struct. Dyn, 28, 273-285.

23. Roberts, J. E., (2005), "Caltrans Structural Control for Bridges in High-Seismic Zones", Earthquake Engrg, and Struct. Dyn., 34(4-5), 449-470.

24. Shinozuka, M., Feng, M. Q, Kim, H., Uzawa, T., and Uada, T., (2003a), "Statistical Analysis of Fragility Curves", Technical Report MCEER-03-0002, Multidisciplinary Center for Earthquake Engineering Research, The State University of New York at Buffalo.

25. Shinozuka, M., Murachi, Y., Dong, X., Zhou, Y., and Orlikowski, M. J., (2003b), "Effect of Seismic Retrofit of Bridges on Transportation Networks", Earthquake Engg. and Engg. Vibration, 2(2), 169-180.

26. Shinozuka, M., Feng, M. Q, Lee, J., and Naganuma, T., (2000), "Statistical Analysis of Fragility Curves", Journal of Engineering Mechanics, ASCE, Vol.126, No.12, 1224-1231.

27. Shinozuka, M. and Deodatis, G., (1996), "Simulation of Multi-Dimensional Gaussian Stochastic Fields by Spectral Representation", Applied Mechanics Review Vol. 49, No. 1, 29-53.

28. Stefano, M. D., Faella, G., and Ramasco, R., (1998), "Inelastic Seismic Response of One-way Plan-Asymmetric Systems under Bi-directional Ground Motions", J. Earthquake Engrg, and Struct. Dyn., 27, 363-376.

29. Wilson, E. L., and Button, M. R., (1982), "Three-dimensional Dynamic Analysis for Multi-component Earthquake Spectra", J. Earthquake Engineering and Structural Dynamics, 10, 471–476.

30. Wilson, E. L., Suharwardy, I., and Habibullah, A., (1995), "A Clarification of Orthogonal Effects in a Three-dimensional Seismic Analysis", Earthquake Spectra, 11(4), 659–666.

31. Zheng, Y., Usami, T. and Ge, H., (2003), "Seismic Response Predictions of Multi-span Steel Bridges Through Pushover Analysis", Earthquake Engineering and Structural Dynamics, 32, 1259-1274.

32. Zhou, Y., (2006), "Probabilistic Seismic Risk Assessment of Highway Transportation Network", Ph.D Dissertation, Department of Civil and Environmental Engineering, University of California, Irvine, USA.

APPENDIX A
MOMENT-CURVATURE RELATIONSHIP OF BRIDGE COLUMNS

The following program on moment-rotation analysis of bridge columns is developed by Dr. Shigeru Kushiyama (Kushiyama 2002) with collaboration with Professor Masanobu Shinozuka. This is done by utilizing the concept and equations presented in Priestley *et al*. (1996).

A.1 Basic Approach and Assumptions

In nonlinear analysis of reinforced concrete structures, moment-rotation relationship (M-θ relationship) of anti-symmetric members is necessary input data. In US codes, there is no empirical formula available to calculate M-θ relationship. Hence, this report focuses on the development of moment-rotation relationship (M-ϕ relationship) of structural members and background assumptions.

For this purpose, M-ϕ relationship is determined first from the stress balancing condition in a member section and then M-θ relationship is determined by evaluating damage zones and corresponding flexibility of these zone. Following are the assumption made for M-ϕ analysis.

1. Longitudinal strain in a section of a structural member is proportion to the distance of that section from the neutral axis, and this strain changes linearly.
2. Tensile stress of concrete is ignored.
3. The stress-strain curves of concrete and longitudinal steel reinforcement are defined as shown in Figures A.1 and A.2, respectively with reference to Priestley *et al*. (1996). Detail explanation is presented in the succeeding section.

Moment-rotation analysis is performed based on two basic assumptions; (1) Bending moment in a member changes linearly and (2) Material and cross-sectional properties of a member section remain identical along one of the member axes.

According to these assumptions, damage at the mid-span of a member will be smaller than that at the end. In cases when load such as vertical load is applied at the mid-span of the member or the arrangement of steel bars differs from end to the mid-span, problems can easily be solved by dividing the member into several segments.

A.2 Stress-Strain Curve of Concrete and Longitudinal Steel Reinforcement

A.2.1 Stress-Strain Curve of Concrete

The stress-strain relation of confined concrete surrounded by shear reinforcement is expressed in the following equations and presented in Figure A-1.

$$f_c = \frac{f'_{cc}\, xr}{r-1+x^r} \quad \text{for } (\varepsilon_c \le \varepsilon_{cu}) \tag{A-1}$$

where

$$f'_{cc} = f'_c \left(2.254\sqrt{1+\frac{7.94 f'_l}{f'_c}} - \frac{2 f'_l}{f'_c} - 1.254 \right) \tag{A-2}$$

$$x = \frac{\varepsilon_c}{\varepsilon_{cc}} \tag{A-3}$$

$$\varepsilon_{cc} = 0.002\left[1+5\left(\frac{f'_{cc}}{f'_c}-1\right)\right] \tag{A-4}$$

$$r = \frac{E_c}{E_c - E_{\sec}} \tag{A-5}$$

$$E_c = 5000\sqrt{f'_c} \text{ MPa} \tag{A-6}$$

$$E_{\sec} = \frac{f'_{cc}}{\varepsilon_{cc}} \tag{A-7}$$

where f'_c is the compressive strength of unconfined concrete, f'_{cc} and ε_{cc} are the stress and strain of confined concrete at peak stress and f'_l is the effective lateral confining stress. For circular or elliptic section,

$$f'_l = K_e f_l \tag{A-8}$$

where $K_e = 0.95$ and $f_l = \dfrac{2 f_{yh} A_{sp}}{D' s}$. For rectangular section,

$$f'_l = K_e f_{yh} (\rho_x + \rho_y) \tag{A-9}$$

where $K_e = 0.75$, $\rho_x = \dfrac{2A_{sp}}{D' s}$ and $\rho_y = \dfrac{2A_{sp}}{b' s}$.

In these equations, f_{yh}, A_{sp} and s respectively represent the yield stress, cross sectional area and spacing of the shear reinforcement, b' is the core width of confined concrete and D' is the diameter and side of the core respectively for circular and rectangular column.

Maximum tensile strain in steel reinforcement (ε_{cu}) is computed as

$$\varepsilon_{cu} = 0.004 + \frac{1.4 \rho_s f_{yh} \varepsilon_{su}}{f'_{cc}} \tag{A-10}$$

where $\rho_s = \dfrac{4A_{sp}}{D' s}$ for circular or elliptic section and $\rho_s = \rho_x + \rho_y$ for rectangular section.

For cover concrete, confining stress f'_l is zero. Hence, $f'_{cc} = f'_c$ and the stress-strain relation becomes

$$f_c = \frac{f'_c \, xr}{r - 1 + x^r} \text{ for } (\varepsilon_c < 2\varepsilon_{co}) \tag{A-11}$$

For $2\varepsilon_{co} \le \varepsilon_c \le \varepsilon_{sp}$, a straight line is assumed that connects f_c at $\varepsilon_c = 2\varepsilon_{co}$ with $f_c = 0$ at ε_{sp}. Beyond this point (i.e., $\varepsilon_c > \varepsilon_{sp}$), $f_c = 0$.

(a)

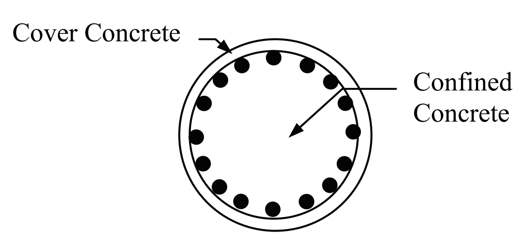

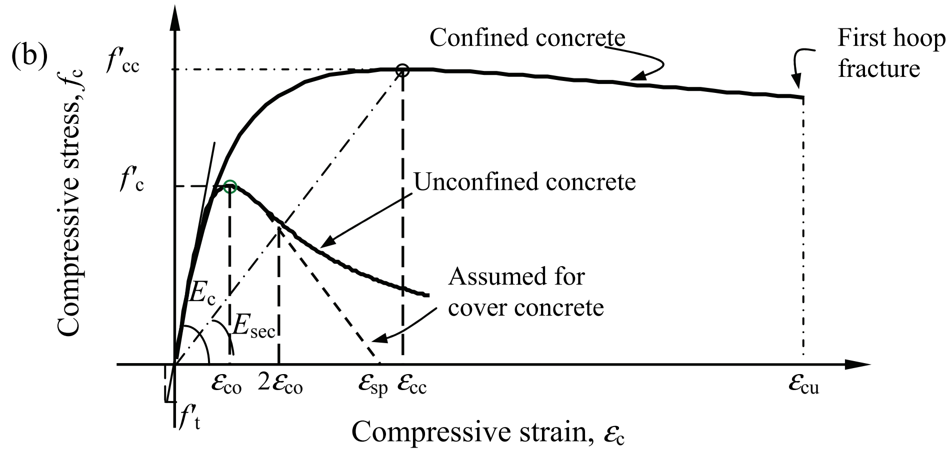

FIGURE A-1 (a) Column Cross-Section and (b) Stress- Strain Curve of Concrete

In a RC member confined with the steel jacket, confining effect is also expected in the zone between the jacket and shear reinforcement. Therefore, lateral confining stress (f'_l) is computed considering A_{sp} as combined area of lateral reinforcement and steel jacket for core concrete (i.e., inside the lateral reinforcement), while A_{sp} for cover concrete (i.e., outside the lateral reinforcement) is only the area of steel jackets.

A.2.2 Stress - Strain Curve of Longitudinal Steel Reinforcement

Stress-strain curve of longitudinal steel reinforcement includes strain hardening as shown in the following equations. For grade 60 reinforcement, normally used in the United States, this relation is expressed as below and shown in Figure A-2.

$$f_s = E_s \varepsilon_s \text{ for } (\varepsilon_s < \varepsilon_y) \quad \text{(A-12)}$$

$$f_s = f_y \text{ for } (\varepsilon_y \le \varepsilon_s \le \varepsilon_{sh}) \quad \text{(A-13)}$$

$$\text{and } f_s = f_y \left[1.5 - 0.5 \left(\frac{0.12 - \varepsilon_s}{0.112} \right)^2 \right] \text{ for } (\varepsilon_{sh} < \varepsilon_s \le \varepsilon_{su}) \quad \text{(A-14)}$$

where, $\varepsilon_{sh} = 0.008$, $\varepsilon_{su} = 0.12$ and $f_y = 1.1 \times$ Nominal yield strength of steel.

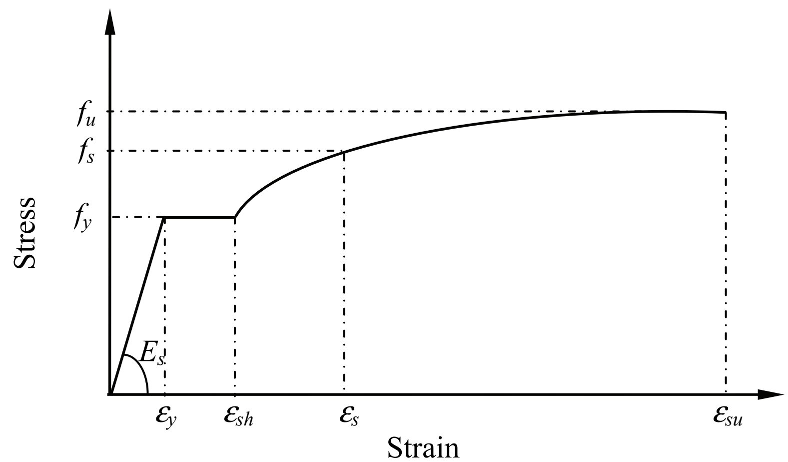

FIGURE A-2 Stress-Strain Curve of Steel

A.3 Calculation of Moment-Curvature (M-ϕ) Relationship

A.3.1 Crack Moment and Curvature (M_c and ϕ_c)

Crack develops in the tension side of a RC member when tensile stress at the tensile lower edge reaches to the tensile strength of concrete under stress balancing condition. However, in many cases crack moment (M_c) at which crack develops is very small. Here M_c is expressed by the following equation.

$$M_c = \left\{ f_t + \frac{N}{A_c + (E_s/E_c - 1)A_s} \right\} Z \tag{A-15}$$

where N is the axial force caused by dead load, f_t is the tensile strength of concrete that is given by $9.0\sqrt{(f'_c)}$ and f'_c is 28 days compressive strength of concrete. A_c is the cross-sectional area of the member; for rectangular section $A_c = BD$ and for elliptic section $A_c = \pi ab$ in which a and b are the radii of major and minor axes. $A_s = A_{sp} + A_s$ in which A_{sp} and A_s are the gross cross-sectional area of compressive reinforcement and tensile reinforcement, respectively. Section modulus, Z can be written as $Z = I_Z/(D/2)$ in which conversion moment of inertia, $I_Z = (I_c + I_s)$. Here, I_c represents the moment of inertia around the strong axis which is $bD^3/12$ for rectangular section and $\pi ba^3/4$ for elliptical section and I_s is the moment of inertia for reinforcement of multi-level bar arrangement that can be expressed as follows.

$$I_s = (E_s/E_c - 1)\sum_{i=1}^{n} A_{sp}^i\left(\frac{D}{2} - dp^i\right)^2 + (E_s/E_c - 1)\sum_{i=1}^{m} A_s^i\left(d^i - \frac{D}{2}\right)^2 \quad \text{(A-16)}$$

where n and m are the number of levels in compression and tension side, respectively. Therefore, the crack curvature, ϕ_c, can be expressed by

$$\phi_c = \frac{M_c}{EI} \quad \text{(A-17)}$$

where EI is the elastic bending rigidity. It should be noted here that immediately after the formation of crack, concrete in the tension side of the member cannot contribute to the moment of inertia. Hence, ϕ_c as computed from the above equation is the curvature just before crack appears.

A.3.2 Moment and Curvature at Yield (M_y and ϕ_y)

Yield moment (M_y) of a member depends on the level at which its tensile reinforcement yields. In a member with multi-level reinforcement arrangement, there is a possibility of having multiple M_y. In this case, under the same axial force (P), M_y is larger when inner reinforcement yields than that when outer reinforcement yields in the tension side of this member. This is because when inner reinforcement yields, outer reinforcement already exceeds its yield strain. Therefore, P and M_y have to be computed for all possible balanced conditions when reinforcement in a certain level yields and simultaneously, strain in the outer edge of confined concrete at compression side reaches to its maximum level of compressive strain, ε_{cu}. Thus, for a particular location of neutral axis c (where c is the distance from compressive upper edge to the neutral axis), M_y and P are calculated first at certain level considering that longitudinal reinforcement in that level maintains yield strain. Then, M_y and P are computed repeatedly by gradually reducing c so that strain at the compressive upper edge (ε_{upper}) reduces from ε_{cu} and thus M-P interaction curve for yield moment is developed. In this way multiple interaction curves are drawn for multi-level reinforcement arrangements.

Yield curvature (ϕ_y) can be computed using the following equation as longitudinal strain (ε) is equal to the product of the curvature (ϕ) and the position of neutral axis c.

$$\phi_y = \frac{\varepsilon_{upper}}{c} \tag{A-18}$$

It is assumed here that c is the distance from the compressive upper edge of the cover concrete to the neutral axis of the member when it is confined with steel jacket. Therefore, this assumption is not valid for members not confined with steel jacket. In such cases, compressive stress of cover concrete at the level of maximum compressive strain (ε_{cu}) is zero as already demonstrated in Figure A-1. However for the sake of simplicity, the above assumption is considered valid for the case of without jacket.

M_y of a member under axial force P (caused by dead load) is obtained as the intersection point of the straight line defined by $P_N = P$ and the interaction curve. From such M-P interaction curves, M_y and ϕ_y can be calculated immediately under axial loads different from dead load.

A.3.3 Maximum Moment and Curvature (M_{max} and ϕ_{max})

Maximum moment (M_{max}) is obtained in following three steps. In step I, moment at balanced reinforcement condition (M_b) and corresponding position of neutral axis (c_b) are calculated. Here, M_b is obtained under the condition that compression strain at the outer edge of confined concrete is ε_{cu} and at the same time, tensile reinforcement of the member at the first level yields.

In step II, maximum axial force (P_{max}) in pure compressive condition is calculated considering the variation in compressive strain as shown in Figure A-3. As this figure clearly indicates, it is not necessary that axial force becomes maximum (P_{max}) only at maximum compressive strain ε_{cu}.

In step III, M_{max} is calculated for certain location of neutral axis (c) when compressive strain at the upper edge of confined concrete is ε_{cu}. This is done in two ways; (*i*) by gradually increasing c_b so that c approaches to a value corresponding to the pure axial condition and (*ii*) by gradually reducing c_b so that c approaches to a value corresponding to the pure bending condition (i.e., axial force $P = 0$). Then, M-P interaction curve for maximum moment is drawn.

Figure A-4 shows an example of interaction curve developed utilizing the above procedure. As shown in this figure, maximum moment is not always larger than the yield moment in the entire range. This occurs depending on the shape of the stress-strain curves of concrete and reinforcing steel.

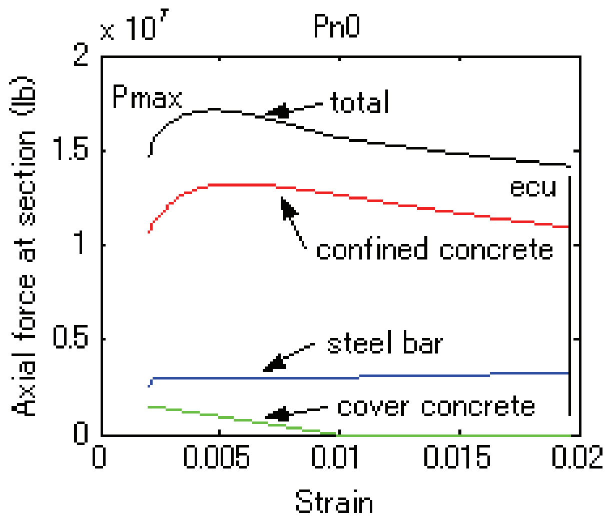

FIGURE A-3 Maximum Axial Force under Pure Compressive Condition

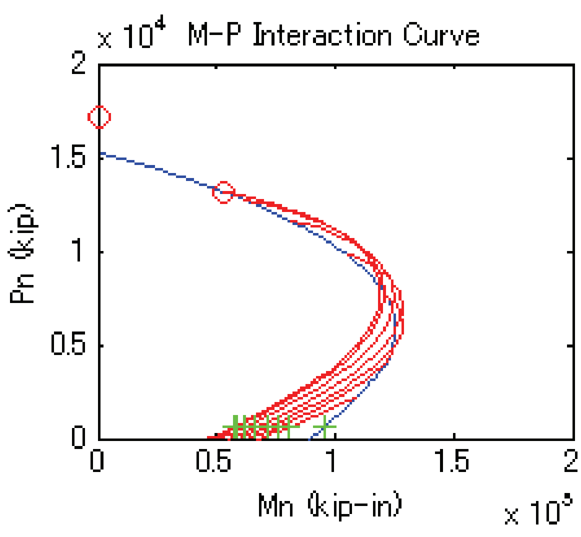

FIGURE A-4 *M-P* Interaction Curve

Therefore, curvature for the maximum moment is expressed as

$$\phi_{\max} = \frac{\varepsilon_{cu}}{c} \tag{A-19}$$

Maximum moment (M_{max}) under the axial force P can be obtained easily from the intersecting point of the straight line of P and the interaction curve (symbol + in Figure A-4). With these, M-ϕ relationship is derived and presented in Figure A-5.

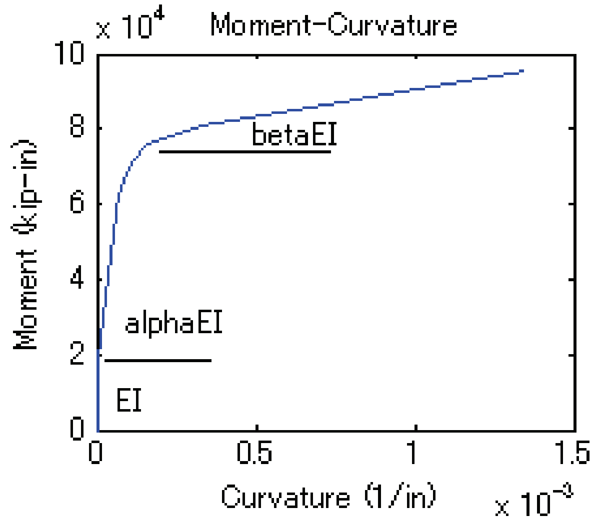

FIGURE A-5 Moment-Curvature Relationship

A.4 Calculation of Moment-Rotation (M-θ) Relationship

This section discusses about the development of moment-rotation (M-θ) relationship of structural members. The relation developed is considering members are anti-symmetric as it is not practical to obtain M-θ relationship for members with arbitrary moment distributions.

As indicated before, it is assumed that moment changes linearly along the member axis. Therefore, rotations θ_c, θ_y and θ_{max} correspond to moments M_c, M_y and M_{max} respectively. Fundamental approach to calculate rotation at the end of a member is:

(1) Flexibility for each damage zone is obtained by taking inverse of gradients of polygonal lines in M-ϕ relationship.

(2) Based on the moment distribution figure, range of each damage zone is determined. Contribution of each damage zone to the rotation at the end of member is calculated by

considering each range separately and corresponding flexibility. Finally, rotation at the end of member is obtained by adding all these contributions.

A.4.1 Distribution of Bending Moment and Curvature along a Member Axis

Prior to the development of moment-rotation relation, bending moment distribution and curvature distribution over the member axis are evaluated. Moment-curvature analysis is performed by assuming that

1. the longitudinal strain in a member section is proportional to its distance from the neutral axis of this member, and this strain changes linearly,
2. tensile stress of concrete is negligent, and
3. stress-strain curves of concrete and longitudinal steel reinforcement are defined as given in Priestley *et al*. (1996) and presented in Figures A-1 and A-2.

Obtained moment-rotation relation can be approximated in bi-linear or tri-linear fashion.

Distributions of bending moment and curvature along the member axis are shown in Figures 6(a) and (b), respectively. As indicated in these figures, curvature distribution is discontinuous at the point when crack moment (M_c) develops. This happens because concrete looses its tensile strength after crack appears and simultaneously, bending rigidity decreases from EI to EI_c. Therefore, before cracking curvature is computed as $\phi_c = \dfrac{M_c}{EI}$ while after cracking this is $\phi_c = \dfrac{M_c}{EI_c}$. This also results in the increase of member flexibility. Figure A-7 shows the distribution of inverse bending rigidity of a member (i.e., flexibility). Bending rigidity is EI when the member is in elastic zone. The same is respectively as αEI and βEI when the member is in between cracking and yield zone, and at maximum moment zone. These values correspond to the gradients of polygonal lines in M-ϕ relation as shown in Figure A-5. Therefore, member flexibility remains constant in each damage zone and increases with the progression of damage.

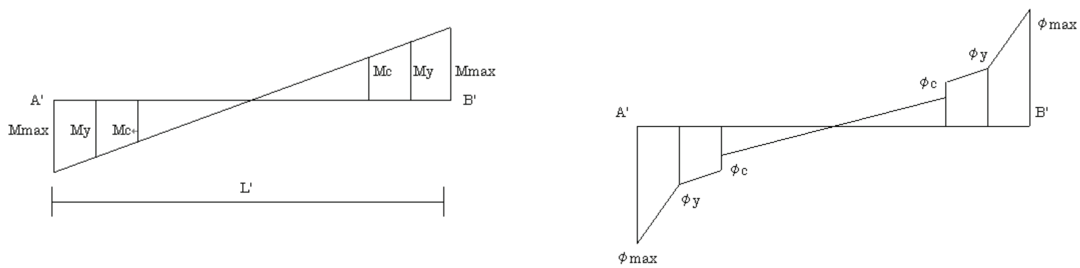

(a) (b)

Figure A.6 (a) Moment and (b) Curvature Distribution

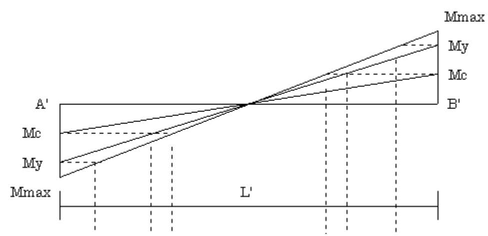

(a) Moment

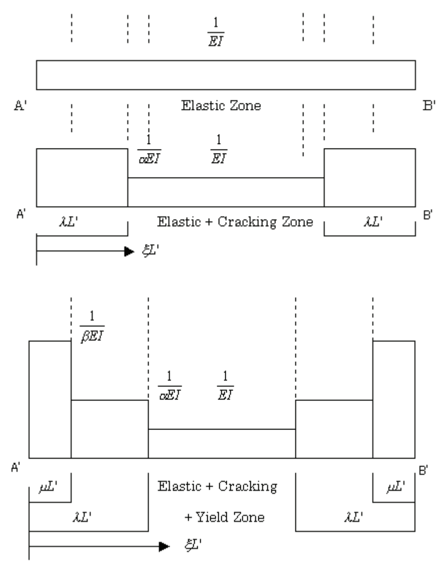

(b) Flexibility

FIGYRE A-7 Member Flexibility According to Generated Moment

A.4.2 Moment-Curvature (M- θ) Relationship at the End of the Member

If the bending rigidity distribution along a member axis is $EI(\xi)$, bending moment at an arbitrary point is expressed as $M(\xi) = M_{A'} - (M_{A'} + M_{B'})\xi$, where $M_{A'}$ and $M_{B'}$ are the moments at end A' and B', respectively. Therefore bending moment, by considering unit moment at A', is given by $\overline{M}_A(\xi) = 1 - \xi$ and the same, by considering unit moment at B', is $\overline{M}_B(\xi) = -\xi$. Hence, from the principle of virtual work, rotations at A' and B' are

$$\theta_{A'} = L'\int_0^1 \frac{M(\xi)\overline{M}_A(\xi)}{EI(\xi)} d\xi \tag{A-20}$$

$$\theta_{B'} = L'\int_0^1 \frac{M(\xi)\overline{M}_B(\xi)}{EI(\xi)} d\xi \tag{A-21}$$

If the flexibility in an arbitrary damage zone is as shown in Figure A-8, the contribution to rotation of end A' can be expressed by following equation.

$$\theta_{A'} = \frac{L'}{rEI}\int_a^b M(\xi)(1-\xi)d\xi \tag{A-22}$$

where, r represents 1, α, β.

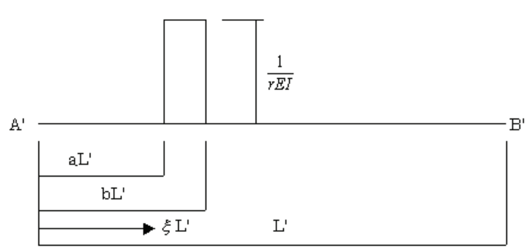

FIGURE A-8 Member Flexibility at any Arbitrary Range

If the end moment is equal to the crack moment, i.e., $M_{A'} = M_{B'} = M_c$, corresponding flexibility is $1/EI$ as the whole member is in elastic zone. Considering the integral range, $0 \le \xi \le 1$, crack rotation θ_c can be expressed as

$$\theta_c (= \theta_{A'}) = \frac{L'}{EI}\int_0^1 (M_c - 2M_c\xi)(1-\xi)d\xi = \frac{L'M_c}{6EI} \tag{A-23}$$

This value is equal to the rotation of an anti-symmetric member in the theory of elasticity.

Rotation corresponding to yield moment M_y is referred to as yield rotation θ_y. As depicted from Figure A.7(b), θ_y is obtained by adding up all contributions to rotation coming from three damage zones: two crack zones at section edges, elastic zone at the mid-span. At that time, $M(\xi)$ is written as $M(\xi) = (M_y - 2M_y\xi)$ in the equation (A-22), and three integral ranges are as $0 \sim \lambda$, $\lambda \sim (1\text{-}\lambda)$, $(1\text{-}\lambda) \sim 1$, respectively, where $\lambda = (1 - M_c/M_y)/2$. After integrating, rotation at end A' can be obtained by adding all contributions from three abovementioned damage zones.

As already discussed, yield moment (M_y) is a particular value either obtained exclusively or regarded as the minimum among all calculated yield moments of a member. The usage for M_y after the second or the maximum moment (M_{max}) is as follows. If M_y after the second or the maximum moment (M_{max}) is given by $\widetilde{M}$, $M(\xi)$ is expressed as $M(\xi) = \widetilde{M} - 2\widetilde{M}\xi$. Integration ranges are $0 \sim \mu_i$, $\mu_i \sim \mu_{i\text{-}1}$,…, $\mu_2 \sim \mu_1$, $\mu_1 \sim \lambda$, $\lambda \sim (1\text{-}\lambda)$, $(1\text{-}\lambda) \sim (1\text{-} \mu_1)$, $(1\text{-} \mu_1) \sim (1\text{-} \mu_2)$,…, $(1\text{-}\mu_{i-1}) \sim (1\text{-} \mu_i)$, $(1\text{-} \mu_i) \sim 1$, respectively, where $\lambda = (1 - M_c / \widetilde{M})/2$, $\mu_j = (1 - M_{y\_j} / \widetilde{M})/2$ and $j = 1 \sim i$, $M_{y\_j} > M_{y\_j\text{-}1} >\ldots> M_{y\_1}$. Therefore, rotation at end A' is obtained by adding all contributions from all damage zones. Figure A-9 is an example of the M-θ relationship obtained using the above procedure for a member with clear-span length of 4.57 m (15 ft).

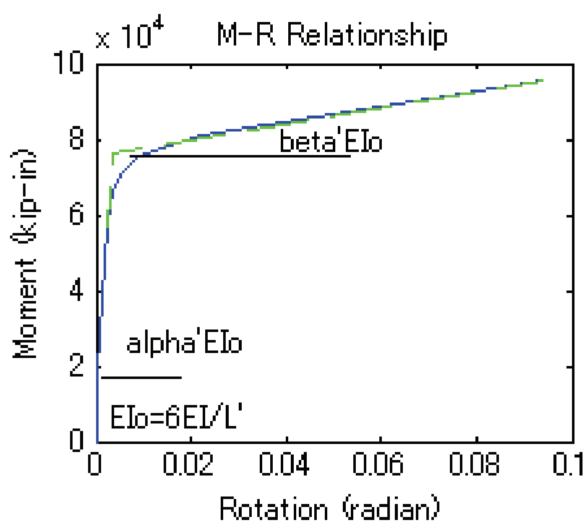

FIGURE A-9 Moment-Rotation Relationship

A.5 Moment-Rotation Curves of Example Bridges

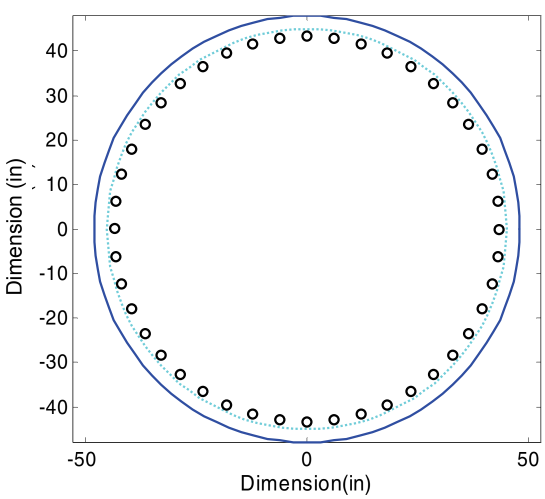

Section of Column

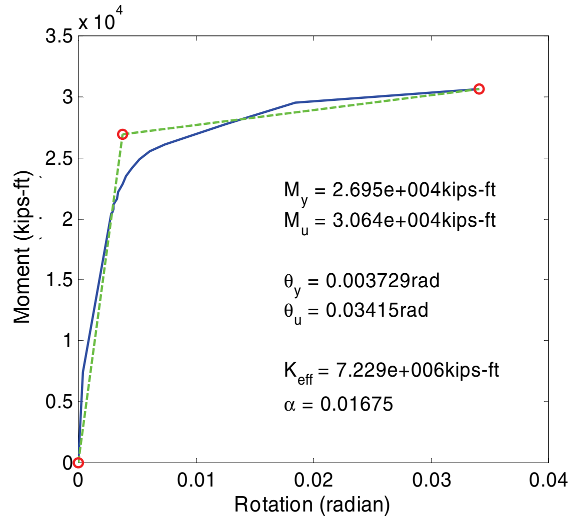

Moment-Rotation Curve

(a) Before Retrofit

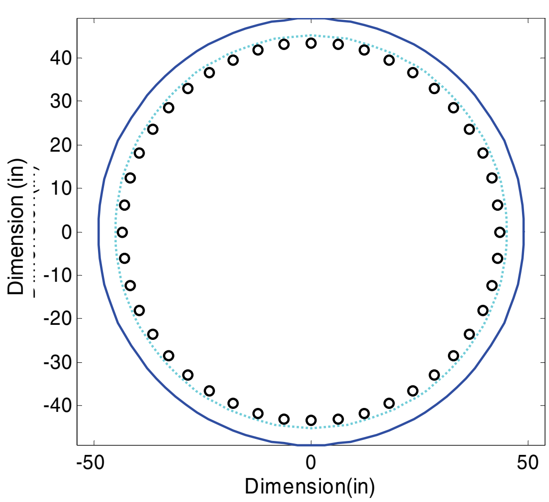

(a) Section of Column

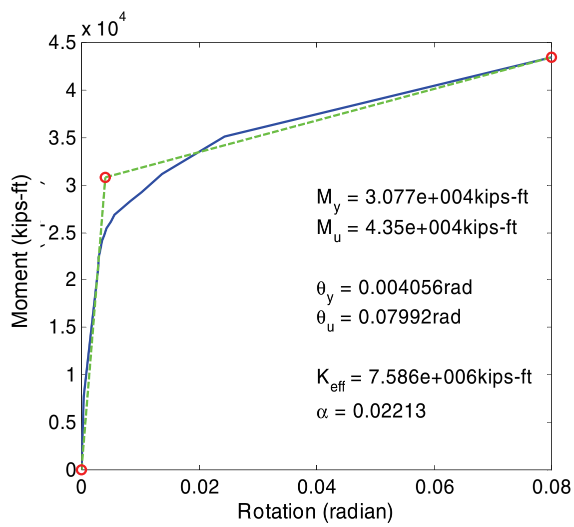

(b) Moment-Rotation Curve

(b) After Retrofit

FIGURE A-10 Moment-Curvature Analysis of Column 1 of Bridge 2

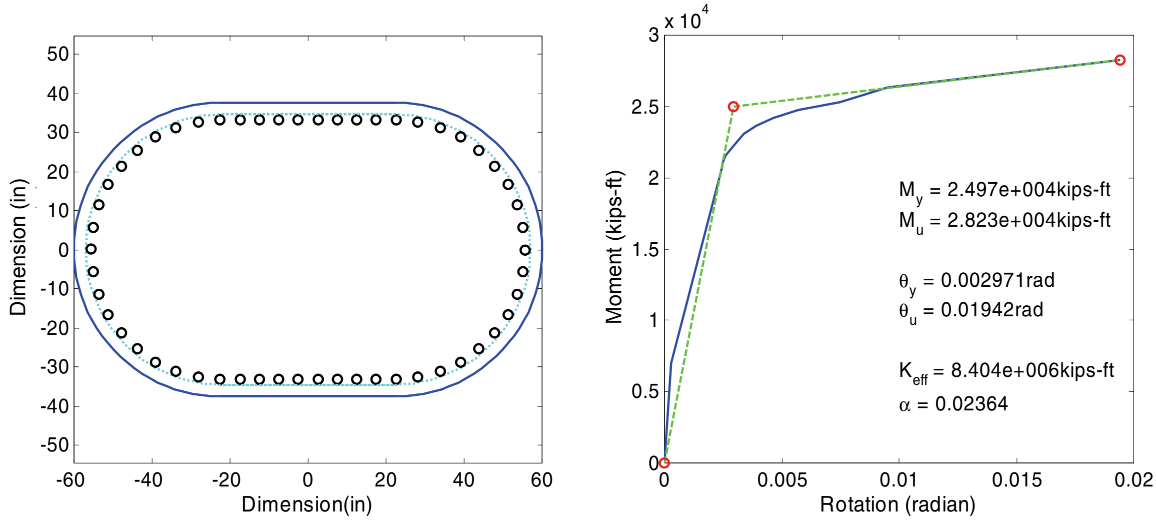

Section of Column | Moment-Rotation Curve

(a) Before Retrofit

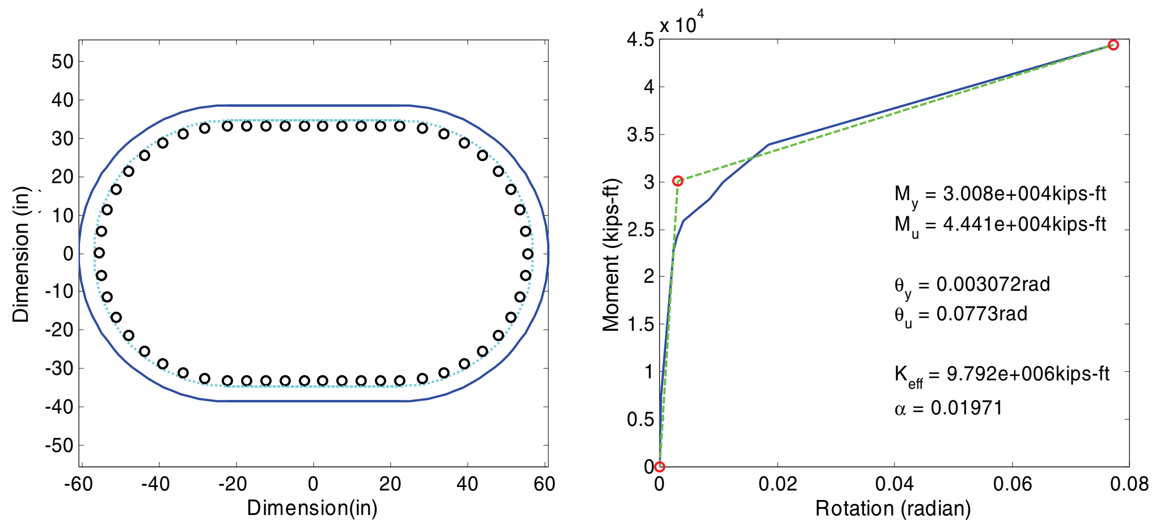

Section of Column | Moment-Rotation Curve

(b) After Retrofit

FIGURE A-11 Moment-Curvature Analysis of Column 1 of Bridge 3 in Longitudinal Direction

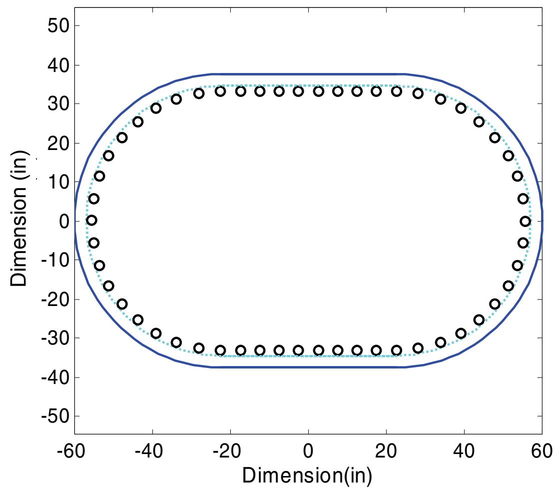

Section of Column

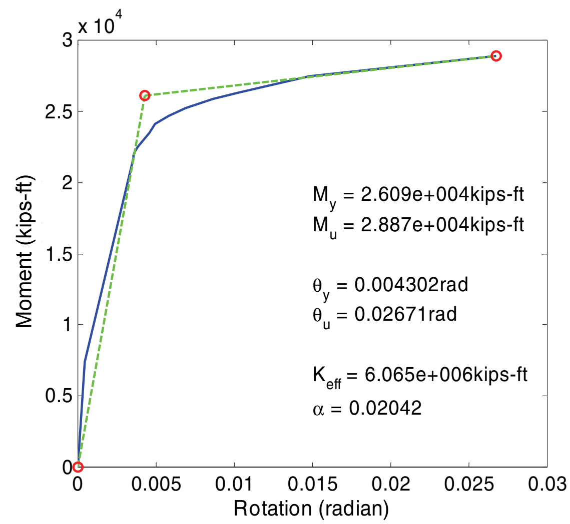

Moment-Rotation Curve

(a) Before Retrofit

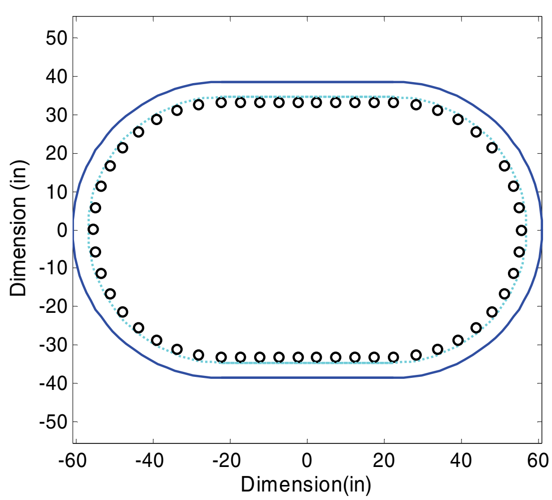

Section of Column

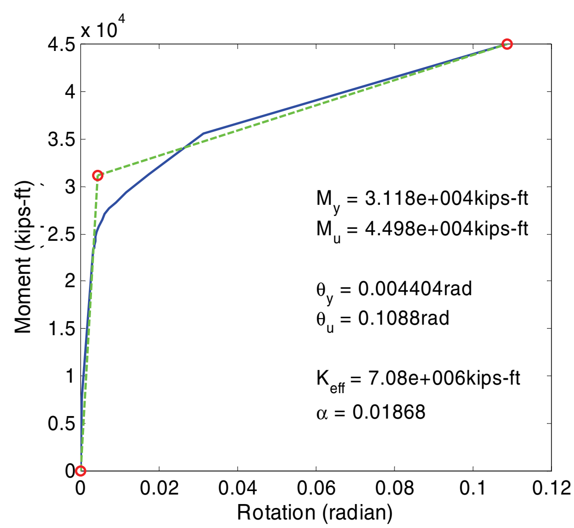

Moment-Rotation Curve

(b) After Retrofit

FIGURE A-12 Moment-Curvature Analysis of Column 2 of Bridge 3 in Longitudinal Direction

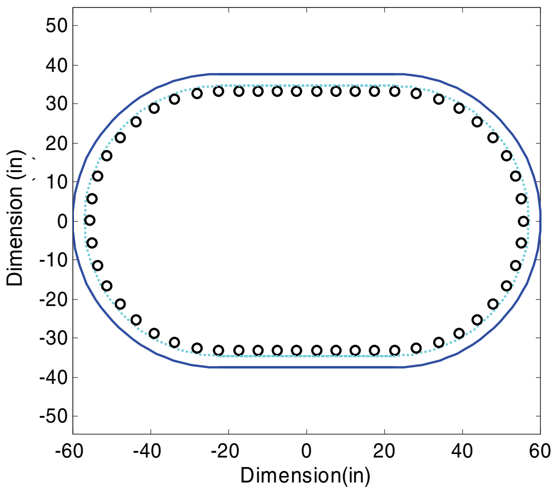

Section of Column

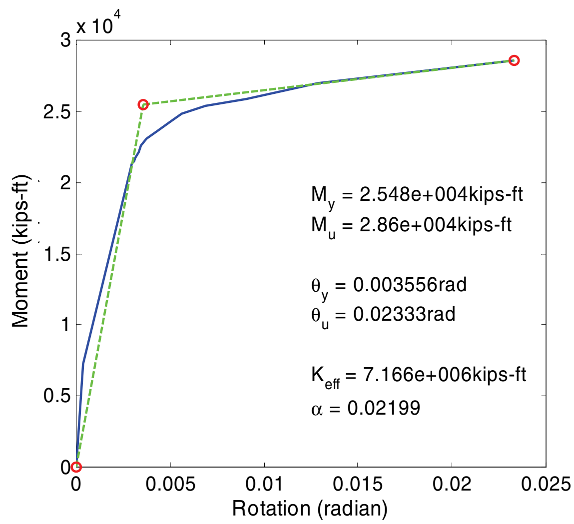

Moment-Rotation Curve

(a) Before Retrofit

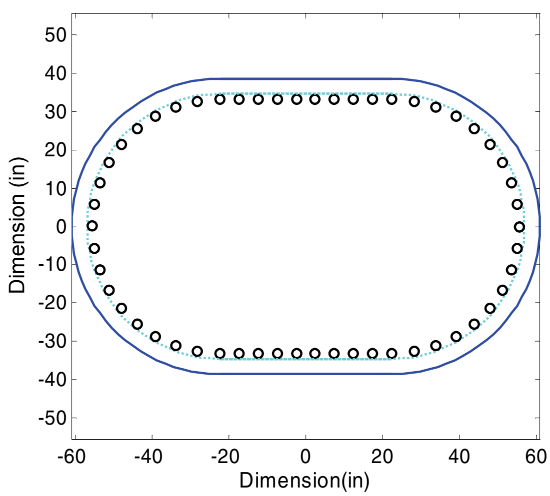

Section of Column

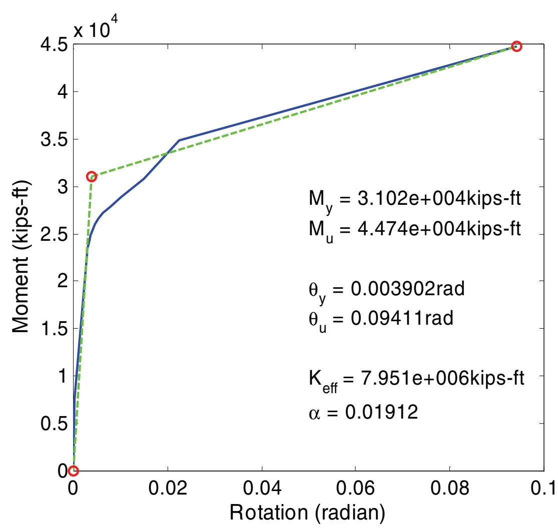

Moment-Rotation Curve

(b3) Column 3 of Bridge 3 after retrofit

FIGURE A-13 Moment-Curvature Analysis of Column 3 of Bridge 3 in Longitudinal Direction

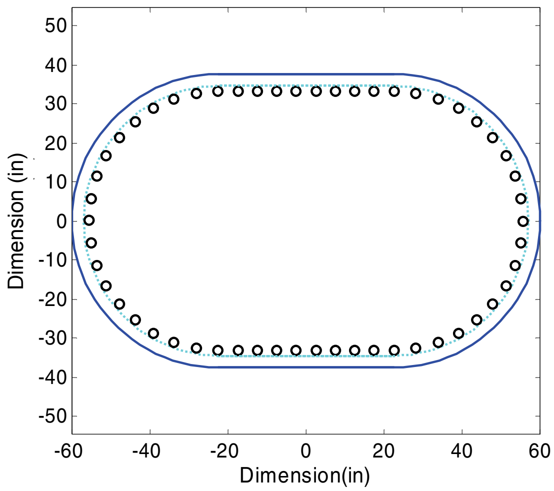

Section of Column

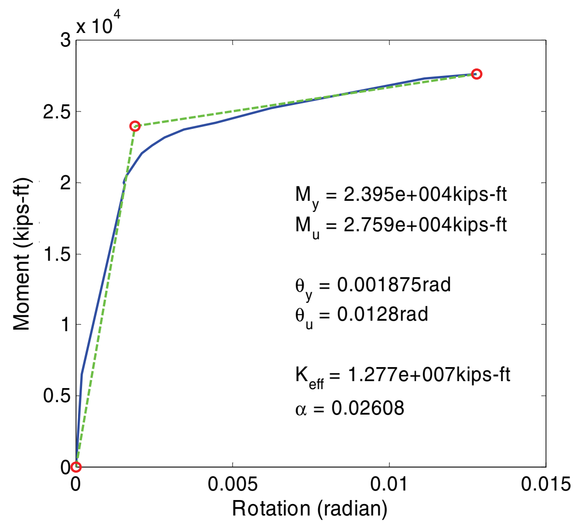

Moment-Rotation Curve

(a) Before Retrofit

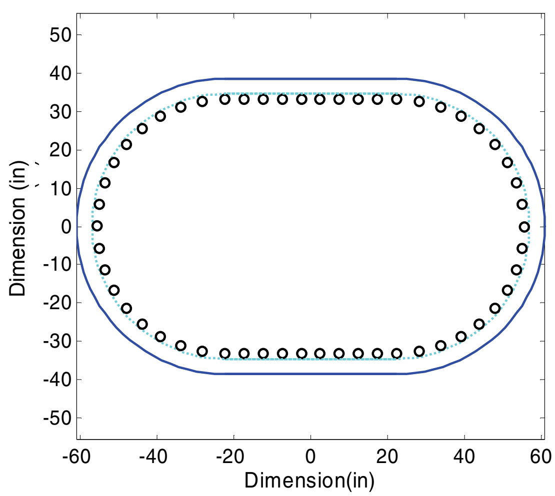

Section of Column

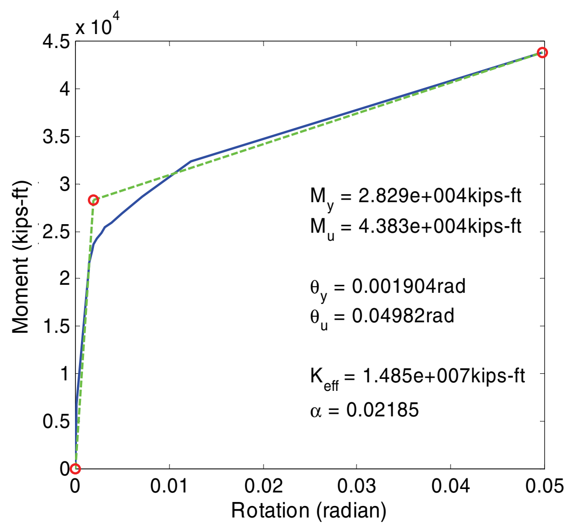

Moment-Rotation Curve

(b) After Retrofit

FIGURE A-14 Moment-Curvature Analysis of Column 4 of Bridge 3 in Longitudinal Direction

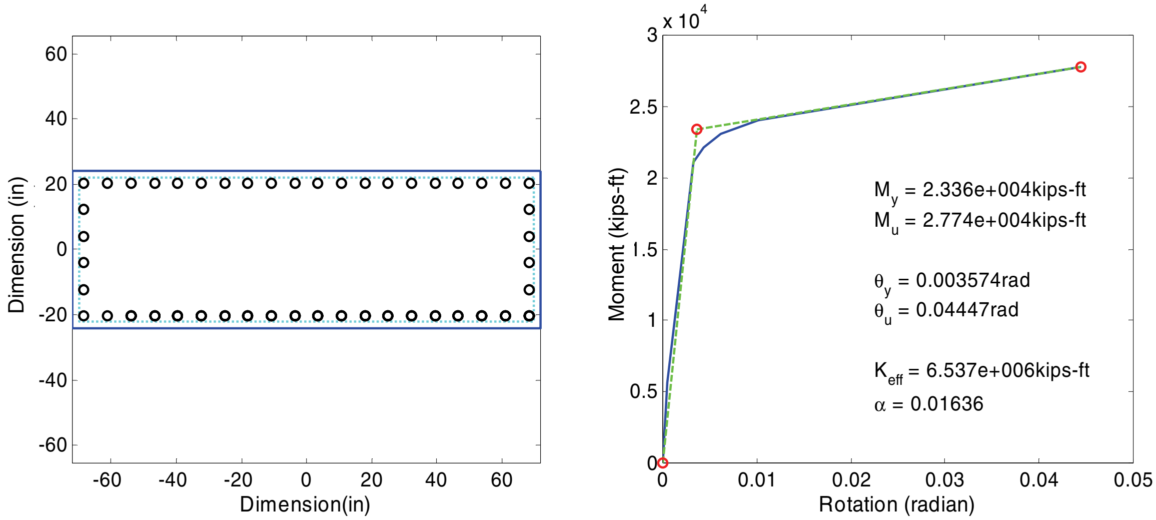

Section of Column

Moment-Rotation Curve

(a) Before Retrofit

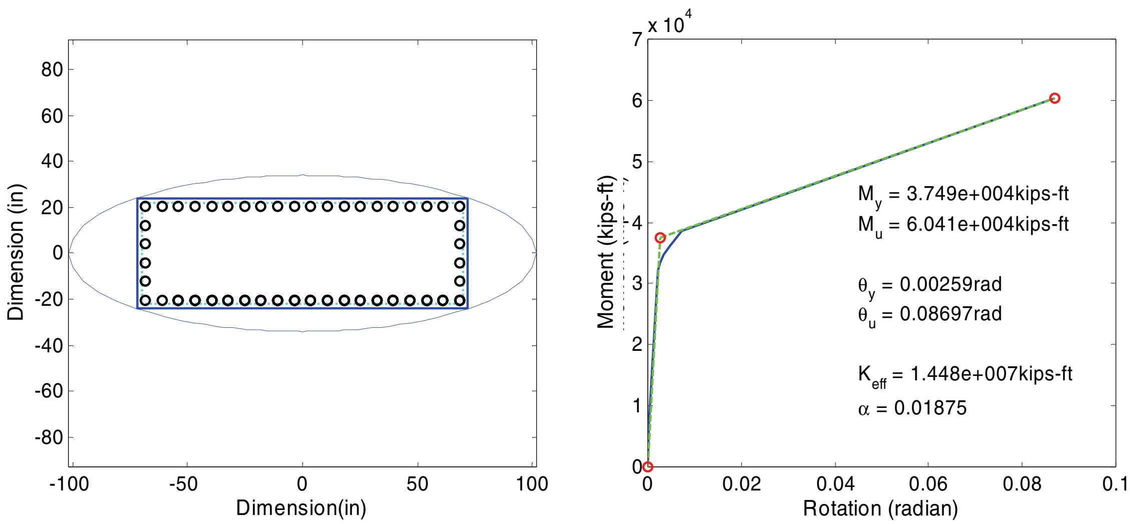

Section of Column

Moment-Rotation Curve

(b) After Retrofit

FIGURE A-15 Moment-Curvature Analysis of Column 1 of Bridge 4 in Longitudinal Direction

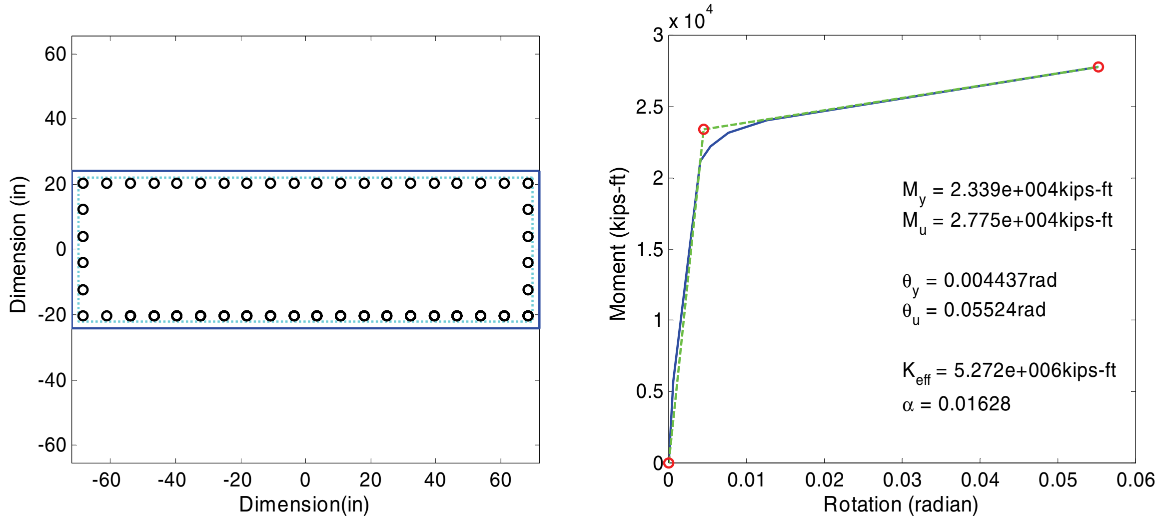

Section of Column Moment-Rotation Curve

(a) Before Retrofit

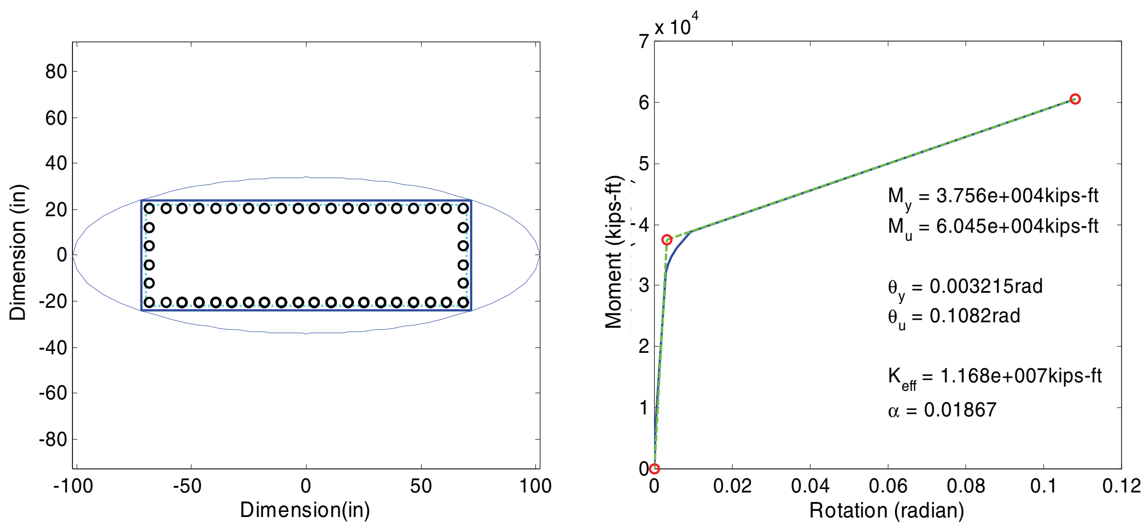

Section of Column Moment-Rotation Curve

(b) After Retrofit

FIGURE A-16 Moment-Curvature Analysis of Column 2 of Bridge 4 in Longitudinal Direction

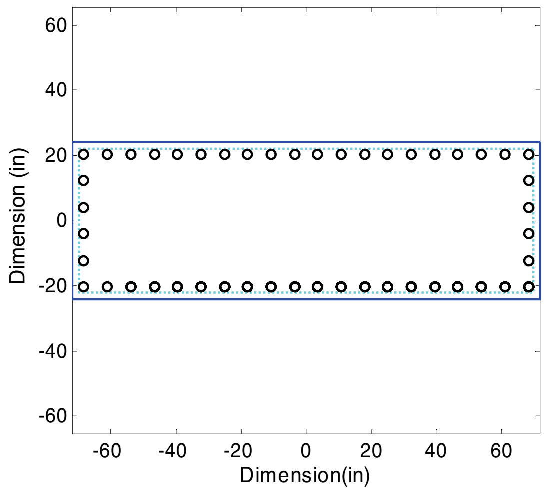

Section of Column

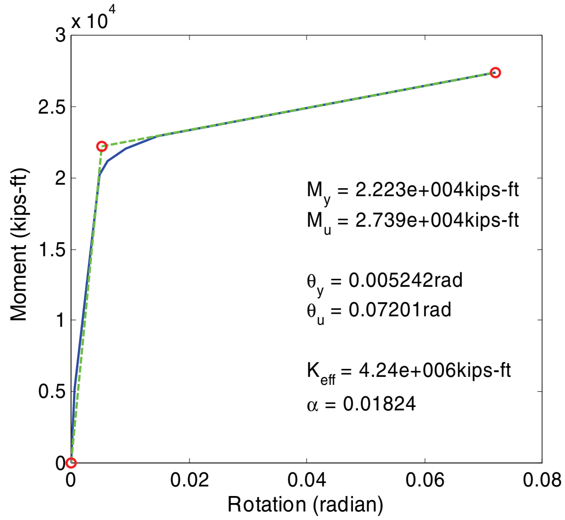

Moment-Rotation Curve

(a) Before Retrofit

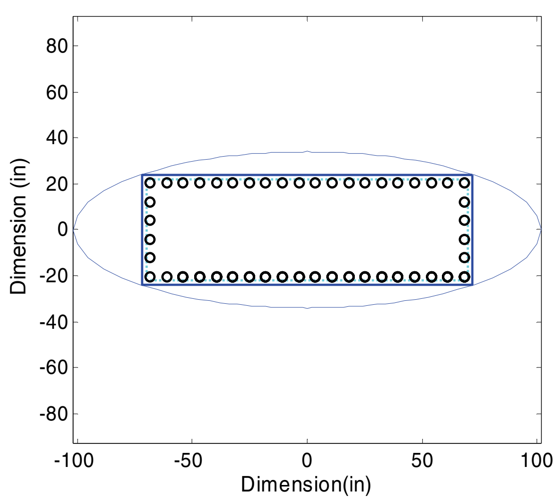

Section of Column

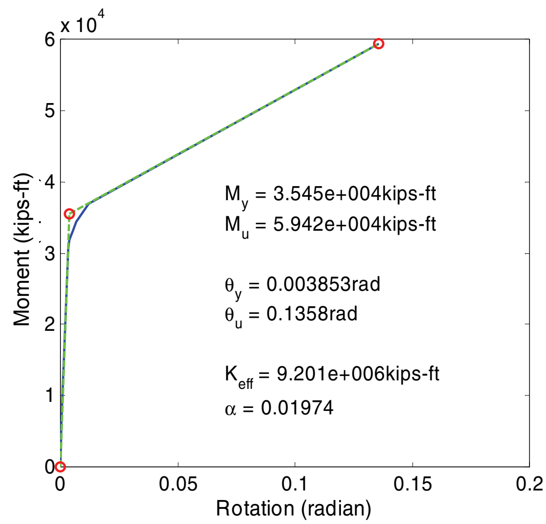

Moment-Rotation Curve

(b) After Retrofit

FIGURE A-17 Moment-Curvature Analysis of Column 3 of Bridge 4 in Longitudinal Direction

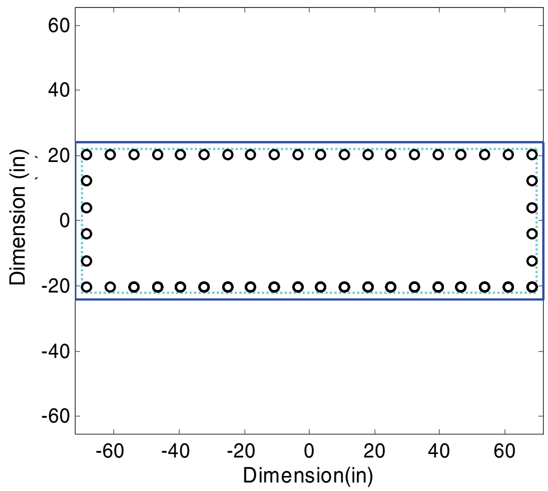

Section of Column

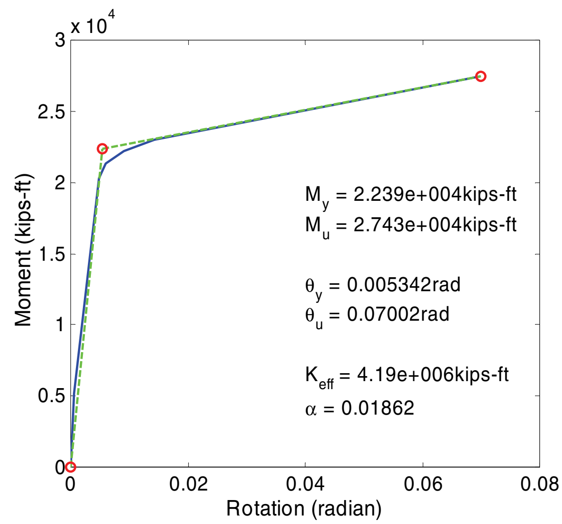

Moment-Rotation Curve

(a) Before Retrofit

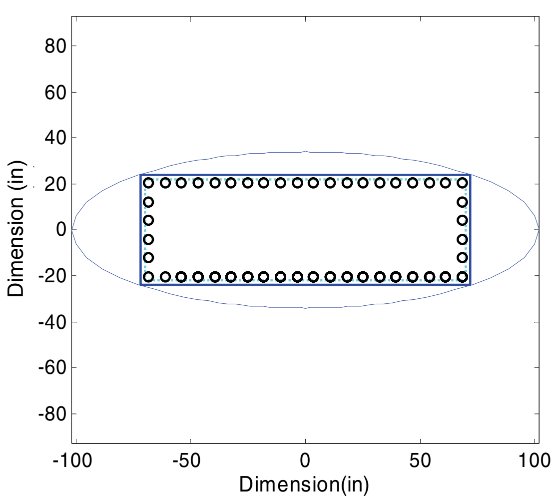

Section of Column

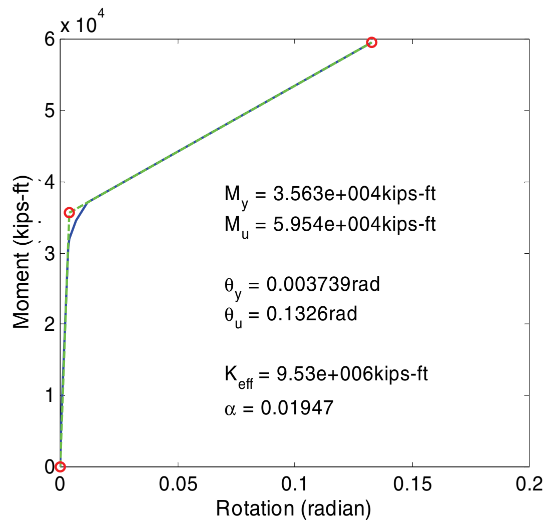

Moment-Rotation Curve

(b) After Retrofit

FIGURE A-18 Moment-Curvature Analysis of Column 4 of Bridge 4 in Longitudinal Direction

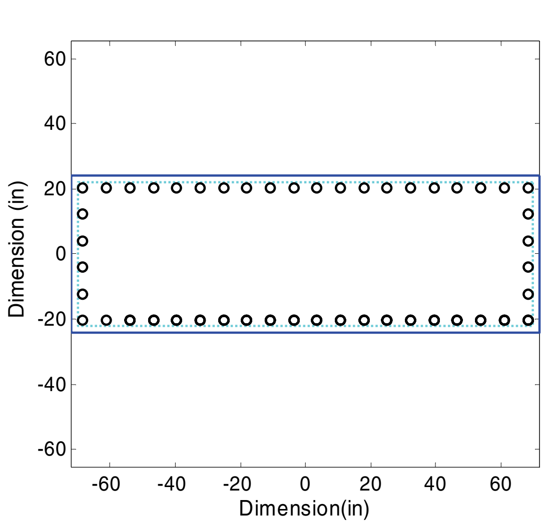

Section of Column

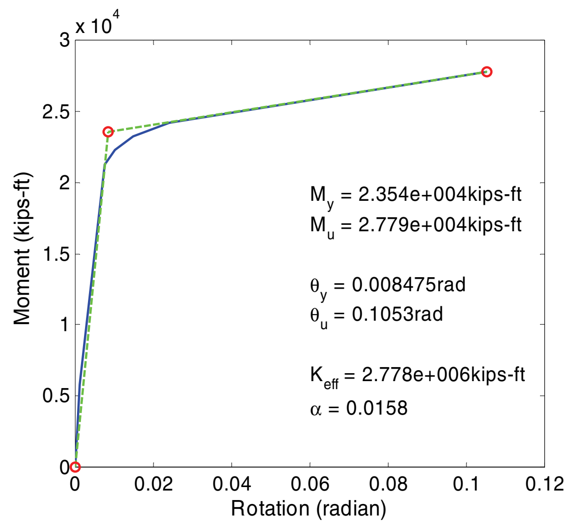

Moment-Rotation Curve

(a) Before Retrofit

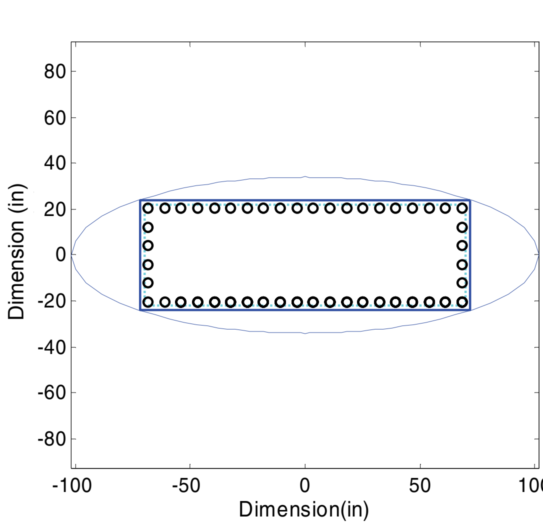

Section of Column

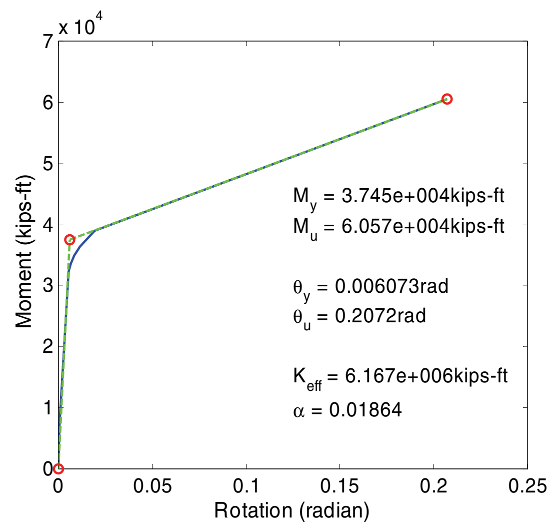

Moment-Rotation Curve

(b) After Retrofit

FIGURE A-19 Moment-Curvature Analysis of Column 5 of Bridge 4 in Longitudinal Direction

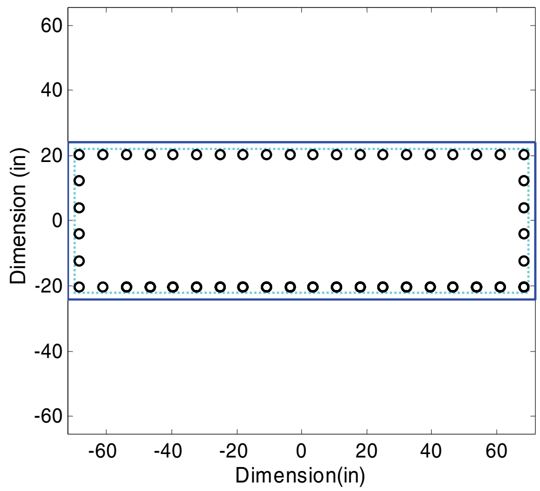

Section of Column

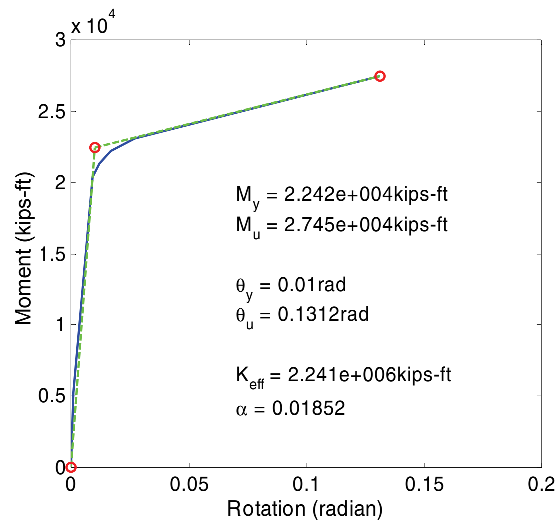

Moment-Rotation Curve

(a) Before Retrofit

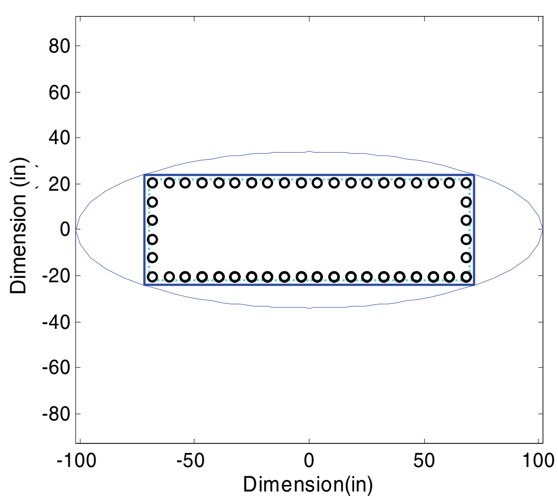

Section of Column

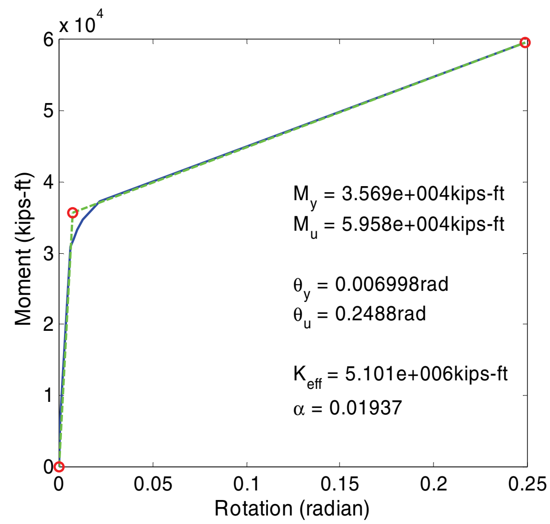

Moment-Rotation Curve

(b) After Retrofit

FIGURE A-20 Moment-Curvature Analysis of Column 6 of Bridge 4 in Longitudinal Direction

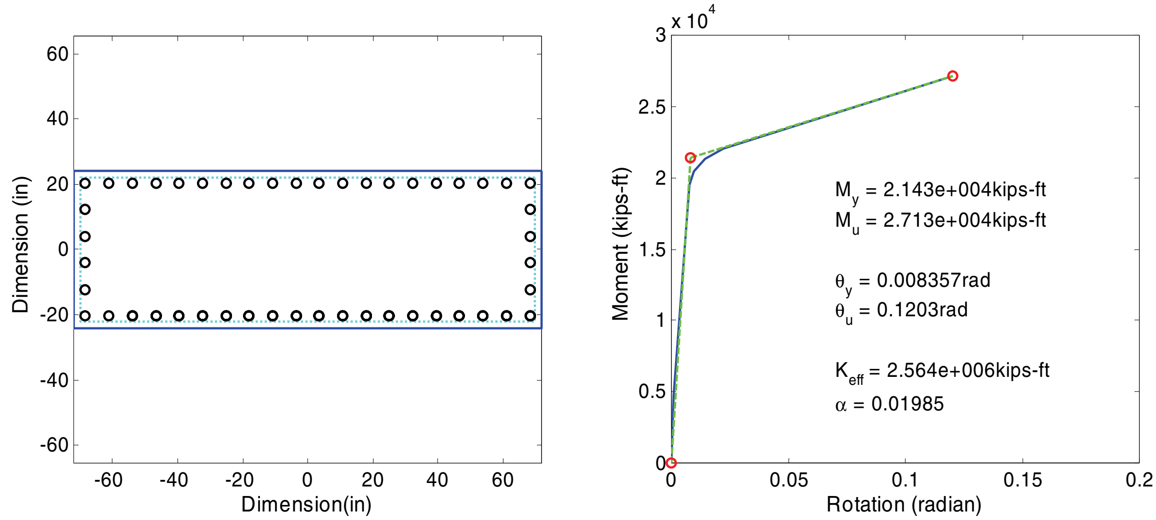

Section of Column Moment-Rotation Curve

(a) Before Retrofit

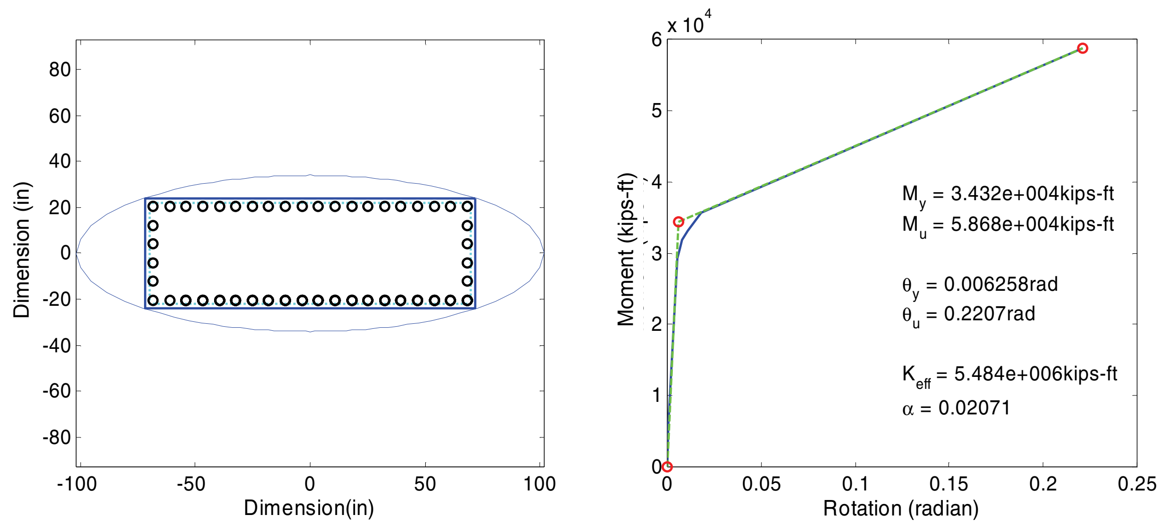

Section of Column Moment-Rotation Curve

(b) After Retrofit

FIGURE A-21 Moment-Curvature Analysis of Column 7 of Bridge 4 in Longitudinal Direction

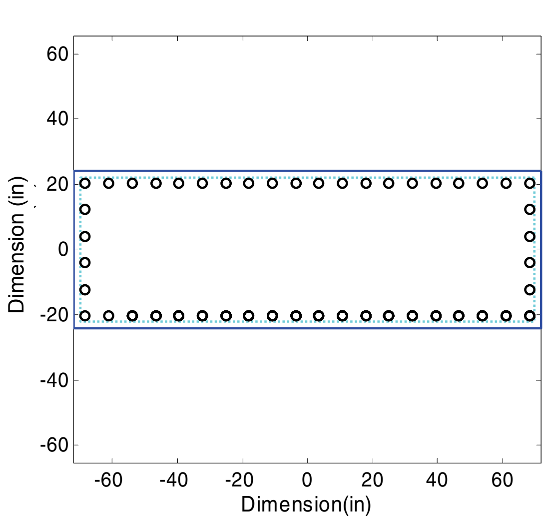

Section of Column

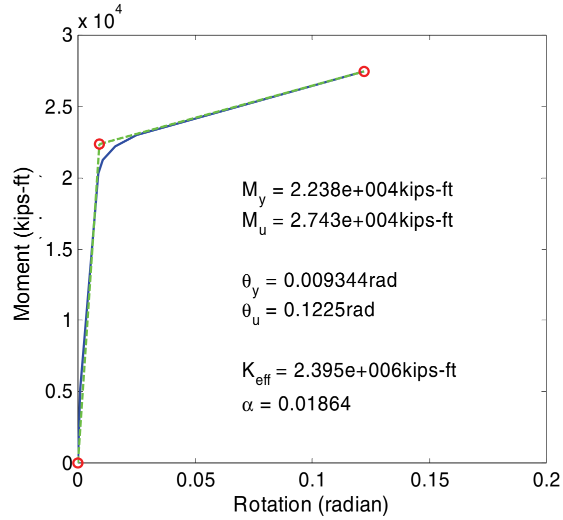

Moment-Rotation Curve

(a) Before Retrofit

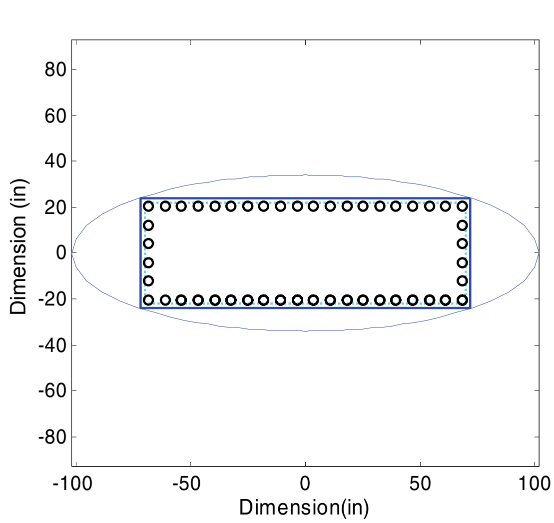

Section of Column

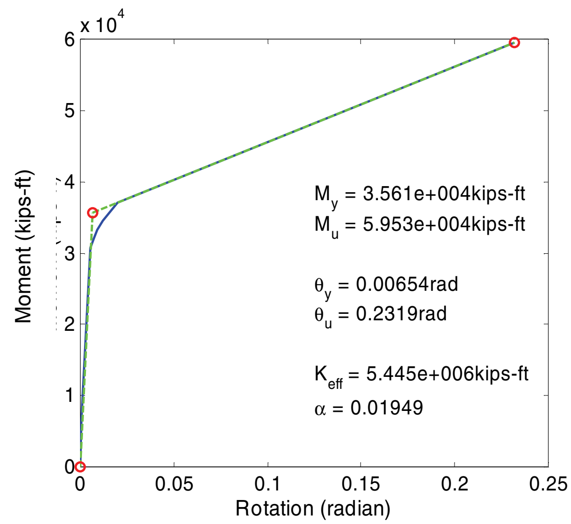

Moment-Rotation Curve

(b) After Retrofit

FIGURE A-22 Moment-Curvature Analysis of Column 8 of Bridge 4 in Longitudinal Direction

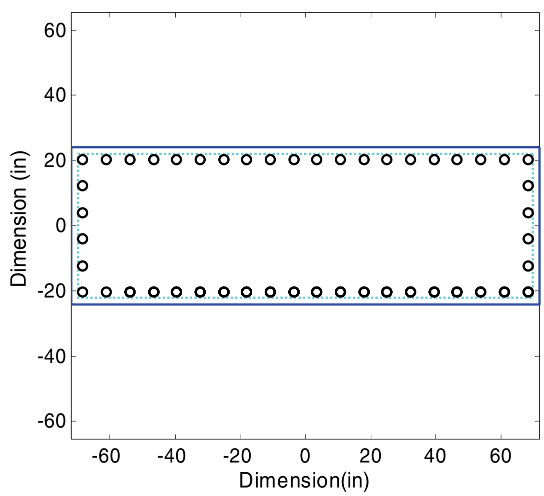

Section of Column

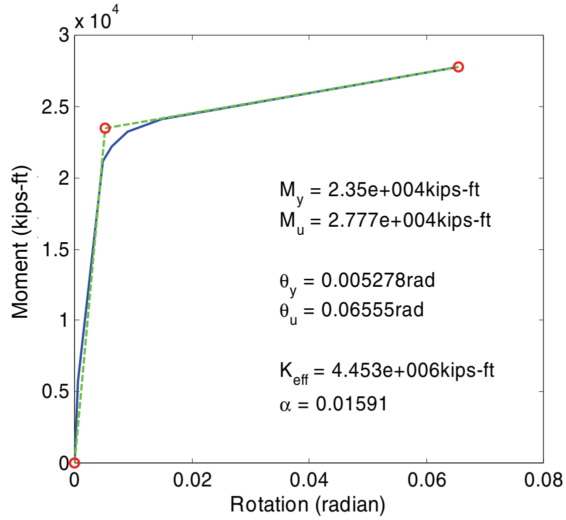

Moment-Rotation Curve

(a) Before Retrofit

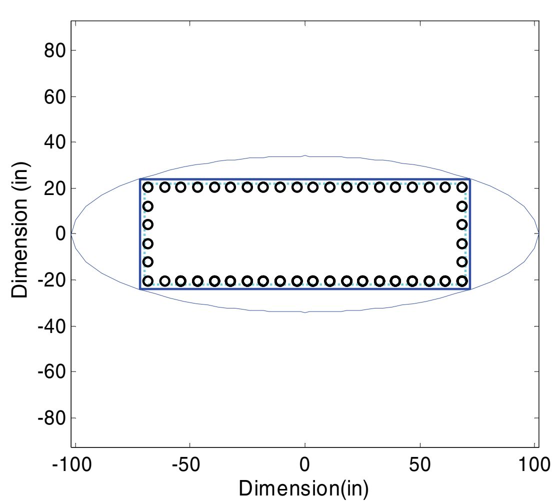

Section of Column

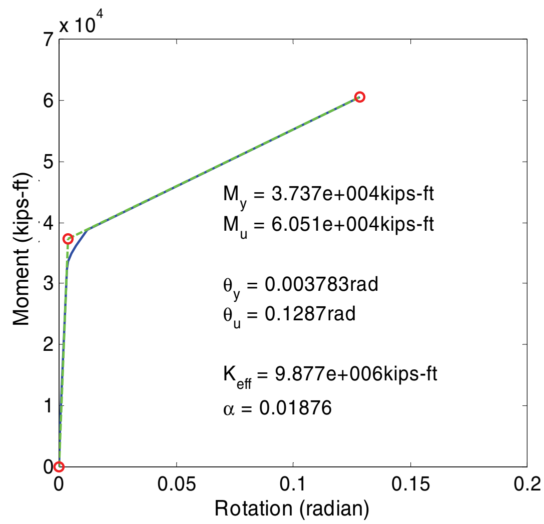

Moment-Rotation Curve

(b) After Retrofit

FIGURE A-23 Moment-Curvature Analysis of Column 9 of Bridge 4 in Longitudinal Direction

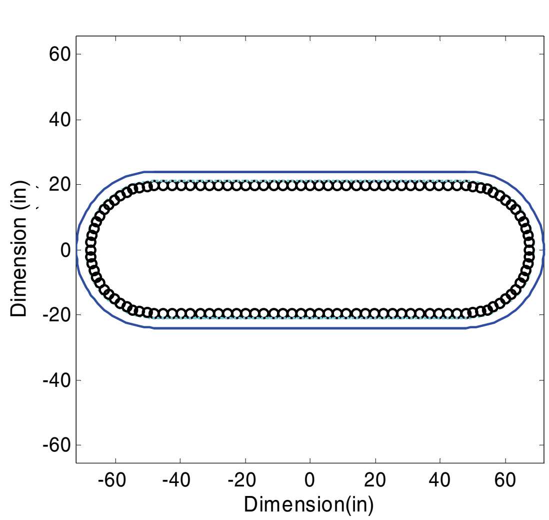

Section of Column

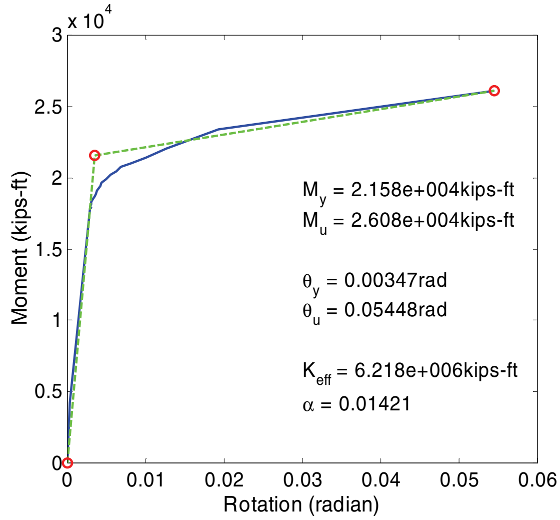

Moment-Rotation Curve

(a) Before Retrofit

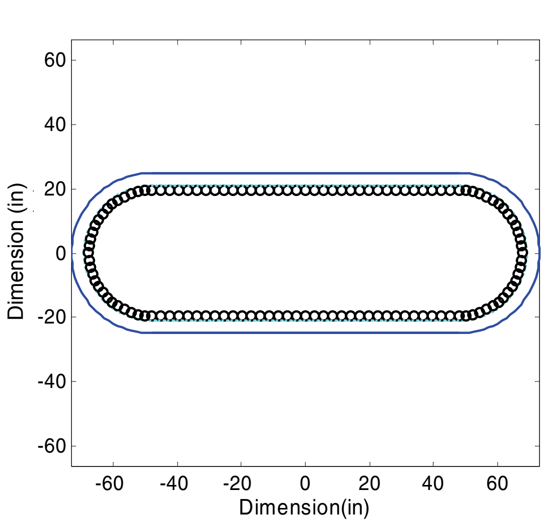

Section of Column

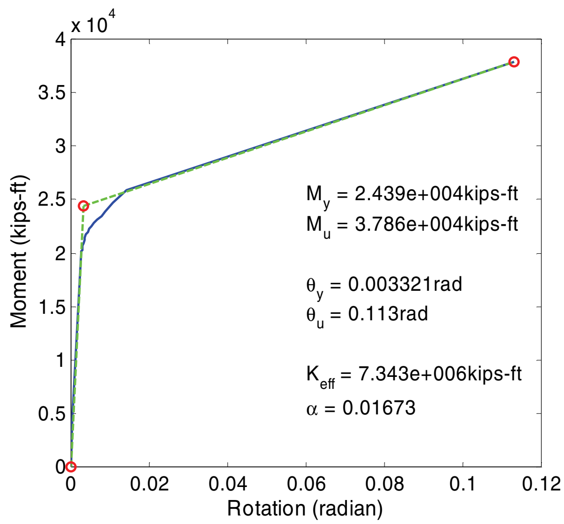

Moment-Rotation Curve

(b) After Retrofit

FIGURE A-24 Moment-Curvature Analysis of Column 1 of Bridge 5 in Longitudinal Direction

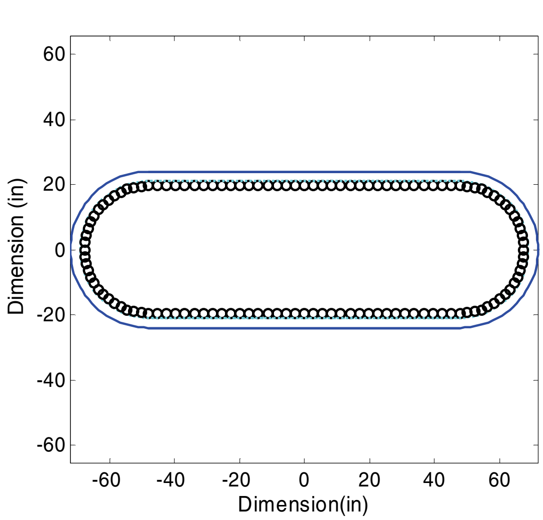

Section of Column

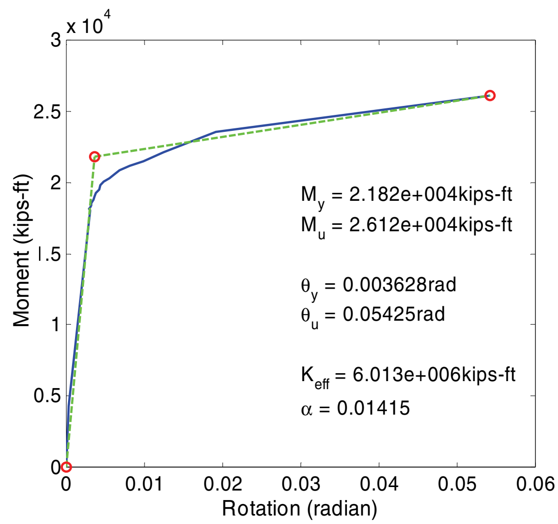

Moment-Rotation Curve

(a) Before Retrofit

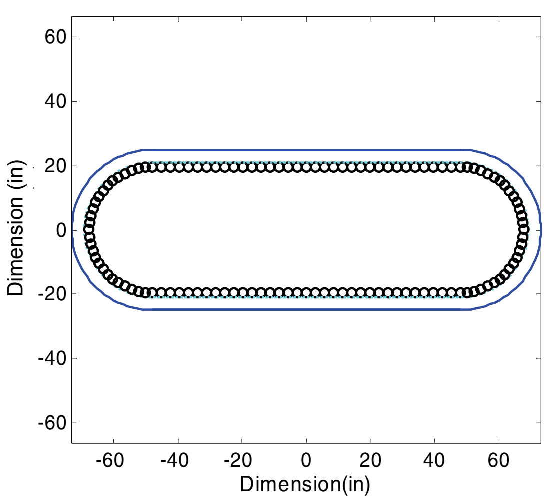

Section of Column

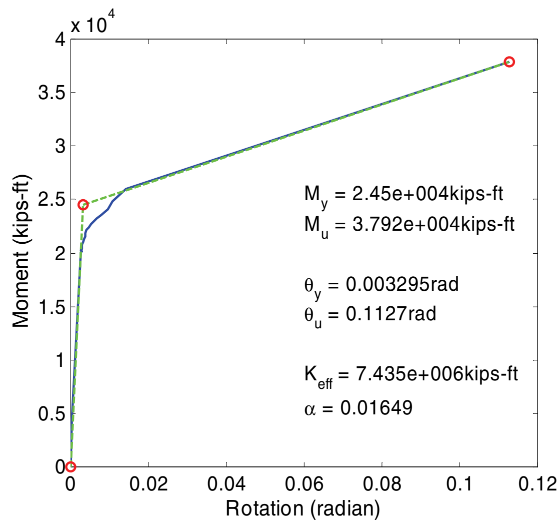

Moment-Rotation Curve

(b) After Retrofit

FIGURE A-25 Moment-Curvature Analysis of Column 2 of Bridge 5 in Longitudinal Direction

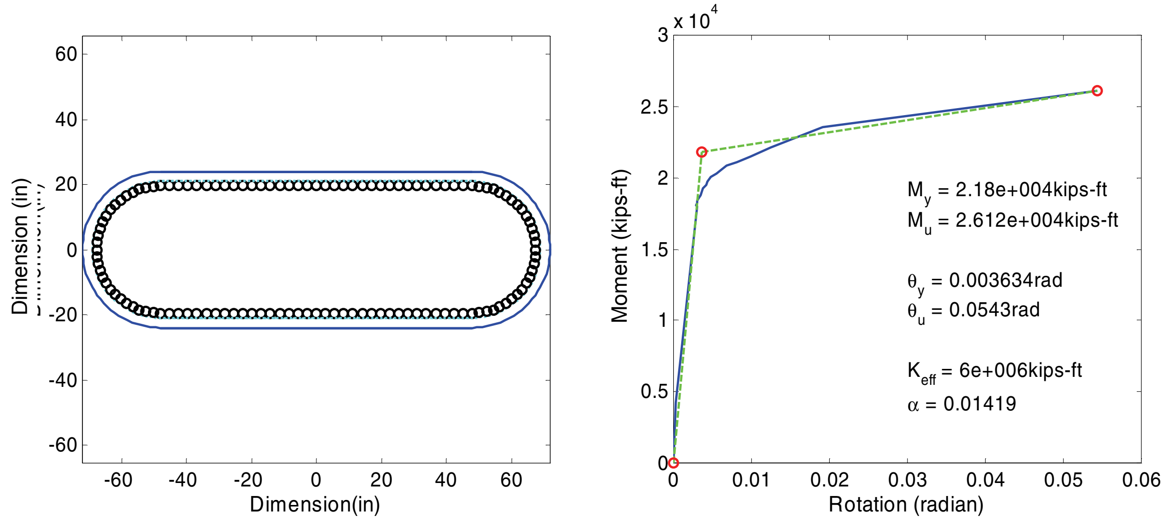

Section of Column

Moment-Rotation Curve

(a) Before Retrofit

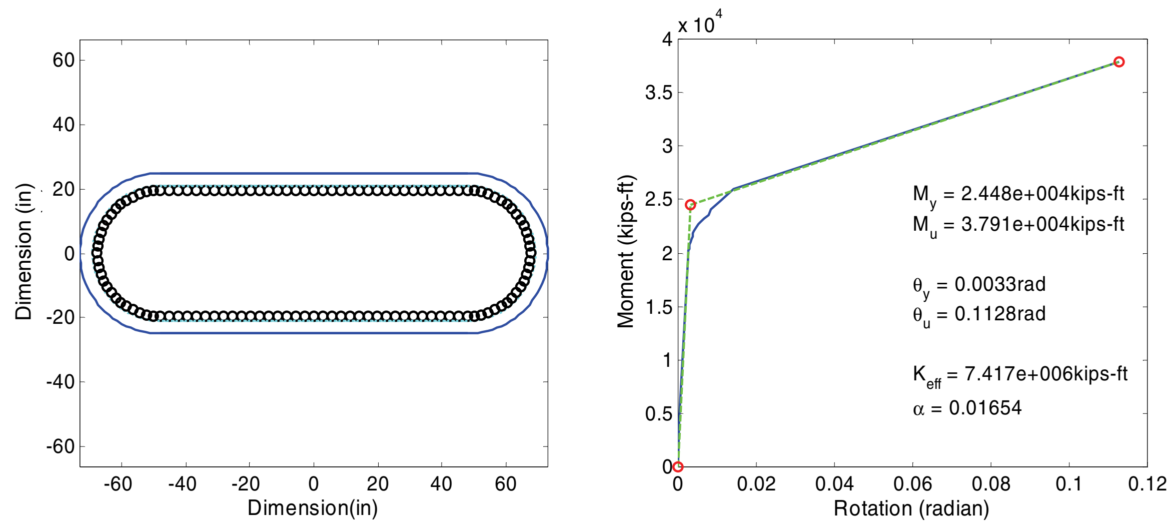

Section of Column

Moment-Rotation Curve

(b) After Retrofit

FIGURE A-26 Moment-Curvature Analysis of Column 3 of Bridge 5 in Longitudinal Direction

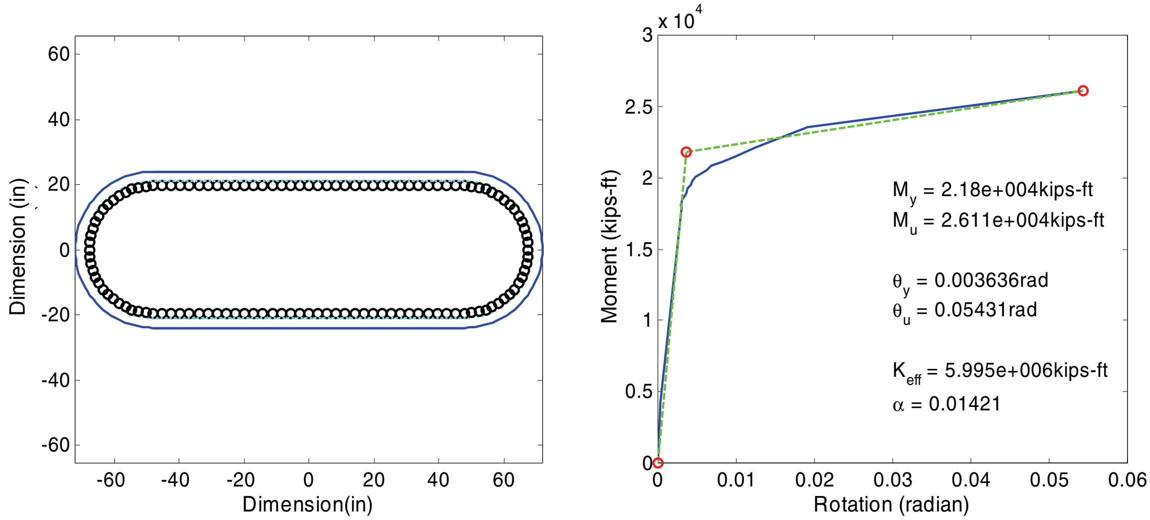

Section of Column Moment-Rotation Curve

(a) Before Retrofit

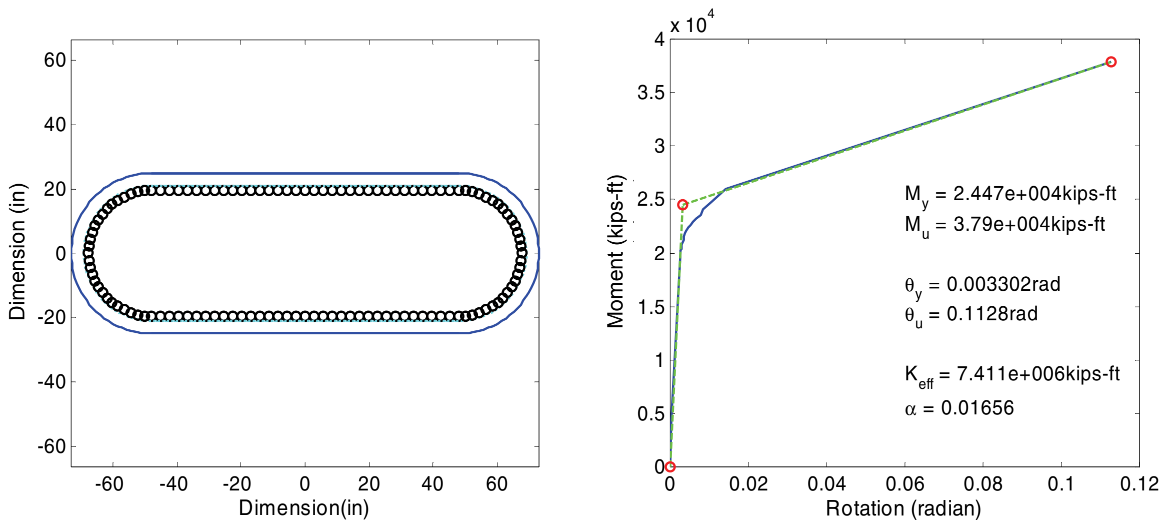

Section of Column Moment-Rotation Curve

(b) After Retrofit

FIGURE A-27 Moment-Curvature Analysis of Column 4 of Bridge 5 in Longitudinal Direction

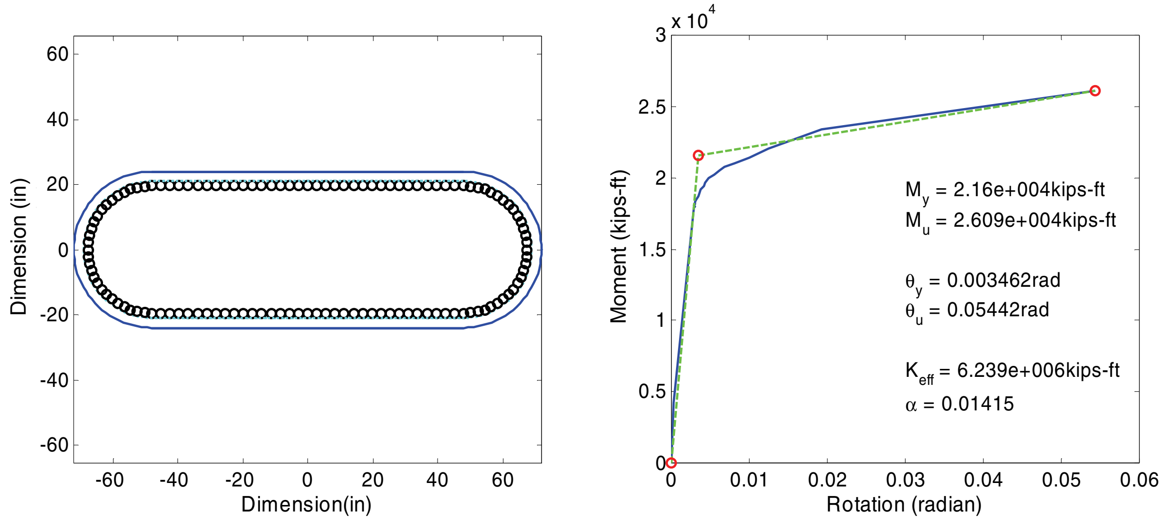

Section of Column　　　Moment-Rotation Curve

(a) Before Retrofit

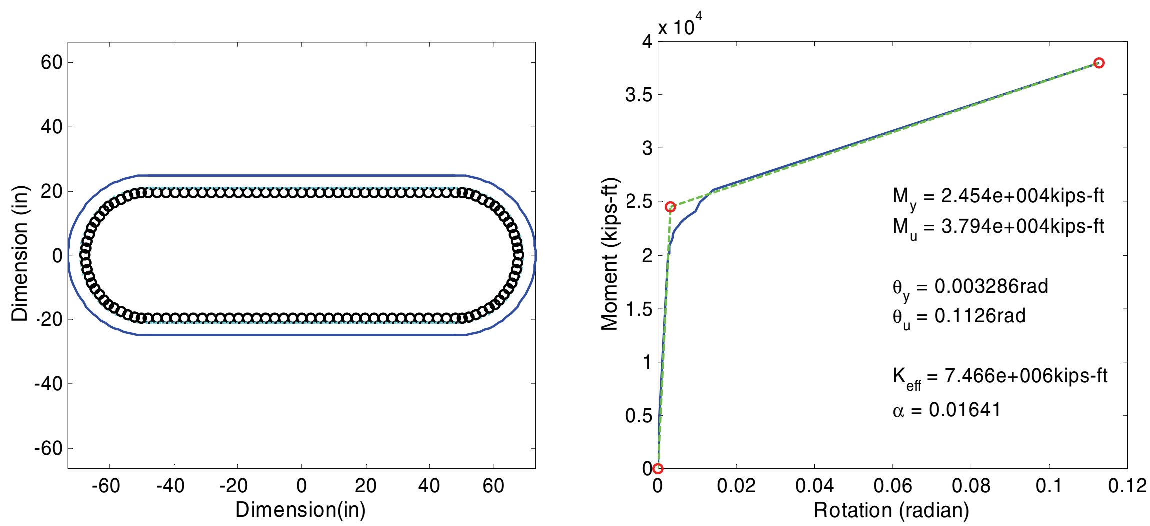

Section of Column　　　Moment-Rotation Curve

(b) After Retrofit

FIGURE A-28 Moment-Curvature Analysis of Column 5 of Bridge 5 in Longitudinal Direction

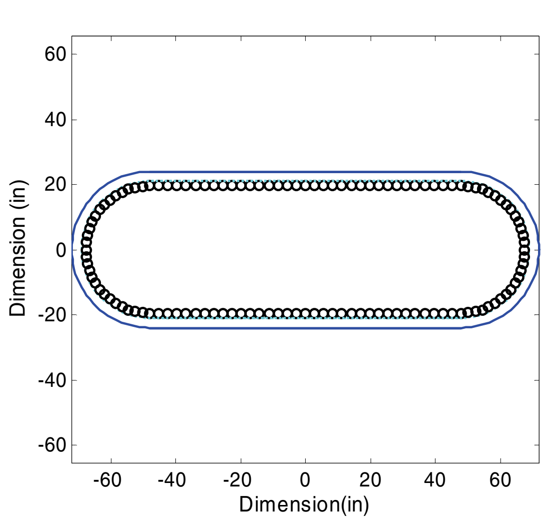

Section of Column

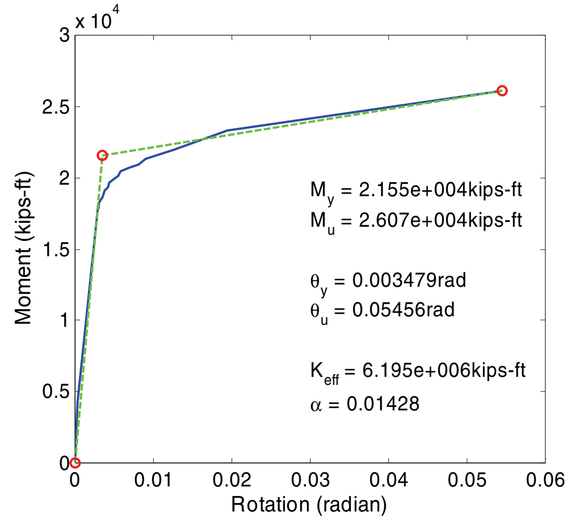

Moment-Rotation Curve

(a) Before Retrofit

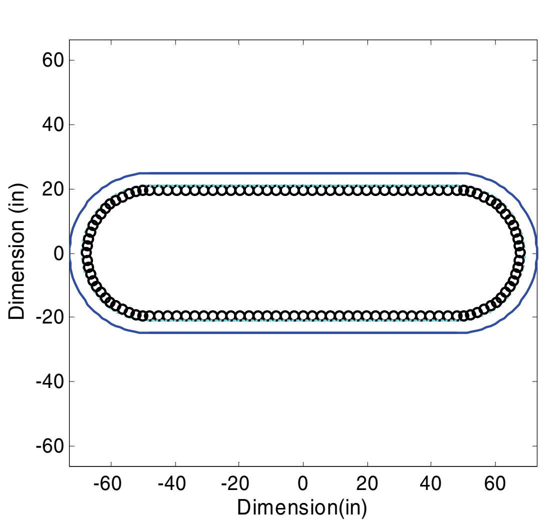

Section of Column

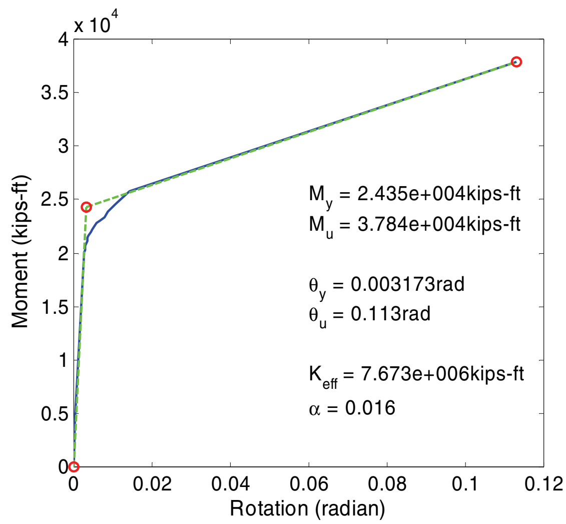

Moment-Rotation Curve

(b) After Retrofit

FIGURE A-29 Moment-Curvature Analysis of Column 6 of Bridge 5 in Longitudinal Direction

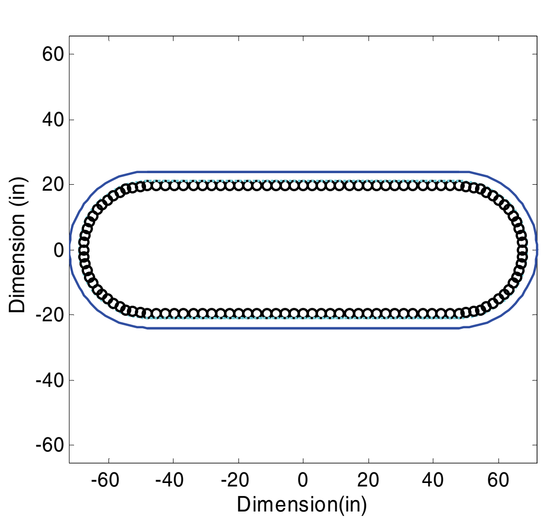

Section of Column

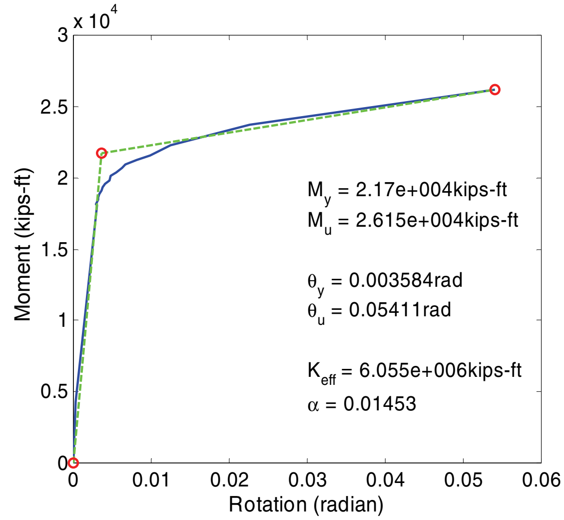

Moment-Rotation Curve

(a) Before Retrofit

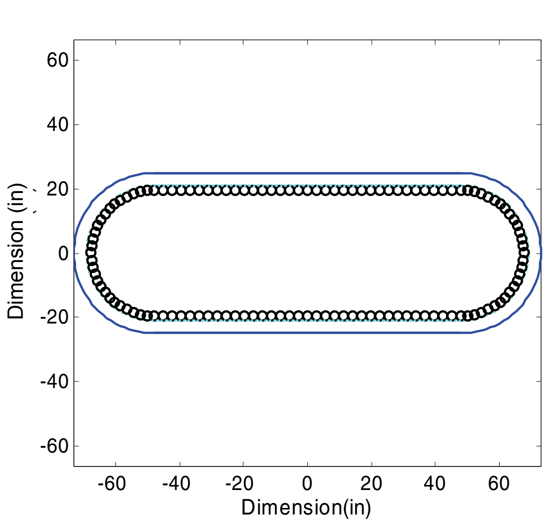

Section of Column

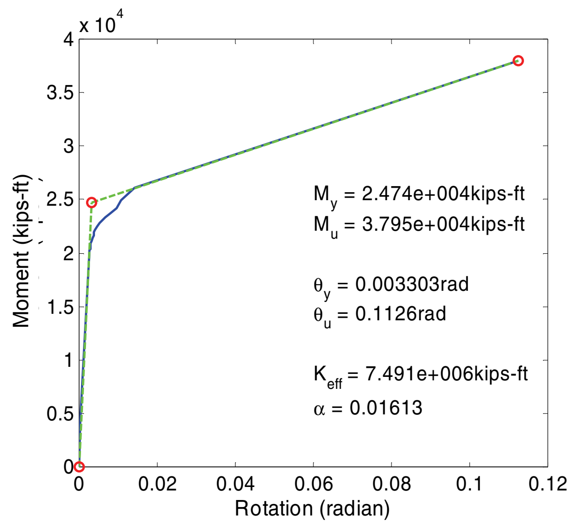

Moment-Rotation Curve

(b) After Retrofit

FIGURE A-30 Moment-Curvature Analysis of Column 7 of Bridge 5 in Longitudinal Direction

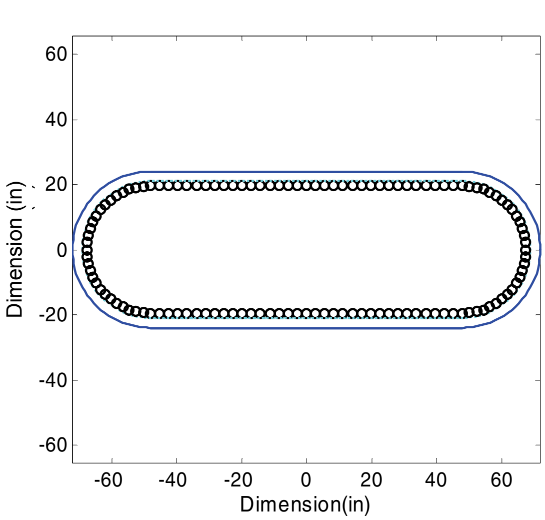

Section of Column

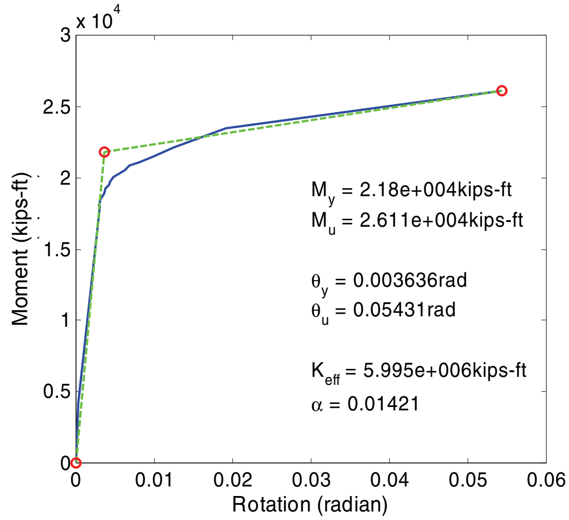

Moment-Rotation Curve

(a) Before Retrofit

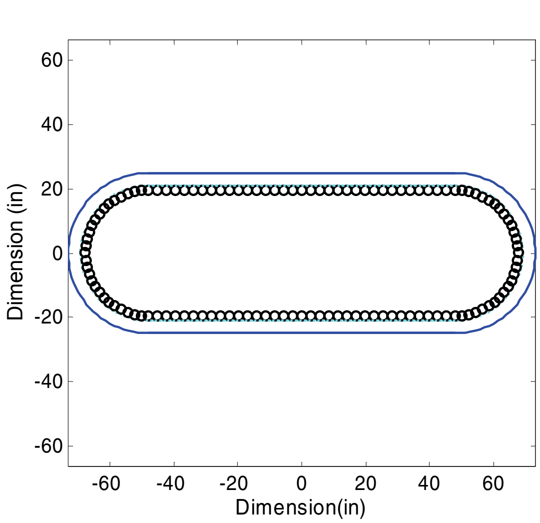

Section of Column

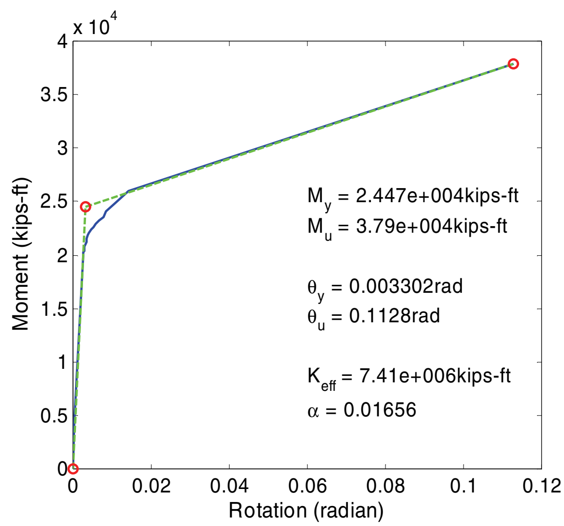

Moment-Rotation Curve

(b) After Retrofit

FIGURE A-31 Moment-Curvature Analysis of Column 8 of Bridge 5 in Longitudinal Direction

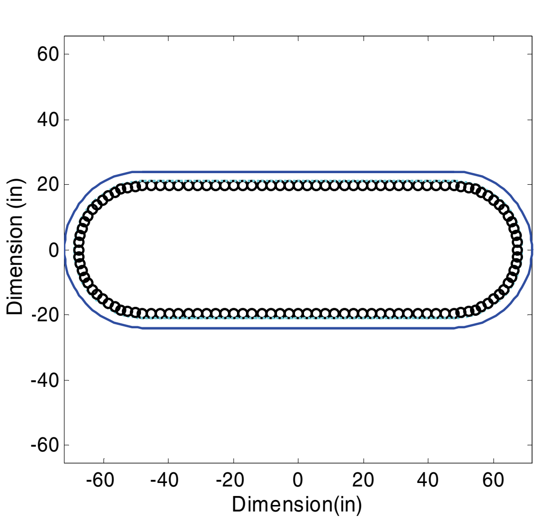

Section of Column

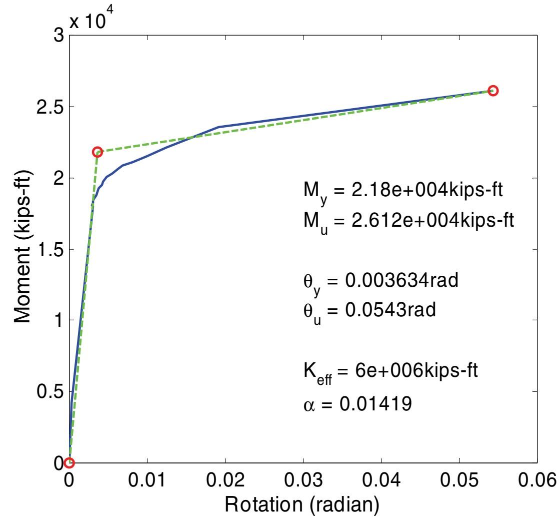

Moment-Rotation Curve

(a) Before Retrofit

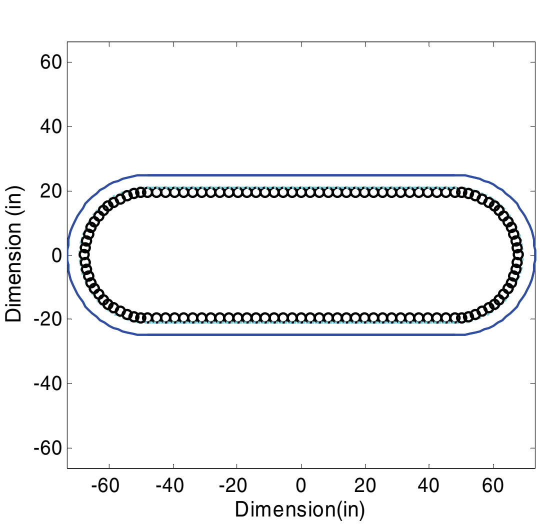

Section of Column

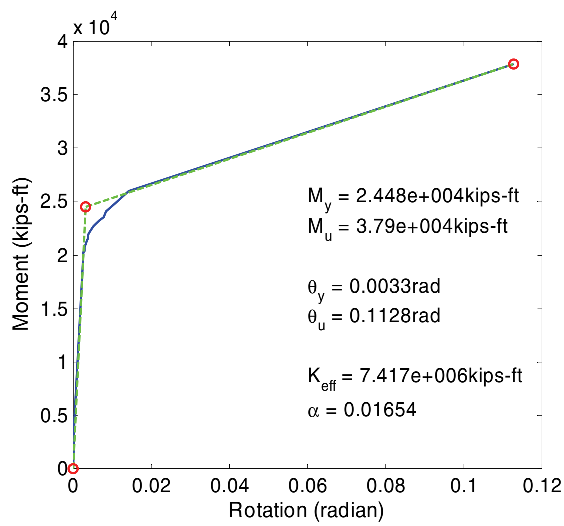

Moment-Rotation Curve

(b) After Retrofit

FIGURE A-32 Moment-Curvature Analysis of Column 9 of Bridge 5

in Longitudinal **Direction**

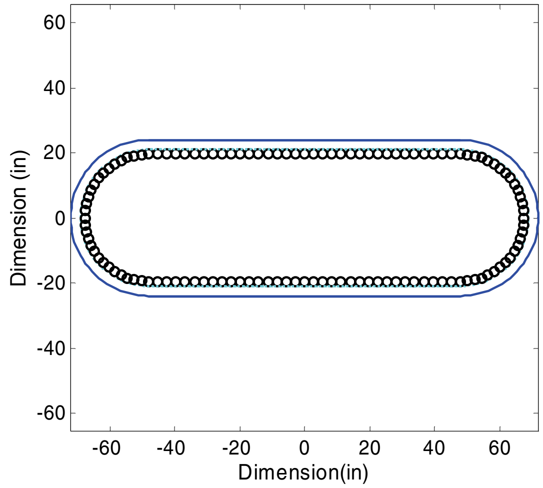

Section of Column

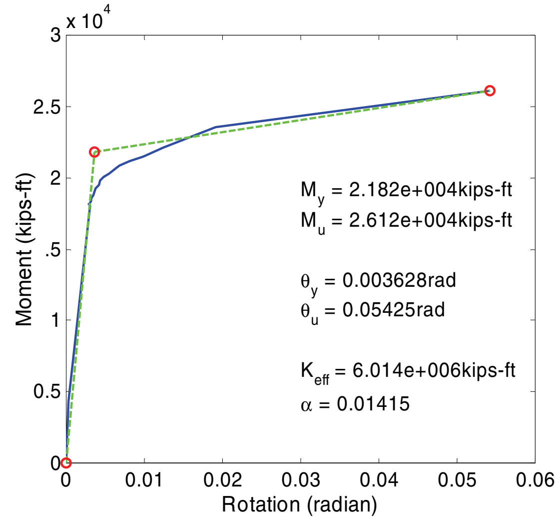

Moment-Rotation Curve

(a) Before Retrofit

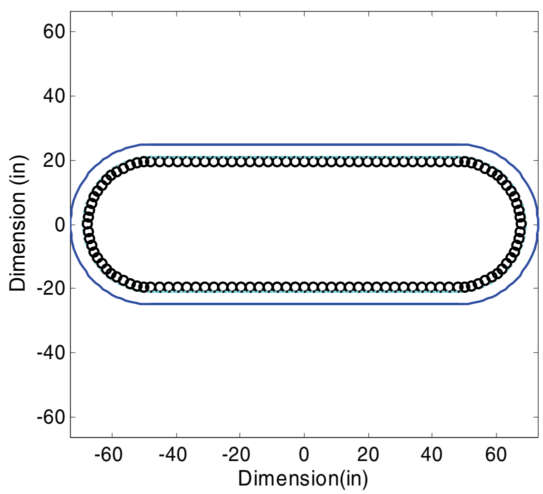

Section of Column

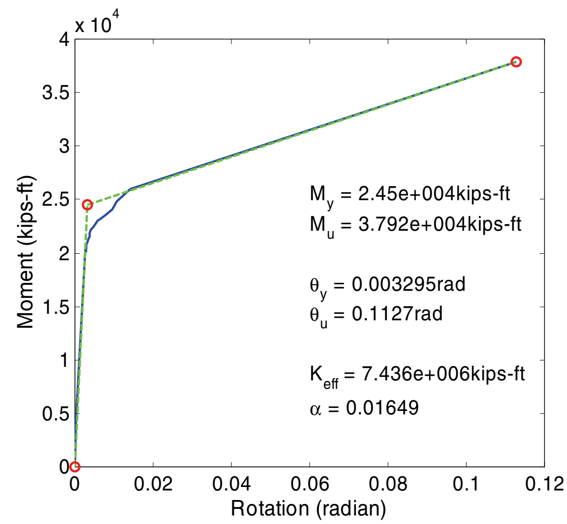

Moment-Rotation Curve

(b) After Retrofit

FIGURE A-33 Moment-Curvature Analysis of Column 10 of Bridge 5 in Longitudinal Direction

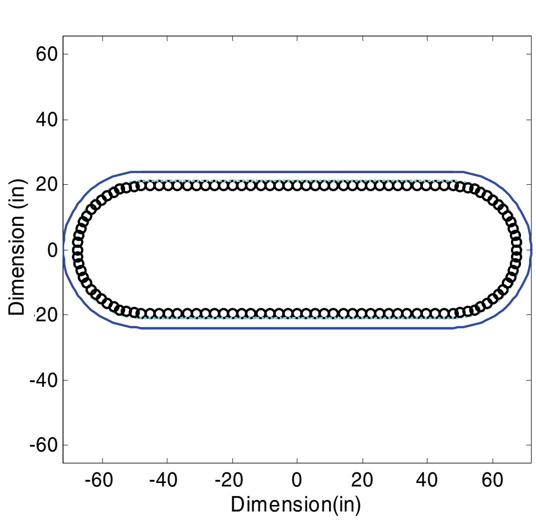

Section of Column

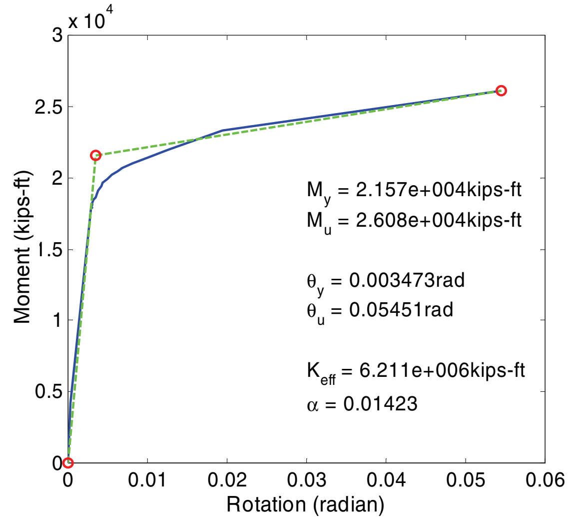

Moment-Rotation Curve

(a) Before Retrofit

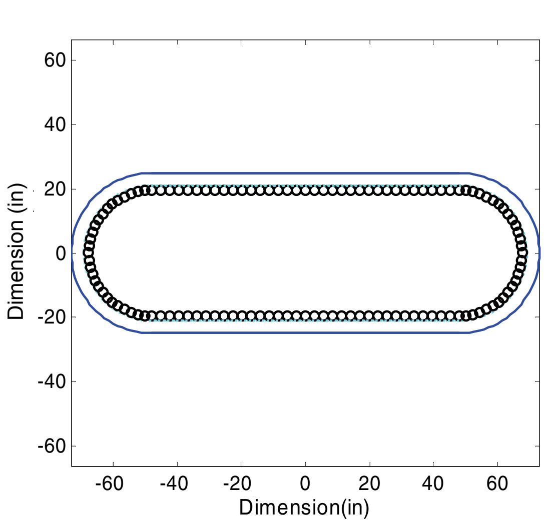

Section of Column

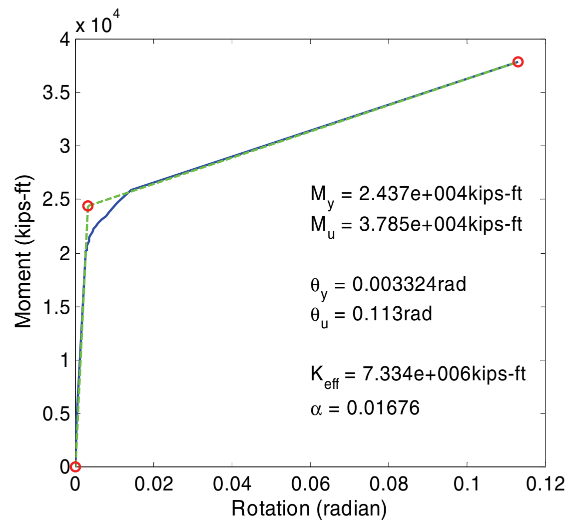

Moment-Rotation Curve

(b) After Retrofit

FIGURE A-34 Moment-Curvature Analysis of Column 11 of Bridge 5 in Longitudinal Direction

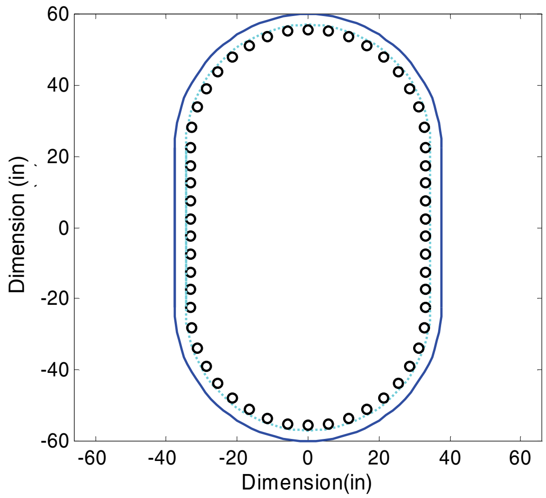

Section of Column

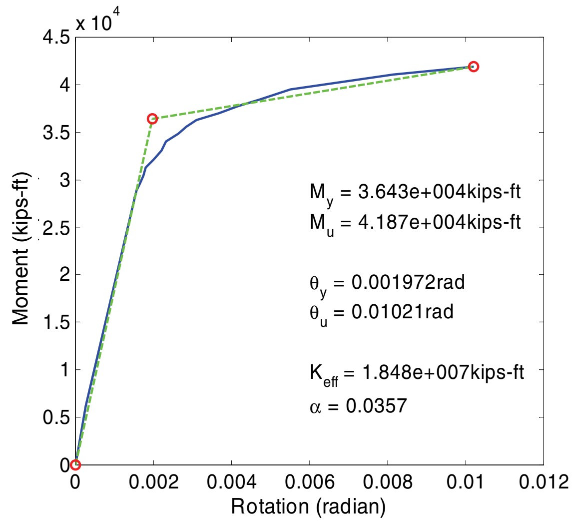

Moment-Rotation Curve

(a) Before Retrofit

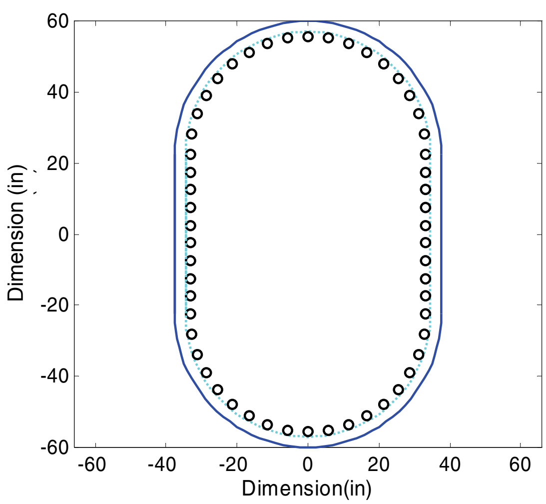

Section of Column

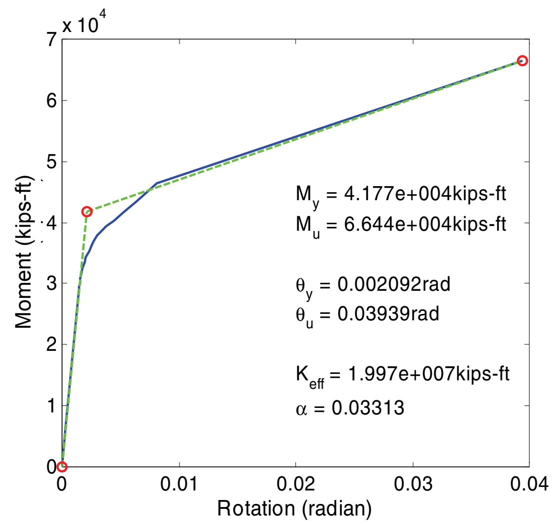

Moment-Rotation Curve

(b) After Retrofit

FIGURE A-35 Moment-Curvature Analysis of Column 1 of Bridge 3 in Transverse Direction

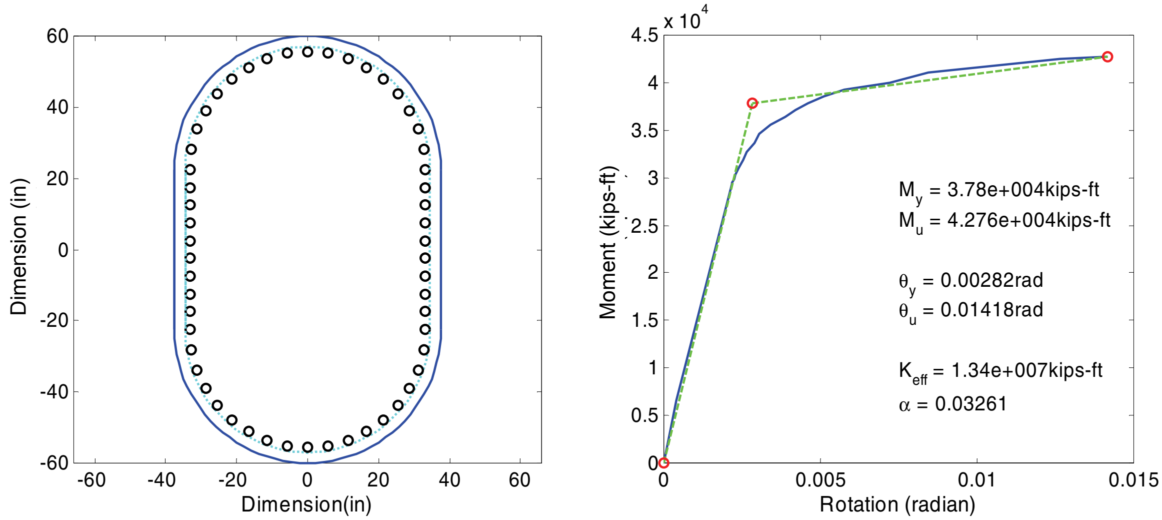

Section of Column Moment-Rotation Curve

(a) Before Retrofit

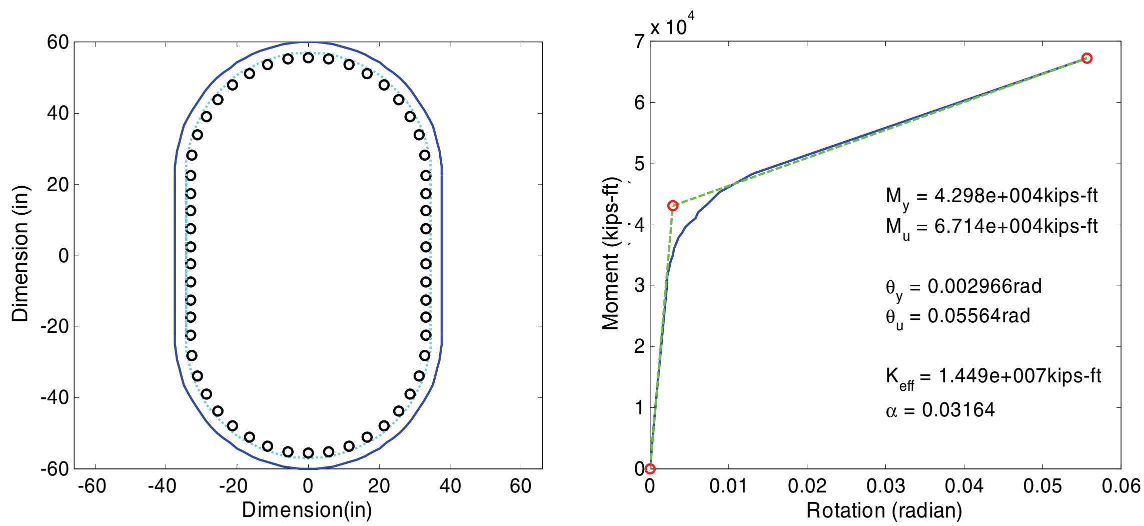

Section of Column Moment-Rotation Curve

(b) After Retrofit

FIGURE A-36 Moment-Curvature Analysis of Column 2 of Bridge 3 in Transverse Direction

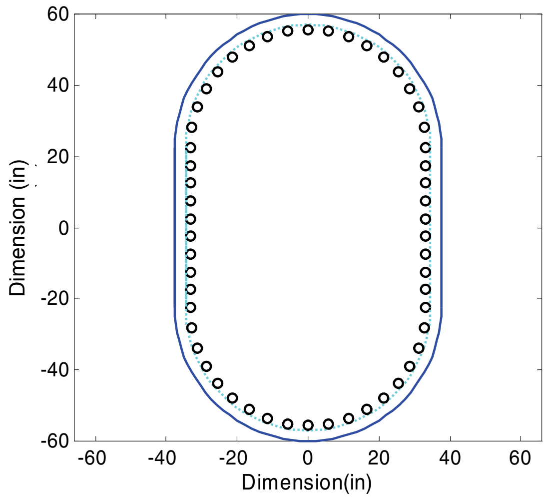

Section of Column

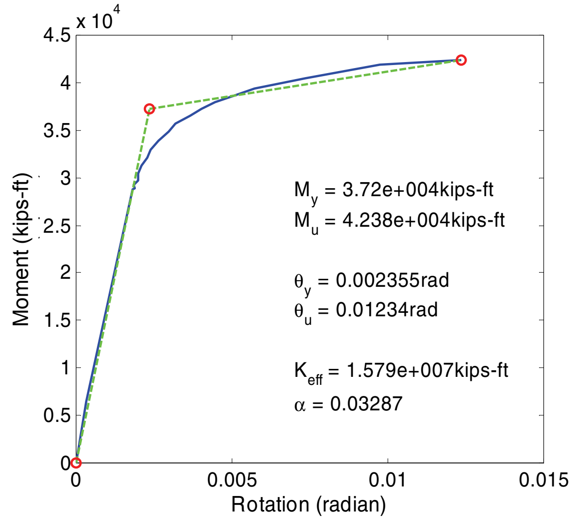

Moment-Rotation Curve

(a) Before Retrofit

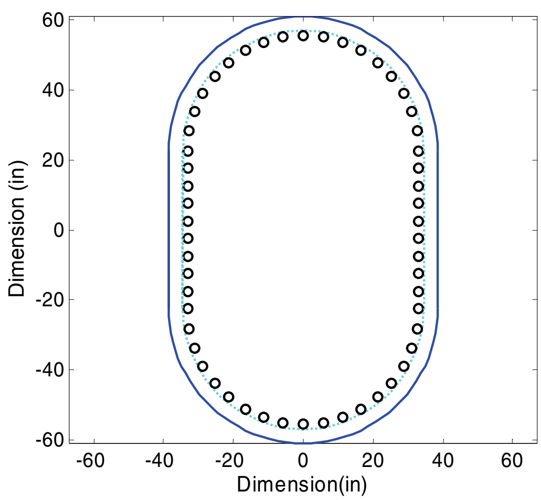

Section of Column

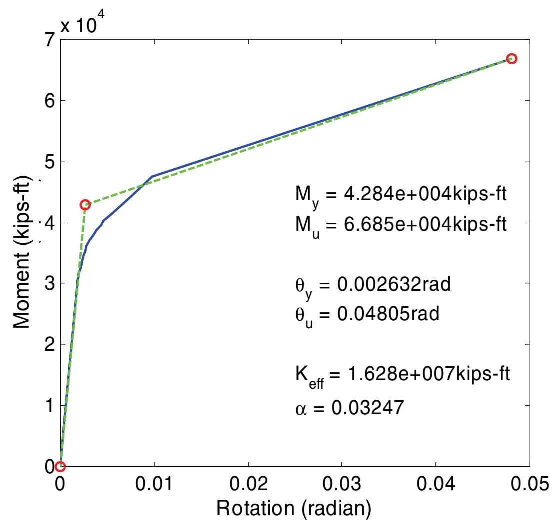

Moment-Rotation Curve

(b) After Retrofit

FIGURE A-37 Moment-Curvature Analysis of Column 3 of Bridge 3 in Transverse Direction

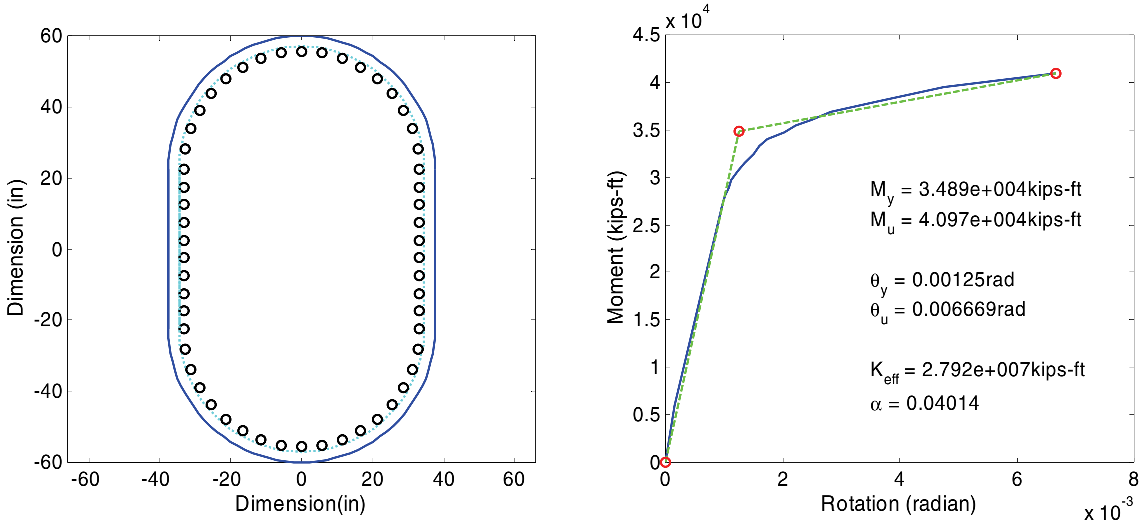

Section of Column Moment-Rotation Curve

(a) Before Retrofit

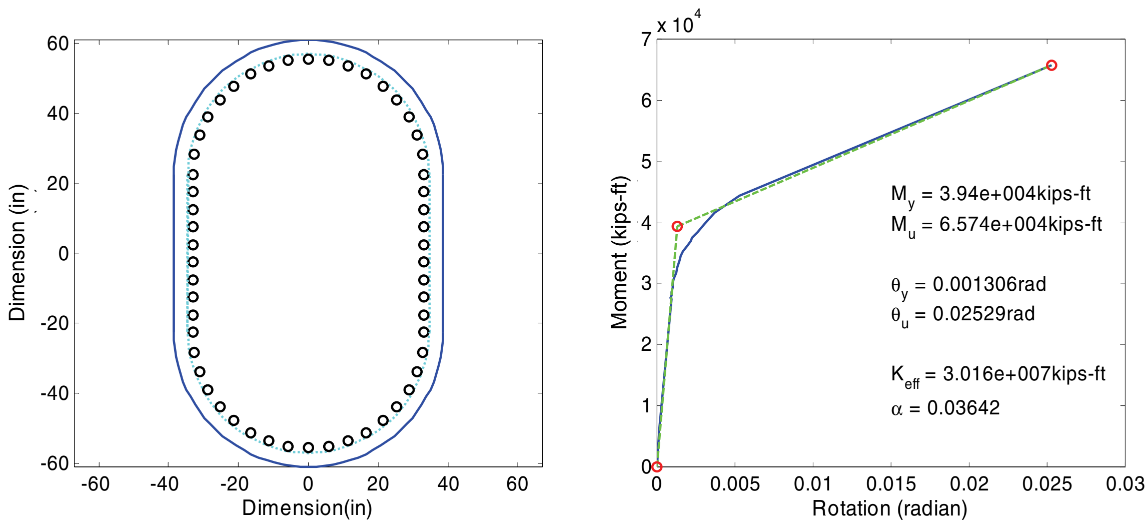

Section of Column Moment-Rotation Curve

(b) After Retrofit

FIGURE A-38 Moment-Curvature Analysis of Column 4 of Bridge 3 in Transverse Direction

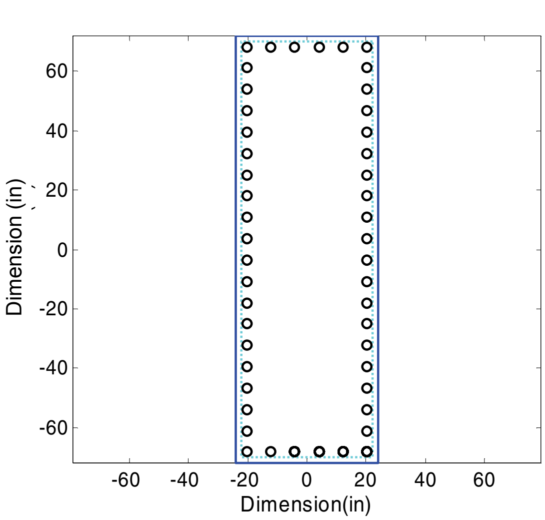

Section of Column

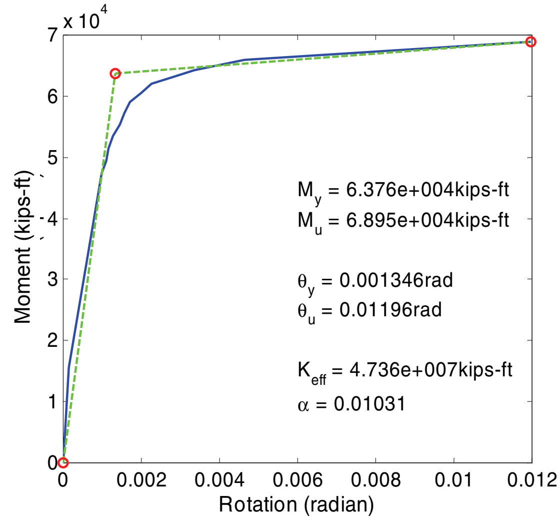

Moment-Rotation Curve

(a) Before Retrofit

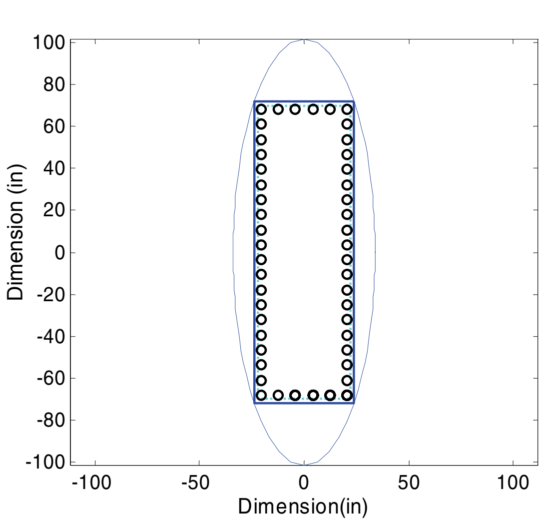

Section of Column

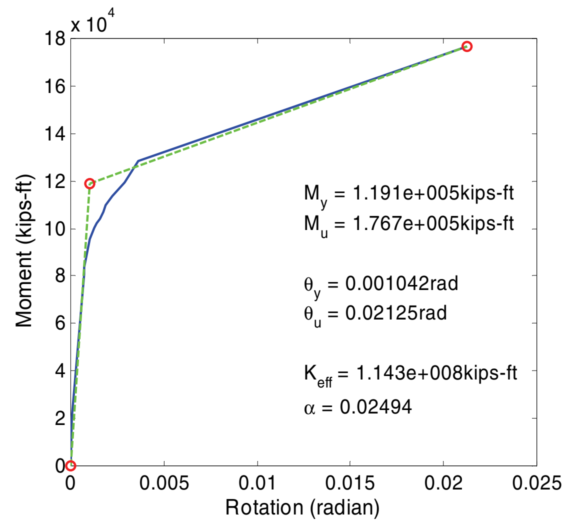

Moment-Rotation Curve

(b) After Retrofit

FIGURE A-39 Moment-Curvature Analysis of Column 1 of Bridge 4 in Transverse Direction

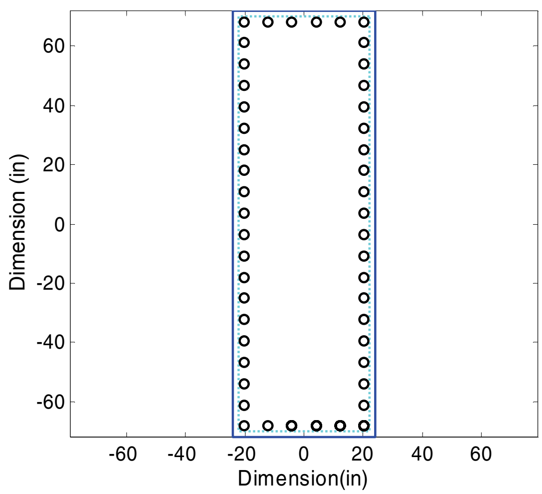

Section of Column

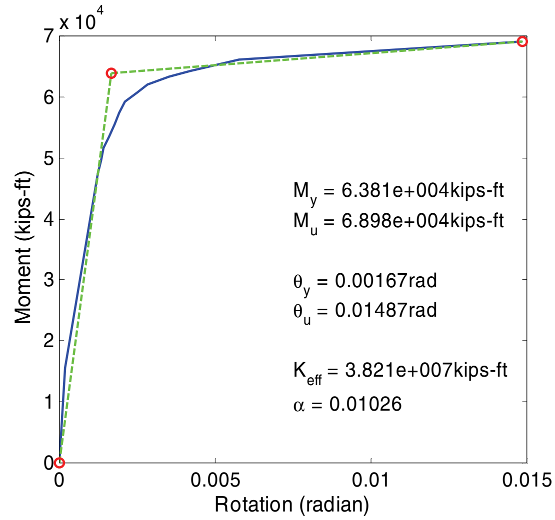

Moment-Rotation Curve

(a) Before Retrofit

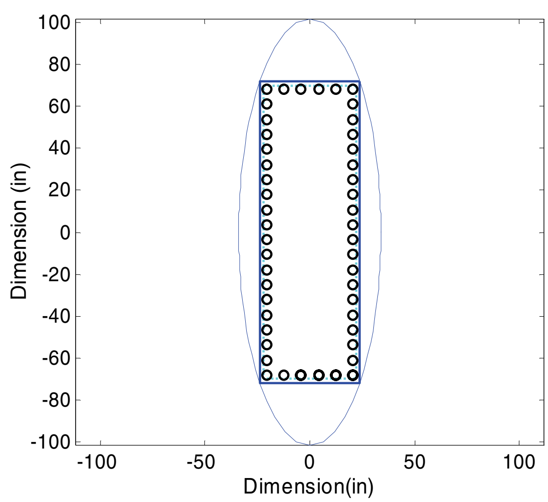

Section of Column

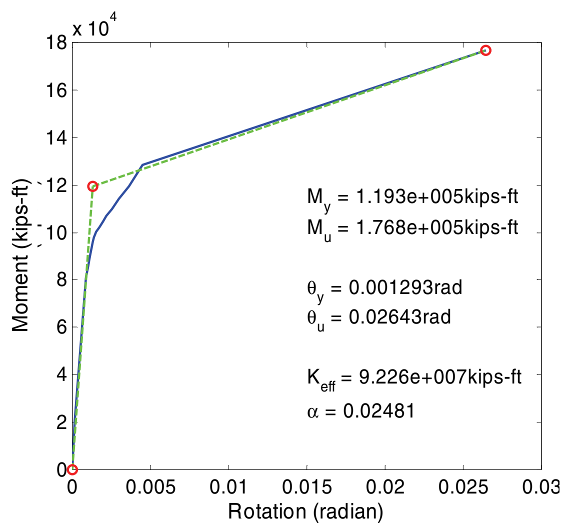

Moment-Rotation Curve

(b) After Retrofit

FIGURE A-40 Moment-Curvature Analysis of Column 2 of Bridge 4 in Transverse Direction

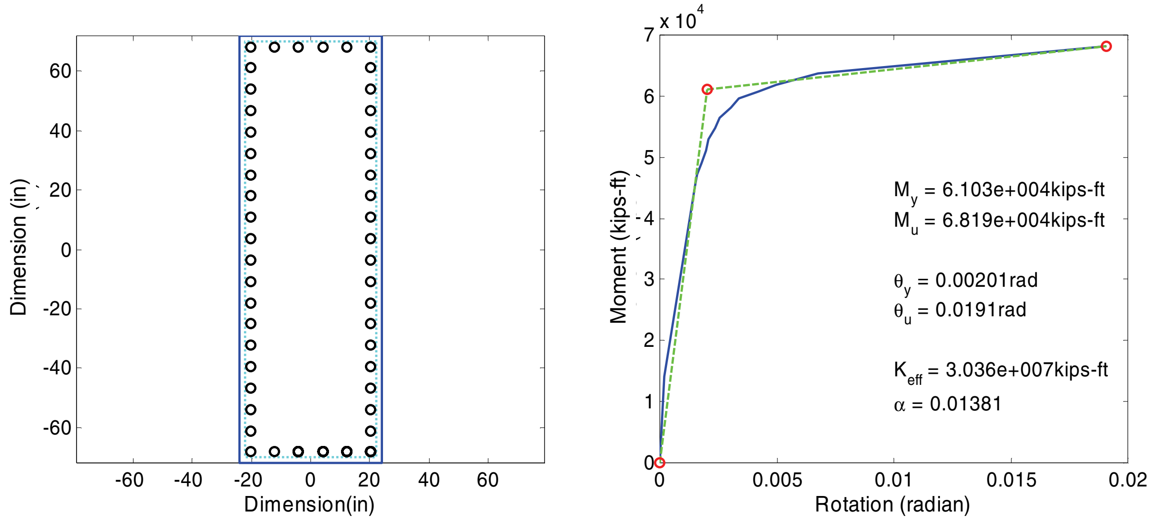

Section of Column　　　　Moment-Rotation Curve

(a) Before Retrofit

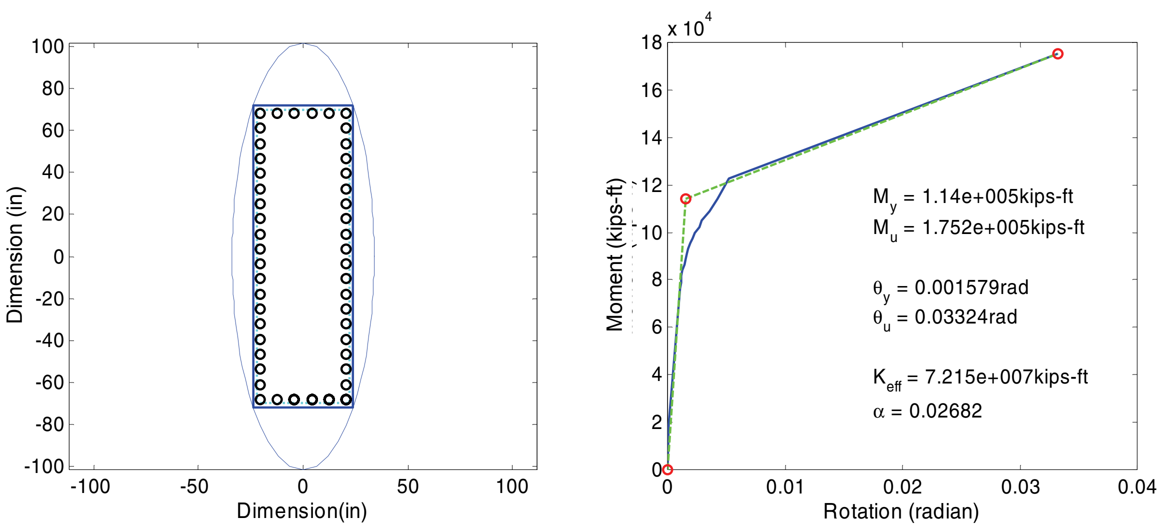

Section of Column　　　　Moment-Rotation Curve

(b) After Retrofit

FIGURE A-41 Moment-Curvature Analysis of Column 3 of Bridge 4 in Transverse Direction

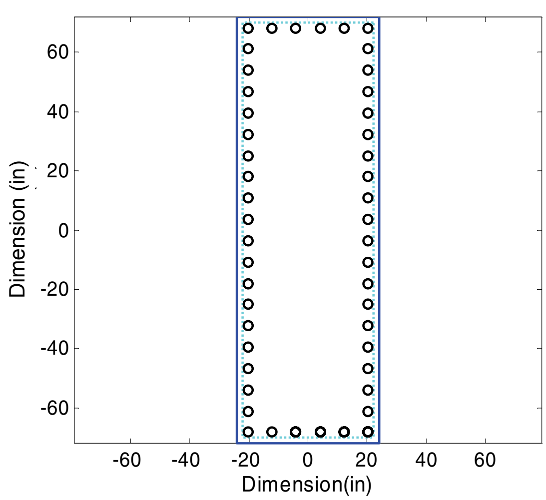

Section of Column

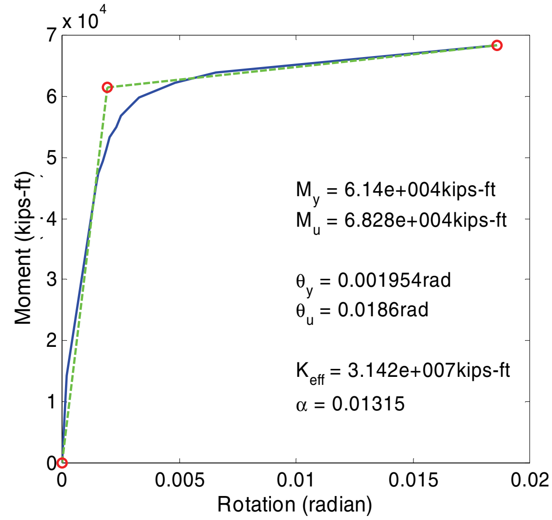

Moment-Rotation Curve

(a) Before Retrofit

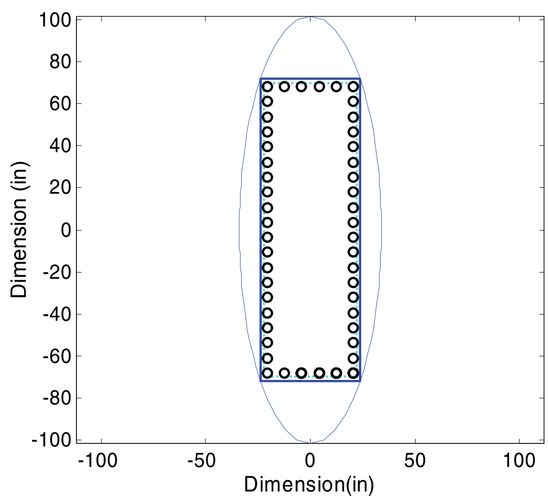

Section of Column

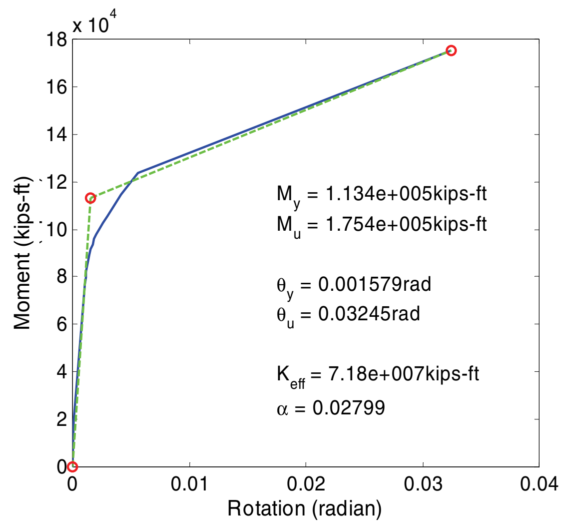

Moment-Rotation Curve

(b) After Retrofit

FIGURE A-42 Moment-Curvature Analysis of Column 4 of Bridge 4 in Transverse Direction

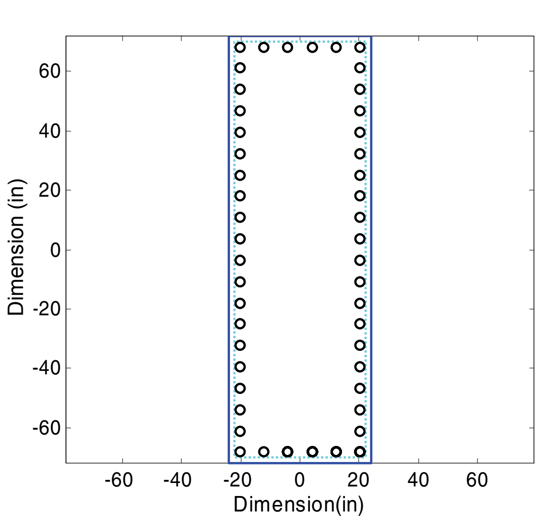

Section of Column

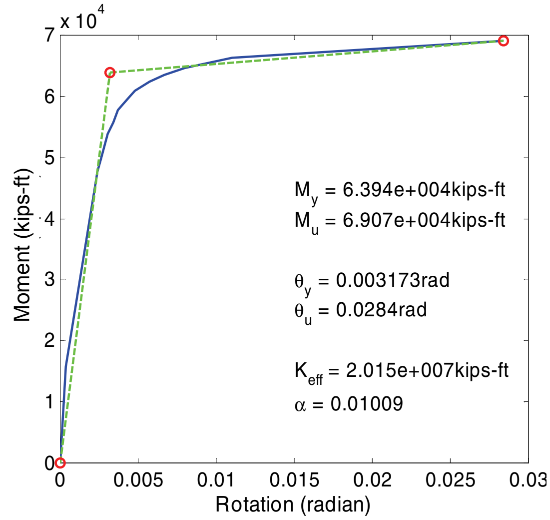

Moment-Rotation Curve

(a) Before Retrofit

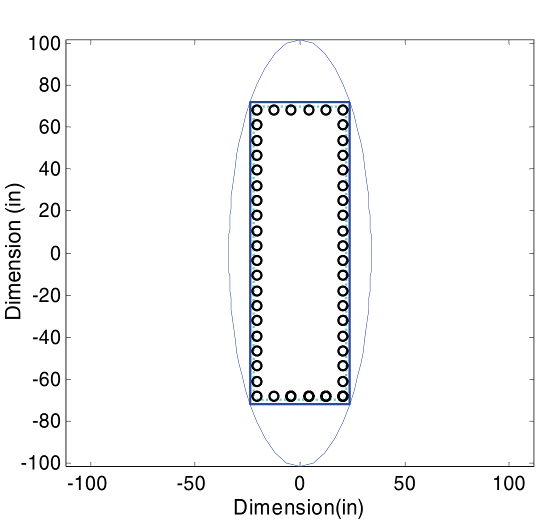

Section of Column

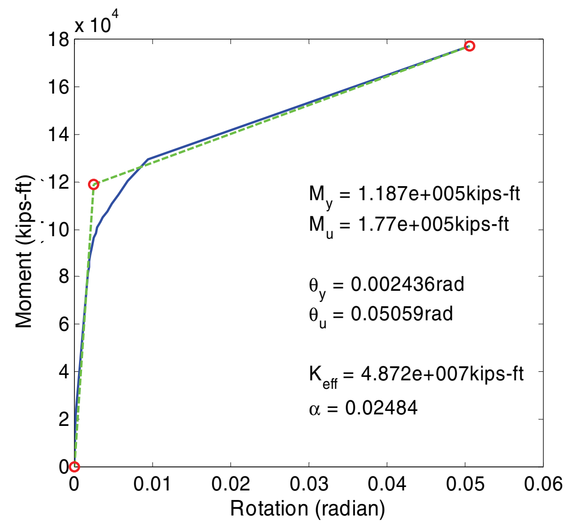

Moment-Rotation Curve

(b) After Retrofit

FIGURE A-43 Moment-Curvature Analysis of Column 5 of Bridge 4 in Transverse Direction

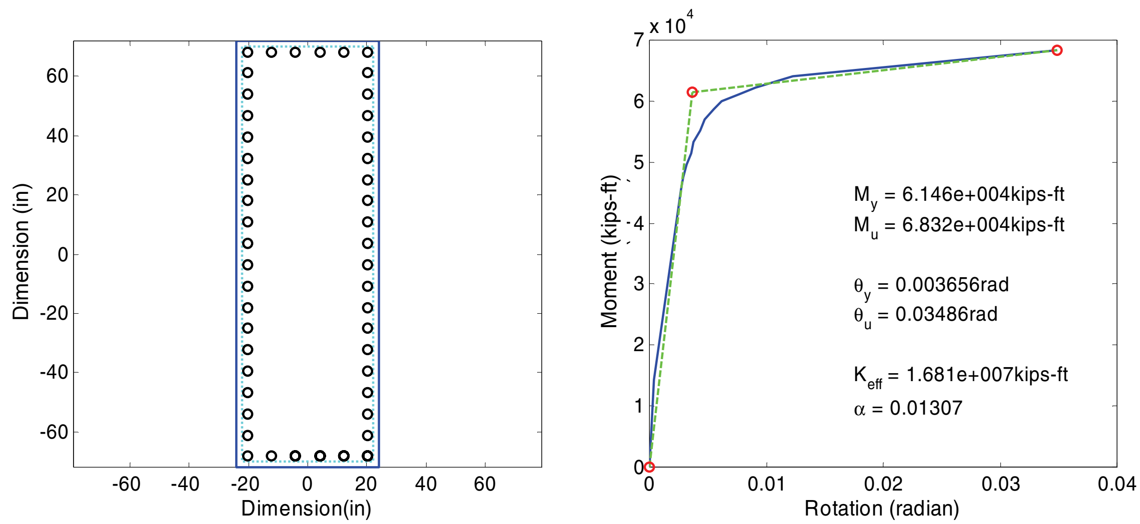

Section of Column Moment-Rotation Curve

(a) Before Retrofit

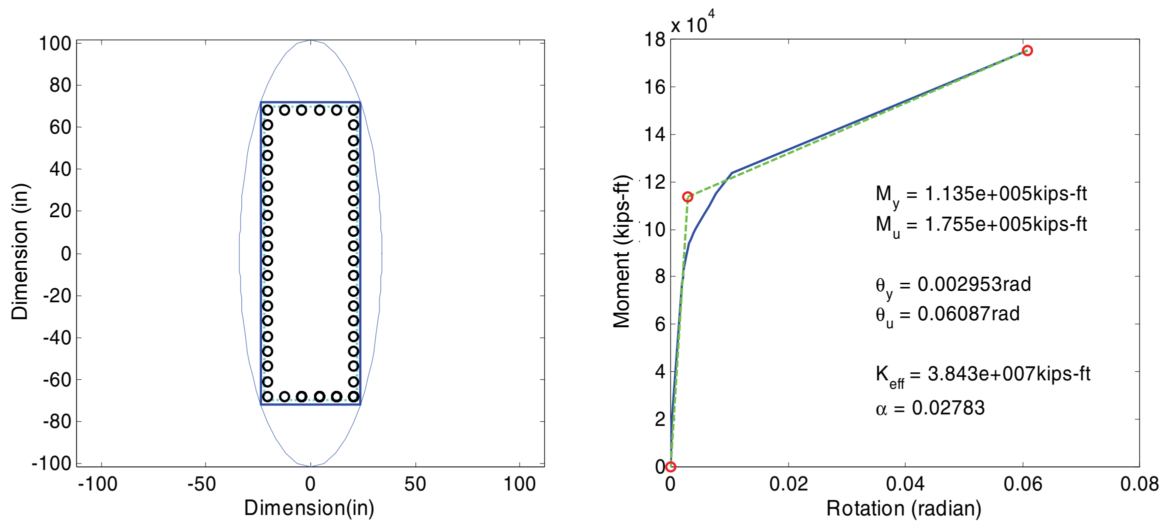

Section of Column Moment-Rotation Curve

(b) After Retrofit

FIGURE A-44 Moment-Curvature Analysis of Column 6 of Bridge 4 in Transverse Direction

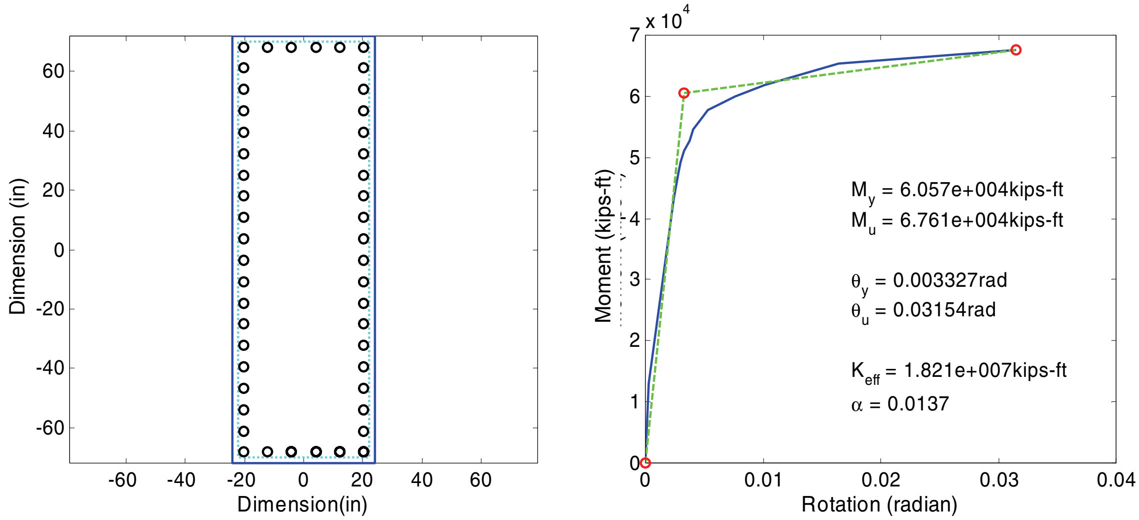

Section of Column — Moment-Rotation Curve

(a) Before Retrofit

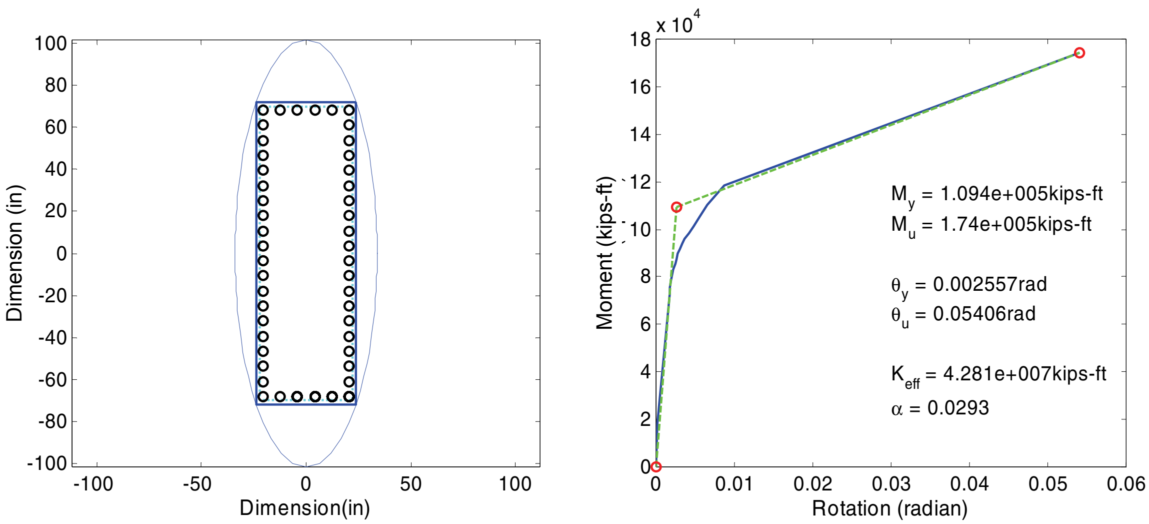

Section of Column — Moment-Rotation Curve

(b) After Retrofit

FIGURE A-45 Moment-Curvature Analysis of Column 7 of Bridge 4 in Transverse Direction

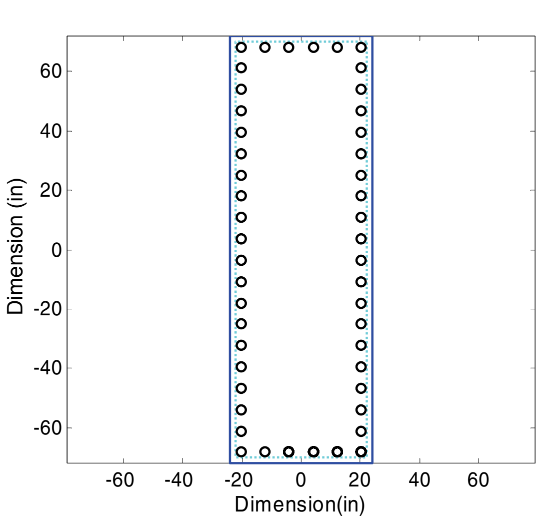

Section of Column

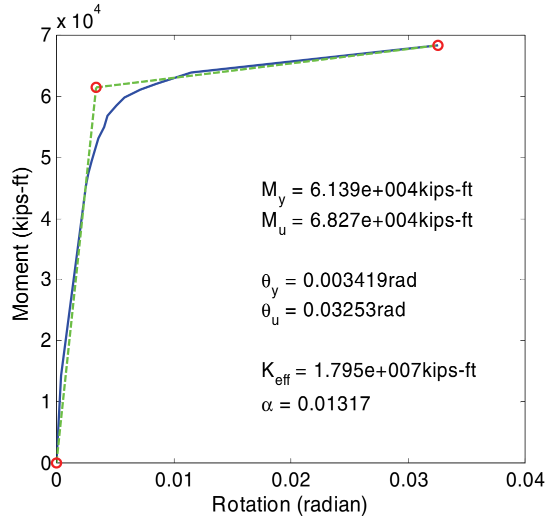

Moment-Rotation Curve

(a) Before Retrofit

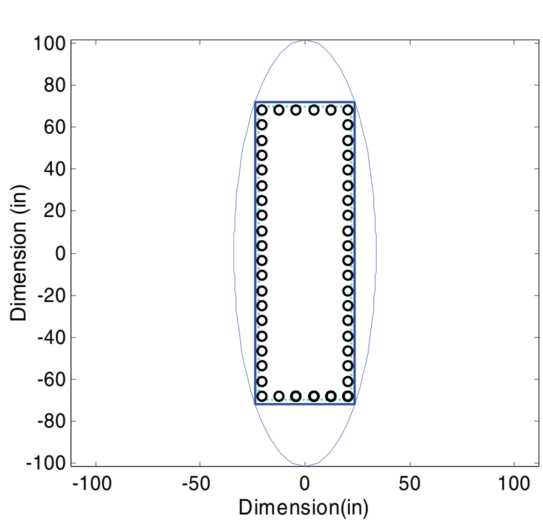

Section of Column

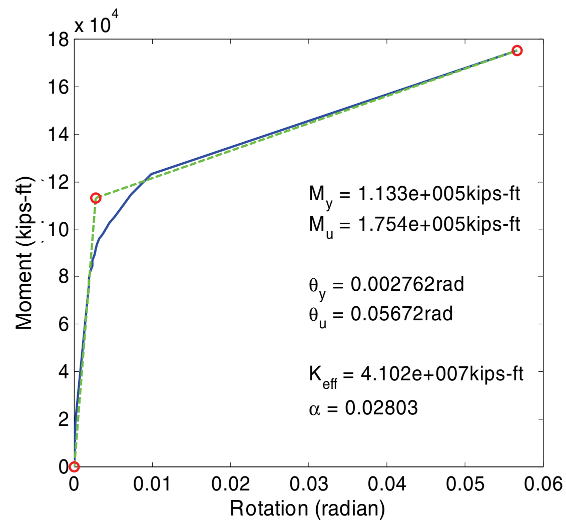

Moment-Rotation Curve

(b) After Retrofit

FIGURE A-46 Moment-Curvature Analysis of Column 8 of Bridge 4 in Transverse Direction

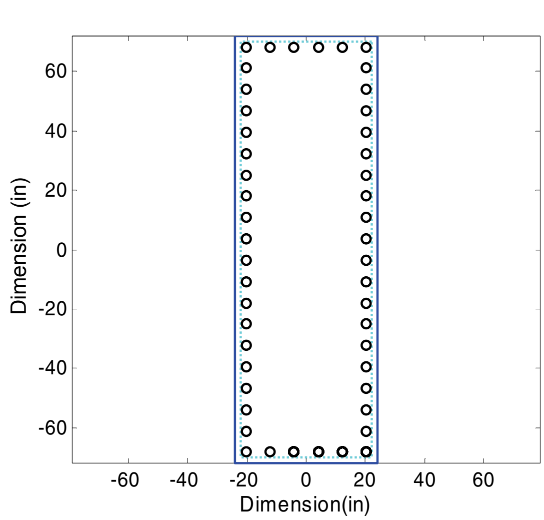

Section of Column

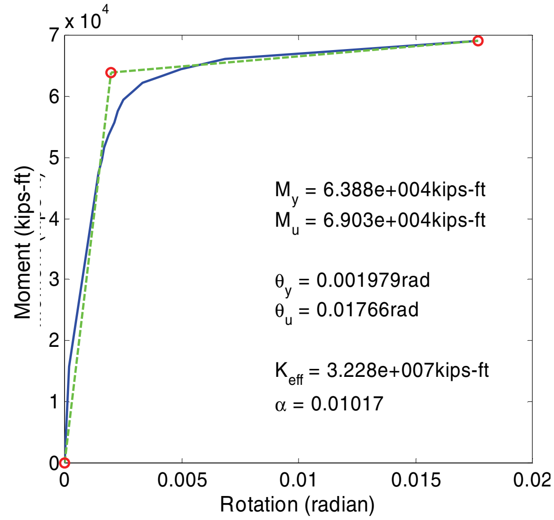

Moment-Rotation Curve

(a) Before Retrofit

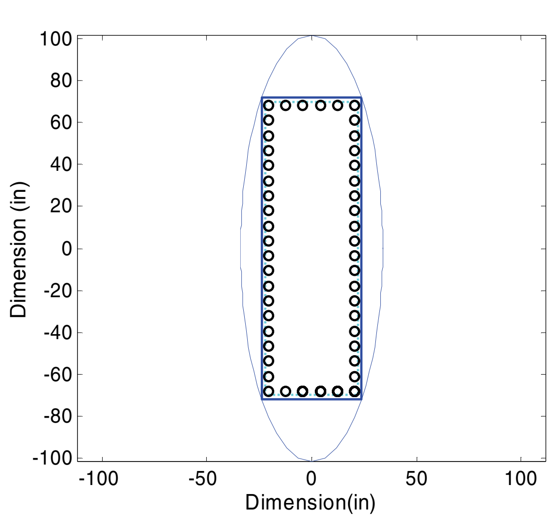

Section of Column

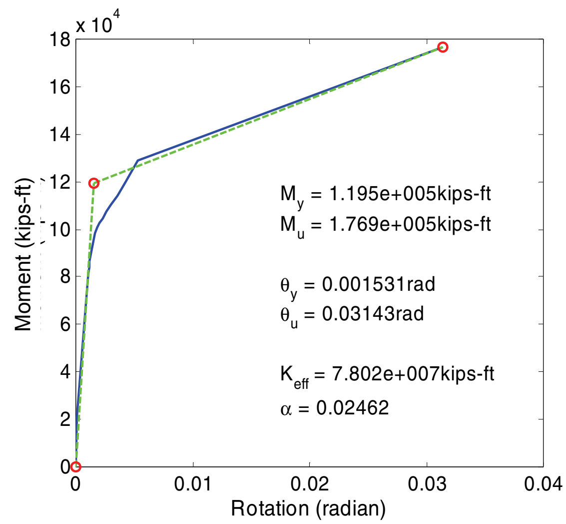

Moment-Rotation Curve

(b) After Retrofit

FIGURE A-47 Moment-Curvature Analysis of Column 9 of Bridge 4 in Transverse Direction

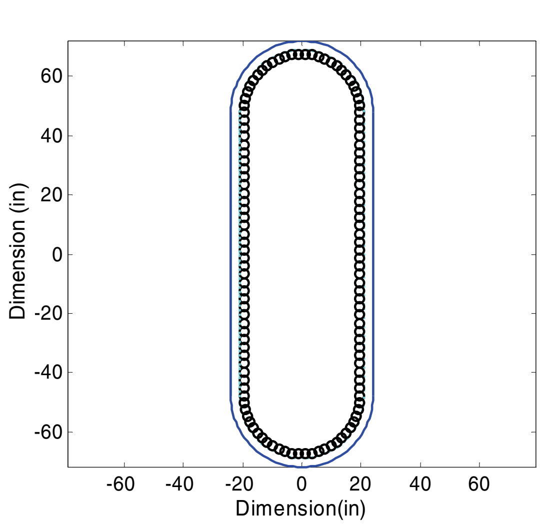

Section of Column

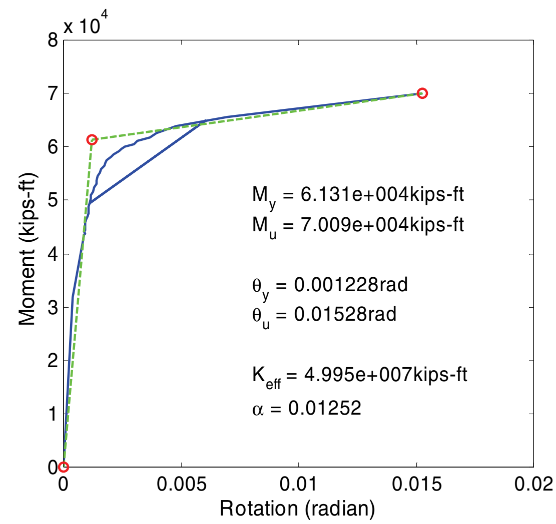

Moment-Rotation Curve

(a) Before Retrofit

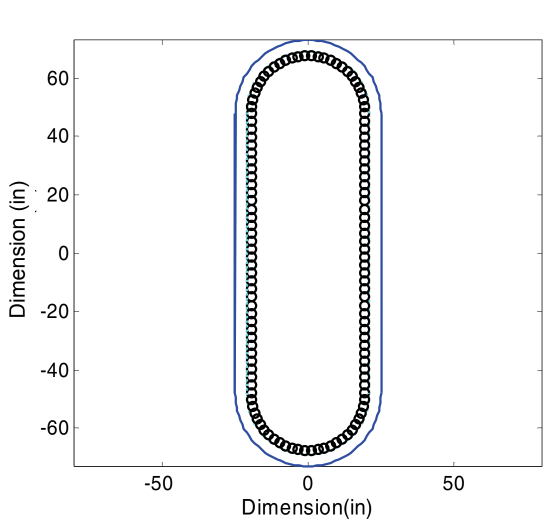

Section of Column

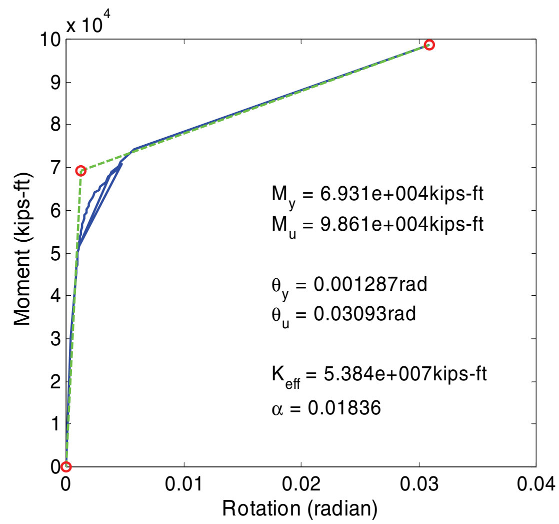

Moment-Rotation Curve

(b) After Retrofit

FIGURE A-48 Moment-Curvature Analysis of Column 1 of Bridge 5 in Transverse Direction

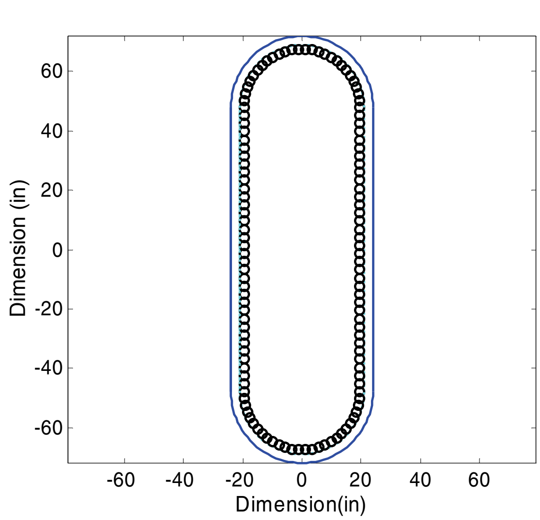

Section of Column

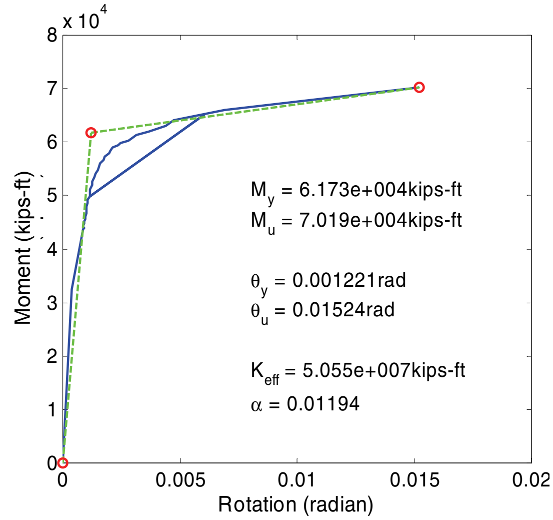

Moment-Rotation Curve

(a) Before Retrofit

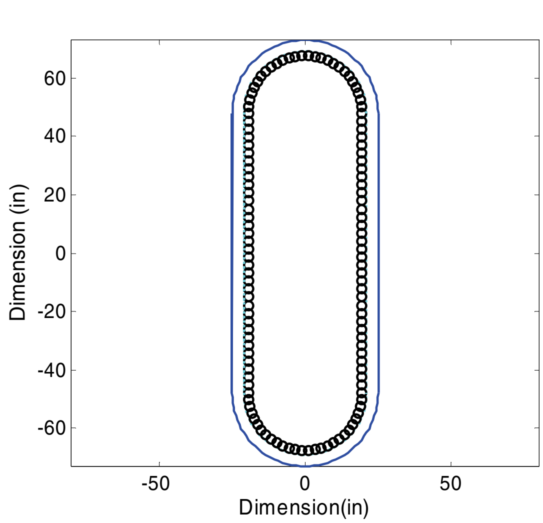

Section of Column

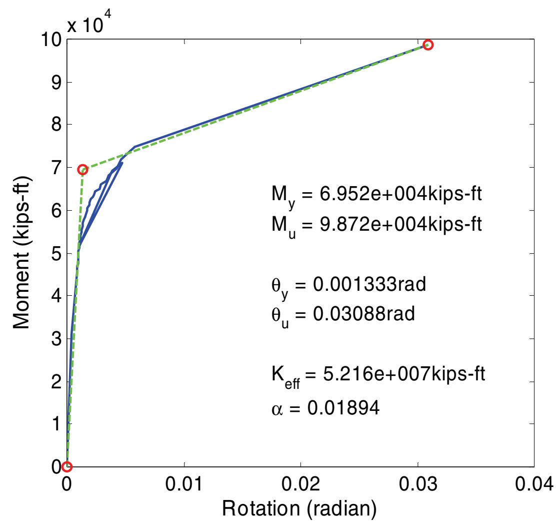

Moment-Rotation Curve

(b) After Retrofit

FIGURE A-49 Moment-Curvature Analysis of Column 2 of Bridge 5 in Transverse Direction

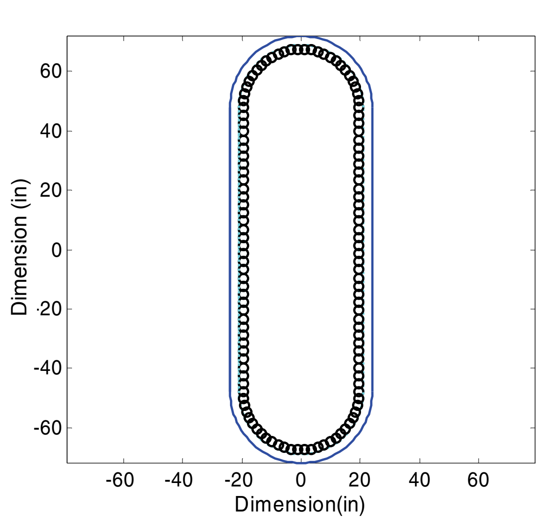

Section of Column

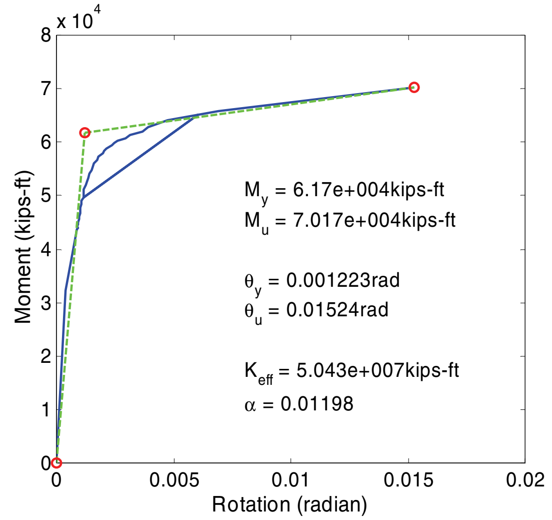

Moment-Rotation Curve

(a) Before Retrofit

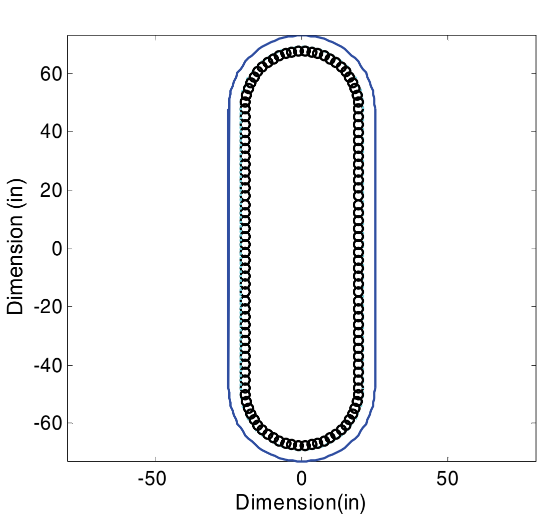

Section of Column

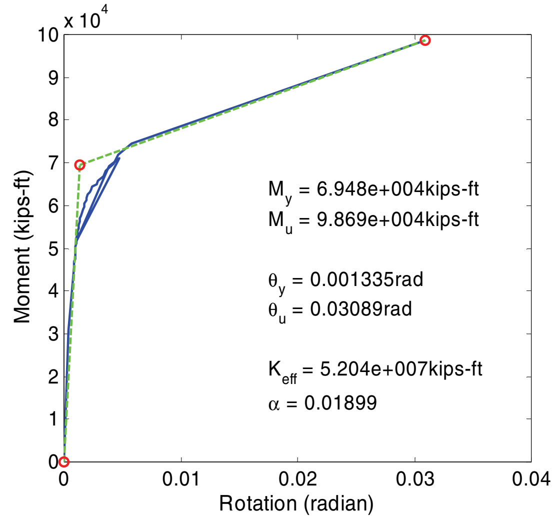

Moment-Rotation Curve

(b) After Retrofit

FIGURE A-50 Moment-Curvature Analysis of Column 3 of Bridge 5 in Transverse Direction

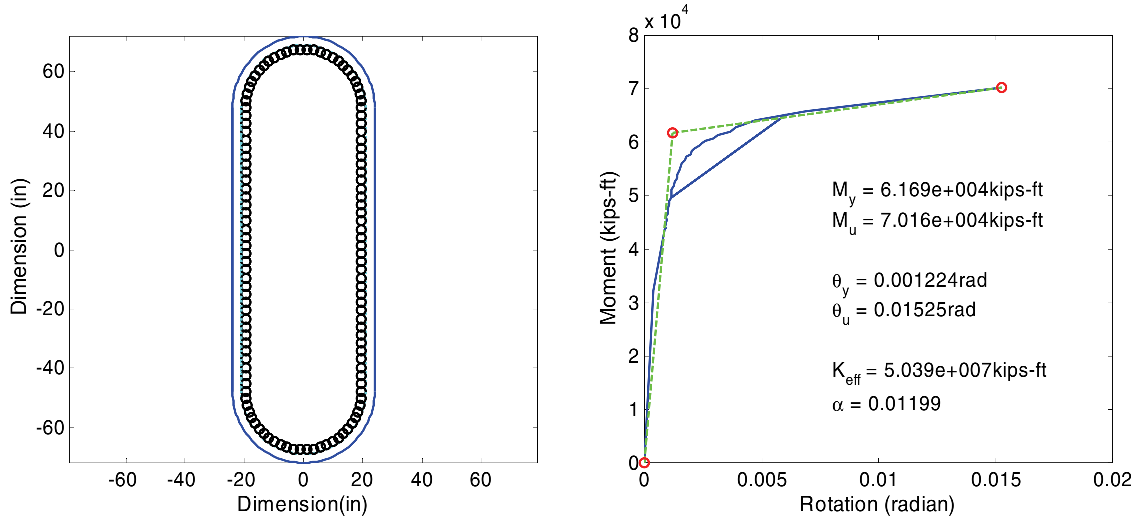

Section of Column

Moment-Rotation Curve

(a) Before Retrofit

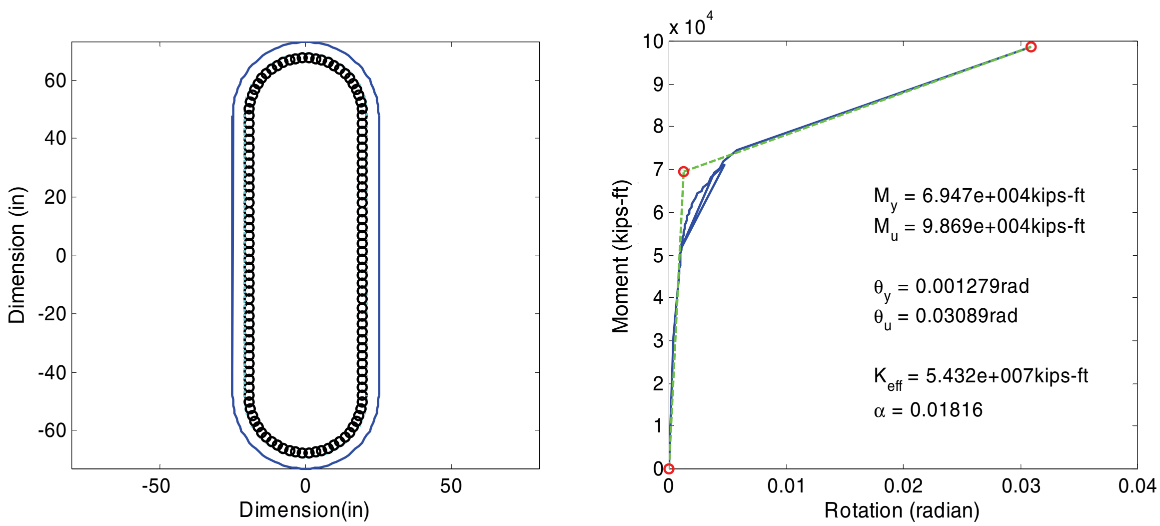

Section of Column

Moment-Rotation Curve

(b) After Retrofit

FIGURE A-51 Moment-Curvature Analysis of Column 4 of Bridge 5 in Transverse Direction

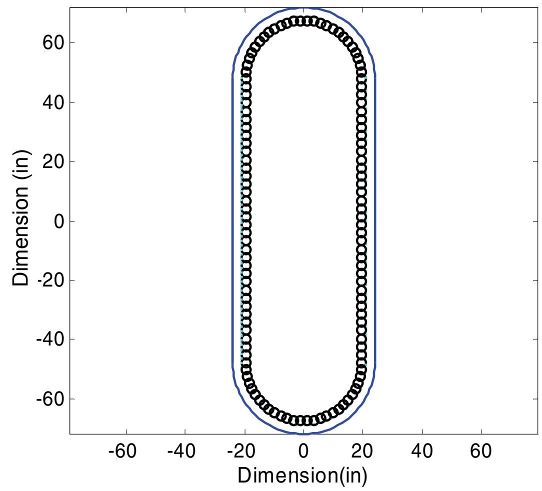

Section of Column

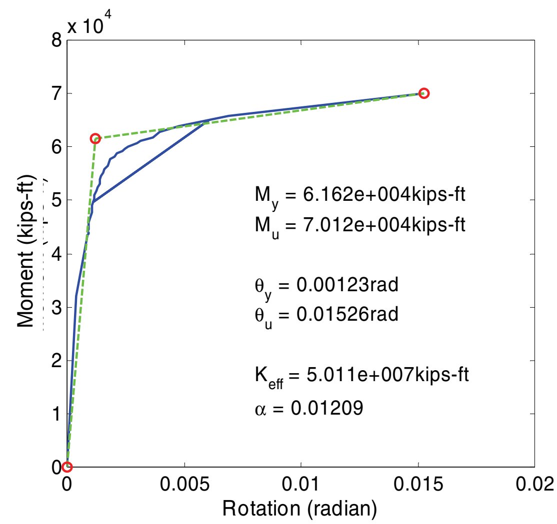

Moment-Rotation Curve

(a) Before Retrofit

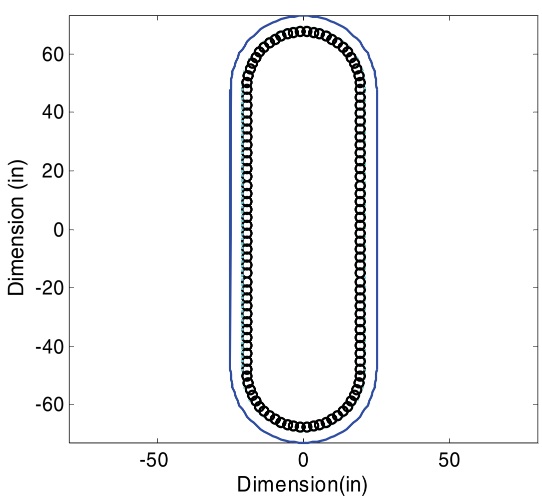

Section of Column

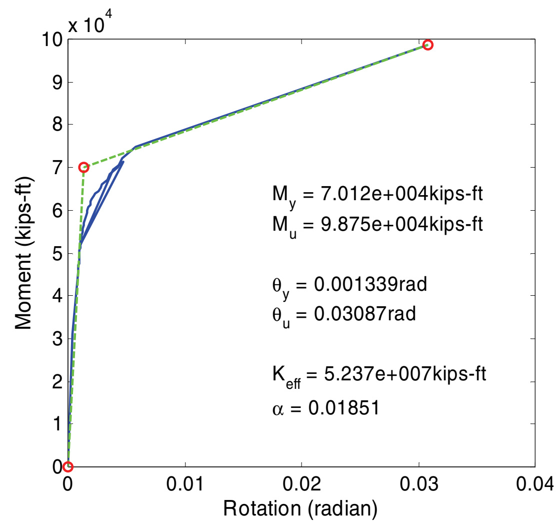

Moment-Rotation Curve

(b) After Retrofit

FIGURE A-52 Moment-Curvature Analysis of Column 5 of Bridge 5 in Transverse Direction

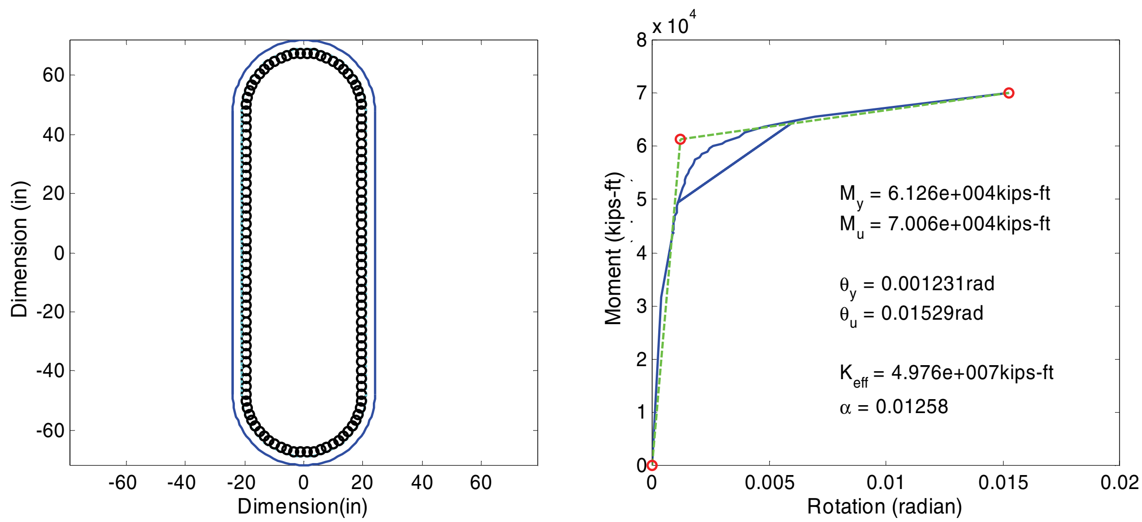

Section of Column Moment-Rotation Curve

(a) Before Retrofit

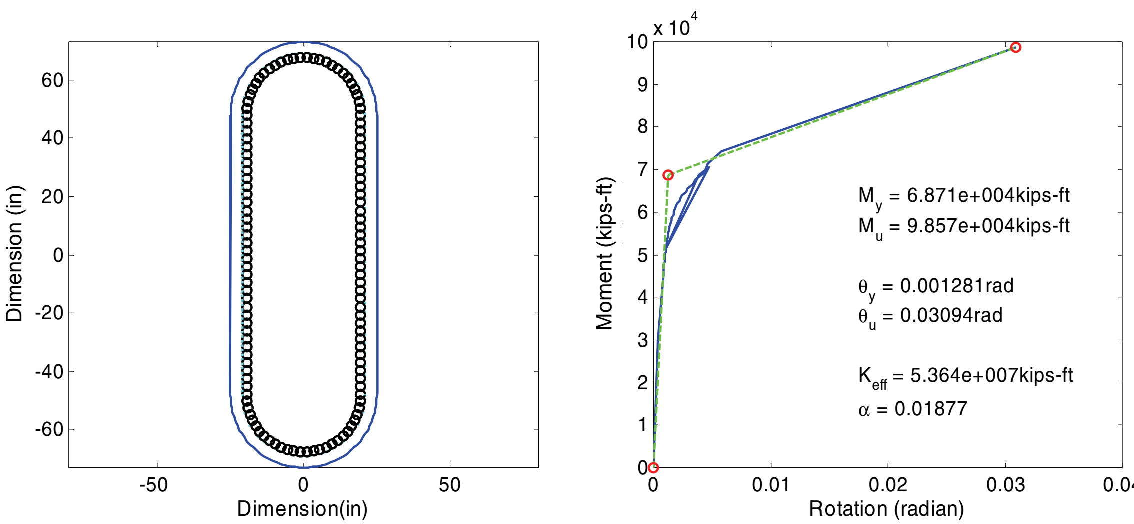

Section of Column Moment-Rotation Curve

(b) After Retrofit

FIGURE A-53 Moment-Curvature Analysis of Column 6 of Bridge 5 in Transverse Direction

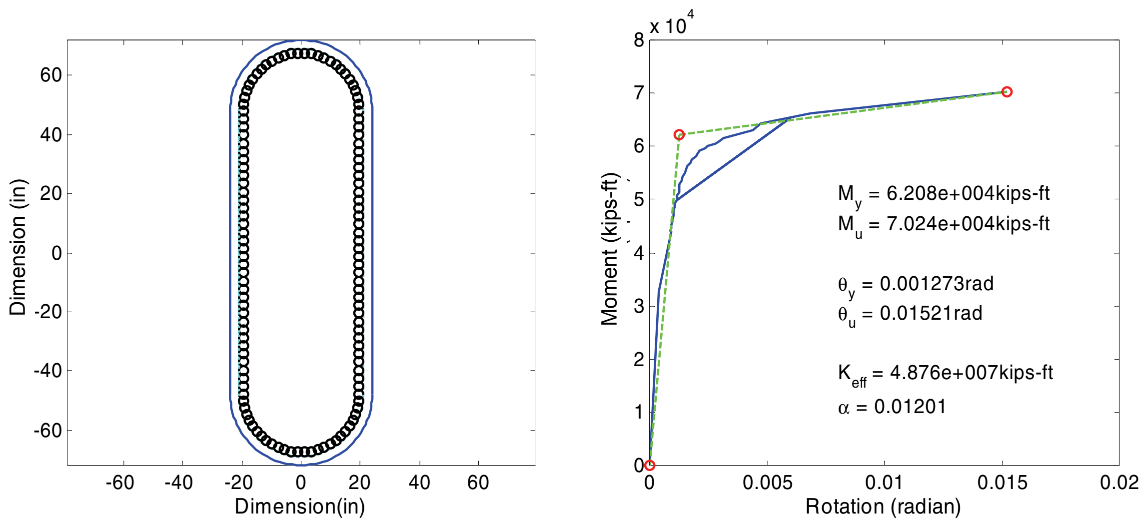

Section of Column

Moment-Rotation Curve

(a) Before Retrofit

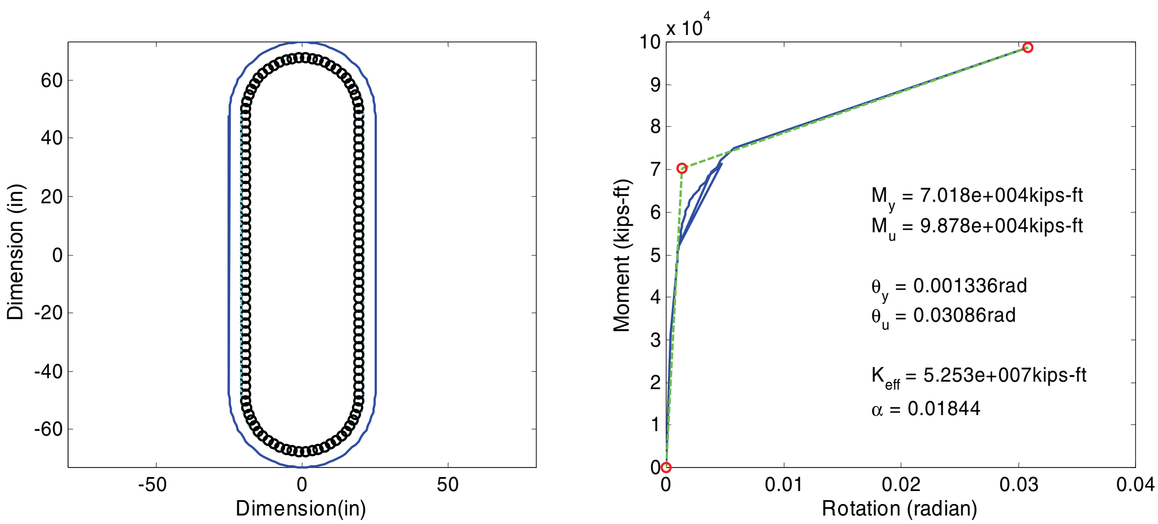

Section of Column

Moment-Rotation Curve

(b) After Retrofit

FIGURE A-54 Moment-Curvature Analysis of Column 7 of Bridge 5 in Transverse Direction

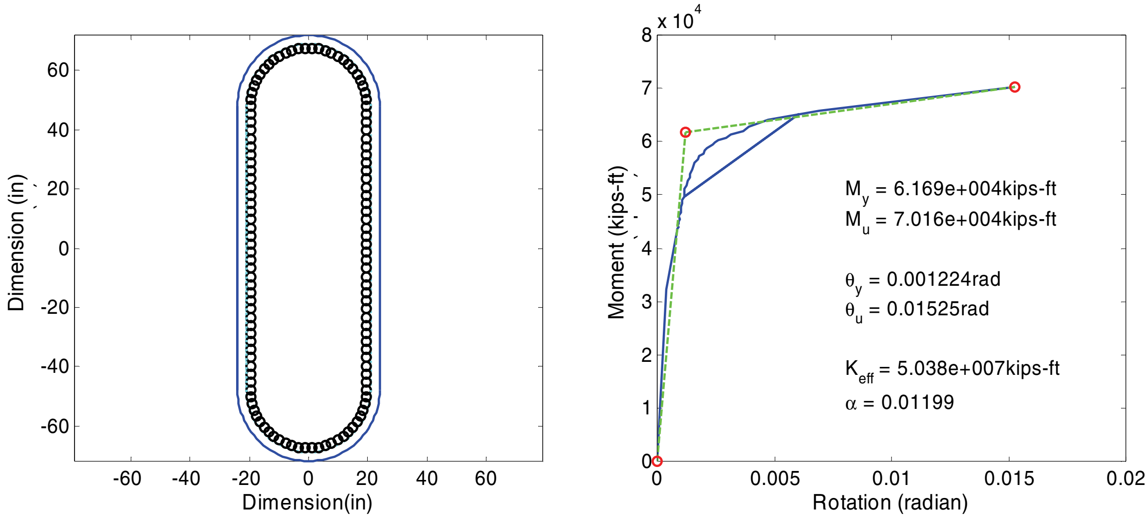

Section of Column Moment-Rotation Curve

(a) Before Retrofit

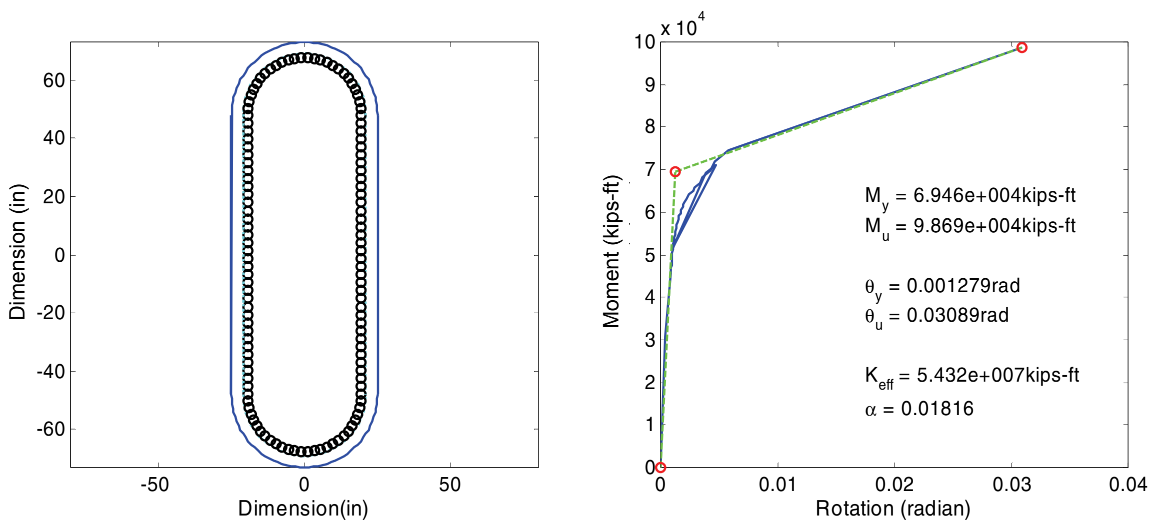

Section of Column Moment-Rotation Curve

(b) After Retrofit

FIGURE A-55 Moment-Curvature Analysis of Column 8 of Bridge 5 in Transverse Direction

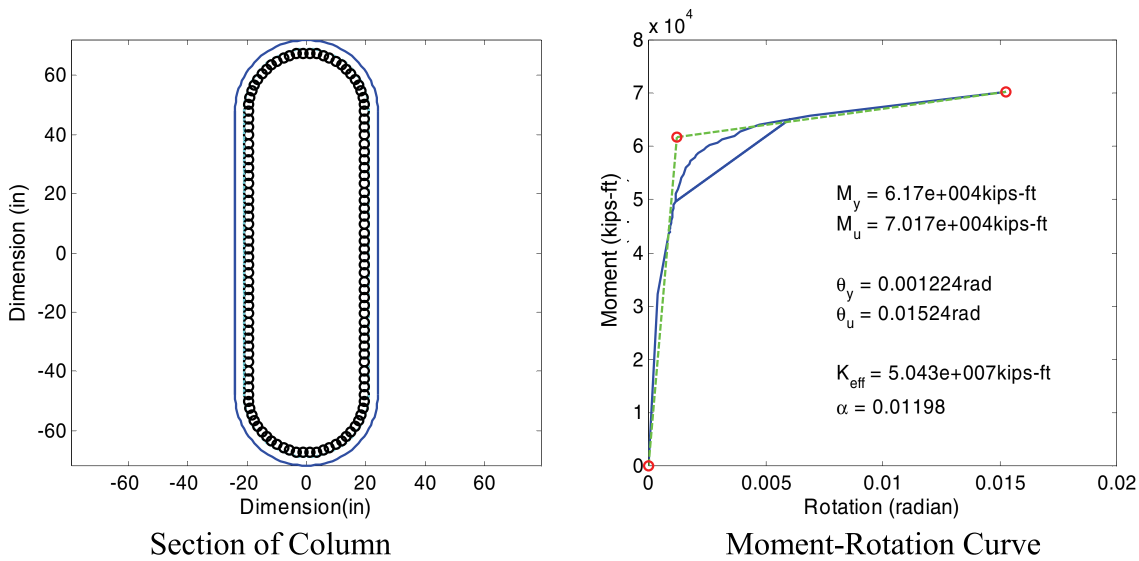

(a) Before Retrofit

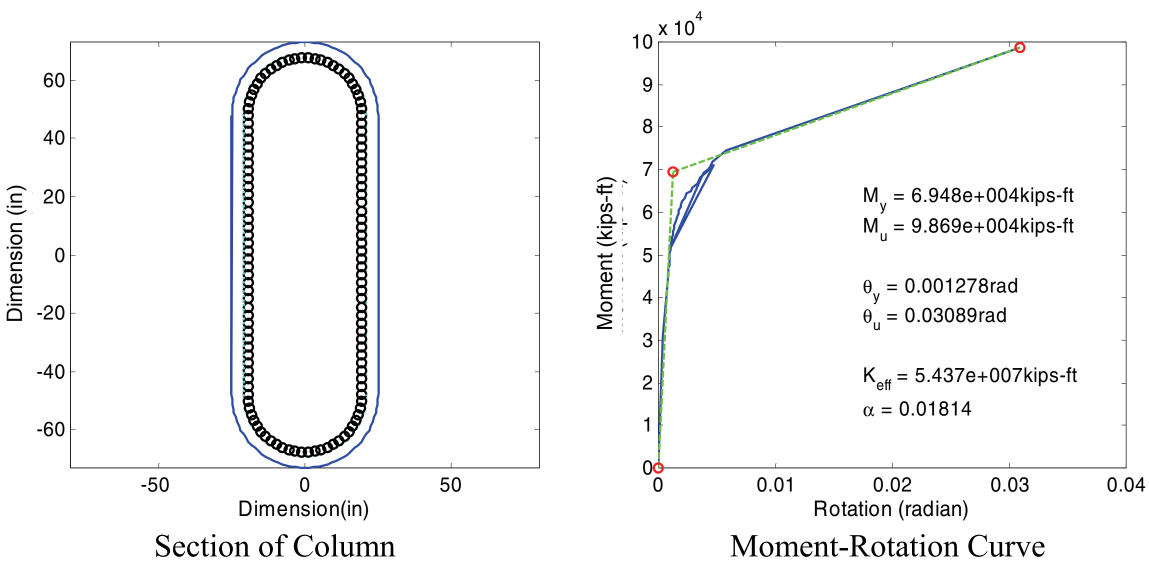

(b) After Retrofit

FIGURE A-56 Moment-Curvature Analysis of Column 9 of Bridge 5 in Transverse Direction

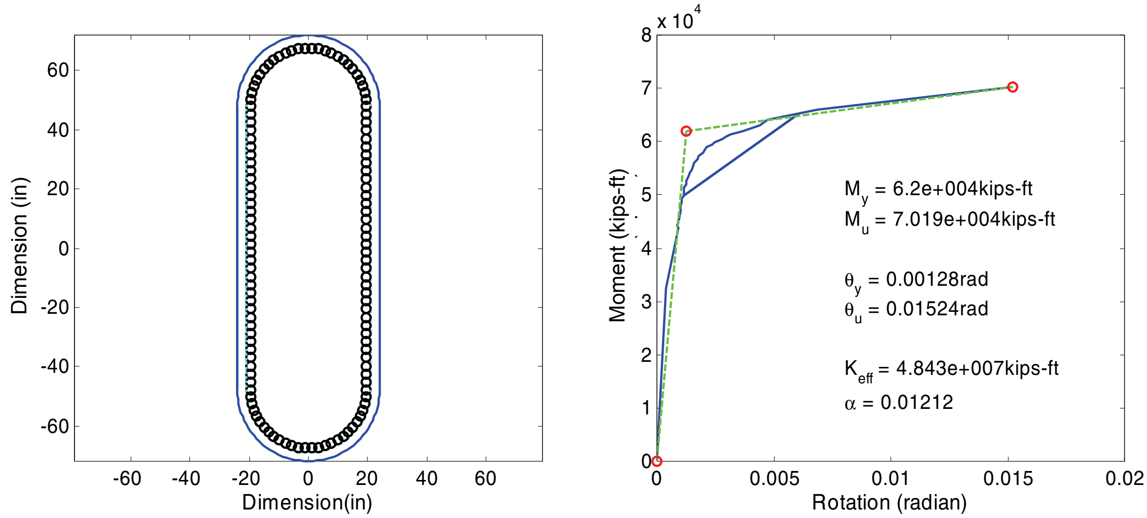

Section of Column Moment-Rotation Curve

(a) Before Retrofit

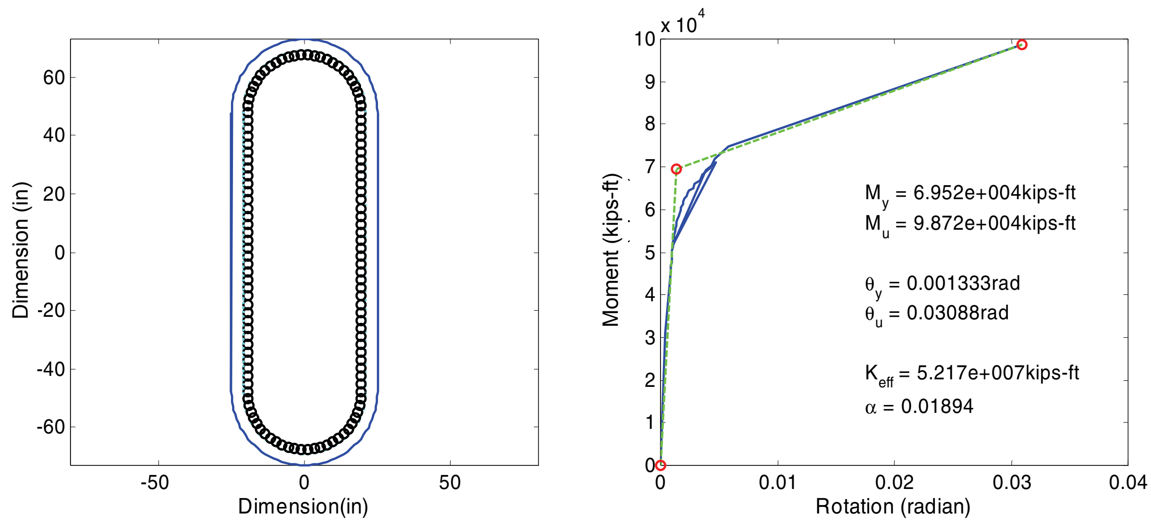

Section of Column Moment-Rotation Curve

(b) After Retrofit

FIGURE A-57 Moment-Curvature Analysis of Column 10 of Bridge 5 in Transverse Direction

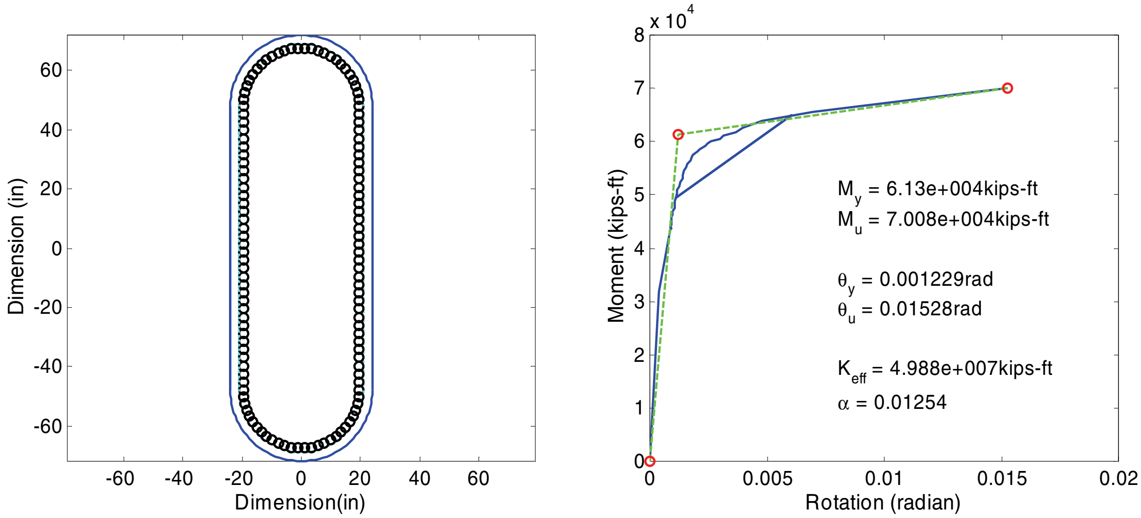

Section of Column Moment-Rotation Curve

(a) Before Retrofit

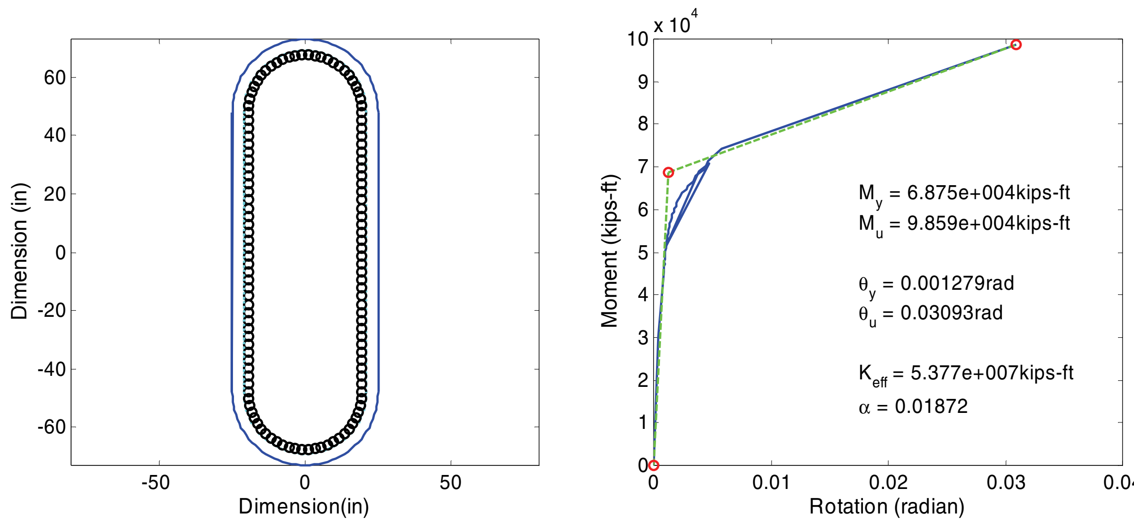

Section of Column Moment-Rotation Curve

(b) After Retrofit

FIGURE A-58 Moment-Curvature Analysis of Column 11 of Bridge 5 in Transverse Direction

APPENDIX B
STIFFNESS AND STRENGTH DEGRADATION OF MOMENT-ROTATION RELATIONSHIP

In this study, Bridge 1 is analyzed under 60 ground motions for the following models of moment-rotation relation; elastic-plastic, bi-linear, stiffness degradation, and stiffness and strength degradation. For all cases, the same yield moment and yield rotation are used. The above four moment-rotation relationships at plastic hinge locations are plotted in Figure B-1.

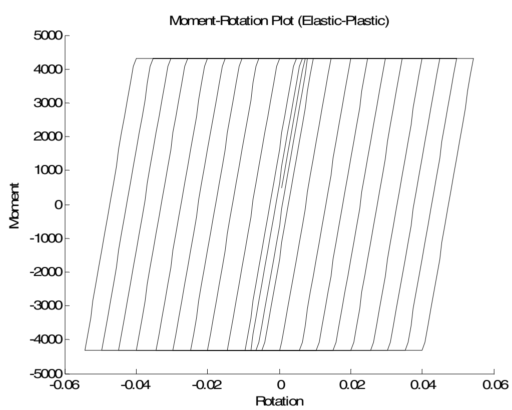

(a) Elastic-Plastic Model

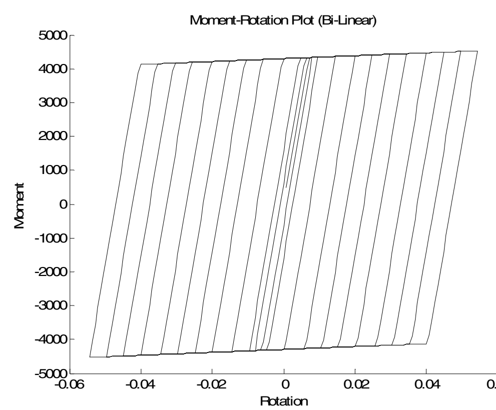

(b) Bi-Linear Model

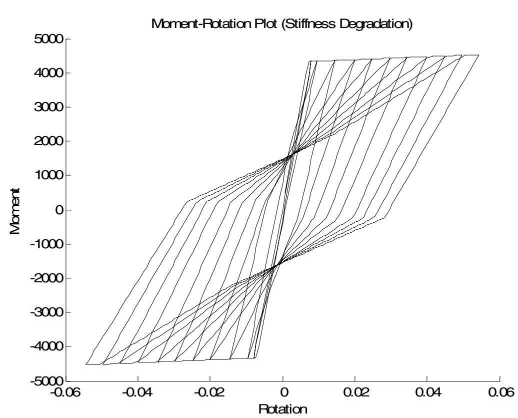

(c) Stiffness-Degradation Model

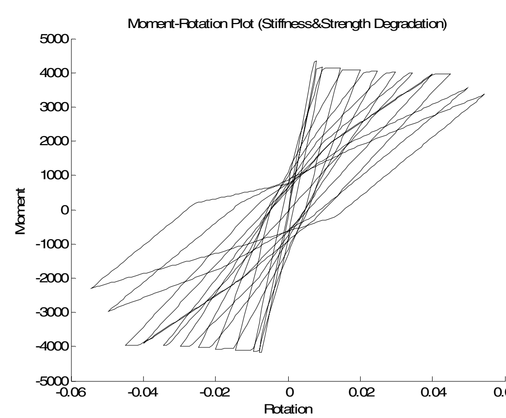

(d) Stiffness & Strength-Degradation Model

FIGURE B-1 Moment-Rotation Relationship

Figures B-2, B-3, B-4 and B-5 represent fragility curves computed with these nonlinear models respectively for almost no, minor, moderate and major damage states. Result indicates that fragility curves at almost no damage are nearly the same for these four models. In other three damage states, fragility curves using stiffness and strength degradation model are the weakest among all curves.

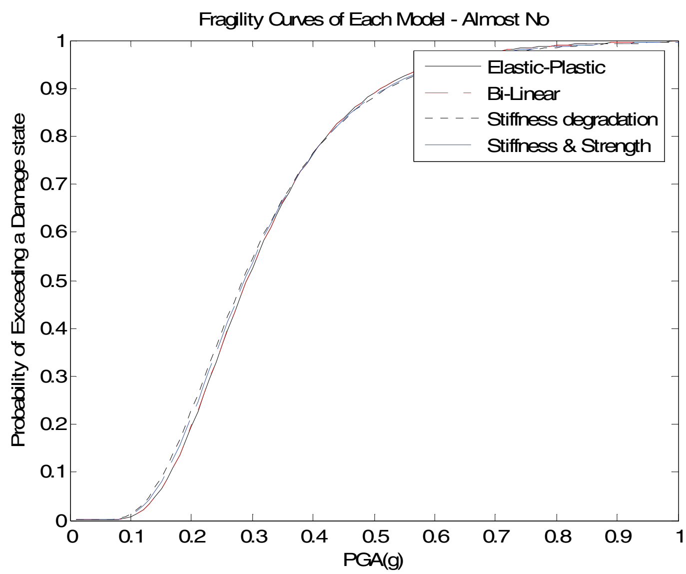

FIGURE B-2 Fragility Curves in Almost No Damage State

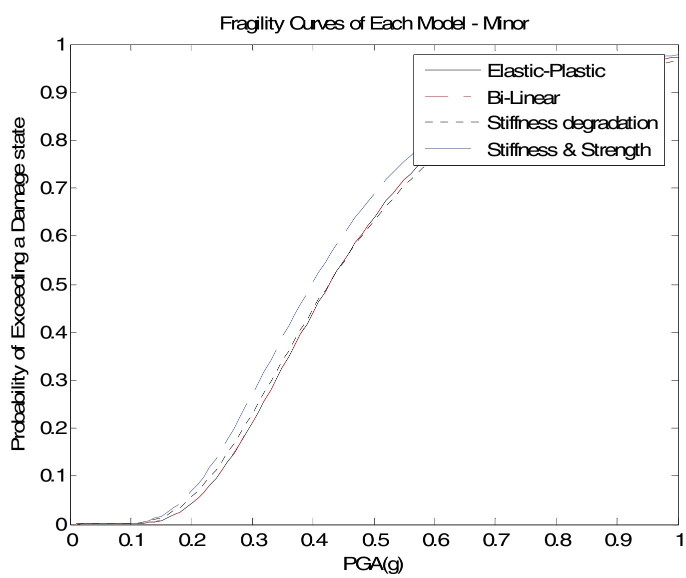

FIGURE B-3 Fragility Curves in Minor Damage State

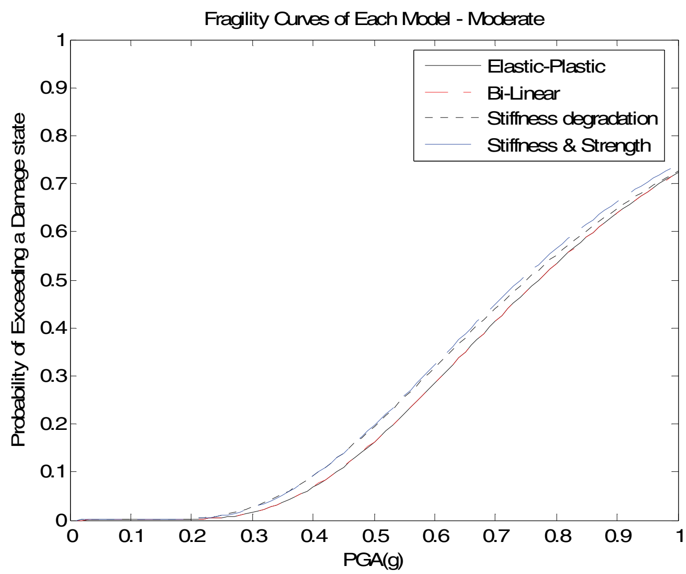

FIGURE B-4 Fragility Curves in Moderate Damage State

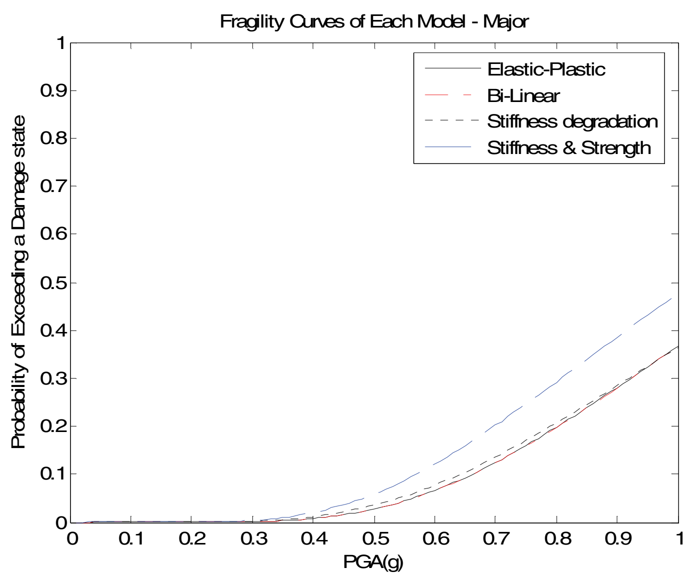

FIGURE B-5 Fragility Curves in Major Damage State

MCEER Technical Reports

MCEER publishes technical reports on a variety of subjects written by authors funded through MCEER. These reports are available from both MCEER Publications and the National Technical Information Service (NTIS). Requests for reports should be directed to MCEER Publications, MCEER, University at Buffalo, State University of New York, Red Jacket Quadrangle, Buffalo, New York 14261. Reports can also be requested through NTIS, 5285 Port Royal Road, Springfield, Virginia 22161. NTIS accession numbers are shown in parenthesis, if available.

NCEER-87-0001 "First-Year Program in Research, Education and Technology Transfer," 3/5/87, (PB88-134275, A04, MF-A01).

NCEER-87-0002 "Experimental Evaluation of Instantaneous Optimal Algorithms for Structural Control," by R.C. Lin, T.T. Soong and A.M. Reinhorn, 4/20/87, (PB88-134341, A04, MF-A01).

NCEER-87-0003 "Experimentation Using the Earthquake Simulation Facilities at University at Buffalo," by A.M. Reinhorn and R.L. Ketter, to be published.

NCEER-87-0004 "The System Characteristics and Performance of a Shaking Table," by J.S. Hwang, K.C. Chang and G.C. Lee, 6/1/87, (PB88-134259, A03, MF-A01). This report is available only through NTIS (see address given above).

NCEER-87-0005 "A Finite Element Formulation for Nonlinear Viscoplastic Material Using a Q Model," by O. Gyebi and G. Dasgupta, 11/2/87, (PB88-213764, A08, MF-A01).

NCEER-87-0006 "Symbolic Manipulation Program (SMP) - Algebraic Codes for Two and Three Dimensional Finite Element Formulations," by X. Lee and G. Dasgupta, 11/9/87, (PB88-218522, A05, MF-A01).

NCEER-87-0007 "Instantaneous Optimal Control Laws for Tall Buildings Under Seismic Excitations," by J.N. Yang, A. Akbarpour and P. Ghaemmaghami, 6/10/87, (PB88-134333, A06, MF-A01). This report is only available through NTIS (see address given above).

NCEER-87-0008 "IDARC: Inelastic Damage Analysis of Reinforced Concrete Frame - Shear-Wall Structures," by Y.J. Park, A.M. Reinhorn and S.K. Kunnath, 7/20/87, (PB88-134325, A09, MF-A01). This report is only available through NTIS (see address given above).

NCEER-87-0009 "Liquefaction Potential for New York State: A Preliminary Report on Sites in Manhattan and Buffalo," by M. Budhu, V. Vijayakumar, R.F. Giese and L. Baumgras, 8/31/87, (PB88-163704, A03, MF-A01). This report is available only through NTIS (see address given above).

NCEER-87-0010 "Vertical and Torsional Vibration of Foundations in Inhomogeneous Media," by A.S. Veletsos and K.W. Dotson, 6/1/87, (PB88-134291, A03, MF-A01). This report is only available through NTIS (see address given above).

NCEER-87-0011 "Seismic Probabilistic Risk Assessment and Seismic Margins Studies for Nuclear Power Plants," by Howard H.M. Hwang, 6/15/87, (PB88-134267, A03, MF-A01). This report is only available through NTIS (see address given above).

NCEER-87-0012 "Parametric Studies of Frequency Response of Secondary Systems Under Ground-Acceleration Excitations," by Y. Yong and Y.K. Lin, 6/10/87, (PB88-134309, A03, MF-A01). This report is only available through NTIS (see address given above).

NCEER-87-0013 "Frequency Response of Secondary Systems Under Seismic Excitation," by J.A. HoLung, J. Cai and Y.K. Lin, 7/31/87, (PB88-134317, A05, MF-A01). This report is only available through NTIS (see address given above).

NCEER-87-0014 "Modelling Earthquake Ground Motions in Seismically Active Regions Using Parametric Time Series Methods," by G.W. Ellis and A.S. Cakmak, 8/25/87, (PB88-134283, A08, MF-A01). This report is only available through NTIS (see address given above).

NCEER-87-0015 "Detection and Assessment of Seismic Structural Damage," by E. DiPasquale and A.S. Cakmak, 8/25/87, (PB88-163712, A05, MF-A01). This report is only available through NTIS (see address given above).

NCEER-87-0016 "Pipeline Experiment at Parkfield, California," by J. Isenberg and E. Richardson, 9/15/87, (PB88-163720, A03, MF-A01). This report is available only through NTIS (see address given above).

NCEER-87-0017 "Digital Simulation of Seismic Ground Motion," by M. Shinozuka, G. Deodatis and T. Harada, 8/31/87, (PB88-155197, A04, MF-A01). This report is available only through NTIS (see address given above).

NCEER-87-0018 "Practical Considerations for Structural Control: System Uncertainty, System Time Delay and Truncation of Small Control Forces," J.N. Yang and A. Akbarpour, 8/10/87, (PB88-163738, A08, MF-A01). This report is only available through NTIS (see address given above).

NCEER-87-0019 "Modal Analysis of Nonclassically Damped Structural Systems Using Canonical Transformation," by J.N. Yang, S. Sarkani and F.X. Long, 9/27/87, (PB88-187851, A04, MF-A01).

NCEER-87-0020 "A Nonstationary Solution in Random Vibration Theory," by J.R. Red-Horse and P.D. Spanos, 11/3/87, (PB88-163746, A03, MF-A01).

NCEER-87-0021 "Horizontal Impedances for Radially Inhomogeneous Viscoelastic Soil Layers," by A.S. Veletsos and K.W. Dotson, 10/15/87, (PB88-150859, A04, MF-A01).

NCEER-87-0022 "Seismic Damage Assessment of Reinforced Concrete Members," by Y.S. Chung, C. Meyer and M. Shinozuka, 10/9/87, (PB88-150867, A05, MF-A01). This report is available only through NTIS (see address given above).

NCEER-87-0023 "Active Structural Control in Civil Engineering," by T.T. Soong, 11/11/87, (PB88-187778, A03, MF-A01).

NCEER-87-0024 "Vertical and Torsional Impedances for Radially Inhomogeneous Viscoelastic Soil Layers," by K.W. Dotson and A.S. Veletsos, 12/87, (PB88-187786, A03, MF-A01).

NCEER-87-0025 "Proceedings from the Symposium on Seismic Hazards, Ground Motions, Soil-Liquefaction and Engineering Practice in Eastern North America," October 20-22, 1987, edited by K.H. Jacob, 12/87, (PB88-188115, A23, MF-A01). This report is available only through NTIS (see address given above).

NCEER-87-0026 "Report on the Whittier-Narrows, California, Earthquake of October 1, 1987," by J. Pantelic and A. Reinhorn, 11/87, (PB88-187752, A03, MF-A01). This report is available only through NTIS (see address given above).

NCEER-87-0027 "Design of a Modular Program for Transient Nonlinear Analysis of Large 3-D Building Structures," by S. Srivastav and J.F. Abel, 12/30/87, (PB88-187950, A05, MF-A01). This report is only available through NTIS (see address given above).

NCEER-87-0028 "Second-Year Program in Research, Education and Technology Transfer," 3/8/88, (PB88-219480, A04, MF-A01).

NCEER-88-0001 "Workshop on Seismic Computer Analysis and Design of Buildings With Interactive Graphics," by W. McGuire, J.F. Abel and C.H. Conley, 1/18/88, (PB88-187760, A03, MF-A01). This report is only available through NTIS (see address given above).

NCEER-88-0002 "Optimal Control of Nonlinear Flexible Structures," by J.N. Yang, F.X. Long and D. Wong, 1/22/88, (PB88-213772, A06, MF-A01).

NCEER-88-0003 "Substructuring Techniques in the Time Domain for Primary-Secondary Structural Systems," by G.D. Manolis and G. Juhn, 2/10/88, (PB88-213780, A04, MF-A01).

NCEER-88-0004 "Iterative Seismic Analysis of Primary-Secondary Systems," by A. Singhal, L.D. Lutes and P.D. Spanos, 2/23/88, (PB88-213798, A04, MF-A01).

NCEER-88-0005 "Stochastic Finite Element Expansion for Random Media," by P.D. Spanos and R. Ghanem, 3/14/88, (PB88-213806, A03, MF-A01).

NCEER-88-0006 "Combining Structural Optimization and Structural Control," by F.Y. Cheng and C.P. Pantelides, 1/10/88, (PB88-213814, A05, MF-A01).

NCEER-88-0007 "Seismic Performance Assessment of Code-Designed Structures," by H.H-M. Hwang, J-W. Jaw and H-J. Shau, 3/20/88, (PB88-219423, A04, MF-A01). This report is only available through NTIS (see address given above).

NCEER-88-0008 "Reliability Analysis of Code-Designed Structures Under Natural Hazards," by H.H-M. Hwang, H. Ushiba and M. Shinozuka, 2/29/88, (PB88-229471, A07, MF-A01). This report is only available through NTIS (see address given above).

NCEER-88-0009 "Seismic Fragility Analysis of Shear Wall Structures," by J-W Jaw and H.H-M. Hwang, 4/30/88, (PB89-102867, A04, MF-A01).

NCEER-88-0010 "Base Isolation of a Multi-Story Building Under a Harmonic Ground Motion - A Comparison of Performances of Various Systems," by F-G Fan, G. Ahmadi and I.G. Tadjbakhsh, 5/18/88, (PB89-122238, A06, MF-A01). This report is only available through NTIS (see address given above).

NCEER-88-0011 "Seismic Floor Response Spectra for a Combined System by Green's Functions," by F.M. Lavelle, L.A. Bergman and P.D. Spanos, 5/1/88, (PB89-102875, A03, MF-A01).

NCEER-88-0012 "A New Solution Technique for Randomly Excited Hysteretic Structures," by G.Q. Cai and Y.K. Lin, 5/16/88, (PB89-102883, A03, MF-A01).

NCEER-88-0013 "A Study of Radiation Damping and Soil-Structure Interaction Effects in the Centrifuge," by K. Weissman, supervised by J.H. Prevost, 5/24/88, (PB89-144703, A06, MF-A01).

NCEER-88-0014 "Parameter Identification and Implementation of a Kinematic Plasticity Model for Frictional Soils," by J.H. Prevost and D.V. Griffiths, to be published.

NCEER-88-0015 "Two- and Three- Dimensional Dynamic Finite Element Analyses of the Long Valley Dam," by D.V. Griffiths and J.H. Prevost, 6/17/88, (PB89-144711, A04, MF-A01).

NCEER-88-0016 "Damage Assessment of Reinforced Concrete Structures in Eastern United States," by A.M. Reinhorn, M.J. Seidel, S.K. Kunnath and Y.J. Park, 6/15/88, (PB89-122220, A04, MF-A01). This report is only available through NTIS (see address given above).

NCEER-88-0017 "Dynamic Compliance of Vertically Loaded Strip Foundations in Multilayered Viscoelastic Soils," by S. Ahmad and A.S.M. Israil, 6/17/88, (PB89-102891, A04, MF-A01).

NCEER-88-0018 "An Experimental Study of Seismic Structural Response With Added Viscoelastic Dampers," by R.C. Lin, Z. Liang, T.T. Soong and R.H. Zhang, 6/30/88, (PB89-122212, A05, MF-A01). This report is available only through NTIS (see address given above).

NCEER-88-0019 "Experimental Investigation of Primary - Secondary System Interaction," by G.D. Manolis, G. Juhn and A.M. Reinhorn, 5/27/88, (PB89-122204, A04, MF-A01).

NCEER-88-0020 "A Response Spectrum Approach For Analysis of Nonclassically Damped Structures," by J.N. Yang, S. Sarkani and F.X. Long, 4/22/88, (PB89-102909, A04, MF-A01).

NCEER-88-0021 "Seismic Interaction of Structures and Soils: Stochastic Approach," by A.S. Veletsos and A.M. Prasad, 7/21/88, (PB89-122196, A04, MF-A01). This report is only available through NTIS (see address given above).

NCEER-88-0022 "Identification of the Serviceability Limit State and Detection of Seismic Structural Damage," by E. DiPasquale and A.S. Cakmak, 6/15/88, (PB89-122188, A05, MF-A01). This report is available only through NTIS (see address given above).

NCEER-88-0023 "Multi-Hazard Risk Analysis: Case of a Simple Offshore Structure," by B.K. Bhartia and E.H. Vanmarcke, 7/21/88, (PB89-145213, A05, MF-A01).

NCEER-88-0024 "Automated Seismic Design of Reinforced Concrete Buildings," by Y.S. Chung, C. Meyer and M. Shinozuka, 7/5/88, (PB89-122170, A06, MF-A01). This report is available only through NTIS (see address given above).

NCEER-88-0025 "Experimental Study of Active Control of MDOF Structures Under Seismic Excitations," by L.L. Chung, R.C. Lin, T.T. Soong and A.M. Reinhorn, 7/10/88, (PB89-122600, A04, MF-A01).

NCEER-88-0026 "Earthquake Simulation Tests of a Low-Rise Metal Structure," by J.S. Hwang, K.C. Chang, G.C. Lee and R.L. Ketter, 8/1/88, (PB89-102917, A04, MF-A01).

NCEER-88-0027 "Systems Study of Urban Response and Reconstruction Due to Catastrophic Earthquakes," by F. Kozin and H.K. Zhou, 9/22/88, (PB90-162348, A04, MF-A01).

NCEER-88-0028 "Seismic Fragility Analysis of Plane Frame Structures," by H.H-M. Hwang and Y.K. Low, 7/31/88, (PB89-131445, A06, MF-A01).

NCEER-88-0029 "Response Analysis of Stochastic Structures," by A. Kardara, C. Bucher and M. Shinozuka, 9/22/88, (PB89-174429, A04, MF-A01).

NCEER-88-0030 "Nonnormal Accelerations Due to Yielding in a Primary Structure," by D.C.K. Chen and L.D. Lutes, 9/19/88, (PB89-131437, A04, MF-A01).

NCEER-88-0031 "Design Approaches for Soil-Structure Interaction," by A.S. Veletsos, A.M. Prasad and Y. Tang, 12/30/88, (PB89-174437, A03, MF-A01). This report is available only through NTIS (see address given above).

NCEER-88-0032 "A Re-evaluation of Design Spectra for Seismic Damage Control," by C.J. Turkstra and A.G. Tallin, 11/7/88, (PB89-145221, A05, MF-A01).

NCEER-88-0033 "The Behavior and Design of Noncontact Lap Splices Subjected to Repeated Inelastic Tensile Loading," by V.E. Sagan, P. Gergely and R.N. White, 12/8/88, (PB89-163737, A08, MF-A01).

NCEER-88-0034 "Seismic Response of Pile Foundations," by S.M. Mamoon, P.K. Banerjee and S. Ahmad, 11/1/88, (PB89-145239, A04, MF-A01).

NCEER-88-0035 "Modeling of R/C Building Structures With Flexible Floor Diaphragms (IDARC2)," by A.M. Reinhorn, S.K. Kunnath and N. Panahshahi, 9/7/88, (PB89-207153, A07, MF-A01).

NCEER-88-0036 "Solution of the Dam-Reservoir Interaction Problem Using a Combination of FEM, BEM with Particular Integrals, Modal Analysis, and Substructuring," by C-S. Tsai, G.C. Lee and R.L. Ketter, 12/31/88, (PB89-207146, A04, MF-A01).

NCEER-88-0037 "Optimal Placement of Actuators for Structural Control," by F.Y. Cheng and C.P. Pantelides, 8/15/88, (PB89-162846, A05, MF-A01).

NCEER-88-0038 "Teflon Bearings in Aseismic Base Isolation: Experimental Studies and Mathematical Modeling," by A. Mokha, M.C. Constantinou and A.M. Reinhorn, 12/5/88, (PB89-218457, A10, MF-A01). This report is available only through NTIS (see address given above).

NCEER-88-0039 "Seismic Behavior of Flat Slab High-Rise Buildings in the New York City Area," by P. Weidlinger and M. Ettouney, 10/15/88, (PB90-145681, A04, MF-A01).

NCEER-88-0040 "Evaluation of the Earthquake Resistance of Existing Buildings in New York City," by P. Weidlinger and M. Ettouney, 10/15/88, to be published.

NCEER-88-0041 "Small-Scale Modeling Techniques for Reinforced Concrete Structures Subjected to Seismic Loads," by W. Kim, A. El-Attar and R.N. White, 11/22/88, (PB89-189625, A05, MF-A01).

NCEER-88-0042 "Modeling Strong Ground Motion from Multiple Event Earthquakes," by G.W. Ellis and A.S. Cakmak, 10/15/88, (PB89-174445, A03, MF-A01).

NCEER-88-0043 "Nonstationary Models of Seismic Ground Acceleration," by M. Grigoriu, S.E. Ruiz and E. Rosenblueth, 7/15/88, (PB89-189617, A04, MF-A01).

NCEER-88-0044 "SARCF User's Guide: Seismic Analysis of Reinforced Concrete Frames," by Y.S. Chung, C. Meyer and M. Shinozuka, 11/9/88, (PB89-174452, A08, MF-A01).

NCEER-88-0045 "First Expert Panel Meeting on Disaster Research and Planning," edited by J. Pantelic and J. Stoyle, 9/15/88, (PB89-174460, A05, MF-A01).

NCEER-88-0046 "Preliminary Studies of the Effect of Degrading Infill Walls on the Nonlinear Seismic Response of Steel Frames," by C.Z. Chrysostomou, P. Gergely and J.F. Abel, 12/19/88, (PB89-208383, A05, MF-A01).

NCEER-88-0047 "Reinforced Concrete Frame Component Testing Facility - Design, Construction, Instrumentation and Operation," by S.P. Pessiki, C. Conley, T. Bond, P. Gergely and R.N. White, 12/16/88, (PB89-174478, A04, MF-A01).

NCEER-89-0001 "Effects of Protective Cushion and Soil Compliancy on the Response of Equipment Within a Seismically Excited Building," by J.A. HoLung, 2/16/89, (PB89-207179, A04, MF-A01).

NCEER-89-0002 "Statistical Evaluation of Response Modification Factors for Reinforced Concrete Structures," by H.H-M. Hwang and J-W. Jaw, 2/17/89, (PB89-207187, A05, MF-A01).

NCEER-89-0003 "Hysteretic Columns Under Random Excitation," by G-Q. Cai and Y.K. Lin, 1/9/89, (PB89-196513, A03, MF-A01).

NCEER-89-0004 "Experimental Study of `Elephant Foot Bulge' Instability of Thin-Walled Metal Tanks," by Z-H. Jia and R.L. Ketter, 2/22/89, (PB89-207195, A03, MF-A01).

NCEER-89-0005 "Experiment on Performance of Buried Pipelines Across San Andreas Fault," by J. Isenberg, E. Richardson and T.D. O'Rourke, 3/10/89, (PB89-218440, A04, MF-A01). This report is available only through NTIS (see address given above).

NCEER-89-0006 "A Knowledge-Based Approach to Structural Design of Earthquake-Resistant Buildings," by M. Subramani, P. Gergely, C.H. Conley, J.F. Abel and A.H. Zaghw, 1/15/89, (PB89-218465, A06, MF-A01).

NCEER-89-0007 "Liquefaction Hazards and Their Effects on Buried Pipelines," by T.D. O'Rourke and P.A. Lane, 2/1/89, (PB89-218481, A09, MF-A01).

NCEER-89-0008 "Fundamentals of System Identification in Structural Dynamics," by H. Imai, C-B. Yun, O. Maruyama and M. Shinozuka, 1/26/89, (PB89-207211, A04, MF-A01).

NCEER-89-0009 "Effects of the 1985 Michoacan Earthquake on Water Systems and Other Buried Lifelines in Mexico," by A.G. Ayala and M.J. O'Rourke, 3/8/89, (PB89-207229, A06, MF-A01).

NCEER-89-R010 "NCEER Bibliography of Earthquake Education Materials," by K.E.K. Ross, Second Revision, 9/1/89, (PB90-125352, A05, MF-A01). This report is replaced by NCEER-92-0018.

NCEER-89-0011 "Inelastic Three-Dimensional Response Analysis of Reinforced Concrete Building Structures (IDARC-3D), Part I - Modeling," by S.K. Kunnath and A.M. Reinhorn, 4/17/89, (PB90-114612, A07, MF-A01). This report is available only through NTIS (see address given above).

NCEER-89-0012 "Recommended Modifications to ATC-14," by C.D. Poland and J.O. Malley, 4/12/89, (PB90-108648, A15, MF-A01).

NCEER-89-0013 "Repair and Strengthening of Beam-to-Column Connections Subjected to Earthquake Loading," by M. Corazao and A.J. Durrani, 2/28/89, (PB90-109885, A06, MF-A01).

NCEER-89-0014 "Program EXKAL2 for Identification of Structural Dynamic Systems," by O. Maruyama, C-B. Yun, M. Hoshiya and M. Shinozuka, 5/19/89, (PB90-109877, A09, MF-A01).

NCEER-89-0015 "Response of Frames With Bolted Semi-Rigid Connections, Part I - Experimental Study and Analytical Predictions," by P.J. DiCorso, A.M. Reinhorn, J.R. Dickerson, J.B. Radziminski and W.L. Harper, 6/1/89, to be published.

NCEER-89-0016 "ARMA Monte Carlo Simulation in Probabilistic Structural Analysis," by P.D. Spanos and M.P. Mignolet, 7/10/89, (PB90-109893, A03, MF-A01).

NCEER-89-P017 "Preliminary Proceedings from the Conference on Disaster Preparedness - The Place of Earthquake Education in Our Schools," Edited by K.E.K. Ross, 6/23/89, (PB90-108606, A03, MF-A01).

NCEER-89-0017 "Proceedings from the Conference on Disaster Preparedness - The Place of Earthquake Education in Our Schools," Edited by K.E.K. Ross, 12/31/89, (PB90-207895, A012, MF-A02). This report is available only through NTIS (see address given above).

NCEER-89-0018 "Multidimensional Models of Hysteretic Material Behavior for Vibration Analysis of Shape Memory Energy Absorbing Devices, by E.J. Graesser and F.A. Cozzarelli, 6/7/89, (PB90-164146, A04, MF-A01).

NCEER-89-0019 "Nonlinear Dynamic Analysis of Three-Dimensional Base Isolated Structures (3D-BASIS)," by S. Nagarajaiah, A.M. Reinhorn and M.C. Constantinou, 8/3/89, (PB90-161936, A06, MF-A01). This report has been replaced by NCEER-93-0011.

NCEER-89-0020 "Structural Control Considering Time-Rate of Control Forces and Control Rate Constraints," by F.Y. Cheng and C.P. Pantelides, 8/3/89, (PB90-120445, A04, MF-A01).

NCEER-89-0021 "Subsurface Conditions of Memphis and Shelby County," by K.W. Ng, T-S. Chang and H-H.M. Hwang, 7/26/89, (PB90-120437, A03, MF-A01).

NCEER-89-0022 "Seismic Wave Propagation Effects on Straight Jointed Buried Pipelines," by K. Elhmadi and M.J. O'Rourke, 8/24/89, (PB90-162322, A10, MF-A02).

NCEER-89-0023 "Workshop on Serviceability Analysis of Water Delivery Systems," edited by M. Grigoriu, 3/6/89, (PB90-127424, A03, MF-A01).

NCEER-89-0024 "Shaking Table Study of a 1/5 Scale Steel Frame Composed of Tapered Members," by K.C. Chang, J.S. Hwang and G.C. Lee, 9/18/89, (PB90-160169, A04, MF-A01).

NCEER-89-0025 "DYNA1D: A Computer Program for Nonlinear Seismic Site Response Analysis - Technical Documentation," by Jean H. Prevost, 9/14/89, (PB90-161944, A07, MF-A01). This report is available only through NTIS (see address given above).

NCEER-89-0026 "1:4 Scale Model Studies of Active Tendon Systems and Active Mass Dampers for Aseismic Protection," by A.M. Reinhorn, T.T. Soong, R.C. Lin, Y.P. Yang, Y. Fukao, H. Abe and M. Nakai, 9/15/89, (PB90-173246, A10, MF-A02). This report is available only through NTIS (see address given above).

NCEER-89-0027 "Scattering of Waves by Inclusions in a Nonhomogeneous Elastic Half Space Solved by Boundary Element Methods," by P.K. Hadley, A. Askar and A.S. Cakmak, 6/15/89, (PB90-145699, A07, MF-A01).

NCEER-89-0028 "Statistical Evaluation of Deflection Amplification Factors for Reinforced Concrete Structures," by H.H.M. Hwang, J-W. Jaw and A.L. Ch'ng, 8/31/89, (PB90-164633, A05, MF-A01).

NCEER-89-0029 "Bedrock Accelerations in Memphis Area Due to Large New Madrid Earthquakes," by H.H.M. Hwang, C.H.S. Chen and G. Yu, 11/7/89, (PB90-162330, A04, MF-A01).

NCEER-89-0030 "Seismic Behavior and Response Sensitivity of Secondary Structural Systems," by Y.Q. Chen and T.T. Soong, 10/23/89, (PB90-164658, A08, MF-A01).

NCEER-89-0031 "Random Vibration and Reliability Analysis of Primary-Secondary Structural Systems," by Y. Ibrahim, M. Grigoriu and T.T. Soong, 11/10/89, (PB90-161951, A04, MF-A01).

NCEER-89-0032 "Proceedings from the Second U.S. - Japan Workshop on Liquefaction, Large Ground Deformation and Their Effects on Lifelines, September 26-29, 1989," Edited by T.D. O'Rourke and M. Hamada, 12/1/89, (PB90-209388, A22, MF-A03).

NCEER-89-0033 "Deterministic Model for Seismic Damage Evaluation of Reinforced Concrete Structures," by J.M. Bracci, A.M. Reinhorn, J.B. Mander and S.K. Kunnath, 9/27/89, (PB91-108803, A06, MF-A01).

NCEER-89-0034 "On the Relation Between Local and Global Damage Indices," by E. DiPasquale and A.S. Cakmak, 8/15/89, (PB90-173865, A05, MF-A01).

NCEER-89-0035 "Cyclic Undrained Behavior of Nonplastic and Low Plasticity Silts," by A.J. Walker and H.E. Stewart, 7/26/89, (PB90-183518, A10, MF-A01).

NCEER-89-0036 "Liquefaction Potential of Surficial Deposits in the City of Buffalo, New York," by M. Budhu, R. Giese and L. Baumgrass, 1/17/89, (PB90-208455, A04, MF-A01).

NCEER-89-0037 "A Deterministic Assessment of Effects of Ground Motion Incoherence," by A.S. Veletsos and Y. Tang, 7/15/89, (PB90-164294, A03, MF-A01).

NCEER-89-0038 "Workshop on Ground Motion Parameters for Seismic Hazard Mapping," July 17-18, 1989, edited by R.V. Whitman, 12/1/89, (PB90-173923, A04, MF-A01).

NCEER-89-0039 "Seismic Effects on Elevated Transit Lines of the New York City Transit Authority," by C.J. Costantino, C.A. Miller and E. Heymsfield, 12/26/89, (PB90-207887, A06, MF-A01).

NCEER-89-0040 "Centrifugal Modeling of Dynamic Soil-Structure Interaction," by K. Weissman, Supervised by J.H. Prevost, 5/10/89, (PB90-207879, A07, MF-A01).

NCEER-89-0041 "Linearized Identification of Buildings With Cores for Seismic Vulnerability Assessment," by I-K. Ho and A.E. Aktan, 11/1/89, (PB90-251943, A07, MF-A01).

NCEER-90-0001 "Geotechnical and Lifeline Aspects of the October 17, 1989 Loma Prieta Earthquake in San Francisco," by T.D. O'Rourke, H.E. Stewart, F.T. Blackburn and T.S. Dickerman, 1/90, (PB90-208596, A05, MF-A01).

NCEER-90-0002 "Nonnormal Secondary Response Due to Yielding in a Primary Structure," by D.C.K. Chen and L.D. Lutes, 2/28/90, (PB90-251976, A07, MF-A01).

NCEER-90-0003 "Earthquake Education Materials for Grades K-12," by K.E.K. Ross, 4/16/90, (PB91-251984, A05, MF-A05). This report has been replaced by NCEER-92-0018.

NCEER-90-0004 "Catalog of Strong Motion Stations in Eastern North America," by R.W. Busby, 4/3/90, (PB90-251984, A05, MF-A01).

NCEER-90-0005 "NCEER Strong-Motion Data Base: A User Manual for the GeoBase Release (Version 1.0 for the Sun3)," by P. Friberg and K. Jacob, 3/31/90 (PB90-258062, A04, MF-A01).

NCEER-90-0006 "Seismic Hazard Along a Crude Oil Pipeline in the Event of an 1811-1812 Type New Madrid Earthquake," by H.H.M. Hwang and C-H.S. Chen, 4/16/90, (PB90-258054, A04, MF-A01).

NCEER-90-0007 "Site-Specific Response Spectra for Memphis Sheahan Pumping Station," by H.H.M. Hwang and C.S. Lee, 5/15/90, (PB91-108811, A05, MF-A01).

NCEER-90-0008 "Pilot Study on Seismic Vulnerability of Crude Oil Transmission Systems," by T. Ariman, R. Dobry, M. Grigoriu, F. Kozin, M. O'Rourke, T. O'Rourke and M. Shinozuka, 5/25/90, (PB91-108837, A06, MF-A01).

NCEER-90-0009 "A Program to Generate Site Dependent Time Histories: EQGEN," by G.W. Ellis, M. Srinivasan and A.S. Cakmak, 1/30/90, (PB91-108829, A04, MF-A01).

NCEER-90-0010 "Active Isolation for Seismic Protection of Operating Rooms," by M.E. Talbott, Supervised by M. Shinozuka, 6/8/9, (PB91-110205, A05, MF-A01).

NCEER-90-0011 "Program LINEARID for Identification of Linear Structural Dynamic Systems," by C-B. Yun and M. Shinozuka, 6/25/90, (PB91-110312, A08, MF-A01).

NCEER-90-0012 "Two-Dimensional Two-Phase Elasto-Plastic Seismic Response of Earth Dams," by A.N. Yiagos, Supervised by J.H. Prevost, 6/20/90, (PB91-110197, A13, MF-A02).

NCEER-90-0013 "Secondary Systems in Base-Isolated Structures: Experimental Investigation, Stochastic Response and Stochastic Sensitivity," by G.D. Manolis, G. Juhn, M.C. Constantinou and A.M. Reinhorn, 7/1/90, (PB91-110320, A08, MF-A01).

NCEER-90-0014 "Seismic Behavior of Lightly-Reinforced Concrete Column and Beam-Column Joint Details," by S.P. Pessiki, C.H. Conley, P. Gergely and R.N. White, 8/22/90, (PB91-108795, A11, MF-A02).

NCEER-90-0015 "Two Hybrid Control Systems for Building Structures Under Strong Earthquakes," by J.N. Yang and A. Danielians, 6/29/90, (PB91-125393, A04, MF-A01).

NCEER-90-0016 "Instantaneous Optimal Control with Acceleration and Velocity Feedback," by J.N. Yang and Z. Li, 6/29/90, (PB91-125401, A03, MF-A01).

NCEER-90-0017 "Reconnaissance Report on the Northern Iran Earthquake of June 21, 1990," by M. Mehrain, 10/4/90, (PB91-125377, A03, MF-A01).

NCEER-90-0018 "Evaluation of Liquefaction Potential in Memphis and Shelby County," by T.S. Chang, P.S. Tang, C.S. Lee and H. Hwang, 8/10/90, (PB91-125427, A09, MF-A01).

NCEER-90-0019 "Experimental and Analytical Study of a Combined Sliding Disc Bearing and Helical Steel Spring Isolation System," by M.C. Constantinou, A.S. Mokha and A.M. Reinhorn, 10/4/90, (PB91-125385, A06, MF-A01). This report is available only through NTIS (see address given above).

NCEER-90-0020 "Experimental Study and Analytical Prediction of Earthquake Response of a Sliding Isolation System with a Spherical Surface," by A.S. Mokha, M.C. Constantinou and A.M. Reinhorn, 10/11/90, (PB91-125419, A05, MF-A01).

NCEER-90-0021 "Dynamic Interaction Factors for Floating Pile Groups," by G. Gazetas, K. Fan, A. Kaynia and E. Kausel, 9/10/90, (PB91-170381, A05, MF-A01).

NCEER-90-0022 "Evaluation of Seismic Damage Indices for Reinforced Concrete Structures," by S. Rodriguez-Gomez and A.S. Cakmak, 9/30/90, PB91-171322, A06, MF-A01).

NCEER-90-0023 "Study of Site Response at a Selected Memphis Site," by H. Desai, S. Ahmad, E.S. Gazetas and M.R. Oh, 10/11/90, (PB91-196857, A03, MF-A01).

NCEER-90-0024 "A User's Guide to Strongmo: Version 1.0 of NCEER's Strong-Motion Data Access Tool for PCs and Terminals," by P.A. Friberg and C.A.T. Susch, 11/15/90, (PB91-171272, A03, MF-A01).

NCEER-90-0025 "A Three-Dimensional Analytical Study of Spatial Variability of Seismic Ground Motions," by L-L. Hong and A.H.-S. Ang, 10/30/90, (PB91-170399, A09, MF-A01).

NCEER-90-0026 "MUMOID User's Guide - A Program for the Identification of Modal Parameters," by S. Rodriguez-Gomez and E. DiPasquale, 9/30/90, (PB91-171298, A04, MF-A01).

NCEER-90-0027 "SARCF-II User's Guide - Seismic Analysis of Reinforced Concrete Frames," by S. Rodriguez-Gomez, Y.S. Chung and C. Meyer, 9/30/90, (PB91-171280, A05, MF-A01).

NCEER-90-0028 "Viscous Dampers: Testing, Modeling and Application in Vibration and Seismic Isolation," by N. Makris and M.C. Constantinou, 12/20/90 (PB91-190561, A06, MF-A01).

NCEER-90-0029 "Soil Effects on Earthquake Ground Motions in the Memphis Area," by H. Hwang, C.S. Lee, K.W. Ng and T.S. Chang, 8/2/90, (PB91-190751, A05, MF-A01).

NCEER-91-0001 "Proceedings from the Third Japan-U.S. Workshop on Earthquake Resistant Design of Lifeline Facilities and Countermeasures for Soil Liquefaction, December 17-19, 1990," edited by T.D. O'Rourke and M. Hamada, 2/1/91, (PB91-179259, A99, MF-A04).

NCEER-91-0002 "Physical Space Solutions of Non-Proportionally Damped Systems," by M. Tong, Z. Liang and G.C. Lee, 1/15/91, (PB91-179242, A04, MF-A01).

NCEER-91-0003 "Seismic Response of Single Piles and Pile Groups," by K. Fan and G. Gazetas, 1/10/91, (PB92-174994, A04, MF-A01).

NCEER-91-0004 "Damping of Structures: Part 1 - Theory of Complex Damping," by Z. Liang and G. Lee, 10/10/91, (PB92-197235, A12, MF-A03).

NCEER-91-0005 "3D-BASIS - Nonlinear Dynamic Analysis of Three Dimensional Base Isolated Structures: Part II," by S. Nagarajaiah, A.M. Reinhorn and M.C. Constantinou, 2/28/91, (PB91-190553, A07, MF-A01). This report has been replaced by NCEER-93-0011.

NCEER-91-0006 "A Multidimensional Hysteretic Model for Plasticity Deforming Metals in Energy Absorbing Devices," by E.J. Graesser and F.A. Cozzarelli, 4/9/91, (PB92-108364, A04, MF-A01).

NCEER-91-0007 "A Framework for Customizable Knowledge-Based Expert Systems with an Application to a KBES for Evaluating the Seismic Resistance of Existing Buildings," by E.G. Ibarra-Anaya and S.J. Fenves, 4/9/91, (PB91-210930, A08, MF-A01).

NCEER-91-0008 "Nonlinear Analysis of Steel Frames with Semi-Rigid Connections Using the Capacity Spectrum Method," by G.G. Deierlein, S-H. Hsieh, Y-J. Shen and J.F. Abel, 7/2/91, (PB92-113828, A05, MF-A01).

NCEER-91-0009 "Earthquake Education Materials for Grades K-12," by K.E.K. Ross, 4/30/91, (PB91-212142, A06, MF-A01). This report has been replaced by NCEER-92-0018.

NCEER-91-0010 "Phase Wave Velocities and Displacement Phase Differences in a Harmonically Oscillating Pile," by N. Makris and G. Gazetas, 7/8/91, (PB92-108356, A04, MF-A01).

NCEER-91-0011 "Dynamic Characteristics of a Full-Size Five-Story Steel Structure and a 2/5 Scale Model," by K.C. Chang, G.C. Yao, G.C. Lee, D.S. Hao and Y.C. Yeh," 7/2/91, (PB93-116648, A06, MF-A02).

NCEER-91-0012 "Seismic Response of a 2/5 Scale Steel Structure with Added Viscoelastic Dampers," by K.C. Chang, T.T. Soong, S-T. Oh and M.L. Lai, 5/17/91, (PB92-110816, A05, MF-A01).

NCEER-91-0013 "Earthquake Response of Retaining Walls; Full-Scale Testing and Computational Modeling," by S. Alampalli and A-W.M. Elgamal, 6/20/91, to be published.

NCEER-91-0014 "3D-BASIS-M: Nonlinear Dynamic Analysis of Multiple Building Base Isolated Structures," by P.C. Tsopelas, S. Nagarajaiah, M.C. Constantinou and A.M. Reinhorn, 5/28/91, (PB92-113885, A09, MF-A02).

NCEER-91-0015 "Evaluation of SEAOC Design Requirements for Sliding Isolated Structures," by D. Theodossiou and M.C. Constantinou, 6/10/91, (PB92-114602, A11, MF-A03).

NCEER-91-0016 "Closed-Loop Modal Testing of a 27-Story Reinforced Concrete Flat Plate-Core Building," by H.R. Somaprasad, T. Toksoy, H. Yoshiyuki and A.E. Aktan, 7/15/91, (PB92-129980, A07, MF-A02).

NCEER-91-0017 "Shake Table Test of a 1/6 Scale Two-Story Lightly Reinforced Concrete Building," by A.G. El-Attar, R.N. White and P. Gergely, 2/28/91, (PB92-222447, A06, MF-A02).

NCEER-91-0018 "Shake Table Test of a 1/8 Scale Three-Story Lightly Reinforced Concrete Building," by A.G. El-Attar, R.N. White and P. Gergely, 2/28/91, (PB93-116630, A08, MF-A02).

NCEER-91-0019 "Transfer Functions for Rigid Rectangular Foundations," by A.S. Veletsos, A.M. Prasad and W.H. Wu, 7/31/91, to be published.

NCEER-91-0020 "Hybrid Control of Seismic-Excited Nonlinear and Inelastic Structural Systems," by J.N. Yang, Z. Li and A. Danielians, 8/1/91, (PB92-143171, A06, MF-A02).

NCEER-91-0021 "The NCEER-91 Earthquake Catalog: Improved Intensity-Based Magnitudes and Recurrence Relations for U.S. Earthquakes East of New Madrid," by L. Seeber and J.G. Armbruster, 8/28/91, (PB92-176742, A06, MF-A02).

NCEER-91-0022 "Proceedings from the Implementation of Earthquake Planning and Education in Schools: The Need for Change - The Roles of the Changemakers," by K.E.K. Ross and F. Winslow, 7/23/91, (PB92-129998, A12, MF-A03).

NCEER-91-0023 "A Study of Reliability-Based Criteria for Seismic Design of Reinforced Concrete Frame Buildings," by H.H.M. Hwang and H-M. Hsu, 8/10/91, (PB92-140235, A09, MF-A02).

NCEER-91-0024 "Experimental Verification of a Number of Structural System Identification Algorithms," by R.G. Ghanem, H. Gavin and M. Shinozuka, 9/18/91, (PB92-176577, A18, MF-A04).

NCEER-91-0025 "Probabilistic Evaluation of Liquefaction Potential," by H.H.M. Hwang and C.S. Lee," 11/25/91, (PB92-143429, A05, MF-A01).

NCEER-91-0026 "Instantaneous Optimal Control for Linear, Nonlinear and Hysteretic Structures - Stable Controllers," by J.N. Yang and Z. Li, 11/15/91, (PB92-163807, A04, MF-A01).

NCEER-91-0027 "Experimental and Theoretical Study of a Sliding Isolation System for Bridges," by M.C. Constantinou, A. Kartoum, A.M. Reinhorn and P. Bradford, 11/15/91, (PB92-176973, A10, MF-A03).

NCEER-92-0001 "Case Studies of Liquefaction and Lifeline Performance During Past Earthquakes, Volume 1: Japanese Case Studies," Edited by M. Hamada and T. O'Rourke, 2/17/92, (PB92-197243, A18, MF-A04).

NCEER-92-0002 "Case Studies of Liquefaction and Lifeline Performance During Past Earthquakes, Volume 2: United States Case Studies," Edited by T. O'Rourke and M. Hamada, 2/17/92, (PB92-197250, A20, MF-A04).

NCEER-92-0003 "Issues in Earthquake Education," Edited by K. Ross, 2/3/92, (PB92-222389, A07, MF-A02).

NCEER-92-0004 "Proceedings from the First U.S. - Japan Workshop on Earthquake Protective Systems for Bridges," Edited by I.G. Buckle, 2/4/92, (PB94-142239, A99, MF-A06).

NCEER-92-0005 "Seismic Ground Motion from a Haskell-Type Source in a Multiple-Layered Half-Space," A.P. Theoharis, G. Deodatis and M. Shinozuka, 1/2/92, to be published.

NCEER-92-0006 "Proceedings from the Site Effects Workshop," Edited by R. Whitman, 2/29/92, (PB92-197201, A04, MF-A01).

NCEER-92-0007 "Engineering Evaluation of Permanent Ground Deformations Due to Seismically-Induced Liquefaction," by M.H. Baziar, R. Dobry and A-W.M. Elgamal, 3/24/92, (PB92-222421, A13, MF-A03).

NCEER-92-0008 "A Procedure for the Seismic Evaluation of Buildings in the Central and Eastern United States," by C.D. Poland and J.O. Malley, 4/2/92, (PB92-222439, A20, MF-A04).

NCEER-92-0009 "Experimental and Analytical Study of a Hybrid Isolation System Using Friction Controllable Sliding Bearings," by M.Q. Feng, S. Fujii and M. Shinozuka, 5/15/92, (PB93-150282, A06, MF-A02).

NCEER-92-0010 "Seismic Resistance of Slab-Column Connections in Existing Non-Ductile Flat-Plate Buildings," by A.J. Durrani and Y. Du, 5/18/92, (PB93-116812, A06, MF-A02).

NCEER-92-0011 "The Hysteretic and Dynamic Behavior of Brick Masonry Walls Upgraded by Ferrocement Coatings Under Cyclic Loading and Strong Simulated Ground Motion," by H. Lee and S.P. Prawel, 5/11/92, to be published.

NCEER-92-0012 "Study of Wire Rope Systems for Seismic Protection of Equipment in Buildings," by G.F. Demetriades, M.C. Constantinou and A.M. Reinhorn, 5/20/92, (PB93-116655, A08, MF-A02).

NCEER-92-0013 "Shape Memory Structural Dampers: Material Properties, Design and Seismic Testing," by P.R. Witting and F.A. Cozzarelli, 5/26/92, (PB93-116663, A05, MF-A01).

NCEER-92-0014 "Longitudinal Permanent Ground Deformation Effects on Buried Continuous Pipelines," by M.J. O'Rourke, and C. Nordberg, 6/15/92, (PB93-116671, A08, MF-A02).

NCEER-92-0015 "A Simulation Method for Stationary Gaussian Random Functions Based on the Sampling Theorem," by M. Grigoriu and S. Balopoulou, 6/11/92, (PB93-127496, A05, MF-A01).

NCEER-92-0016 "Gravity-Load-Designed Reinforced Concrete Buildings: Seismic Evaluation of Existing Construction and Detailing Strategies for Improved Seismic Resistance," by G.W. Hoffmann, S.K. Kunnath, A.M. Reinhorn and J.B. Mander, 7/15/92, (PB94-142007, A08, MF-A02).

NCEER-92-0017 "Observations on Water System and Pipeline Performance in the Limón Area of Costa Rica Due to the April 22, 1991 Earthquake," by M. O'Rourke and D. Ballantyne, 6/30/92, (PB93-126811, A06, MF-A02).

NCEER-92-0018 "Fourth Edition of Earthquake Education Materials for Grades K-12," Edited by K.E.K. Ross, 8/10/92, (PB93-114023, A07, MF-A02).

NCEER-92-0019 "Proceedings from the Fourth Japan-U.S. Workshop on Earthquake Resistant Design of Lifeline Facilities and Countermeasures for Soil Liquefaction," Edited by M. Hamada and T.D. O'Rourke, 8/12/92, (PB93-163939, A99, MF-E11).

NCEER-92-0020 "Active Bracing System: A Full Scale Implementation of Active Control," by A.M. Reinhorn, T.T. Soong, R.C. Lin, M.A. Riley, Y.P. Wang, S. Aizawa and M. Higashino, 8/14/92, (PB93-127512, A06, MF-A02).

NCEER-92-0021 "Empirical Analysis of Horizontal Ground Displacement Generated by Liquefaction-Induced Lateral Spreads," by S.F. Bartlett and T.L. Youd, 8/17/92, (PB93-188241, A06, MF-A02).

NCEER-92-0022 "IDARC Version 3.0: Inelastic Damage Analysis of Reinforced Concrete Structures," by S.K. Kunnath, A.M. Reinhorn and R.F. Lobo, 8/31/92, (PB93-227502, A07, MF-A02).

NCEER-92-0023 "A Semi-Empirical Analysis of Strong-Motion Peaks in Terms of Seismic Source, Propagation Path and Local Site Conditions, by M. Kamiyama, M.J. O'Rourke and R. Flores-Berrones, 9/9/92, (PB93-150266, A08, MF-A02).

NCEER-92-0024 "Seismic Behavior of Reinforced Concrete Frame Structures with Nonductile Details, Part I: Summary of Experimental Findings of Full Scale Beam-Column Joint Tests," by A. Beres, R.N. White and P. Gergely, 9/30/92, (PB93-227783, A05, MF-A01).

NCEER-92-0025 "Experimental Results of Repaired and Retrofitted Beam-Column Joint Tests in Lightly Reinforced Concrete Frame Buildings," by A. Beres, S. El-Borgi, R.N. White and P. Gergely, 10/29/92, (PB93-227791, A05, MF-A01).

NCEER-92-0026 "A Generalization of Optimal Control Theory: Linear and Nonlinear Structures," by J.N. Yang, Z. Li and S. Vongchavalitkul, 11/2/92, (PB93-188621, A05, MF-A01).

NCEER-92-0027 "Seismic Resistance of Reinforced Concrete Frame Structures Designed Only for Gravity Loads: Part I - Design and Properties of a One-Third Scale Model Structure," by J.M. Bracci, A.M. Reinhorn and J.B. Mander, 12/1/92, (PB94-104502, A08, MF-A02).

NCEER-92-0028 "Seismic Resistance of Reinforced Concrete Frame Structures Designed Only for Gravity Loads: Part II - Experimental Performance of Subassemblages," by L.E. Aycardi, J.B. Mander and A.M. Reinhorn, 12/1/92, (PB94-104510, A08, MF-A02).

NCEER-92-0029 "Seismic Resistance of Reinforced Concrete Frame Structures Designed Only for Gravity Loads: Part III - Experimental Performance and Analytical Study of a Structural Model," by J.M. Bracci, A.M. Reinhorn and J.B. Mander, 12/1/92, (PB93-227528, A09, MF-A01).

NCEER-92-0030 "Evaluation of Seismic Retrofit of Reinforced Concrete Frame Structures: Part I - Experimental Performance of Retrofitted Subassemblages," by D. Choudhuri, J.B. Mander and A.M. Reinhorn, 12/8/92, (PB93-198307, A07, MF-A02).

NCEER-92-0031 "Evaluation of Seismic Retrofit of Reinforced Concrete Frame Structures: Part II - Experimental Performance and Analytical Study of a Retrofitted Structural Model," by J.M. Bracci, A.M. Reinhorn and J.B. Mander, 12/8/92, (PB93-198315, A09, MF-A03).

NCEER-92-0032 "Experimental and Analytical Investigation of Seismic Response of Structures with Supplemental Fluid Viscous Dampers," by M.C. Constantinou and M.D. Symans, 12/21/92, (PB93-191435, A10, MF-A03). This report is available only through NTIS (see address given above).

NCEER-92-0033 "Reconnaissance Report on the Cairo, Egypt Earthquake of October 12, 1992," by M. Khater, 12/23/92, (PB93-188621, A03, MF-A01).

NCEER-92-0034 "Low-Level Dynamic Characteristics of Four Tall Flat-Plate Buildings in New York City," by H. Gavin, S. Yuan, J. Grossman, E. Pekelis and K. Jacob, 12/28/92, (PB93-188217, A07, MF-A02).

NCEER-93-0001 "An Experimental Study on the Seismic Performance of Brick-Infilled Steel Frames With and Without Retrofit," by J.B. Mander, B. Nair, K. Wojtkowski and J. Ma, 1/29/93, (PB93-227510, A07, MF-A02).

NCEER-93-0002 "Social Accounting for Disaster Preparedness and Recovery Planning," by S. Cole, E. Pantoja and V. Razak, 2/22/93, (PB94-142114, A12, MF-A03).

NCEER-93-0003 "Assessment of 1991 NEHRP Provisions for Nonstructural Components and Recommended Revisions," by T.T. Soong, G. Chen, Z. Wu, R-H. Zhang and M. Grigoriu, 3/1/93, (PB93-188639, A06, MF-A02).

NCEER-93-0004 "Evaluation of Static and Response Spectrum Analysis Procedures of SEAOC/UBC for Seismic Isolated Structures," by C.W. Winters and M.C. Constantinou, 3/23/93, (PB93-198299, A10, MF-A03).

NCEER-93-0005 "Earthquakes in the Northeast - Are We Ignoring the Hazard? A Workshop on Earthquake Science and Safety for Educators," edited by K.E.K. Ross, 4/2/93, (PB94-103066, A09, MF-A02).

NCEER-93-0006 "Inelastic Response of Reinforced Concrete Structures with Viscoelastic Braces," by R.F. Lobo, J.M. Bracci, K.L. Shen, A.M. Reinhorn and T.T. Soong, 4/5/93, (PB93-227486, A05, MF-A02).

NCEER-93-0007 "Seismic Testing of Installation Methods for Computers and Data Processing Equipment," by K. Kosar, T.T. Soong, K.L. Shen, J.A. HoLung and Y.K. Lin, 4/12/93, (PB93-198299, A07, MF-A02).

NCEER-93-0008 "Retrofit of Reinforced Concrete Frames Using Added Dampers," by A. Reinhorn, M. Constantinou and C. Li, to be published.

NCEER-93-0009 "Seismic Behavior and Design Guidelines for Steel Frame Structures with Added Viscoelastic Dampers," by K.C. Chang, M.L. Lai, T.T. Soong, D.S. Hao and Y.C. Yeh, 5/1/93, (PB94-141959, A07, MF-A02).

NCEER-93-0010 "Seismic Performance of Shear-Critical Reinforced Concrete Bridge Piers," by J.B. Mander, S.M. Waheed, M.T.A. Chaudhary and S.S. Chen, 5/12/93, (PB93-227494, A08, MF-A02).

NCEER-93-0011 "3D-BASIS-TABS: Computer Program for Nonlinear Dynamic Analysis of Three Dimensional Base Isolated Structures," by S. Nagarajaiah, C. Li, A.M. Reinhorn and M.C. Constantinou, 8/2/93, (PB94-141819, A09, MF-A02).

NCEER-93-0012 "Effects of Hydrocarbon Spills from an Oil Pipeline Break on Ground Water," by O.J. Helweg and H.H.M. Hwang, 8/3/93, (PB94-141942, A06, MF-A02).

NCEER-93-0013 "Simplified Procedures for Seismic Design of Nonstructural Components and Assessment of Current Code Provisions," by M.P. Singh, L.E. Suarez, E.E. Matheu and G.O. Maldonado, 8/4/93, (PB94-141827, A09, MF-A02).

NCEER-93-0014 "An Energy Approach to Seismic Analysis and Design of Secondary Systems," by G. Chen and T.T. Soong, 8/6/93, (PB94-142767, A11, MF-A03).

NCEER-93-0015 "Proceedings from School Sites: Becoming Prepared for Earthquakes - Commemorating the Third Anniversary of the Loma Prieta Earthquake," Edited by F.E. Winslow and K.E.K. Ross, 8/16/93, (PB94-154275, A16, MF-A02).

NCEER-93-0016 "Reconnaissance Report of Damage to Historic Monuments in Cairo, Egypt Following the October 12, 1992 Dahshur Earthquake," by D. Sykora, D. Look, G. Croci, E. Karaesmen and E. Karaesmen, 8/19/93, (PB94-142221, A08, MF-A02).

NCEER-93-0017 "The Island of Guam Earthquake of August 8, 1993," by S.W. Swan and S.K. Harris, 9/30/93, (PB94-141843, A04, MF-A01).

NCEER-93-0018 "Engineering Aspects of the October 12, 1992 Egyptian Earthquake," by A.W. Elgamal, M. Amer, K. Adalier and A. Abul-Fadl, 10/7/93, (PB94-141983, A05, MF-A01).

NCEER-93-0019 "Development of an Earthquake Motion Simulator and its Application in Dynamic Centrifuge Testing," by I. Krstelj, Supervised by J.H. Prevost, 10/23/93, (PB94-181773, A-10, MF-A03).

NCEER-93-0020 "NCEER-Taisei Corporation Research Program on Sliding Seismic Isolation Systems for Bridges: Experimental and Analytical Study of a Friction Pendulum System (FPS)," by M.C. Constantinou, P. Tsopelas, Y-S. Kim and S. Okamoto, 11/1/93, (PB94-142775, A08, MF-A02).

NCEER-93-0021 "Finite Element Modeling of Elastomeric Seismic Isolation Bearings," by L.J. Billings, Supervised by R. Shepherd, 11/8/93, to be published.

NCEER-93-0022 "Seismic Vulnerability of Equipment in Critical Facilities: Life-Safety and Operational Consequences," by K. Porter, G.S. Johnson, M.M. Zadeh, C. Scawthorn and S. Eder, 11/24/93, (PB94-181765, A16, MF-A03).

NCEER-93-0023 "Hokkaido Nansei-oki, Japan Earthquake of July 12, 1993, by P.I. Yanev and C.R. Scawthorn, 12/23/93, (PB94-181500, A07, MF-A01).

NCEER-94-0001 "An Evaluation of Seismic Serviceability of Water Supply Networks with Application to the San Francisco Auxiliary Water Supply System," by I. Markov, Supervised by M. Grigoriu and T. O'Rourke, 1/21/94, (PB94-204013, A07, MF-A02).

NCEER-94-0002 "NCEER-Taisei Corporation Research Program on Sliding Seismic Isolation Systems for Bridges: Experimental and Analytical Study of Systems Consisting of Sliding Bearings, Rubber Restoring Force Devices and Fluid Dampers," Volumes I and II, by P. Tsopelas, S. Okamoto, M.C. Constantinou, D. Ozaki and S. Fujii, 2/4/94, (PB94-181740, A09, MF-A02 and PB94-181757, A12, MF-A03).

NCEER-94-0003 "A Markov Model for Local and Global Damage Indices in Seismic Analysis," by S. Rahman and M. Grigoriu, 2/18/94, (PB94-206000, A12, MF-A03).

NCEER-94-0004 "Proceedings from the NCEER Workshop on Seismic Response of Masonry Infills," edited by D.P. Abrams, 3/1/94, (PB94-180783, A07, MF-A02).

NCEER-94-0005 "The Northridge, California Earthquake of January 17, 1994: General Reconnaissance Report," edited by J.D. Goltz, 3/11/94, (PB94-193943, A10, MF-A03).

NCEER-94-0006 "Seismic Energy Based Fatigue Damage Analysis of Bridge Columns: Part I - Evaluation of Seismic Capacity," by G.A. Chang and J.B. Mander, 3/14/94, (PB94-219185, A11, MF-A03).

NCEER-94-0007 "Seismic Isolation of Multi-Story Frame Structures Using Spherical Sliding Isolation Systems," by T.M. Al-Hussaini, V.A. Zayas and M.C. Constantinou, 3/17/94, (PB94-193745, A09, MF-A02).

NCEER-94-0008 "The Northridge, California Earthquake of January 17, 1994: Performance of Highway Bridges," edited by I.G. Buckle, 3/24/94, (PB94-193851, A06, MF-A02).

NCEER-94-0009 "Proceedings of the Third U.S.-Japan Workshop on Earthquake Protective Systems for Bridges," edited by I.G. Buckle and I. Friedland, 3/31/94, (PB94-195815, A99, MF-A06).

NCEER-94-0010 "3D-BASIS-ME: Computer Program for Nonlinear Dynamic Analysis of Seismically Isolated Single and Multiple Structures and Liquid Storage Tanks," by P.C. Tsopelas, M.C. Constantinou and A.M. Reinhorn, 4/12/94, (PB94-204922, A09, MF-A02).

NCEER-94-0011 "The Northridge, California Earthquake of January 17, 1994: Performance of Gas Transmission Pipelines," by T.D. O'Rourke and M.C. Palmer, 5/16/94, (PB94-204989, A05, MF-A01).

NCEER-94-0012 "Feasibility Study of Replacement Procedures and Earthquake Performance Related to Gas Transmission Pipelines," by T.D. O'Rourke and M.C. Palmer, 5/25/94, (PB94-206638, A09, MF-A02).

NCEER-94-0013 "Seismic Energy Based Fatigue Damage Analysis of Bridge Columns: Part II - Evaluation of Seismic Demand," by G.A. Chang and J.B. Mander, 6/1/94, (PB95-18106, A08, MF-A02).

NCEER-94-0014 "NCEER-Taisei Corporation Research Program on Sliding Seismic Isolation Systems for Bridges: Experimental and Analytical Study of a System Consisting of Sliding Bearings and Fluid Restoring Force/Damping Devices," by P. Tsopelas and M.C. Constantinou, 6/13/94, (PB94-219144, A10, MF-A03).

NCEER-94-0015 "Generation of Hazard-Consistent Fragility Curves for Seismic Loss Estimation Studies," by H. Hwang and J-R. Huo, 6/14/94, (PB95-181996, A09, MF-A02).

NCEER-94-0016 "Seismic Study of Building Frames with Added Energy-Absorbing Devices," by W.S. Pong, C.S. Tsai and G.C. Lee, 6/20/94, (PB94-219136, A10, A03).

NCEER-94-0017 "Sliding Mode Control for Seismic-Excited Linear and Nonlinear Civil Engineering Structures," by J. Yang, J. Wu, A. Agrawal and Z. Li, 6/21/94, (PB95-138483, A06, MF-A02).

NCEER-94-0018 "3D-BASIS-TABS Version 2.0: Computer Program for Nonlinear Dynamic Analysis of Three Dimensional Base Isolated Structures," by A.M. Reinhorn, S. Nagarajaiah, M.C. Constantinou, P. Tsopelas and R. Li, 6/22/94, (PB95-182176, A08, MF-A02).

NCEER-94-0019 "Proceedings of the International Workshop on Civil Infrastructure Systems: Application of Intelligent Systems and Advanced Materials on Bridge Systems," Edited by G.C. Lee and K.C. Chang, 7/18/94, (PB95-252474, A20, MF-A04).

NCEER-94-0020 "Study of Seismic Isolation Systems for Computer Floors," by V. Lambrou and M.C. Constantinou, 7/19/94, (PB95-138533, A10, MF-A03).

NCEER-94-0021 "Proceedings of the U.S.-Italian Workshop on Guidelines for Seismic Evaluation and Rehabilitation of Unreinforced Masonry Buildings," Edited by D.P. Abrams and G.M. Calvi, 7/20/94, (PB95-138749, A13, MF-A03).

NCEER-94-0022 "NCEER-Taisei Corporation Research Program on Sliding Seismic Isolation Systems for Bridges: Experimental and Analytical Study of a System Consisting of Lubricated PTFE Sliding Bearings and Mild Steel Dampers," by P. Tsopelas and M.C. Constantinou, 7/22/94, (PB95-182184, A08, MF-A02).

NCEER-94-0023 “Development of Reliability-Based Design Criteria for Buildings Under Seismic Load,” by Y.K. Wen, H. Hwang and M. Shinozuka, 8/1/94, (PB95-211934, A08, MF-A02).

NCEER-94-0024 “Experimental Verification of Acceleration Feedback Control Strategies for an Active Tendon System,” by S.J. Dyke, B.F. Spencer, Jr., P. Quast, M.K. Sain, D.C. Kaspari, Jr. and T.T. Soong, 8/29/94, (PB95-212320, A05, MF-A01).

NCEER-94-0025 “Seismic Retrofitting Manual for Highway Bridges,” Edited by I.G. Buckle and I.F. Friedland, published by the Federal Highway Administration (PB95-212676, A15, MF-A03).

NCEER-94-0026 “Proceedings from the Fifth U.S.-Japan Workshop on Earthquake Resistant Design of Lifeline Facilities and Countermeasures Against Soil Liquefaction,” Edited by T.D. O’Rourke and M. Hamada, 11/7/94, (PB95-220802, A99, MF-E08).

NCEER-95-0001 "Experimental and Analytical Investigation of Seismic Retrofit of Structures with Supplemental Damping: Part 1 - Fluid Viscous Damping Devices," by A.M. Reinhorn, C. Li and M.C. Constantinou, 1/3/95, (PB95-266599, A09, MF-A02).

NCEER-95-0002 "Experimental and Analytical Study of Low-Cycle Fatigue Behavior of Semi-Rigid Top-And-Seat Angle Connections," by G. Pekcan, J.B. Mander and S.S. Chen, 1/5/95, (PB95-220042, A07, MF-A02).

NCEER-95-0003 "NCEER-ATC Joint Study on Fragility of Buildings," by T. Anagnos, C. Rojahn and A.S. Kiremidjian, 1/20/95, (PB95-220026, A06, MF-A02).

NCEER-95-0004 "Nonlinear Control Algorithms for Peak Response Reduction," by Z. Wu, T.T. Soong, V. Gattulli and R.C. Lin, 2/16/95, (PB95-220349, A05, MF-A01).

NCEER-95-0005 "Pipeline Replacement Feasibility Study: A Methodology for Minimizing Seismic and Corrosion Risks to Underground Natural Gas Pipelines," by R.T. Eguchi, H.A. Seligson and D.G. Honegger, 3/2/95, (PB95-252326, A06, MF-A02).

NCEER-95-0006 "Evaluation of Seismic Performance of an 11-Story Frame Building During the 1994 Northridge Earthquake," by F. Naeim, R. DiSulio, K. Benuska, A. Reinhorn and C. Li, to be published.

NCEER-95-0007 "Prioritization of Bridges for Seismic Retrofitting," by N. Basöz and A.S. Kiremidjian, 4/24/95, (PB95-252300, A08, MF-A02).

NCEER-95-0008 "Method for Developing Motion Damage Relationships for Reinforced Concrete Frames," by A. Singhal and A.S. Kiremidjian, 5/11/95, (PB95-266607, A06, MF-A02).

NCEER-95-0009 "Experimental and Analytical Investigation of Seismic Retrofit of Structures with Supplemental Damping: Part II - Friction Devices," by C. Li and A.M. Reinhorn, 7/6/95, (PB96-128087, A11, MF-A03).

NCEER-95-0010 "Experimental Performance and Analytical Study of a Non-Ductile Reinforced Concrete Frame Structure Retrofitted with Elastomeric Spring Dampers," by G. Pekcan, J.B. Mander and S.S. Chen, 7/14/95, (PB96-137161, A08, MF-A02).

NCEER-95-0011 "Development and Experimental Study of Semi-Active Fluid Damping Devices for Seismic Protection of Structures," by M.D. Symans and M.C. Constantinou, 8/3/95, (PB96-136940, A23, MF-A04).

NCEER-95-0012 "Real-Time Structural Parameter Modification (RSPM): Development of Innervated Structures," by Z. Liang, M. Tong and G.C. Lee, 4/11/95, (PB96-137153, A06, MF-A01).

NCEER-95-0013 "Experimental and Analytical Investigation of Seismic Retrofit of Structures with Supplemental Damping: Part III - Viscous Damping Walls," by A.M. Reinhorn and C. Li, 10/1/95, (PB96-176409, A11, MF-A03).

NCEER-95-0014 "Seismic Fragility Analysis of Equipment and Structures in a Memphis Electric Substation," by J-R. Huo and H.H.M. Hwang, 8/10/95, (PB96-128087, A09, MF-A02).

NCEER-95-0015 "The Hanshin-Awaji Earthquake of January 17, 1995: Performance of Lifelines," Edited by M. Shinozuka, 11/3/95, (PB96-176383, A15, MF-A03).

NCEER-95-0016 "Highway Culvert Performance During Earthquakes," by T.L. Youd and C.J. Beckman, available as NCEER-96-0015.

NCEER-95-0017 "The Hanshin-Awaji Earthquake of January 17, 1995: Performance of Highway Bridges," Edited by I.G. Buckle, 12/1/95, to be published.

NCEER-95-0018 "Modeling of Masonry Infill Panels for Structural Analysis," by A.M. Reinhorn, A. Madan, R.E. Valles, Y. Reichmann and J.B. Mander, 12/8/95, (PB97-110886, MF-A01, A06).

NCEER-95-0019 "Optimal Polynomial Control for Linear and Nonlinear Structures," by A.K. Agrawal and J.N. Yang, 12/11/95, (PB96-168737, A07, MF-A02).

NCEER-95-0020 "Retrofit of Non-Ductile Reinforced Concrete Frames Using Friction Dampers," by R.S. Rao, P. Gergely and R.N. White, 12/22/95, (PB97-133508, A10, MF-A02).

NCEER-95-0021 "Parametric Results for Seismic Response of Pile-Supported Bridge Bents," by G. Mylonakis, A. Nikolaou and G. Gazetas, 12/22/95, (PB97-100242, A12, MF-A03).

NCEER-95-0022 "Kinematic Bending Moments in Seismically Stressed Piles," by A. Nikolaou, G. Mylonakis and G. Gazetas, 12/23/95, (PB97-113914, MF-A03, A13).

NCEER-96-0001 "Dynamic Response of Unreinforced Masonry Buildings with Flexible Diaphragms," by A.C. Costley and D.P. Abrams," 10/10/96, (PB97-133573, MF-A03, A15).

NCEER-96-0002 "State of the Art Review: Foundations and Retaining Structures," by I. Po Lam, to be published.

NCEER-96-0003 "Ductility of Rectangular Reinforced Concrete Bridge Columns with Moderate Confinement," by N. Wehbe, M. Saiidi, D. Sanders and B. Douglas, 11/7/96, (PB97-133557, A06, MF-A02).

NCEER-96-0004 "Proceedings of the Long-Span Bridge Seismic Research Workshop," edited by I.G. Buckle and I.M. Friedland, to be published.

NCEER-96-0005 "Establish Representative Pier Types for Comprehensive Study: Eastern United States," by J. Kulicki and Z. Prucz, 5/28/96, (PB98-119217, A07, MF-A02).

NCEER-96-0006 "Establish Representative Pier Types for Comprehensive Study: Western United States," by R. Imbsen, R.A. Schamber and T.A. Osterkamp, 5/28/96, (PB98-118607, A07, MF-A02).

NCEER-96-0007 "Nonlinear Control Techniques for Dynamical Systems with Uncertain Parameters," by R.G. Ghanem and M.I. Bujakov, 5/27/96, (PB97-100259, A17, MF-A03).

NCEER-96-0008 "Seismic Evaluation of a 30-Year Old Non-Ductile Highway Bridge Pier and Its Retrofit," by J.B. Mander, B. Mahmoodzadegan, S. Bhadra and S.S. Chen, 5/31/96, (PB97-110902, MF-A03, A10).

NCEER-96-0009 "Seismic Performance of a Model Reinforced Concrete Bridge Pier Before and After Retrofit," by J.B. Mander, J.H. Kim and C.A. Ligozio, 5/31/96, (PB97-110910, MF-A02, A10).

NCEER-96-0010 "IDARC2D Version 4.0: A Computer Program for the Inelastic Damage Analysis of Buildings," by R.E. Valles, A.M. Reinhorn, S.K. Kunnath, C. Li and A. Madan, 6/3/96, (PB97-100234, A17, MF-A03).

NCEER-96-0011 "Estimation of the Economic Impact of Multiple Lifeline Disruption: Memphis Light, Gas and Water Division Case Study," by S.E. Chang, H.A. Seligson and R.T. Eguchi, 8/16/96, (PB97-133490, A11, MF-A03).

NCEER-96-0012 "Proceedings from the Sixth Japan-U.S. Workshop on Earthquake Resistant Design of Lifeline Facilities and Countermeasures Against Soil Liquefaction, Edited by M. Hamada and T. O'Rourke, 9/11/96, (PB97-133581, A99, MF-A06).

NCEER-96-0013 "Chemical Hazards, Mitigation and Preparedness in Areas of High Seismic Risk: A Methodology for Estimating the Risk of Post-Earthquake Hazardous Materials Release," by H.A. Seligson, R.T. Eguchi, K.J. Tierney and K. Richmond, 11/7/96, (PB97-133565, MF-A02, A08).

NCEER-96-0014 "Response of Steel Bridge Bearings to Reversed Cyclic Loading," by J.B. Mander, D-K. Kim, S.S. Chen and G.J. Premus, 11/13/96, (PB97-140735, A12, MF-A03).

NCEER-96-0015 "Highway Culvert Performance During Past Earthquakes," by T.L. Youd and C.J. Beckman, 11/25/96, (PB97-133532, A06, MF-A01).

NCEER-97-0001 "Evaluation, Prevention and Mitigation of Pounding Effects in Building Structures," by R.E. Valles and A.M. Reinhorn, 2/20/97, (PB97-159552, A14, MF-A03).

NCEER-97-0002 "Seismic Design Criteria for Bridges and Other Highway Structures," by C. Rojahn, R. Mayes, D.G. Anderson, J. Clark, J.H. Hom, R.V. Nutt and M.J. O'Rourke, 4/30/97, (PB97-194658, A06, MF-A03).

NCEER-97-0003 “Proceedings of the U.S.-Italian Workshop on Seismic Evaluation and Retrofit,” Edited by D.P. Abrams and G.M. Calvi, 3/19/97, (PB97-194666, A13, MF-A03).

NCEER-97-0004 "Investigation of Seismic Response of Buildings with Linear and Nonlinear Fluid Viscous Dampers," by A.A. Seleemah and M.C. Constantinou, 5/21/97, (PB98-109002, A15, MF-A03).

NCEER-97-0005 "Proceedings of the Workshop on Earthquake Engineering Frontiers in Transportation Facilities," edited by G.C. Lee and I.M. Friedland, 8/29/97, (PB98-128911, A25, MR-A04).

NCEER-97-0006 "Cumulative Seismic Damage of Reinforced Concrete Bridge Piers," by S.K. Kunnath, A. El-Bahy, A. Taylor and W. Stone, 9/2/97, (PB98-108814, A11, MF-A03).

NCEER-97-0007 "Structural Details to Accommodate Seismic Movements of Highway Bridges and Retaining Walls," by R.A. Imbsen, R.A. Schamber, E. Thorkildsen, A. Kartoum, B.T. Martin, T.N. Rosser and J.M. Kulicki, 9/3/97, (PB98-108996, A09, MF-A02).

NCEER-97-0008 "A Method for Earthquake Motion-Damage Relationships with Application to Reinforced Concrete Frames," by A. Singhal and A.S. Kiremidjian, 9/10/97, (PB98-108988, A13, MF-A03).

NCEER-97-0009 "Seismic Analysis and Design of Bridge Abutments Considering Sliding and Rotation," by K. Fishman and R. Richards, Jr., 9/15/97, (PB98-108897, A06, MF-A02).

NCEER-97-0010 "Proceedings of the FHWA/NCEER Workshop on the National Representation of Seismic Ground Motion for New and Existing Highway Facilities," edited by I.M. Friedland, M.S. Power and R.L. Mayes, 9/22/97, (PB98-128903, A21, MF-A04).

NCEER-97-0011 "Seismic Analysis for Design or Retrofit of Gravity Bridge Abutments," by K.L. Fishman, R. Richards, Jr. and R.C. Divito, 10/2/97, (PB98-128937, A08, MF-A02).

NCEER-97-0012 "Evaluation of Simplified Methods of Analysis for Yielding Structures," by P. Tsopelas, M.C. Constantinou, C.A. Kircher and A.S. Whittaker, 10/31/97, (PB98-128929, A10, MF-A03).

NCEER-97-0013 "Seismic Design of Bridge Columns Based on Control and Repairability of Damage," by C-T. Cheng and J.B. Mander, 12/8/97, (PB98-144249, A11, MF-A03).

NCEER-97-0014 "Seismic Resistance of Bridge Piers Based on Damage Avoidance Design," by J.B. Mander and C-T. Cheng, 12/10/97, (PB98-144223, A09, MF-A02).

NCEER-97-0015 “Seismic Response of Nominally Symmetric Systems with Strength Uncertainty,” by S. Balopoulou and M. Grigoriu, 12/23/97, (PB98-153422, A11, MF-A03).

NCEER-97-0016 “Evaluation of Seismic Retrofit Methods for Reinforced Concrete Bridge Columns,” by T.J. Wipf, F.W. Klaiber and F.M. Russo, 12/28/97, (PB98-144215, A12, MF-A03).

NCEER-97-0017 “Seismic Fragility of Existing Conventional Reinforced Concrete Highway Bridges,” by C.L. Mullen and A.S. Cakmak, 12/30/97, (PB98-153406, A08, MF-A02).

NCEER-97-0018 “Loss Asssessment of Memphis Buildings,” edited by D.P. Abrams and M. Shinozuka, 12/31/97, (PB98-144231, A13, MF-A03).

NCEER-97-0019 “Seismic Evaluation of Frames with Infill Walls Using Quasi-static Experiments,” by K.M. Mosalam, R.N. White and P. Gergely, 12/31/97, (PB98-153455, A07, MF-A02).

NCEER-97-0020 “Seismic Evaluation of Frames with Infill Walls Using Pseudo-dynamic Experiments,” by K.M. Mosalam, R.N. White and P. Gergely, 12/31/97, (PB98-153430, A07, MF-A02).

NCEER-97-0021 “Computational Strategies for Frames with Infill Walls: Discrete and Smeared Crack Analyses and Seismic Fragility,” by K.M. Mosalam, R.N. White and P. Gergely, 12/31/97, (PB98-153414, A10, MF-A02).

NCEER-97-0022 "Proceedings of the NCEER Workshop on Evaluation of Liquefaction Resistance of Soils," edited by T.L. Youd and I.M. Idriss, 12/31/97, (PB98-155617, A15, MF-A03).

MCEER-98-0001 "Extraction of Nonlinear Hysteretic Properties of Seismically Isolated Bridges from Quick-Release Field Tests," by Q. Chen, B.M. Douglas, E.M. Maragakis and I.G. Buckle, 5/26/98, (PB99-118838, A06, MF-A01).

MCEER-98-0002 "Methodologies for Evaluating the Importance of Highway Bridges," by A. Thomas, S. Eshenaur and J. Kulicki, 5/29/98, (PB99-118846, A10, MF-A02).

MCEER-98-0003 "Capacity Design of Bridge Piers and the Analysis of Overstrength," by J.B. Mander, A. Dutta and P. Goel, 6/1/98, (PB99-118853, A09, MF-A02).

MCEER-98-0004 "Evaluation of Bridge Damage Data from the Loma Prieta and Northridge, California Earthquakes," by N. Basoz and A. Kiremidjian, 6/2/98, (PB99-118861, A15, MF-A03).

MCEER-98-0005 "Screening Guide for Rapid Assessment of Liquefaction Hazard at Highway Bridge Sites," by T. L. Youd, 6/16/98, (PB99-118879, A06, not available on microfiche).

MCEER-98-0006 "Structural Steel and Steel/Concrete Interface Details for Bridges," by P. Ritchie, N. Kauhl and J. Kulicki, 7/13/98, (PB99-118945, A06, MF-A01).

MCEER-98-0007 "Capacity Design and Fatigue Analysis of Confined Concrete Columns," by A. Dutta and J.B. Mander, 7/14/98, (PB99-118960, A14, MF-A03).

MCEER-98-0008 "Proceedings of the Workshop on Performance Criteria for Telecommunication Services Under Earthquake Conditions," edited by A.J. Schiff, 7/15/98, (PB99-118952, A08, MF-A02).

MCEER-98-0009 "Fatigue Analysis of Unconfined Concrete Columns," by J.B. Mander, A. Dutta and J.H. Kim, 9/12/98, (PB99-123655, A10, MF-A02).

MCEER-98-0010 "Centrifuge Modeling of Cyclic Lateral Response of Pile-Cap Systems and Seat-Type Abutments in Dry Sands," by A.D. Gadre and R. Dobry, 10/2/98, (PB99-123606, A13, MF-A03).

MCEER-98-0011 "IDARC-BRIDGE: A Computational Platform for Seismic Damage Assessment of Bridge Structures," by A.M. Reinhorn, V. Simeonov, G. Mylonakis and Y. Reichman, 10/2/98, (PB99-162919, A15, MF-A03).

MCEER-98-0012 "Experimental Investigation of the Dynamic Response of Two Bridges Before and After Retrofitting with Elastomeric Bearings," by D.A. Wendichansky, S.S. Chen and J.B. Mander, 10/2/98, (PB99-162927, A15, MF-A03).

MCEER-98-0013 "Design Procedures for Hinge Restrainers and Hinge Sear Width for Multiple-Frame Bridges," by R. Des Roches and G.L. Fenves, 11/3/98, (PB99-140477, A13, MF-A03).

MCEER-98-0014 "Response Modification Factors for Seismically Isolated Bridges," by M.C. Constantinou and J.K. Quarshie, 11/3/98, (PB99-140485, A14, MF-A03).

MCEER-98-0015 "Proceedings of the U.S.-Italy Workshop on Seismic Protective Systems for Bridges," edited by I.M. Friedland and M.C. Constantinou, 11/3/98, (PB2000-101711, A22, MF-A04).

MCEER-98-0016 "Appropriate Seismic Reliability for Critical Equipment Systems: Recommendations Based on Regional Analysis of Financial and Life Loss," by K. Porter, C. Scawthorn, C. Taylor and N. Blais, 11/10/98, (PB99-157265, A08, MF-A02).

MCEER-98-0017 "Proceedings of the U.S. Japan Joint Seminar on Civil Infrastructure Systems Research," edited by M. Shinozuka and A. Rose, 11/12/98, (PB99-156713, A16, MF-A03).

MCEER-98-0018 "Modeling of Pile Footings and Drilled Shafts for Seismic Design," by I. PoLam, M. Kapuskar and D. Chaudhuri, 12/21/98, (PB99-157257, A09, MF-A02).

MCEER-99-0001 "Seismic Evaluation of a Masonry Infilled Reinforced Concrete Frame by Pseudodynamic Testing," by S.G. Buonopane and R.N. White, 2/16/99, (PB99-162851, A09, MF-A02).

MCEER-99-0002 "Response History Analysis of Structures with Seismic Isolation and Energy Dissipation Systems: Verification Examples for Program SAP2000," by J. Scheller and M.C. Constantinou, 2/22/99, (PB99-162869, A08, MF-A02).

MCEER-99-0003 "Experimental Study on the Seismic Design and Retrofit of Bridge Columns Including Axial Load Effects," by A. Dutta, T. Kokorina and J.B. Mander, 2/22/99, (PB99-162877, A09, MF-A02).

MCEER-99-0004 "Experimental Study of Bridge Elastomeric and Other Isolation and Energy Dissipation Systems with Emphasis on Uplift Prevention and High Velocity Near-source Seismic Excitation," by A. Kasalanati and M. C. Constantinou, 2/26/99, (PB99-162885, A12, MF-A03).

MCEER-99-0005 "Truss Modeling of Reinforced Concrete Shear-flexure Behavior," by J.H. Kim and J.B. Mander, 3/8/99, (PB99-163693, A12, MF-A03).

MCEER-99-0006 "Experimental Investigation and Computational Modeling of Seismic Response of a 1:4 Scale Model Steel Structure with a Load Balancing Supplemental Damping System," by G. Pekcan, J.B. Mander and S.S. Chen, 4/2/99, (PB99-162893, A11, MF-A03).

MCEER-99-0007 "Effect of Vertical Ground Motions on the Structural Response of Highway Bridges," by M.R. Button, C.J. Cronin and R.L. Mayes, 4/10/99, (PB2000-101411, A10, MF-A03).

MCEER-99-0008 "Seismic Reliability Assessment of Critical Facilities: A Handbook, Supporting Documentation, and Model Code Provisions," by G.S. Johnson, R.E. Sheppard, M.D. Quilici, S.J. Eder and C.R. Scawthorn, 4/12/99, (PB2000-101701, A18, MF-A04).

MCEER-99-0009 "Impact Assessment of Selected MCEER Highway Project Research on the Seismic Design of Highway Structures," by C. Rojahn, R. Mayes, D.G. Anderson, J.H. Clark, D'Appolonia Engineering, S. Gloyd and R.V. Nutt, 4/14/99, (PB99-162901, A10, MF-A02).

MCEER-99-0010 "Site Factors and Site Categories in Seismic Codes," by R. Dobry, R. Ramos and M.S. Power, 7/19/99, (PB2000-101705, A08, MF-A02).

MCEER-99-0011 "Restrainer Design Procedures for Multi-Span Simply-Supported Bridges," by M.J. Randall, M. Saiidi, E. Maragakis and T. Isakovic, 7/20/99, (PB2000-101702, A10, MF-A02).

MCEER-99-0012 "Property Modification Factors for Seismic Isolation Bearings," by M.C. Constantinou, P. Tsopelas, A. Kasalanati and E. Wolff, 7/20/99, (PB2000-103387, A11, MF-A03).

MCEER-99-0013 "Critical Seismic Issues for Existing Steel Bridges," by P. Ritchie, N. Kauhl and J. Kulicki, 7/20/99, (PB2000-101697, A09, MF-A02).

MCEER-99-0014 "Nonstructural Damage Database," by A. Kao, T.T. Soong and A. Vender, 7/24/99, (PB2000-101407, A06, MF-A01).

MCEER-99-0015 "Guide to Remedial Measures for Liquefaction Mitigation at Existing Highway Bridge Sites," by H.G. Cooke and J. K. Mitchell, 7/26/99, (PB2000-101703, A11, MF-A03).

MCEER-99-0016 "Proceedings of the MCEER Workshop on Ground Motion Methodologies for the Eastern United States," edited by N. Abrahamson and A. Becker, 8/11/99, (PB2000-103385, A07, MF-A02).

MCEER-99-0017 "Quindío, Colombia Earthquake of January 25, 1999: Reconnaissance Report," by A.P. Asfura and P.J. Flores, 10/4/99, (PB2000-106893, A06, MF-A01).

MCEER-99-0018 "Hysteretic Models for Cyclic Behavior of Deteriorating Inelastic Structures," by M.V. Sivaselvan and A.M. Reinhorn, 11/5/99, (PB2000-103386, A08, MF-A02).

MCEER-99-0019 "Proceedings of the 7th U.S.- Japan Workshop on Earthquake Resistant Design of Lifeline Facilities and Countermeasures Against Soil Liquefaction," edited by T.D. O'Rourke, J.P. Bardet and M. Hamada, 11/19/99, (PB2000-103354, A99, MF-A06).

MCEER-99-0020 "Development of Measurement Capability for Micro-Vibration Evaluations with Application to Chip Fabrication Facilities," by G.C. Lee, Z. Liang, J.W. Song, J.D. Shen and W.C. Liu, 12/1/99, (PB2000-105993, A08, MF-A02).

MCEER-99-0021 "Design and Retrofit Methodology for Building Structures with Supplemental Energy Dissipating Systems," by G. Pekcan, J.B. Mander and S.S. Chen, 12/31/99, (PB2000-105994, A11, MF-A03).

MCEER-00-0001 "The Marmara, Turkey Earthquake of August 17, 1999: Reconnaissance Report," edited by C. Scawthorn; with major contributions by M. Bruneau, R. Eguchi, T. Holzer, G. Johnson, J. Mander, J. Mitchell, W. Mitchell, A. Papageorgiou, C. Scaethorn, and G. Webb, 3/23/00, (PB2000-106200, A11, MF-A03).

MCEER-00-0002 "Proceedings of the MCEER Workshop for Seismic Hazard Mitigation of Health Care Facilities," edited by G.C. Lee, M. Ettouney, M. Grigoriu, J. Hauer and J. Nigg, 3/29/00, (PB2000-106892, A08, MF-A02).

MCEER-00-0003 "The Chi-Chi, Taiwan Earthquake of September 21, 1999: Reconnaissance Report," edited by G.C. Lee and C.H. Loh, with major contributions by G.C. Lee, M. Bruneau, I.G. Buckle, S.E. Chang, P.J. Flores, T.D. O'Rourke, M. Shinozuka, T.T. Soong, C-H. Loh, K-C. Chang, Z-J. Chen, J-S. Hwang, M-L. Lin, G-Y. Liu, K-C. Tsai, G.C. Yao and C-L. Yen, 4/30/00, (PB2001-100980, A10, MF-A02).

MCEER-00-0004 "Seismic Retrofit of End-Sway Frames of Steel Deck-Truss Bridges with a Supplemental Tendon System: Experimental and Analytical Investigation," by G. Pekcan, J.B. Mander and S.S. Chen, 7/1/00, (PB2001-100982, A10, MF-A02).

MCEER-00-0005 "Sliding Fragility of Unrestrained Equipment in Critical Facilities," by W.H. Chong and T.T. Soong, 7/5/00, (PB2001-100983, A08, MF-A02).

MCEER-00-0006 "Seismic Response of Reinforced Concrete Bridge Pier Walls in the Weak Direction," by N. Abo-Shadi, M. Saiidi and D. Sanders, 7/17/00, (PB2001-100981, A17, MF-A03).

MCEER-00-0007 "Low-Cycle Fatigue Behavior of Longitudinal Reinforcement in Reinforced Concrete Bridge Columns," by J. Brown and S.K. Kunnath, 7/23/00, (PB2001-104392, A08, MF-A02).

MCEER-00-0008 "Soil Structure Interaction of Bridges for Seismic Analysis," I. PoLam and H. Law, 9/25/00, (PB2001-105397, A08, MF-A02).

MCEER-00-0009 "Proceedings of the First MCEER Workshop on Mitigation of Earthquake Disaster by Advanced Technologies (MEDAT-1), edited by M. Shinozuka, D.J. Inman and T.D. O'Rourke, 11/10/00, (PB2001-105399, A14, MF-A03).

MCEER-00-0010 "Development and Evaluation of Simplified Procedures for Analysis and Design of Buildings with Passive Energy Dissipation Systems," by O.M. Ramirez, M.C. Constantinou, C.A. Kircher, A.S. Whittaker, M.W. Johnson, J.D. Gomez and C. Chrysostomou, 11/16/01, (PB2001-105523, A23, MF-A04).

MCEER-00-0011 "Dynamic Soil-Foundation-Structure Interaction Analyses of Large Caissons," by C-Y. Chang, C-M. Mok, Z-L. Wang, R. Settgast, F. Waggoner, M.A. Ketchum, H.M. Gonnermann and C-C. Chin, 12/30/00, (PB2001-104373, A07, MF-A02).

MCEER-00-0012 "Experimental Evaluation of Seismic Performance of Bridge Restrainers," by A.G. Vlassis, E.M. Maragakis and M. Saiid Saiidi, 12/30/00, (PB2001-104354, A09, MF-A02).

MCEER-00-0013 "Effect of Spatial Variation of Ground Motion on Highway Structures," by M. Shinozuka, V. Saxena and G. Deodatis, 12/31/00, (PB2001-108755, A13, MF-A03).

MCEER-00-0014 "A Risk-Based Methodology for Assessing the Seismic Performance of Highway Systems," by S.D. Werner, C.E. Taylor, J.E. Moore, II, J.S. Walton and S. Cho, 12/31/00, (PB2001-108756, A14, MF-A03).

MCEER-01-0001 "Experimental Investigation of P-Delta Effects to Collapse During Earthquakes," by D. Vian and M. Bruneau, 6/25/01, (PB2002-100534, A17, MF-A03).

MCEER-01-0002 "Proceedings of the Second MCEER Workshop on Mitigation of Earthquake Disaster by Advanced Technologies (MEDAT-2)," edited by M. Bruneau and D.J. Inman, 7/23/01, (PB2002-100434, A16, MF-A03).

MCEER-01-0003 "Sensitivity Analysis of Dynamic Systems Subjected to Seismic Loads," by C. Roth and M. Grigoriu, 9/18/01, (PB2003-100884, A12, MF-A03).

MCEER-01-0004 "Overcoming Obstacles to Implementing Earthquake Hazard Mitigation Policies: Stage 1 Report," by D.J. Alesch and W.J. Petak, 12/17/01, (PB2002-107949, A07, MF-A02).

MCEER-01-0005 "Updating Real-Time Earthquake Loss Estimates: Methods, Problems and Insights," by C.E. Taylor, S.E. Chang and R.T. Eguchi, 12/17/01, (PB2002-107948, A05, MF-A01).

MCEER-01-0006 "Experimental Investigation and Retrofit of Steel Pile Foundations and Pile Bents Under Cyclic Lateral Loadings," by A. Shama, J. Mander, B. Blabac and S. Chen, 12/31/01, (PB2002-107950, A13, MF-A03).

MCEER-02-0001 "Assessment of Performance of Bolu Viaduct in the 1999 Duzce Earthquake in Turkey" by P.C. Roussis, M.C. Constantinou, M. Erdik, E. Durukal and M. Dicleli, 5/8/02, (PB2003-100883, A08, MF-A02).

MCEER-02-0002 "Seismic Behavior of Rail Counterweight Systems of Elevators in Buildings," by M.P. Singh, Rildova and L.E. Suarez, 5/27/02. (PB2003-100882, A11, MF-A03).

MCEER-02-0003 "Development of Analysis and Design Procedures for Spread Footings," by G. Mylonakis, G. Gazetas, S. Nikolaou and A. Chauncey, 10/02/02, (PB2004-101636, A13, MF-A03, CD-A13).

MCEER-02-0004 "Bare-Earth Algorithms for Use with SAR and LIDAR Digital Elevation Models," by C.K. Huyck, R.T. Eguchi and B. Houshmand, 10/16/02, (PB2004-101637, A07, CD-A07).

MCEER-02-0005 "Review of Energy Dissipation of Compression Members in Concentrically Braced Frames," by K.Lee and M. Bruneau, 10/18/02, (PB2004-101638, A10, CD-A10).

MCEER-03-0001 "Experimental Investigation of Light-Gauge Steel Plate Shear Walls for the Seismic Retrofit of Buildings" by J. Berman and M. Bruneau, 5/2/03, (PB2004-101622, A10, MF-A03, CD-A10).

MCEER-03-0002 "Statistical Analysis of Fragility Curves," by M. Shinozuka, M.Q. Feng, H. Kim, T. Uzawa and T. Ueda, 6/16/03, (PB2004-101849, A09, CD-A09).

MCEER-03-0003 "Proceedings of the Eighth U.S.-Japan Workshop on Earthquake Resistant Design f Lifeline Facilities and Countermeasures Against Liquefaction," edited by M. Hamada, J.P. Bardet and T.D. O'Rourke, 6/30/03, (PB2004-104386, A99, CD-A99).

MCEER-03-0004 "Proceedings of the PRC-US Workshop on Seismic Analysis and Design of Special Bridges," edited by L.C. Fan and G.C. Lee, 7/15/03, (PB2004-104387, A14, CD-A14).

MCEER-03-0005 "Urban Disaster Recovery: A Framework and Simulation Model," by S.B. Miles and S.E. Chang, 7/25/03, (PB2004-104388, A07, CD-A07).

MCEER-03-0006 "Behavior of Underground Piping Joints Due to Static and Dynamic Loading," by R.D. Meis, M. Maragakis and R. Siddharthan, 11/17/03, (PB2005-102194, A13, MF-A03, CD-A00).

MCEER-03-0007 "Seismic Vulnerability of Timber Bridges and Timber Substructures," by A.A. Shama, J.B. Mander, I.M. Friedland and D.R. Allicock, 12/15/03.

MCEER-04-0001 "Experimental Study of Seismic Isolation Systems with Emphasis on Secondary System Response and Verification of Accuracy of Dynamic Response History Analysis Methods," by E. Wolff and M. Constantinou, 1/16/04 (PB2005-102195, A99, MF-E08, CD-A00).

MCEER-04-0002 "Tension, Compression and Cyclic Testing of Engineered Cementitious Composite Materials," by K. Kesner and S.L. Billington, 3/1/04, (PB2005-102196, A08, CD-A08).

MCEER-04-0003 "Cyclic Testing of Braces Laterally Restrained by Steel Studs to Enhance Performance During Earthquakes," by O.C. Celik, J.W. Berman and M. Bruneau, 3/16/04, (PB2005-102197, A13, MF-A03, CD-A00).

MCEER-04-0004 "Methodologies for Post Earthquake Building Damage Detection Using SAR and Optical Remote Sensing: Application to the August 17, 1999 Marmara, Turkey Earthquake," by C.K. Huyck, B.J. Adams, S. Cho, R.T. Eguchi, B. Mansouri and B. Houshmand, 6/15/04, (PB2005-104888, A10, CD-A00).

MCEER-04-0005 "Nonlinear Structural Analysis Towards Collapse Simulation: A Dynamical Systems Approach," by M.V. Sivaselvan and A.M. Reinhorn, 6/16/04, (PB2005-104889, A11, MF-A03, CD-A00).

MCEER-04-0006 "Proceedings of the Second PRC-US Workshop on Seismic Analysis and Design of Special Bridges," edited by G.C. Lee and L.C. Fan, 6/25/04, (PB2005-104890, A16, CD-A00).

MCEER-04-0007 "Seismic Vulnerability Evaluation of Axially Loaded Steel Built-up Laced Members," by K. Lee and M. Bruneau, 6/30/04, (PB2005-104891, A16, CD-A00).

MCEER-04-0008 "Evaluation of Accuracy of Simplified Methods of Analysis and Design of Buildings with Damping Systems for Near-Fault and for Soft-Soil Seismic Motions," by E.A. Pavlou and M.C. Constantinou, 8/16/04, (PB2005-104892, A08, MF-A02, CD-A00).

MCEER-04-0009 "Assessment of Geotechnical Issues in Acute Care Facilities in California," by M. Lew, T.D. O'Rourke, R. Dobry and M. Koch, 9/15/04, (PB2005-104893, A08, CD-A00).

MCEER-04-0010 "Scissor-Jack-Damper Energy Dissipation System," by A.N. Sigaher-Boyle and M.C. Constantinou, 12/1/04 (PB2005-108221).

MCEER-04-0011 "Seismic Retrofit of Bridge Steel Truss Piers Using a Controlled Rocking Approach," by M. Pollino and M. Bruneau, 12/20/04 (PB2006-105795).

MCEER-05-0001 "Experimental and Analytical Studies of Structures Seismically Isolated with an Uplift-Restraint Isolation System," by P.C. Roussis and M.C. Constantinou, 1/10/05 (PB2005-108222).

MCEER-05-0002 "A Versatile Experimentation Model for Study of Structures Near Collapse Applied to Seismic Evaluation of Irregular Structures," by D. Kusumastuti, A.M. Reinhorn and A. Rutenberg, 3/31/05 (PB2006-101523).

MCEER-05-0003 "Proceedings of the Third PRC-US Workshop on Seismic Analysis and Design of Special Bridges," edited by L.C. Fan and G.C. Lee, 4/20/05, (PB2006-105796).

MCEER-05-0004 "Approaches for the Seismic Retrofit of Braced Steel Bridge Piers and Proof-of-Concept Testing of an Eccentrically Braced Frame with Tubular Link," by J.W. Berman and M. Bruneau, 4/21/05 (PB2006-101524).

MCEER-05-0005 "Simulation of Strong Ground Motions for Seismic Fragility Evaluation of Nonstructural Components in Hospitals," by A. Wanitkorkul and A. Filiatrault, 5/26/05 (PB2006-500027).

MCEER-05-0006 "Seismic Safety in California Hospitals: Assessing an Attempt to Accelerate the Replacement or Seismic Retrofit of Older Hospital Facilities," by D.J. Alesch, L.A. Arendt and W.J. Petak, 6/6/05 (PB2006-105794).

MCEER-05-0007 "Development of Seismic Strengthening and Retrofit Strategies for Critical Facilities Using Engineered Cementitious Composite Materials," by K. Kesner and S.L. Billington, 8/29/05 (PB2006-111701).

MCEER-05-0008 "Experimental and Analytical Studies of Base Isolation Systems for Seismic Protection of Power Transformers," by N. Murota, M.Q. Feng and G-Y. Liu, 9/30/05 (PB2006-111702).

MCEER-05-0009 "3D-BASIS-ME-MB: Computer Program for Nonlinear Dynamic Analysis of Seismically Isolated Structures," by P.C. Tsopelas, P.C. Roussis, M.C. Constantinou, R. Buchanan and A.M. Reinhorn, 10/3/05 (PB2006-111703).

MCEER-05-0010 "Steel Plate Shear Walls for Seismic Design and Retrofit of Building Structures," by D. Vian and M. Bruneau, 12/15/05 (PB2006-111704).

MCEER-05-0011 "The Performance-Based Design Paradigm," by M.J. Astrella and A. Whittaker, 12/15/05 (PB2006-111705).

MCEER-06-0001 "Seismic Fragility of Suspended Ceiling Systems," H. Badillo-Almaraz, A.S. Whittaker, A.M. Reinhorn and G.P. Cimellaro, 2/4/06 (PB2006-111706).

MCEER-06-0002 "Multi-Dimensional Fragility of Structures," by G.P. Cimellaro, A.M. Reinhorn and M. Bruneau, 3/1/06 (PB2007-106974, A09, MF-A02, CD A00).

MCEER-06-0003 "Built-Up Shear Links as Energy Dissipators for Seismic Protection of Bridges," by P. Dusicka, A.M. Itani and I.G. Buckle, 3/15/06 (PB2006-111708).

MCEER-06-0004 "Analytical Investigation of the Structural Fuse Concept," by R.E. Vargas and M. Bruneau, 3/16/06 (PB2006-111709).

MCEER-06-0005 "Experimental Investigation of the Structural Fuse Concept," by R.E. Vargas and M. Bruneau, 3/17/06 (PB2006-111710).

MCEER-06-0006 "Further Development of Tubular Eccentrically Braced Frame Links for the Seismic Retrofit of Braced Steel Truss Bridge Piers," by J.W. Berman and M. Bruneau, 3/27/06 (PB2007-105147).

MCEER-06-0007 "REDARS Validation Report," by S. Cho, C.K. Huyck, S. Ghosh and R.T. Eguchi, 8/8/06 (PB2007-106983).

MCEER-06-0008 "Review of Current NDE Technologies for Post-Earthquake Assessment of Retrofitted Bridge Columns," by J.W. Song, Z. Liang and G.C. Lee, 8/21/06 06 (PB2007-106984).

MCEER-06-0009 "Liquefaction Remediation in Silty Soils Using Dynamic Compaction and Stone Columns," by S. Thevanayagam, G.R. Martin, R. Nashed, T. Shenthan, T. Kanagalingam and N. Ecemis, 8/28/06 06 (PB2007-106985).

MCEER-06-0010 "Conceptual Design and Experimental Investigation of Polymer Matrix Composite Infill Panels for Seismic Retrofitting," by W. Jung, M. Chiewanichakorn and A.J. Aref, 9/21/06 (PB2007-106986).

MCEER-06-0011 "A Study of the Coupled Horizontal-Vertical Behavior of Elastomeric and Lead-Rubber Seismic Isolation Bearings," by G.P. Warn and A.S. Whittaker, 9/22/06 (PB2007-108679).

MCEER-06-0012 "Proceedings of the Fourth PRC-US Workshop on Seismic Analysis and Design of Special Bridges: Advancing Bridge Technologies in Research, Design, Construction and Preservation," Edited by L.C. Fan, G.C. Lee and L. Ziang, 10/12/06.

MCEER-06-0013 "Cyclic Response and Low Cycle Fatigue Characteristics of Plate Steels," by P. Dusicka, A.M. Itani and I.G. Buckle, 11/1/06 06 (PB2007-106987).

MCEER-06-0014 "Proceedings of the Second US-Taiwan Bridge Engineering Workshop," edited by W.P. Yen, J. Shen, J-Y. Chen and M. Wang, 11/15/06.

MCEER-06-0015 "User Manual and Technical Documentation for the REDARS™ Import Wizard," by S. Cho, S. Ghosh, C.K. Huyck and S.D. Werner, 11/30/06.

MCEER-06-0016 "Hazard Mitigation Strategy and Monitoring Technologies for Urban and Infrastructure Public Buildings: Proceedings of the China-US Workshops," edited by X.Y. Zhou, A.L. Zhang, G.C. Lee and M. Tong, 12/12/06.

MCEER-07-0001 "Static and Kinetic Coefficients of Friction for Rigid Blocks," by C. Kafali, S. Fathali, M. Grigoriu and A.S. Whittaker, 3/20/07.

MCEER-07-0002 "Hazard Mitigation Investment Decision Making: Organizational Response to Legislative Mandate," by L.A. Arendt, D.J. Alesch and W.J. Petak, 4/9/07.

MCEER-07-0003 "Seismic Behavior of Bidirectional-Resistant Ductile End Diaphragms with Unbonded Braces in Straight or Skewed Steel Bridges," by O. Celik and M. Bruneau, 4/11/07.

MCEER-07-0004 "Modeling Pile Behavior in Large Pile Groups Under Lateral Loading," by A.M. Dodds and G.R. Martin, 4/16/07.

MCEER-07-0005 "Experimental Investigation of Blast Performance of Seismically Resistant Concrete-Filled Steel Tube Bridge Piers," by S. Fujikura, M. Bruneau and D. Lopez-Garcia, 4/20/07.

MCEER-07-0006 "Seismic Analysis of Conventional and Isolated Liquefied Natural Gas Tanks Using Mechanical Analogs," by I.P. Christovasilis and A.S. Whittaker, 5/1/07.

MCEER-07-0007 "Experimental Seismic Performance Evaluation of Isolation/Restraint Systems for Mechanical Equipment – Part 1: Heavy Equipment Study," by S. Fathali and A. Filiatrault, 6/6/07.

MCEER-07-0008 "Seismic Vulnerability of Timber Bridges and Timber Substructures," by A.A. Sharma, J.B. Mander, I.M. Friedland and D.R. Allicock, 6/7/07.

MCEER-07-0009 "Experimental and Analytical Study of the XY-Friction Pendulum (XY-FP) Bearing for Bridge Applications," by C.C. Marin-Artieda, A.S. Whittaker and M.C. Constantinou, 6/7/07.

MCEER-07-0010 "Proceedings of the PRC-US Earthquake Engineering Forum for Young Researchers," Edited by G.C. Lee and X.Z. Qi, 6/8/07.

MCEER-07-0011 "Design Recommendations for Perforated Steel Plate Shear Walls," by R. Purba and M. Bruneau, 6/18/07.

MCEER-07-0012 "Performance of Seismic Isolation Hardware Under Service and Seismic Loading," by M.C. Constantinou, A.S. Whittaker, Y. Kalpakidis, D.M. Fenz and G.P. Warn, 8/27/07.

MCEER-07-0013 "Experimental Evaluation of the Seismic Performance of Hospital Piping Subassemblies," by E.R. Goodwin, E. Maragakis and A.M. Itani, 9/4/07.

MCEER-07-0014 "A Simulation Model of Urban Disaster Recovery and Resilience: Implementation for the 1994 Northridge Earthquake," by S. Miles and S.E. Chang, 9/7/07.

MCEER-07-0015 "Statistical and Mechanistic Fragility Analysis of Concrete Bridges," by M. Shinozuka, S. Banerjee and S-H. Kim, 9/10/07.

MCEER
EARTHQUAKE ENGINEERING TO EXTREME EVENTS
University at Buffalo, The State University of New York
Red Jacket Quadrangle ▪ Buffalo, New York 14261
Phone: (716) 645-3391 ▪ Fax: (716) 645-3399
E-mail: *mceer@buffalo.edu* ▪ WWW Site *http://mceer.buffalo.edu*
University at Buffalo *The State University of New York*

ISSN 1520-295X